AFRL-HE-WP-TR-2002-0247

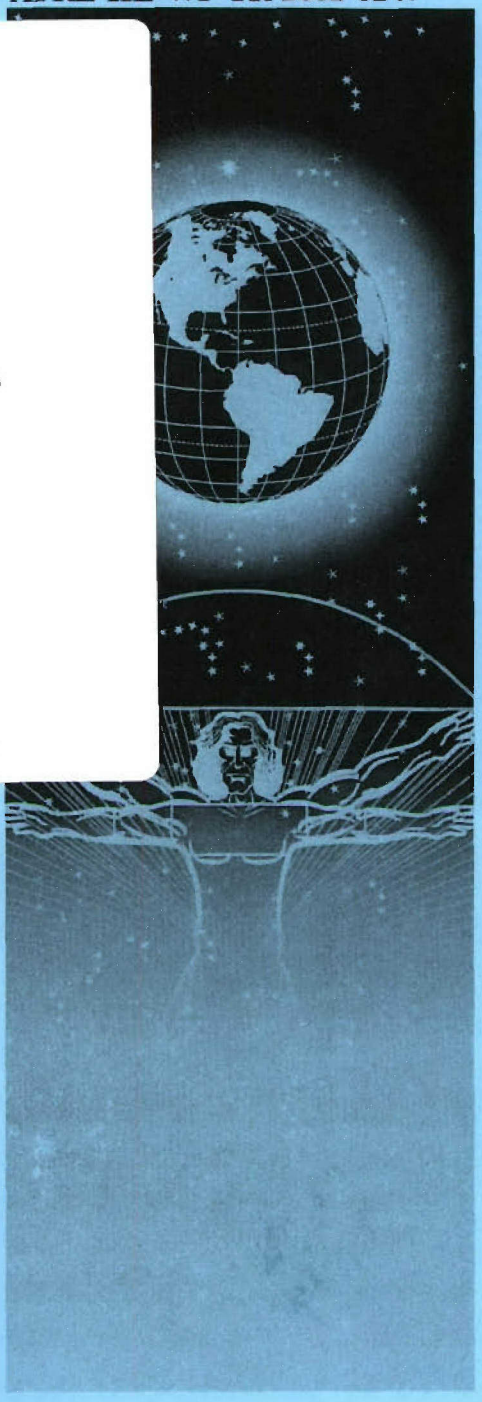

UNITED STATES AIR FORCE RESEARCH LABORATORY

ADVANCED NEUROSCIENCE INTERFACE RESEARCH

Bilal Ezzedine, Ph.D.
Mehdi Adineh, Ph.D.
Martin Satter, Ph.D.
Joseph Mantil, M.D., Ph.D.

Wallace-Kettering Neuroscience Institute
3533 Southern Blvd., Suite 5200
Kettering, OH 45429

May 2002

FINAL REPORT FOR THE PERIOD JULY 1997 TO MAY 2002

Human Effectiveness Directorate
Integration & Operations Division
2610 Seventh Street
Wright-Patterson AFB OH 45433-7901

NOTICES

When US Government drawings, specifications or other data are used for any purpose other than a definitely related Government procurement operation, the Government thereby incurs no responsibility nor any obligation whatsoever, and the fact that the Government may have formulated, furnished, or in any way supplied the said drawings, specifications or other data, is not to be regarded by implication or otherwise, as in any manner licensing the holder or any other person or corporation, or conveying any rights or permission to manufacture, use, or sell any patented invention that may in any way be related thereto.

Please do not request copies of this report from the Air Force Research Laboratory. Additional copies my be purchased from:

National Technical Information Service
5285 Port Royal Road
Springfield, VA 22161

Federal Government Agencies registered with the Defense Technical Information Center should direct requests for copies of this report to:

Defense Technical Information Center
8725 John J. Kingman Rd., Ste 0944
Ft. Belvoir, VA 22060-6218

TECHNICAL REVIEW AND APPROVAL

AFRL-HE-WP-TR-2002-0247

The voluntary informed consent of the subjects in this research was obtained as required by Air Force Instruction 40-402.

This report has been reviewed by the Office of Public Affairs (PA) and is releasable to the National Technical Information Service (NTIS). At NTIS, it will be available to the general public, including foreign nations.

This technical report has been reviewed and is approved for publication.

FOR THE DIRECTOR

GLENN HARSHBERGER, CHIEF
Integration & Operations Division
Air Force Research Laboratory

REPORT DOCUMENTATION PAGE

Form Approved
OMB No. 0704-0188

1. REPORT DATE *(DD-MM-YYYY)*	2. REPORT TYPE	3. DATES COVERED *(From - To)*
01-05-2002	Final	July 1997-May 2002

4. TITLE AND SUBTITLE

Advanced Neuroscience Interface Research

5a. CONTRACT NUMBER
F33615-98-2-6002

5b. GRANT NUMBER
n/a

5c. PROGRAM ELEMENT NUMBER
63231F

6. AUTHOR(S)

Adineh, Mehda, Ph.D.
Ezzedine, Bilal, Ph.D.
Satter, Martin, Ph.D.
Mantil, Joseph, C., M.D., Ph.D.

5d. PROJECT NUMBER
n/a

5e. TASK NUMBER
n/a

5f. WORK UNIT NUMBER
n/a

7. PERFORMING ORGANIZATION NAME(S) AND ADDRESS(ES)

Wallace Kettering Neuroscience Institute
Kettering Medical Center
3533 Southern Blvd., Suite 5200
Kettering OH 45429

8. PERFORMING ORGANIZATION REPORT NUMBER
n/a

9. SPONSORING/MONITORING AGENCY NAME(S) AND ADDRESS(ES)

AFRL/HEOX
ATTN: SCOTT HALL
2610 Seventh St
WPAFB OH 45433-7901

DFAS-CO/New Dominion
PO Box 182041
Columbus OH 43218-2041

10. SPONSOR/MONITOR'S ACRONYM(S)

11. SPONSOR/MONITOR'S REPORT NUMBER(S)
AFRL-HE-WP-TR-2002-0247

12. DISTRIBUTION/AVAILABILITY STATEMENT

Approved for public release; distribution is unlimited

13. SUPPLEMENTARY NOTES

n/a

14. ABSTRACT

WKNI completed a Cooperative Agreement with AFRL to attempt to develop an infrastructure and demonstration project to exhibit and utilize technological developments with applications potentially valuable to both a military and civilian mission. Integrating mission critical information from a variety of formats and sources, and making them available to a highly trained operator, were seen as parallels between Air Force pilot and flight crew needs and the needs of a neurosurgeon and surgery team. Using the specialized knowledge and experience of the Human Effectiveness Directorate, we attempted to apply this knowledge to a civilian environment in the application and development of this technology.

15. SUBJECT TERMS

MRI	Perfusion	neuronavigation	PET scan
MR Spectroscopy	fMRI	co-registration software	radiopharmaceuticals
Diffusion	presurgical planning	interactive 3-D omages	radiotracers

16. SECURITY CLASSIFICATION OF:			17. LIMITATION OF ABSTRACT	18. NUMBER OF PAGES	19a. NAME OF RESPONSIBLE PERSON
a. REPORT	b. ABSTRACT	c. THIS PAGE			Gerald M. Szkotnicki
U	U	U	UL	244	19b. TELEPHONE NUMBER *(Include area code)* (937)396-8002

Cooperative Agreement F33615-98-2-6002

Advanced Neuroscience Interface Research

Advanced MR Imaging Visualization and Segmentation

Bilal Ezzedine, Ph.D.
Mehdi Adineh, Ph.D.

Next-Generation Image-Guided Neuronavigation System

Martin Satter, Ph.D.

PET Biochemical Imaging Project

Joseph Mantil, M.D., Ph.D.

May 01, 2002

Wallace-Kettering Neuroscience Institute
3533 Southern Blvd., Suite 5200
Kettering, OH 45429

Abstract

The Cooperative Agreement entitled "Advanced Neuroscience Interface Research," was generated out of a recognized need for a neuroscience institute in the Dayton area to address research and technology issues concerning both public and military health, and human factors concerns.

The Advanced Neuroscience Interface Research Program is divided into three separate project categories that each has a demonstrated list of technologies with potential neuroscience and military applications which focus on improved targeting and recognition of abnormalities in the brain. Specifically, all three projects investigate the unexpected similarities in the specialized skills required of pilots and neurosurgeons, including the improvement of effective instantaneous decision-making utilizing multiple sources of data, minimization of distractions and stress, and the use of hand-eye coordination to make delicate, decisive maneuvers.

The objective of the **Advanced MR Imaging Visualization and Segmentation** project was to develop, and more importantly integrate, advances in neuroscience imaging, processing and data management in order to improve clinical outcomes for patients with additional applications for advancing neuroscience capabilities for the USAF. Advanced-imaging techniques were developed to detect neurological changes in a variety of diseases in a clinical setting. These and existing techniques were combined, compared and contrasted to give the most complete visual and biochemical view of what was occurring in patients, incorporating several MR imaging techniques including spectroscopy both of patients and surgically-excised tissue. While each method, or modality, gave a certain amount of information, combining methods complemented each other to give a more thorough understanding of pathological changes for decision-making by the clinician. In order to make this new information useful, the data had to be put in forms that it could be combined, compared and contrasted; computer programs were developed and implemented to achieve this.

The information had to be made available in an intelligible, user-friendly interface. Software programs were developed and implemented to securely share information and provide the clinicians with the ability to access and analyze the information with speed and ease. In addition, claustrophobia and excessive noise, obstacles that have deprived some patients of these valuable assays, were addressed through development and use of new devices.

The overall purpose of the **Next Generation Image-Guided Neuronavigation System** project was to enhance the neurosurgical capabilities at Kettering Medical Center by integrating hardware and software with elements potentially useful in both military and civilian applications. The Air Force pilot requires a wide variety of information from different sources to navigate through a predefined air space around barriers to a predefined target. This is analogous to a neurosurgeon accessing multiple sources of information, such as MR and PET images, input to image-based computer guidance systems to enable precise navigation through brain anatomy during surgery. Using multiple data inputs, this project sought to obtain and couple (co-register) data from these disparate sources thus augmenting the ability to accomplish a successful surgery or mission to the operator (pilot or surgeon).

The IGNS project was executed along two parallel tracks involving hardware assessment and acquisition along with software development and deployment. Time is a mission-critical factor for both pilots and neurosurgeons. A drawn-out mission leads to increased exposure, potential detection and unnecessary conflict for the pilot, whereas an extended surgery increases the rate of infection and complications due to anesthesia. Fatigue translates to a greater probability for human error in both disciplines. Therefore, a primary goal in this project was to investigate technologies to input information from a number of sources and integrate them into a single sensory display system, culminating in reduced fatigue and increased attention levels throughout the operating field. The Principle Investigator studied improvements in man-machine interface by electronically combining input from disparate components and presenting information in approximate real-time where possible to the surgeon and the surgical team.

Using AFRL input and participation where possible, we developed a set of instruments combined with software development that allows for the rapid co-registration and display of 3-D image data. In addition, we sought to update computer images based on the position of the aircraft or surgeon's tools, thereby presenting the operator with the most relevant data at a specific time and place.

The **PET Biochemical Imaging** project focuses on using biochemical imaging of tumors for improved diagnosis, target delineation and treatment evaluation.

By measuring chemical changes within the body, PET biochemical imaging offers many advantages over other technologies available for the detection and treatment of brain tumors and other neurological diseases. Noninvasive biochemical brain mapping performed by PET scan can immediately elucidate the marked differences between normal brain tissue and tumor tissue for the physician, long before the anatomical changes recorded by computerized tomography or magnetic resonance imaging can be detected.

In order to understand the biochemical processes in tumor, PET allows the use of selective radiotracers (or biomarkers) that enables the analysis of tumor pathology, location and volume. Biochemical imaging thus assists in the efficacy of neurosurgery, radiotherapy, and chemotherapy. The development of new radiotracers for use in PET scanning aids studies of patients with brain tumors, schizophrenia, stroke, Alzheimer's disease (AD) and Parkinson's disease. A protocol was developed to utilize three target radiotracers to study brain tumors in human subjects: ^{18}F-fluorodeoxyglucose (^{18}F-FDG) for glucose metabolism; ^{11}C-methionine (^{11}C-MET) for amino acid transport and protein synthesis and; ^{11}C-choline for lipid synthesis. The uptake and incorporation of these radiotracers were evaluated using PET in astrocytoma patients who were suspected of having World Health Organization (WHO) grade II or grade III tumors.

Table of Contents

PET Biochemical Imaging Project

Figures List

Advanced MR Visualization and Segmentation

Next Generation Image Guided Neuronavigation System

PET Biochemical Imaging Project

List of Tables and Attachments

Advanced MR Imaging and Visualization

Tables

Attachments

1. ANR Patent
2. Human Factors Study

Next Generation Image Guided Neuronavigation

Tables

Attachments

1. CRASIS
2. 3-D Editing of Digital Shapes for the Rapid Segmentation of Medical Volumtric Images

PET Biochemical Imaging Project

None

Foreward

Cooperative Agreement Number F33615-98-2-6002 was generated from a recognized need for the development of an advanced neuroscience institute in the Dayton area, and the unique opportunity for collaboration between the Air Force Research Laboratory and the Wallace Kettering Neuroscience Institute on demonstration projects that have potential mutual benefit to both the medical and military communities.

The **Advanced Neuroscience Interface Research Program** is divided into three separate project categories that each has a demonstrated list of technologies with potential neuroscience and military applications which focus on improved targeting and recognition of abnormalities in the brain. Specifically, all three projects investigate the unexpected similarities in the specialized skills required of pilots and neurosurgeons, including the improvement of effective instantaneous decision-making utilizing multiple sources of data, minimization of distractions and stress, and the use of hand-eye coordination to make delicate, decisive maneuvers.

The **Advanced MR Visualization and Segmentation** project includes studies in the evaluation of brain function and alertness in healthy as well as impaired pilots, and patients to determine and enhance the ability to function in a challenging environment. Through studies with functional magnetic resonance imaging, stimulus and response, visual perception pathways and degenerative disease, hippocampal pathways were investigated. Human factors issues were also addressed in the stroke protocol, such as the effective and rapid communication techniques to improve overall team performance.

Technological developments and advancements in the **Next Generation Image-Guided Neuronavigation System** project investigated issues of man-machine interface, and the importance to the operator of having critical information pre-processed and delivered rapidly and in an easily, accessible manner, as well as making complex information available in real-time to various people on the team. Human effectiveness issues were

researched and addressed in order to afford the surgeon or pilot a more user-friendly environment, thereby increasing the operator's overall effectiveness in the completion of the mission. Surface mapping, and global deployment of supplies and resources and other areas of common interest were also studied to improve overall mission effectiveness.

The **PET Biochemical Imaging** project included investigation of neuroreceptors and the use of radiotracers in PET imaging to target abnormalities such as tumor or other central nervous system disorders in the brain. The technologies investigated and developed have potential military application in the areas of posttraumatic stress disorder, the detection and counteraction of neurotoxins, modulation of tissue sensitivity to radiation used in both the medical and nuclear power environment.

The development of all of these technologies in the various neuroscience interfaces have potential dual use in both the medical and military environments, and therefore provide opportunities to leverage DoD and private sector resources for economic and military benefit.

Acknowledgment

The studies reported herein represent a team effort among the scientists, clinicians, and support staff at a number of different institutions as follows:

Physicians:

The successes resulting from this project reflect significant contributions from the following healthcare professionals who, amid their exhausting schedules, provided us with continued support and direction:

Our neurosurgeons–*Dr. Theodore Bernstein, Dr. Raymond Poelstra, and Dr. Gary Kraus.*

Our radiologists–*Dr. John German, Dr. Ronald Faddel, Dr. Jerry Andrews, and Dr. Theodore Miller.*

Our neurologists–*Dr. Robert Simpkins* and *Dr. David White.*

Institutions:

Department of Acoustics, Department of the Human Factors Engineering, and Department of Radiology at Wright-Patterson AFB; Dayton, Ohio.

Deepest thanks to *Mr. Scott Hall*, Technology Transfer Manager of the Air Force Research Laboratory Human Effectiveness Directorate and AF Project Manager of this effort, for his interest and active participation.

Department of Biochemistry and Molecular Biology, Department of Physics, Department of Microbiology and Immunology, Department of Emergency Medicine, and Department of Medicine at the Wright State University (WSU); Dayton, Ohio for assistance in various areas of this project including our epilepsy and brain tumor research.

Harvard Brain Bank; Boston, Massachusetts for providing us with normal brain tissue.

Dr. Thomas P. Greco, Yale School of Medicine; New Haven, Connecticut, for assistance with our MS project.

General Electric; Dayton, Ohio, *Dr. Thomas Raiddy*, for providing research material.

Support Staff:

Mr. Michael Kent, Wallace-Kettering Neuroscience Institute (WKNI) and WSU, for his important role in many of our scientific projects. We are very grateful to have had his input while preparing this report.

Mr. Basil Bakri, WKNI, for graphic and computer assistance.

The MRI technologists at Kettering Medical Center (KMC), particularly *Ms. Cathy Swick*, for generous help with the project.

WKNI students/interns *Ms. Lisa Jacola, Ms. Katie Kimble, Ms. Brittany Cleveland*, and *Mr. Jeremy Olson* who put an exhausting amount of hours into this project.

Ms. Sharon Kerestes, WKNI, for her patience and assistance in completing this project.

Ms. Candi Lee and *Ms. Jean Ruppert*, nurses at KMC, who were the bridges to our patients.
Ms. Pam Sequeira, Pathology, KMC

Special thanks to *Mr. Gerald Szkotnicki*, WKNI Executive Director, whose door was always open and helped us to develop a strong research infrastructure at WKNI. His diligence and guidance were invaluable.

Most importantly, we thank our research patients who put their trust in us. Their generosity will never be forgotten.

Advanced MR Imaging and Visualization

1.0 Executive Summary

1.1 Overview

The objective of the Advanced MR Imaging Visualization and Segmentation project was to develop, and more importantly integrate, advances in neuroscience imaging, processing and data management in order to improve clinical outcomes for patients with additional applications for advancing neuroscience capabilities for the USAF. Advanced-Imaging techniques were developed to detect neurological changes in a variety of diseases in a clinical setting. These and existing techniques were combined, compared and contrasted to give the most complete visual and biochemical view of what was occurring in patients, incorporating several MR imaging techniques including spectroscopy both of patients and surgically-excised tissue. While each method, or modality, gave a certain amount of information, combining methods complemented each other to give a more thorough understanding of pathological changes for decision-making by the clinician. In order to make this new information useful, the data had to be put in forms that it could be combined, compared and contrasted; computer programs were developed and implemented to achieve this.

The information had to be made available in an intelligible, user-friendly interface. Software programs were developed and implemented to securely share information and provide the clinicians with the ability to access and analyze the information with speed and ease. In addition, claustrophobia and excessive noise, obstacles that have deprived some patients of these valuable assays, were addressed through development and use of new devices.

1.2 Major Accomplishments and Key Products and Deliverables

Major accomplishments and key products and deliverables include the following:

1) Utilizing a multimodal approach including in vivo and in vitro magnetic resonance spectroscopy (MRS), chemical shift imaging (CSI), fluid-attentuated inversion recovery (FLAIR), fast spin echo sequence-inversion recovery (FSE-IR) MR, and functional

magnetic resonance imaging (fMRI) in the characterization of neurological diseases studied, this project demonstrated clinical advances affecting patient outcomes. Our understanding of heretofore unknown biochemical changes sheds insight into disease progression and may impact the search for prevention and cure.

2) Advances in image segmentation, database development, and creation of Internet Browser-Based Imaging Access networks and programs allowed for optimal remote communication and utilization of data by clinicians in a rapidly and easily acquired environment.

3) An advance in noise reduction in the MR environment holds promise for making MR available to greater numbers of patients and with greater safety at the present and as higher power MR becomes available. A joint patent was filed for this device in conjunction with Wright-Patterson Air Force Base (WPAFB), Department of Acoustics.

4) We provided the community with the first state-of -the-art neuroimaging capability for the management of hyperacute stroke.

5) A prototype device to alleviate claustrophobia in the MR environment was developed and tested. This device may make MR available to a large category of patients for whom this essential diagnostic tool was previously unavailable.

6) A new MR instrument equipped with Echo-Planar Imaging (EPI) was acquired and utilized in each of the following portions of the project.

7) In vivo characterization of human brain tumors by MRS is now regularly performed to evaluate tumor classification in monitoring response to treatment, and WKNI/KMCN surgeons have begun using MRS data as a valuable tool in the operating room to determine tissue state and mapping.

8) Advanced MRI techniques in management of stroke: CT examination is ineffective in the diagnosis of hyperacute stroke. Recently, a significant body of evidence suggests that

the combined application of the diffusion-weighted imaging (DWI) and perfusion-weighted imaging (PWI) can be effective in detecting ischemic changes in early time-points post the onset of stroke. We developed an original experimental design to examine the feasibility of advanced MR techniques in the management of hyperacute stroke in our community-oriented hospital. In order to conduct and accommodate such a large-scale study, a CT/MRI suite was built adjacent to the emergency department (ED). Indeed, we are pleased that our hyperacute MR stroke sequences are matched only by the leading stroke research centers in the world. Unfortunately, we were challenged by our ability to recruit patients into the study. Nonetheless, we were able to provide our community with the state of the art stroke imaging. Work is in the progress to reengage our stroke study by including the identification of a highly skilled stroke team who will help us educate the community regarding the importance of time in management of stroke.

9) Choline metabolism in human brain tumors with ^{13}C-Positron Emission Tomography (PET) and ^{1}H-CSI: the need for prompt and accurate recognition of a low to high grade progression and/or of a post-therapeutic recurrence in cerebral neoplasms has given impetus to the search for novel neuroimaging methods. This is the first documented study of complementing in vivo choline metabolism determined from MRS with radio-labeled PET imaging. Data from our investigation clearly showed the feasibility of performing correlative investigations with PET and MRS. Such data may prove useful for characterizing tumor proliferation status in vivo.

10) Feasibility of performing in vivo choline metabolism studies in biological tissue was investiagted. The results of the pilot kinetic study indicated that metabolites derived from exogenous choline can be monitored using MRS. Future studies will increase our understanding of the biosynthesis and metabolism of choline-derived phospholipids (PL) that affect processes of signal transduction, cell proliferation, differentiation and apoptosis, including carcinogenesis in brain tumors.

11) CSI of human central neurocytoma (CN): We were able to provide an in vivo profile of this rare brain tumor. Our studies were presented to American Society of Neuroradiology in the spring of 2001. Our work will aid clinicians in better diagnosing this brain tumor. In addition, our in vitro MRS data provided a more detailed biochemical profile of CN brain tumors. Our original work further emphasized the importance of quantitation in proton (^{1}H)-MRS studies for detecting altered brain metabolism.

12) PL changes in hippocampus of epileptics were investigated. In a multi-center and multi-institutional investigation involving scientists at the Wallace-Kettering Neuroscience Institute (WKNI), Wright State University (WSU) and Harvard Brain Bank (Boston, MA), the underlying mechanism of seizure in patients was explored.

13) A comparative analysis of CT and FLAIR for the detection of hemorrhage was completed. Our results reflect the fact that more work is needed to determine MR FLAIR's role in the detection of hematoma. The higher percent error rates for the radiologists' interpretation of the MR FLAIR images suggest that this method may not be as diagnostically accurate for the detection of acute and hyperacute intracranial hemorrhage (HICH). However, the limited number of patient cases led to us to search our databases to retrieve more patients with active intracranial hemorrhage (as defined by CT scan) who also had a MR-FLAIR within 24 h. In a blinded investigation, radiologists at WKNI/KMCN and WPAFB are further evaluating these images.

14) Hippocampal volumetric measurements. Hippocampus is a brain structure involved in short-term memory processing. Unfortunately, the hippocampus is known to be severely affected by the characteristic neuropathology of mesial temporal lobe epilepsy (MTLE), Alzheimer's disease (AD), schizophrenia and many others central nervous system (CNS) related pathologies [1-5]. In a productive partnership among research scientists and epileptologists at WKNI and Department of Radiology at WPAFB, several major clinical research projects were completed. The results had immediate clinical benefit, they include:

a. We demonstrated that 3-D spoiled gradient recalled acquisition steady state-inversion recovery (SPGR-IR) MR sequence using a standard head coil could enhance clinical utilization of hippocampal volumetric measurements when used in conjunction with Vitrea™ (Vital Images; Minneaplis, MN).
b. A newly developed and optimized MR pulse sequence was developed and utilized to determine asymmetrical atrophy associated with hippocampal sclerosis.

15) Alleviating claustrophobia with 3-D Audio Display. A mockup MRI machine was constructed to appear similar to a real MRI, and a 3-D audio display for virtual environment (VE) was constructed. Subjects' subjective ratings of comfort were higher in the VE condition than in the non-VE condition, but this difference failed to reach significance. However, subjective ratings of their ability to cope with the situation were significantly higher in the VE than the non-VE condition. This display may prove valuable in reducing obstacles that deny claustrophobic patients of this valuable tool.

16) Active noise reduction in the MRI environment. An active noise reduction device, improving noise reduction from previous devices, was designed and patented. This device may improve safety and allow MRI of patients that previously could not tolerate this examination.

17) Distributed neuroscience database project. A database software and application was developed, with an engaging, easy-to-use interface, in which common data can easily be shared between all users.

18) Internet Browser-Based Imaging Access. The WKNI and WPAFB Hospital, in conjunction with KMCN, implemented a cost-effective solution to resolve the issue of broad image distribution. This solution was the Stentor's iSite web server, which is fed directly from KMCN's PACS system.

19) Multi-modalities biochemical imaging in tumefaction of multiple sclerosis (MS). Using MRI, MRS and positron emission tomography (PET), we were able to distinguish an unusual case of MS from a tumor. These findings determined a successful treatment and outcome, and demonstrate clear benefits to utilizing a multiplicity of modalities in distinguishing clinical conditions.

20) Software tool development for MRS analysis. To integrate the area under the spectral peaks, we developed a new software tool at WKNI called *Integrex*. This software is easy, flexible and capable of input from various data format, which subsequently eased our data analysis.

21) A pattern recognition software tool kit was developed. This unique program recognizes common signals in MR spectra and associates them with common findings through mathematical modeling. Such association will aid in diagnosis and follow-up, and help to ensure consistency and precision in evaluating images and spectra.

22) 3-D brain functional imaging data were delivered to stereotactic neuronavigational instruments utilized in neurosurgery operating theatre. The main objectives of this projects were accomplished in a close collaborative effort among between the neuroimaging team and neurosurgeons in the following three phases:

a. Optimizing MR data acquisition methods;
b. Image transformation and post-processing; and
c. 3-D neuronavigational compatibility of functional data.

23) Publications and meetings: The works of this project were published, patented, presented and recognized at national and international meetings including: International Society of Magnetic Resonance in Medicine and the American Society of Neuroradiology.

2.0 Summary of Objectives

In order to provide for the improved imaging visualization and segmentation to support optimum patient diagnosis, treatment and care, the following objectives were determined:

1. Utilize existing as well as develop new magnetic resonance (MR) technologies to improve the medical imaging environment by allowing for image data acquisition in a more rapid and precise manner;
2. Employ the techniques of diffusion and perfusion imaging, task activation and spectroscopy to improve information differentiation and classification at the beginning of patient examination for optimum diagnosis, treatment, and care;
3. Advance functional imaging modalities, particularly multi-nuclear spectroscopy (MNS) and chemical shift imaging (CSI) to determine the behavioral characteristics of several prominent neurological disorders including tumors (specifically the aggressiveness of tumor), multiple sclerosis (MS) and epilepsy;
4. Utilize a headset developed by the USAF and the Wright State University (WSU) that produces an auditory 3-D display as a means to abate claustrophobia experienced by patients subject to magnetic resonance imaging (MRI) and MR spectroscopy (MRS);
5. Compare and contrast the utility and accuracy of MR-fluid attenuated inversion recovery (FLAIR) to computerized tomography (CT) in brain hemorrhage detection; and
6. Develop software and integrate the database and imaging modalities to optimize use of the multi-parametric data acquired from a multiplicity of sources in a user-friendly, secure computer environment.

3.0 Background

3.1 Overview

Existing MR technology did not provide for the necessary imaging visualization and segmentation to support optimum patient diagnosis, treatment and care. Neurosurgeons and neurologists are now able to more accurately identify anatomical, functional, and biochemical markers for defining targets for therapeutic action. A primary consideration was the development of a medical-imaging environment suitable for 3-D interaction of data in a more rapid and precise manner for use by the physician end-user. A neurovascular optimized MRI instrument equipped with echo planar imaging (EPI) capability was acquired in the first year of this project that allows the techniques of perfusion and diffusion imaging, task activation and spectroscopy to accomplish this task. At the same time, valuable information from new techniques was becoming more readily available. However, integration of these new data was either virtually impossible or the time interval for integration so great as to make the new information useless.

MR spectroscopy (MRS) utilizes the same hardware as conventional MRI. However, where MRI delineates well-detailed anatomical and pathological information, MRS provides insight into the biochemical changes that precede morphological changes detected in MRI or other imaging modalities. Rather than generating an image, MRS produces a graph of the peaks of various brain metabolites. Each brain metabolite has its own unique resonance frequency. Therefore, unlike other imaging techniques, MRS can provide both qualitative and quantitative information, as the areas of metabolite peaks are related to the steady-state cellular concentration of metabolites visible with MRS, which changes with pathology. Any nucleus that has a nonzero spin such as: ^{1}H (proton), ^{13}C (carbon) and ^{31}P (phosphorous) can be used for MRS analysis. Currently, our spectroscopic capabilities at WKNI are limited to performing only ^{1}H spectroscopy. However, we are in the process of upgrading our system to a multi-nuclear package, so we can detect a significant number of other brain metabolites including those that contain phosphorous such as ATP and inorganic phosphate (Pi).

In the brain, ^{1}H-MRS allows detection of several compounds including *N*-acetly-aspartate (NAA), lipids, choline, creatine (Cr), glutamate, glutamine, lactate and myo-inostitol (***Figure 1***). Changes in choline resonance intensities are likely related to changes in levels of phosphocholine (Pcho) and glycerophosphocholine (GPC), and probably reflect alterations in cell membrane integrity. Increases in lactate resonance intensity are found in the presence of impaired energy metabolism or inflammation. Changes in NAA are indicative of expression of neuronal or axonal loss or dysfunction, as NAA in found exclusively in neurons and the neuronal process in the mature brain.

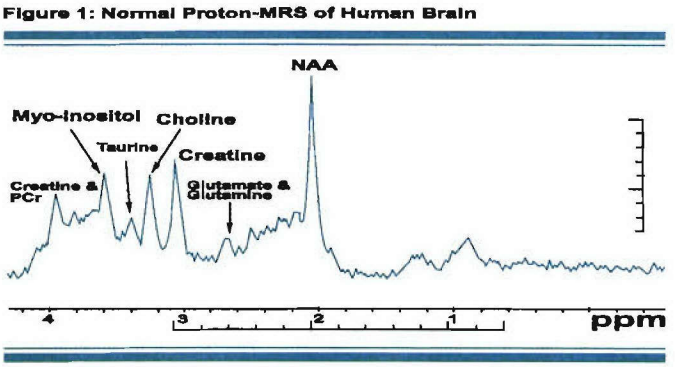

Figure 1. ^{1}H-MRS allows detection of several brain metabolites including NAA, lipids, choline, Cr, glutamate, glutamine, lactate, and myo-inositol.

We use two ^{1}H-MRS techniques routinely at WKNI, the single-voxel (SV-MRS) technique and CSI. In the SV-MRS, a volume of interest (VOI) is identified on the anatomical MRI, and a single MR spectrum is obtained from that VOI. The VOI can be as small as 1 cm^3. Recently, we have begun using a more advanced ^{1}H-MRS technique in which we can generate metabolic images showing the distribution of metabolites in the spectrum over one or more slices of brain. This technique is called CSI and offers marked improvements over SV-MRS by providing images of the regional distribution of metabolites with increased spatial resolution. CSI is analogous to conventional MRI except that the signal intensity of each voxel is based on the proton signal from metabolites, other than water. Because the concentration of metabolites is at least 10,000 times less than of water, the resolution and signal to noise of metabolite images are much less than of water-based images. Currently, we are capable of generating 2-D CSI

(***Figure 2***) and we are working hard to provide our clinicians with multi-slice CSI and 3-D CSI.

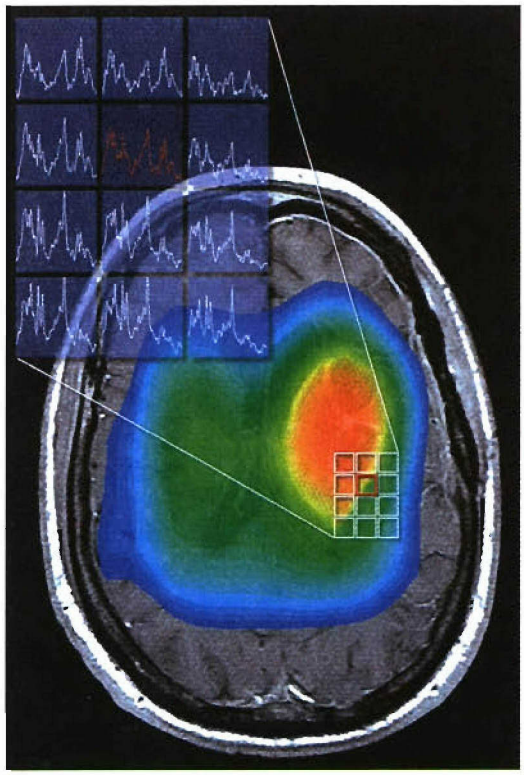

Figure 2. CSI of a Patient with a Brain Tumor.

MRS has diagnostic value for evaluating and monitoring the progression of stroke, intracranial tumors, epilepsy, multiple sclerosis (MS), AD, Parkinson's disease and many others. Herein, we describe some of the applications of this imaging modality as it relates to brain tumors, MS and epilepsy that were utilized throughout our project.

Furthermore, we were able to integrate various conventional/anatomical MR imaging techniques with MRS in hope of providing a more complete view of the changes occurring in patients suffering with various neuropathologies. MRS has significantly advanced our understanding, as we were able to identify specific biochemical changes. While each MR imaging type, or MRS spectrum, provided a certain amount of information by itself, adding, comparing and contrasting modalities truly provided "a whole that was greater than the sum of the parts."

This integrative approach has promise for clinical and military application. Treatments can be improved through improved biochemical and anatomical characterization of disease. Military application may include better characterization in neurotoxicological circumstances, as well as overcoming problems such as claustrophobia that may be encountered by personnel in enclosed settings such as cockpits. Improved image segmentation and database integration and sharing will benefit utilization of the information gathered from each study.

3.2 In Vivo Characterization of Human Brain Tumors by MRS

An extensive amount of research in the past decade has shown that in the nearly 100% of the primary brain tumors at time of presentation, the ^{1}H-MRS is abnormal [1]. Therefore, MRS could be a more sensitive imaging modality in detection of neoplasia than CT or MRI. ^{1}H-MRS has also shown to be a promising technique for the early detection of metabolic changes in tumor tissue during the course of radiotherapy and chemotherapy [2, 3]. Such alterations in brain metabolism post-radiation can aid clinicians in distinguishing between the areas of induced brain necrosis from recurrent tumor (***Figure 3***). Although, further research is needed, MRS can potentially provide a method for the tailoring of radiation, chemotherapy and treatment schedules to the needs of the individual patients.

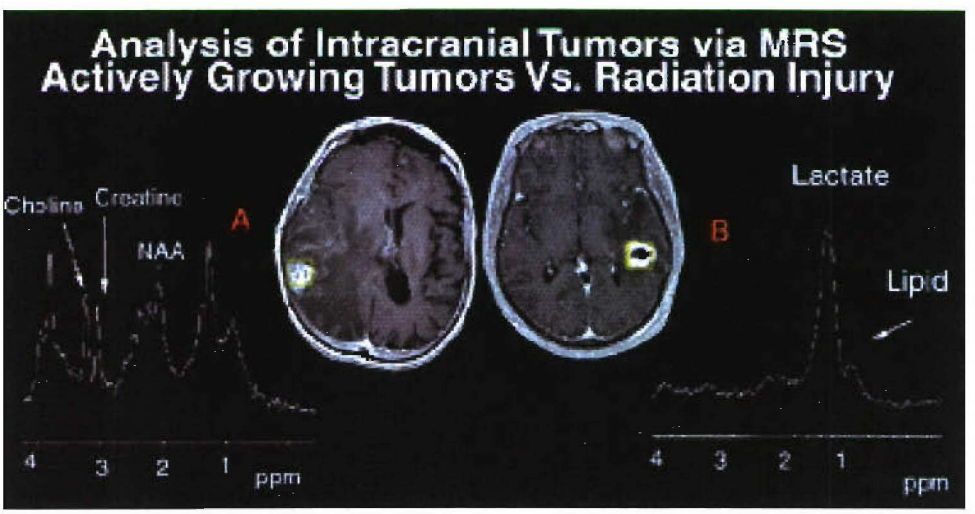

Figure 3

At WKNI, image data obtained using MRI are routinely used supplemented with MRS data to evaluate brain tumors. More importantly, several studies have suggested that MRS can also improve the in vivo classification of intracranial tumors and monitoring response to treatment [4]. Indeed, we are among several other research laboratories which are in the process of developing mathematical models to perform pattern recognition (PR) analysis of MRS spectra for the characterization of brain tumor types. We are correlating the in vivo spectroscopic data with surgical pathologic findings and supplemental MRS studies performed on surgical tissue specimens to determine the clinical value of the MRS in characterization of tumor types in vivo.

3.3 Choline Metabolism in Human Brain Tumors with ^{11}C-PET and ^{1}H-CSI

Choline is a precursor for cellular membranes and acetylcholine synthesis [5]. Choline metabolism has shown to be impacted by various neuropathologies including neurodegenerative diseases and neoplasms [5]. It is therefore important to gain knowledge about choline metabolism in vivo in an attempt to understand the role of this important metabolite in disease processes. Herein, we report the first documented study of in vivo choline metabolism with MRS in conjunction with ^{11}C-positron emission tomography (PET).

Despite the inherent advantages of in vivo MRS imaging, this technique has some drawbacks. Perhaps the most complex problem with the in vivo MRS is a compounding of observable metabolic signals. For example, the elevation in choline signal within pathological tissue does not solely represent free choline. Many different choline-containing compounds such as GPC, Pcho or CDP-choline are represented in one choline signal. One way to address the issues associated with in vivo MRS is to extract specific metabolites from the tumor tissue and examine them in vitro. Herein, we also report on the utilization of in vitro high-resolution MRS of a specimen of the same tumor with the expectation of providing better interpretation of the in vivo spectra.

3.4 Choline Metabolism in Human Brian Tumors

Choline is a precursor for cellular membranes and acetylcholine synthesis. Choline metabolism has been shown to be influenced by various neuropathologies including neurodegenerative diseases and neoplasms. It is therefore important to gain knowledge about choline metabolism in vivo and in vitro in an attempt to understand the role of this important metabolite in disease processes. We have developed several important techniques at WKNI in understanding choline metabolism in our tumor patients, including ^{11}C-labled choline for PET studies. We have presented our work at major international scientific conferences.

Phosphatidylcholine (PtdC) is the major component of biological membranes. Biosynthesis and metabolism of this PL affect processes of signal transduction, cell proliferation, and differentiation and apoptosis, including brain carcinogenesis. Yet our understanding of this metabolism and its regulation is far from complete. PtdC is synthesized mainly from choline via the CDP-choline pathway (de novo). Recent studies suggest that processes that control PtdC biosynthesis may play a role in cell proliferation and carcinogenesis [6]. Radioisotope methods have previously been used to measure rates of PtdC synthesis, but these methods lack the specificity to analyze the metabolic pathways.

This is a multi-phase investigation that will be conducted in the following order: 1) feasibility of studying choline incorporation into PL by in vivo MRS and developing the kinetic models to describe fluxes; 2) choline metabolism in tumor cell lines and analyzing data using the kinetic models developed in the first phase; and 3) ^{13}C-labled choline studies in patients using ^{13}C-multi-nuclear spectroscopic (MNS) imaging in hope of in vivo grading of tumors based on the fluxes through PL biosynthetic pathways.

Herein we report on the completion of the first phase of these studies. In collaboration with the Department of Biochemistry/Molecular Biology and Department of Physics at Wright State University (WSU), we used ^{13}C and ^{31}P-MRS to investigate the biosynthesis of PtdC in vivo during a 60-min infusion of [$^{1\text{-}13}$C]choline, and conducted a kinetic model analysis of the data. We concluded that, because of our ability to optimize the techniques

and analysis, we were ready to begin the second phase of our investigations, in vitro brain tumor cells.

3.5 CSI of Human CN

Although CN accounts for only 1% of all central nervous system (CNS) tumors, it is responsible for nearly half of all of the supratentorial intraventricular tumors. The five-year survival rate for all CNs is 81%, with 100% survival rate, without recurrence, being reported with total resection of the tumor. CN differentiation and diagnosis have become vital. Herein, we report the first documented ^{1}H-CSI of a human CN.

A significant body of evidence suggests that CSI could provide a more sensitive complementary imaging modality in detection of neoplasia with CT or MRI. The results of our current investigation provide an in vivo biochemical profile of this rare brain tumor.

One of the major drawbacks of utilizing CSI in routine clinical setting is the absolute quantitation of alterations in metabolite concentrations. Most in vivo brain MRS studies describe the impact of disease on living tissue in terms of ratio of metabolites. However, the interpretation of the data is difficult because the signal intensity of the in vivo MR spectra is significantly dependent upon the acquisition parameters. Herein, we also report on utilization of in vitro high-resolution MRS of a human CN tumor extract in hope of providing a better interpretation of the spectra obtained by CSI-MR.

3.6 PL Changes in Hippocampus of Epileptics

Epilepsy surgery is one of the most effective treatments in patients with intractable partial epilepsy. Partial seizures emanate from the temporal lobe structures of the brain in approximately 80% of patients evaluated for such a surgery [7]. The most epileptogenic region in the temporal lobe is the medial temporal lobe structures involving the amygdala and hippocampus.

The hippocampus is a complex curved structure with an elongated shape and variable angle. The hippocampus has been and continues to be a major target structure for the investigation of links between brain processes and psychologically-experienced memory. Unfortunately, the hippocampus is known to be severely affected by the characteristic neuropathology of mesial temporal lobe epilepsy (MTLE), AD, schizophrenia and many others CNS-related pathologies [8-12]. In fact, hippocampal sclerosis is the most common abnormality associated with MTLE [8]. The MRI characteristics of hippocampal sclerosis include increased T_2 signal intensity (i.e., indicative of atrophy) in the hippocampus and decreased size of the hippocampus.

Furthermore, ^{1}H-MRS has also shown to be a useful adjunctive pre-surgical test for the localization of the epileptogenic foci in patients with partial epilepsy, especially those with extratemporal foci [13]. The reduction in the NAA signal is due to the loss of neurons associated with hippocampal atrophy. However, the source of the elevation of the choline and Cr signals in the ^{1}H-MRS in vivo of epileptic foci is not clear. Several possibilities that will be examined in this study will include choline and Cr-containing brain metabolites such as: GPC, phosphatidylcholine (PC), Pcho, CDP-choline and phosphocreatine (PCr).

Apoptosis or programmed cell death is an inducible and organized, form of cellular demise that results in the removal of apoptotic cells by macrophages. Interestingly, recent evidence implicating apoptosis in the etiology and pathophysiology of known human diseases, such as heart diseases, cancer, AIDS, and neurodegenerative and autoimmune diseases are continually surfacing [14, 15]. Apoptosis is induced when cells undergo severe injury to their nucleus, as occurs following exposure to radiation. One of the early responses to apoptotic signals involves exposing phosphatidylserine (PS) on the outer leaflet of the plasma membrane. PS is an important component of cell membrane PL, and is normally restricted to the inner leaflet. PS exposure to the outer leaflet has several potential biological consequences, two of which are recognition and removal of the apoptotic cell by phagocytes. Thus, membrane-bound PS expression serves as a signal to surrounding cells, identifying the expressing cell as undergoing apoptosis [15-17].

Whether PS is the sole ligand recognized by phagocytes or it is associated with other molecules to form a complex ligand remains to be determined. Conversely, excessive PS exposure may lead to thrombosis or may explain formation of so-called antiphospholipid (aPL) antibodies as occurring in patients with aPL syndrome [18, 19].

Based on the in vivo MRS data and immunohistochemical studies, it is well established that atrophy associated with hippocampal sclerosis is connected to neuronal loss. We, thus, hypothesize that neuronal loss associated with hippocampal sclerosis in TLE patients might be due to a shift in the PS distribution in the bilayer membrane. Interestingly, in animal models, several investigators have demonstrated that during seizures, levels of PS-associated second messengers and their precursors in neuronal membranes are altered. More specifically, the levels of diacylglycerol (DAG), as well as free fatty acid levels, have shown to be elevated in rats undergoing evoked seizures. PS is an anionic membrane PL integral to protein kinase C (PKC) activation via interactions with DAG [20].

During seizures, levels and distribution of PS and other PL in neuronal membranes are altered. PS is an important component of cell membrane PL, and is normally restricted to the inner leaflet. Early responses to apoptotic signal cause PS to migrate to the outer leaflet of the plasma membrane.

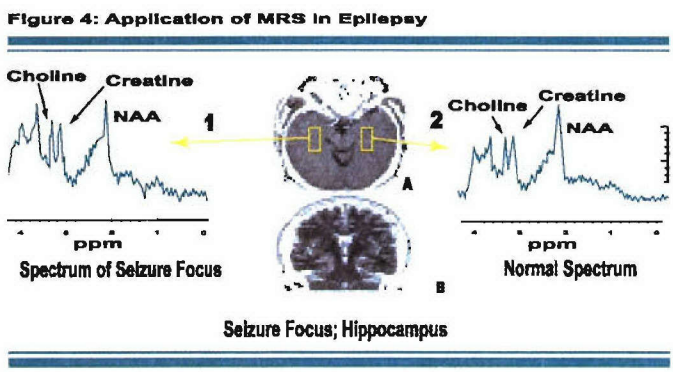

Figure 4

Herein, we report on alteration in the PS distribution in cells and MRS observed PL that may contribute to mechanisms in hippocampal sclerosis associated with MTLE. By

studying MTLE patient biopsies with normal control brain tissue, we expect to uncover correlations previously unknown. The Harvard Brain Bank (Boston, MA) provided us with the normal human brain hippocampi.

3.7 Comparative Analysis of CT and FLAIR for the Detection of Hemorrhage

Presently, patients who present to the emergency room (ER) with acute neurological deficits are entered into the area "stroke protocol." This is generally centered on the results of the CT scan. The usefulness of multiple mode (diffusion, perfusion, and fluid-attenuated inversion recovery; FLAIR) MRI in the diagnosis of acute ischemic stroke has already been proven [11]. *Barber et al.* discussed the superiority of DWI and PWI in the diagnosis of major cerebral ischemic changes [21]. Conversely, many authors have stated and reiterated their confidence in the CT scan as the initial and primary assessment tool for the diagnosis of spontaneous intracerebral hemorrhage [22, 23]. Until recently, the superiority of the CT scan has not been challenged.

Many researchers have used animal models to show that MRI is a superior tool to the CT scan for the diagnosis of both ischemic and hemorrhagic strokes [24]; researchers have found these same results with human models. The issue now is whether the MRI is as accurate of a medium as the CT scan for diagnosis of intracerebral hemorrhage and if so, what form of MRI should be used. Indeed, several authors have demonstrated that MR-FLAIR is an accurate diagnostic instrument in the diagnosis of acute, subacute, and chronic subarachnoid hemorrhage [25, 26]. *Bakshi et al.* showed that MR-FLAIR could also be used to detect intraventricular hemorrhage at the acute and subacute phases [27]. *Linfante et al.* proved that MRI could be both diagnostically accurate and practically feasible even within the hyperacute 2-h onset window [28]. We are building our research on the foundation provided by these studies.

This study was designed to be done retrospectively using readily available patient data. The null hypothesis for this study was that the MR-FLAIR is just as effective at detecting both intraparenchymal and extraparenchymal intracranial hemorrhage as the CT scan.

We searched our databases and medical records of hundreds of patients who were admitted to KMCN since 1995. Our criterion was finding a subgroup of patients who had known brain hemorrhage as determined from CT examination and also had a MR-FLAIR within 30 h.

3.8 Hippocampal Volumetric Measurements

As previously stated, the hippocampus has been and continues to be a major target structure for the investigation of links between brain processes and psychologically-experienced memory. Unfortunately, the hippocampus is known to be severely affected by the characteristic neuropathology of AD [29, 30], TLE [29, 30], schizophrenia [29] and many others CNS-related pathologies [29]. In fact, hippocampal sclerosis is the most common abnormality associated with TLE [29]. Several studies have established a high degree of correlation among MR visual analysis of hippocampal sclerosis, pathology and the electroencephalographic (EEG) focus [29, 30]. The MR characteristics of hippocampal sclerosis include increased T_2 signal intensity in the hippocampus and decreased size of the hippocampus. However, detection of subtle unilateral hippocampal atrophy or bilateral symmetrical atrophy is difficult by simple visual inspection even on the high-resolution MRI exams. Several studies have suggested the utilization of quantitative MRI-based volume measurements of the hippocampus to improve the sensitivity of hippocampal atrophy detection in TLE. Hippocampal atrophy detected by volumetric MRI has also been found to be a sensitive feature of early AD [29, 30]

Precise in vivo volumetric measurements of small brain structures such as basal ganglia, amygdala, and hippocampus have been possible due to a significant improvement in the resolution of MR images. However, hippocampal volumetric measurements have been difficult in routine clinical settings due to the complex anatomical nature of the hippocampus. Furthermore, there is concern that since the volumes have to be measured manually with contouring, the variability of the inter-operator and intra-operator could cause a problem.

This project addressed the following questions: 1) Could improved volumetric measurements with improved clinical utility be produced from enhanced hippocampal imaging by MRI? 2) Would a localized temporal coil prove more effective than the conventional MRI head coil? and 3) Would radiologists in a clinical setting find hippocampal volumetric measurement by either method equally or more valuable in determining patient care and outcome?

3.8.1 Phase 1 Objectives

Our neuroimaging team has recently demonstrated a simple method for fully interactive 3-D segmentation and brain volumetric measurements using a single modified pulse sequence. The fast 3-D-Spoiled Gradient Recalled Acquisition Steady State (SPGR) is a fast pulse sequence and thus can easily be added in a clinical setting. By using an inversion recovery time of 500ms (TI = 500 ms), we have demonstrated a good contrast between white/gray matter and cerebral spinal fluid (CSF) in a series of contiguous T_1-weighted (T_1W) images (i.e., without any space gap). By reconstructing the images with commercially available 3-D analysis state-of-the-art image-processing software Vitrea™ which had recently been acquired by WKNI, volumetric brain analysis can be performed based on a combination of manual thresholding and tracing. No image pre-processing is needed. The whole process of 3-D reconstruction of the hippocampus, thresholding and surface rendering is relatively fast and user-friendly.

3.8.1.1 Main Focus of the Investigation

The aim of this study was to assess the reliability and accuracy of hippocampal volumetric measurements using Vitrea™ via modified 3-D SPGR-IR prepped pulse sequence.

Study-study variation was assessed in healthy volunteers scanned on two different occasions and the inter- and intra-operator variations will be assessed in healthy subjects. The accuracy of our technique will be further evaluated by measurements of a phantom with known volume. In addition, the results of our volumetric measurements were

compared to results obtained using 3-D reformatting software on Advantage Windows™ Workstation, which is available on all GE MR instruments.

3.8.1.2 Clinical Relevance

Routine use of the quantitative approach for MRI analysis of hippocampal atrophy using commercially available image-processing software Vitrea™ could remove subjectivity in interpretation and improve the field of MRI by detecting these atrophic changes. Furthermore, the capacity for the routine in vivo clinical volumetric measurements will potentially benefit the investigation of neuropsychiatric disorders. Also, since MRI does not involve ionizing radiation, repeated measures over time pose no risk to the subjects. Therefore, the effectiveness and monitoring of therapy including pharmacotherapy in various hippocampal-related pathologies would be possible. By combining MR volumetric studies with all other currently employed techniques, the accuracy of TLE diagnosis can be greatly improved.

3.8.1.3 Advantages of Using Vitrea™

Enumerated below are some advantages to using Vitrea™:

1) User-friendly software that can be used routinely in clinical settings.
   Vitrea™ allows both surface and volume rendering which can theoretically improve the accuracy of visual delineation as well as the volumetric measurement of the hippocampus. It is interesting to note that the 3-D measurement feature of Vitrea™ with real-time volume rendering feedback allows the measurement of the entire volume of a segmented structure, but also excludes the regional lesions within the structure as depicted by various signal intensities. We must emphasis that this unique feature of Vitrea™ has significant clinical implications. Examples of when this would be helpful are: 1) tumor volume assessment, 2) volume measurement of necrotic portions of tumors and, 3) determination of the entire volume a tumor. This is an important tool for monitoring the effectiveness of tumor therapy. This feature also has significant benefits for hippocampal volumetric measurements. In several neuropathologies including TLE, the visual inspection of the hippocampus may overestimate its exact size by not excluding the interior hippocampal lesions, which

have marked signal difference relative to the normal hippocampus tissue. Thus, using Vitrea's™ 3-D measurement feature with instant volume-rendering feedback, one can easily exclude such areas.

2) The post-processing requires less time for this particular application relative to other image-processing softwares including the more widely used AWW 3.0.
3) Ability to fly around the hippocampus in 3-D in real-time.
   There is no need to use histogram data in making decision about the voxels' relative signal intensity (e.g., AWW 3-D software). Instead, the voxels' relative signal intensity can be done simply be leveling the window and instant visual feedback. These features can potentially making volumetric measurements more practical in routine clinical settings.

3.8.2 Phase 2

Having demonstrated the utility of improved volumetric measurement using improved sequences Vitrea™, the next phase sought to further overcome artifacts and noise that still pose obstacles to optimal clinical utility. High-resolution imaging with localized MR coils, which provide significant improvement in the signal/noise ratio of the temporal lobe region, has shown to be a valuable tool in generating very high-resolution imaging of hippocampal anatomy. In this phase of the study, we used localized MR coils in conjunction with a fast spin echo sequence (FSE), the highest anatomical resolution for hippocampal delineation without magnetic susceptibility artifacts that can be achieved. Using this technique, improved contrast between white/gray matter and CSF was generated in a series of contiguous and heavily tilted T_2-W images. Furthermore, by combining MR images with MinIP (Minimum Intensity Projection) image-processing and visualization, we have significantly expedited the hippocampal delineation procedure.

3.8.3 Phase 3

In the first two phases of the project, hippocampal volumetric measurement was demonstrated as a valuable tool and significantly improved upon. Such high-resolution

images have eased the process of hippocampal contouring and paved the way for routine volumetric measurements in our center.

Even with the drastic improvement in MR image quality for hippocampal volumetric measurements, routine use of the quantitative approach for MRI analysis of hippocampal atrophy is not widespread, especially in community-based healthcare systems. Implementation of volumetric analysis requires training, costly computer hardware and software and time. Moreover, there is concern with regard to the subjectivity in the structural delineation.

Our center has been generating high-resolution images with small localized surface coils for volumetric analysis during the course of this project (see phase 2 above). The issue addressed in phase 3 was whether the high-resolution imaging of the temporal lobe with the localized coil is as accurate a medium as the hippocampal volumetric analysis with the standard head coil for the diagnosis of hippocampal sclerosis. It may be that the two approaches prove complimentary in improving diagnosis.

In a multi-center blinded study involving radiologists at KMC and WPAFB, we are retrospectively comparing the radiologists' interpretation of hippocampal atrophy (versus sclerosis) based on the high-resolution images with the corresponding volumetric analysis.

3.8.3.1 Project Importance

Routine use of the quantitative approach for MRI analysis of hippocampal sclerosis is very challenging in community-based healthcare centers. Data from the current investigation demonstrates whether the radiological interpretation based on the utilization of high-resolution imaging is better for detection of hippocampal sclerosis, or volumetric analysis by standard head coil is required.

Hippocampus is a brain structure involved in short-term memory processing. The volume of this structure is impacted by various neuropathologies including AD and

epilepsy. In this study, we optimized MR images in order to delineate this structure and measure its volume.

3.9 Alleviating Claustrophobia with 3-D Audio Display

Claustrophobia is perhaps the negative side effect most widely associated with MRI examination. Utilizing 3-D audio displays developed at WSU and WPAFB, WKNI evaluated a virtual environment (VE) to alleviate anxiety associated with MRI exams.

MRI scans are becoming standard diagnostic tools in many areas of medicine and are widely used for research purposes. Despite the utility of MRI, a significant number of patients fail to complete, or have difficulty with, the procedure because of anxiety and claustrophobia [31]. We investigated the use of VE technology to alleviate these responses, thereby making MRI procedures more readily available to a wider array of patients.

The prior use of VEs to treat phobias has centered on the repeated presentation of the fear-inducing stimulus to the patient in such a manner that the phobic response diminishes over time, i.e., systematic desensitization or exposure therapy [32-34]. However, exposure therapies are generally very time-consuming (requiring multiple therapy sessions) and are therefore not practical with MRI. In this experiment, we utilized the VE during the MRI procedure, rather than before the procedure (as in exposure therapy). The goal was to create a compelling and spatial virtual experience, such that the patient felt that he/she was in the VE rather than the MRI scanner. The ability of a VE to create the illusion of being in a different environment is known as presence. The constraints of the MRI enclosure limit the ability to create a realistic VE and a significant sense of presence. Typically, motor-control interfaces within a VE allow the user to move around and interact with virtual objects as they would in a real environment with real objects, reinforcing the sense of presence. Because the patient must remain still during the MRI scan to prevent motion artifact, this type of interaction is not possible. The lack of motor interfaces within the MRI emphasizes the importance of high-fidelity sensory displays. Most work on VEs has focused on the role of high-quality visual stimulation for

creating presence. However, in our previous work, we have argued strongly for the importance of high-fidelity spatial audio stimulation for producing a compelling sense of presence. Moreover, virtual audio provides a sense of spaciousness not commonly associated with audio presented over headphones, which seems likely to be particularly relevant to the alleviation of claustrophobia.

3.10 Active Noise Reduction in the MRI Environment

MRI is an important and useful medical diagnostic tool; however, many patients experience anxiety that is exacerbated by the acoustic noise associated with the scanning process. In the past, both active and passive attenuation have been used to mitigate MRI noise, but this system works by sampling the noise at the patient's earphones. This sample is sent to a computer that analyzes the noise signal and generates a new signal, which feeds back into the earphones to cancel the noise signals at the patient's ears, as measured by two fiber optic microphones.

In the past, both passive and active attenuation have been used to mitigate MRI noise [35]. The passive attenuation usually consists either of foam insert ear plugs or ear muffs. Under normal circumstances these systems can provide 20-30 dB of attenuation. Commonly these hearing protection devices are combined with a pneumatic-driven system carrying sound to the patient's ears via plastic tubes (similar to the type of headset once commonly used on commercial aircraft). The pneumatic sound system allows the operator to give verbal instructions to the patient or play music, but probably somewhat reduced the passive attenuation of the hearing protection devices. Recently, a noise-attenuating headset has been developed by *Ziarati et al.* that uses shielded non-magnetic (piezoelectric) electro-acoustic transducers to generate an audio signal inside the MRI without the considerable delays inherent in pneumatic headphones (as sound propagates from the driver unit into the MRI magnet bore through a tube) [36].

At least two active MRI attenuation noise cancellation systems have been implemented, and an additional system is described. *Goldman, Grossman*, and *Friedlander* [37] developed a system using a standard pneumatic headset system in which polyethylene

tubes carry an acoustic signal from a pneumatic driver unit outside the MRI system to a pair of earmuffs worn by the patient. The pneumatic headset was modified with two additional polyethylene tubes that carried the sound signal inside the earmuff away from the headset to a pair of electret microphones located inside the MRI room. The electret microphones were connected to an electro-optical transducer which carried the earmuff noise signal to the shielded control room via fiber optic cables. Apparently the system consisted only of a "compensation amplifier" that produced an anti-noise signal by filtering the noise signal measured by the microphones and playing this signal back through the pneumatic headphones. *Goldman et al.* reported an average attenuation of 11.1 dB from this system, which is very impressive.

However, there are a number of issues with this MRI system that remain unresolved. The first involves the frequency spectrum where the noise was cancelled. The system apparently was only effective at low frequencies (from 40 Hz to 500 Hz), where *Goldman* reported finding the majority of the energy from the scan. This is inconsistent with our own measurements of imager noise (and those reported by *Ravicz et al.*) which indicate that most of the MRI noise occurs around 1kHz. In fact, our own calculations found that, in a T_1 pre-scan, 95% of the acoustic power in the noise signal was in the range from 840 Hz- 1920 Hz. Thus it does not appear that this MRI system would be capable of attenuating the MRI scans we measured by 10 dBA. The second unresolved issue with the system is the handling of the large time delays between the acoustic noise signal and its measurement by the electret microphones, and between the generation of the acoustic anti-noise signal by the compensation and its arrival at the listener's ear. Both the measurement and production of sound in the system are limited by the propagation speed of sound. The signal at the patient's ear must travel down the tube before reaching the electret microphones, a distance of at least 5 ft and a delay of at least 5 ms, and the anti-noise signal must travel back down the tube before reaching the listener's ears, at distance of perhaps 20 ft and a delay of 20 ms. Thus there is a built in delay in the control loop of this system of at least 20 ms, or 10 periods of a 500 Hz signal. *Goldman et al.* do not explain how their noise canceling system works or how they compensated for such a long delay in the control loop, which would compromise most

traditional noise canceling algorithms such as the LMS algorithm. Finally, very little information is given about how the attenuation performance of the system was measured. It is not clear over what time period the attenuation was measured, and how the sound levels were weighted over time. In summary, it is difficult to determine many details about the operation of the noise cancellation system developed by *Goldman* and colleagues.

Pla, Summerfeldt, and *Heddeen* [38] reported an active MRI noise cancellation system in considerably greater detail than the description *Goldman et al.* provided about their system. The 1995 system uses non-magnetic microphones located at fixed locations inside the magnet bore to record the error signal, and non-magnetic piezoceramic loudspeakers located at fixed locations to generate the noise cancellation signal. Thus, the 1995 system cancels the MRI noise signal at fixed locations inside the MRI, rather than at the locations of the patient's ears. The system uses a two-stage adaptive processing algorithm to generate the noise cancellation signal. The first stage performs a real-time system identification on the transfer function from each noise cancellation speaker to each error microphone. The output of this system is used as the error path model in a Filtered-X LMS algorithm that adapts to the optimal linear combination of the input signal from a reference microphone located near the gradient coils, but away from the piezoceramic noise-canceling loudspeakers. (The Filtered-X LMS algorithm is discussed in more detail below.) *Pla et al.* report that the system is capable of reducing acoustic noise by 15-25 dB in fast-scan sequences and by up to 10 dB in slower "impulsive" scan sequences. However, it should be noted that this cancellation occurs at the location of the error microphones, and not necessarily at the location of the patients' ears. Consequently, the actual noise attenuation experienced by the patient may be substantially lower. *Shimode et al.* describe an active noise cancellation system similar in structure to the one described by *Pla et al.*, but also incorporating some features of the system described by *Goldman et al.* [39].

Like the *Pla* system, the *Shimode* system is a feed-forward system in which a reference signal is processed to generate an anti-noise signal played by an electro-acoustic

transducer to cancel the MRI noise at the location of error microphones placed inside the MRI near the patient's head. The cancellation sound is generated by a loudspeaker located outside the magnet bore and transmitted to the patient's ears through tubes (i.e., a standard pneumatic headset as described by *Goldman et al.*). Two alternative means are suggested for measuring the error signal-placing non-magnetic (capacitance type) microphones inside the magnet bore near the patient's head (as described by *Pla*), or running pneumatic tubes from the headset to microphones located outside the magnet bore (as described by *Shimode*). Two methods are also suggested for measuring the reference noise signal: a microphone placed near the gradient coils (as described by *Pla*) or direct access to the electrical currents (pulse codes) driving the gradient magnet coils. The current signals for the x, y, and z axes are passed through waveform filters representing the transfer characteristic from the gradient magnet coils to the acoustic noise signal, and the three resulting signals are combined and used as the reference signal in a traditional LMS algorithm similar to the one described by *Pla*.

The direct use of the current signals to derive the reference signal for the noise cancellation algorithm is the most substantial improvement of the *Shimode* system. Since the acoustic noise results directly from the pulse code currents, which are controlled precisely for each type of scan, the acoustic noise for a given scan can be predicted accurately from the pulse codes. Furthermore, since the pulse codes are controlled by software in the MRI scanner, it is possible to determine the exact pulse codes being sent to the scanner well before the codes are actually sent. Thus by using the pulse codes it is possible to predict the acoustic noise generated by the MRI *before* the noise is actually created. This is a tremendous advantage in the active cancellation of MRI noise for two reasons. First, it allows the noise cancellation system to construct a nearly perfect inverse noise waveform a priori without exposure to the current noise generated by the MRI. Traditional noise cancellation algorithms require the noise canceling system to listen to the noise and adaptively seek the transformation of the current noise that provides the best cancellation. The system is reactive and must wait until the characteristics of the noise change before starting to adapt to the new noise. Thus, each time the noise changes, a traditional adaptive noise cancellation (ANC) system will cease canceling the

noise effectively until the algorithm has time to adapt to the change. In contrast, an active noise cancellation system that uses a priori information from the pulse code sequence can generate a noise cancellation signal before the noise signal is measured by the system and does not have to adapt to changes in the signal. Thus the ANC system using information from the pulse code is always acting at maximum efficiency and does not suffer from "down time" while adapting to changes in the noise characteristics.

The second major advantage of using the pulse code sequence to create the inverse noise waveform is that it overcomes the problems associated with the propagation time from the pneumatic headphone driver located outside the MRI machine to the pneumatic headphones worn by the patient. In a typical MRI installation, the headphone tube is 8-10-feet-long, corresponding to a 10-ms delay from the time the inverse acoustic noise is generated at the driver unit to the time the sound reaches the patient's ears. This 10-ms delay reduces the convergence rate and compromises the stability of any adaptive algorithm processing the signal at the listener's ears because the system must wait 10 ms after the noise cancellation signal is changed to evaluate the consequences of the change on cancellation performance. It also makes it almost impossible to cancel impulsive noise with a traditional noise cancellation algorithm because the noise cancellation signal cannot be produced until the impulsive noise arrives at the reference microphone, and the delay from the reference microphone to the patient's ears is shorter than the propagation time for the sound through the tubes. The use of a non-magnetic driver inside the magnet alleviates this problem, but requires the presence of conductive material inside the magnet bore. However, having access to the pulse code currents before they are sent to the magnet allows the cancellation signal to be generated in advance so it reaches the patient's ears at the same time as the acoustic noise.

The present device was similar in overall structure to the *Shimode* algorithm, but incorporated a new method of measuring the error signal inside the magnet bore without the use of conductive material, and incorporates information from the radio frequency (RF) signal in addition to the x, y, and z gradient pulses. Like the *Pla* and *Shimode*

system, the present system uses the Filtered-X LMS algorithm. This algorithm is described in detail in the methods.

3.11 Distributed Neuroscience Database Project

Current medical record-keeping at WKNI did not provide a way for doctors and researchers to electronically gather specific research information. The creation of a research database application has provided a way to store data efficiently and retrieve common data quickly. Incorporated in the design are search and statistical reporting capabilities to further assist in the analysis of research data.

The Epilepsy Center at WKNI has grown tremendously in the past few years. We have designed a computer patient database for the clinical and research epilepsy center. All important patient demographics will be at the physician's fingertips (name, address, age, medications, allergies, special notes, insurance, family doctor, and more). Availability of this database will allow our physicians and researchers to better access their patient data and for future retrospective analysis.

3.12 Internet Browser-Based Imaging Access

Traditional modes of imaging are changing. Where once imaging modalities such as MRI, CT, and radiography-rendered hardcopy films, they now give us digital images that are archived on Picture Archives and Communication systems (PACS). This new technology reduces the costs associated with producing and storing hard copy film but poses the new challenge of image distribution. When using hard copy film, the actual film could be sent to a physician's office, a nursing unit, the ER, and even into the operating room (OR). Some drawbacks to this method were the potential for film, and the fact that the films could only be in one place at a given time.

We utilized and implemented the Stentor's iSyntax^{TM} technology to deliver images instantaneously over our existing hospital network. Digital interfaces were developed to complement Stentor's technology with our imaging networks. Such technology could

provide full-resolution images in real- ɔ without compromising speed and image quality.

3.13 Functional Imaging In Tumefactant MS

Brain lesions in MS may present as solitary mass lesions located in the white-matter and gray-white junction [40]. Atypical clinical and radiographic features of large demyelinating plaques may lead to several erroneous differential diagnoses such as tumors, infection or demyelination from other causes [40, 41].

The diagnosis of MS, till recently, largely depended on the clinical course, which typically features an exacerbation and remission of multi-focal neurological deficits, electrophysiological tests, CSF analysis and imaging studies [42]. The advent of functional/ metabolic imaging modalities such as MRS [17-19, 43] and PET has revolutionized our concepts in many brain diseases, including MS.

We report an unusual case of MS presenting with subacute onset of focal neurological signs and a single, large enhancing lesion on the MRI. MRS and various PET techniques were utilized to further characterize the MS lesion

3.14 Spectroscopic Imaging Biopsy Guidance

Histological examination of a tumor specimen on a core or open biopsy is considered the gold standard for the diagnosis of brain tumors. While the non-invasive technique of MRI can direct some of the diagnostic decision-making, it has limitations and disadvantages, that can be partly overcome with the use of in vivo MRS. In vivo MRS is able to provide a specific biochemical profile on tumor tissue compared to normal tissue. We have utilized a simple model to predict the site within tumor that might possibly provide the highest yield for biopsy. Data were post-processed and delivered to the surgical suite. Surgical biopsies were obtained from locations referenced on MR images by guidance with a surgical navigation system.

3.15 High-Speed Neuroimaging in Management of Stroke

The combined application of diffusion-weighted imaging (DWI) and perfusion-weighted imaging (PWI) has significantly improved the diagnosis and management of acute cerebral infarction. Such novel MRI methods provide valuable information regarding the early ischemic changes in the first hours post-stroke. PWI provides the earliest information regarding a significant decrease in regional cerebral blood flow (CBF), the event that precedes cerebral ischemia. Indeed, if carried out during the first few hours post-stroke, PWI delineates the area of compromised CBF, which is significantly larger than the areas of actual cell death (i.e., the irreversible ischemic lesions). However, as time passes, cellular dysfunction occurs as a result of Na^+-ATP pump failure caused by a diminished CBF, which in turn causes water accumulation in the intracellular compartment. Thus, at the onset of acute cerebral ischemia, a reduction in the apparent diffusion coefficient (ADC) of water molecules is observed. ADC value is reduced due to a dramatic shift in water movement from extracellular to intracellular compartments. Such diffusion abnormalities, which can be detected by DWI as early as 90 min, reflect the formation of irreversible ischemic lesions.

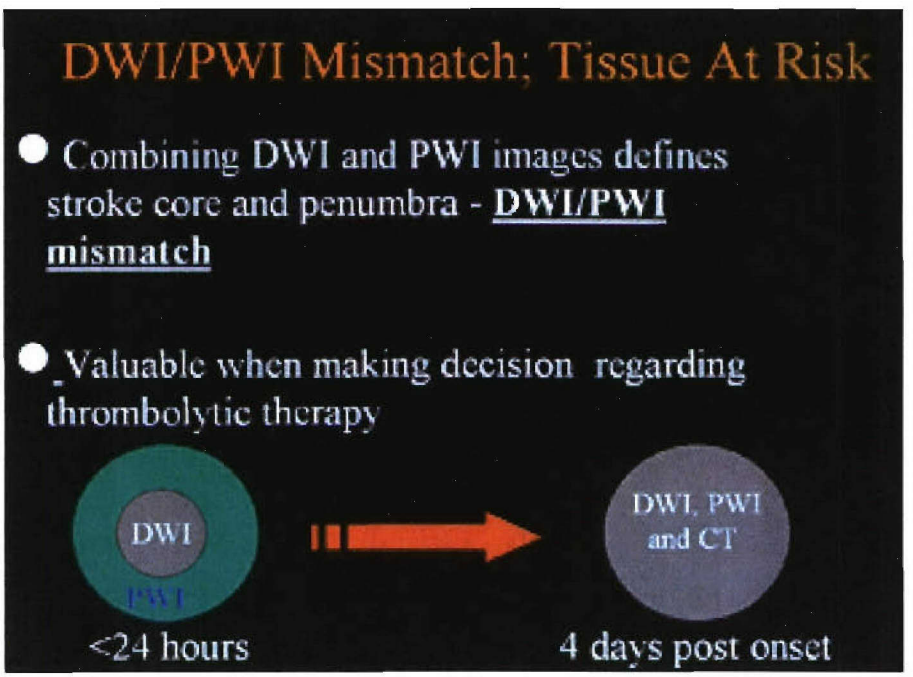

Figure 5

Data acquired from both DWI and PWI can demonstrate the core of the infarct comprising the area of irreversible damage as defined by DWI, and the penumbra, which is the surrounding area of salvageable tissue defined by the PWI. Presence of such mismatch in PWI/ DWI examination will enable clinicians to assess the presence or absence of salvageable brain tissue, as well as the risk of hemorrhage into injured tissue, and make an objective decision regarding administration of tissue plasminogen activator (rTPA), a thrombolytic therapy that can successfully reperfuse brain tissue. The main objectives of this study was that in a blinded multimode investigation: 1) we intended to examine the predictive value of DWI/PWI mismatch, estimated in hyperacute stroke ($\leq$24 post-onset of symptoms), in determination of the final infarct size (6-10 days post-onset of symptoms); and 2) we planned to examine the possible correlation between the National Institutes of Health Stroke Study (NIHSS) test score and the infarct size as a function of time.

In order to conduct and accommodate such a large-scale study, a world class CT/MRI suite was built adjacent to the ER. Indeed, we are pleased that our hyperacute MR-stroke sequences are matched only by the leading stroke research centers in the world. Unfortunately, we were challenged by our inability to recruit patients into the study. However, we were able to provide our community with the state-of-the-art stroke imaging. Work is in progress to rejuvenate our stroke study including the formation of a highly skilled stroke team who will help us educate the staff and community regarding the importance of time in management of stroke.

3.16 3-D Brain Functional Imaging Data Deliverance to Stereotactic Neuronavigational Instruments

Previous brain-imaging investigations utilizing conventional MRI studies have demonstrated various anatomical changes of a mainly atrophic and to some extent reversal in the brain of alcohol-dependent patients. However, data regarding the significance of the functional implications (i.e., cognition, memory, etc.) of such brain dysmorphology have been inconclusive. In light of the recently developed fMRI technique, it is now feasible to non-invasively obtain images of the working brain in real-

time. This technique relies on the local physiological changes that are associated with activation of the visual, motor or other brain systems. Thus, fMRI has opened the gates for the investigators to perform repeated measurements of the brain function in correlation with the underlying anatomy and cognitive processes in the same person.

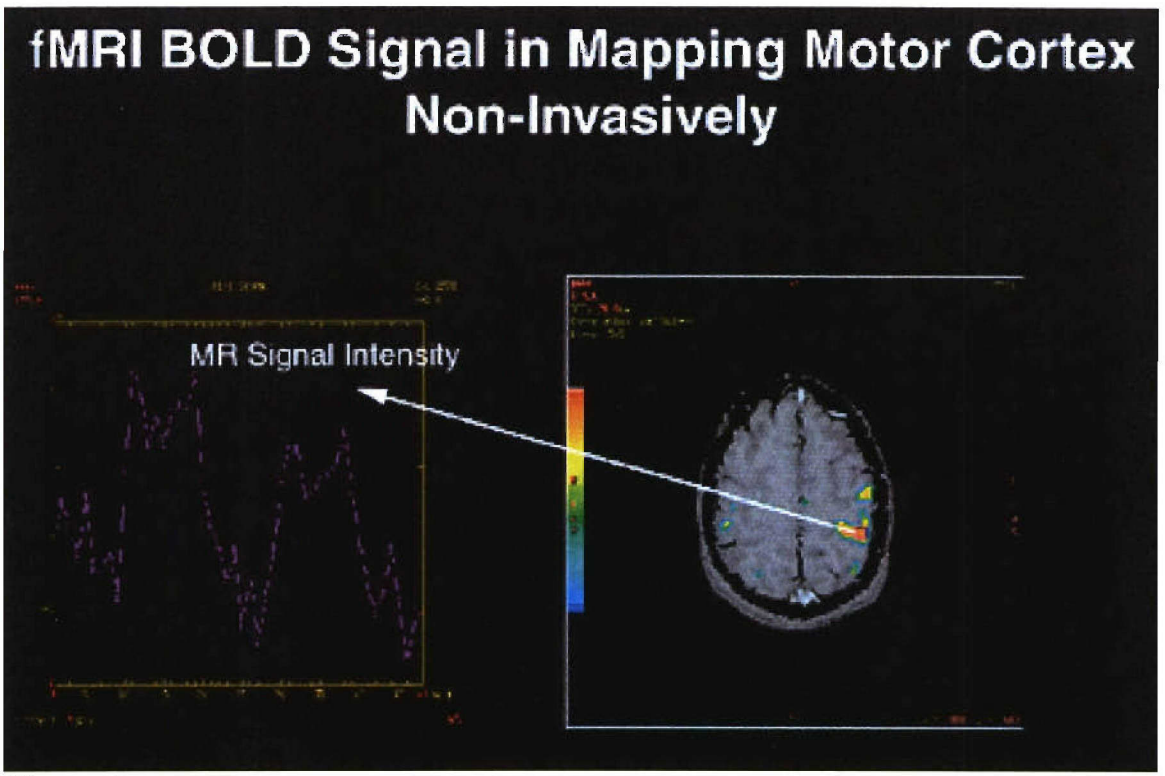

Figure 6

Herein we describe the utility of fMRI data for surgical guidance and visualization systems. We have defined the motor strip on fMRI data and fused them with anatomical data from various preoperative scans T_1W and T_2W MRI. We have further post-processed these data for segmentation to generate 3-D surface models of key anatomical and functional structures. Work is in progress to provide our neurosurgeons with speech and language functional maps.

4.0 Methods and Procedures

4.1 In Vivo Characterization of Human Brain Tumors by MRS

Retrospectively, we have been collecting data from patients with suspected brain neoplasms or recurrent neoplasia referred for MRS. Control spectra from healthy adult volunteers were also included in this database and a PR model has been developed. The possible methods for development of a PR model are described herein: the first tested PR model involves unsupervised learning methods such principal component analysis (PCA), ANN (neural networks) and cluster analysis. These methods assume no preexisting group structure (tumors types in our case) but try to suggest such structure based on its own analysis. We have further evaluated our results using supervised learning methods. These methods are based on the existence of a group structure (tumors types) on one hand and the existence of a pre-assigned set of cases (tumors type already known) and a new set for which an assignment is required (into one of the predefined tumor types).

The second PR model has been employed in our studies, since our group structure is already known and we have a pre-assigned set. The first PR model might suggest a group structure that does match with medical definitions. Data were input to our model after preprocessing; preprocessing is the transformation from the free induction decay (FID) to the sample vector. The choice of preprocessing method and the dynamic range of MR data determine which classification method can be chosen.

Preprocessing of data involved transformation of the FID, phasing and baseline correction. Concentration can be evaluated by area integration to form a vector in form: V=[c1,c2,..., cn].

This method suffers from operator bias in picking resonance of interest, correct phase and baseline, adequate determination of the area, and overlapping resonance.

A supervised learning PR method began by an optional phase which is the discriminatary analysis (DA). Basically, the DA (also called feature extraction) role is to select spectral features that have a high potency to separate the different tumor types. Examples of such

analysis include Lineare discriminatory analysis (LDA), PCA and optimum discriminatory vector (ODV). We are aware of the availability of at least LDA in statistical packages such as SPSS and STATS.

Our next phase of our PR method will involve estimating the sensitivity and specificity of our predictions with those of qualitative blinded interpretations from two readers (board-certified neuroradiologists), qualitative unblinded interpretations of a spectroscopist, and a quantitative Cho/NAA amplitude ratio > 1 threshold for tumor. Participants were from the KMC patient population and recruited volunteers. In addition to participants being scanned, a sub-study to incorporate retrospective data was conducted. Data was obtained from the KMC Radiology Department records, KMC pathology results, Gamma Knife patient medical record files and referring physician's files (when necessary). Patient data was entered into a computer database designed by WKNI. A large database was constructed of MR spectra from patients about whom data was compiled and analyzed.

4.2 Choline Metabolism in Human Brain Tumors with ^{11}C-PET and ^{1}H-CSI

The subject of the study was a 57-year-old female patient suffering with astrocytoma (World Health Organization; WHO grade III). A portion of this brain tumor was extirpated and processed for in vitro MRS analyses. Aqueous and lipid extracts of brain sample were prepared by dual-phase extraction [44]. High-resolution proton-decoupled ^{31}P, and ^{1}H on the brain extract samples were acquired at 145.8 and 360 MHz, respectively. In vivo MRI/MRS data were obtained using WKNI GE Signa instrument equipped with ProbeSI package.

PET studies were carried out on a high-resolution Siemens EXACT HR+ scanner (in-plane FWHM =4.6 mm, axial FWHM = 3.5 mm, axial field of view (FOV) = 15.52 cm). Dynamic ^{11}C-labeled choline study was accomplished post 20mCi of labeled choline.

4.3 Choline PL Metabolism in Human Brain Tumor Cell Lines

Preliminary data were generated using a rat model in order to develop the kinetic model for use in brain cell lines.

Rats were infused with an equimolar solution of ^{13}C-labeled choline for 0, 15, 30, 45 and 60 min (n = 4 to 5 at each time point). After infusion, livers were surgically exposed and freeze-clamped. Chemical extracts of the tissues were prepared using a dual-phase extraction procedure [44]. High-resolution proton-decoupled ^{31}P and ^{13}C spectra on the extract samples were acquired at 8.5T, respectively. MR spectral intensities from aqueous and lipid extracts yielded metabolite concentrations, and an assessment of the ^{13}C-enrichment of the metabolite pools. All data were considered statistically significant at the 95% confidence level. Kinetic models were coded using a numerical integration package, Advanced Computing Simulation Language. The blood plasma choline was assumed to be 100% ^{13}C-labeled at the appropriate carbon positions, and these metabolite pools are inexhaustible.

4.4 CSI of Human CN

A 17-year-old male presented to the ER with a one-week history of severe headache, nausea and left upper extremity weakness. He denied any vomiting, or history of head trauma. The biopsy result indicated sections of numerous cauterized and some well-preserved fragments of a moderately to markedly cellular neoplasm composed of relatively round to oval cells with oval nuclei and minimal cytoplasm, dispersed within a fibrillary background. Most of the tumor was arranged in varying-sized nests separated by delicate fibrillarity and arborizing capillary-like blood vessels. Areas of hypercellularity with zones of necrosis, nuclear anaplasia and mitoses were evident. In latter areas, microvascular proliferation was identified. Extensive areas of calcification were seen (***Figure 7***). The overall histologic features were consistent with a CN, corresponding to WHO grade II. Immunoperoxidase stain for neuron-specific enolase (NSE) indicated positivity of the well-preserved tumor cells (***Figure 8***). Immunoperoxidase stain for glial fibrillary acidic protein (GFAP) was negative except for the background fibrillarity. In addition, the presence of anaplastic nuclear features accompanied by mitoses, vascular proliferation, and areas of necrosis suggest that this tumor may have potential aggressive growth and/or local recurrence.

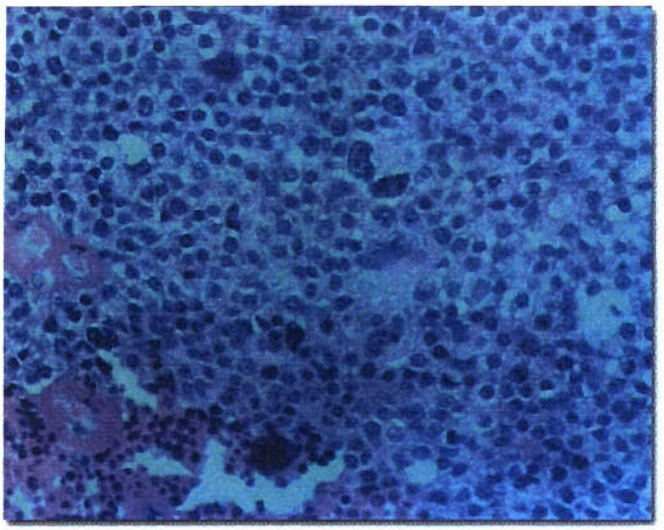

Figure 7. CN. *Figure depicts selectively uniform cells with moderate nuclear plimorphian within a fibrillary background. Prominent areas of necrosis are seen.*

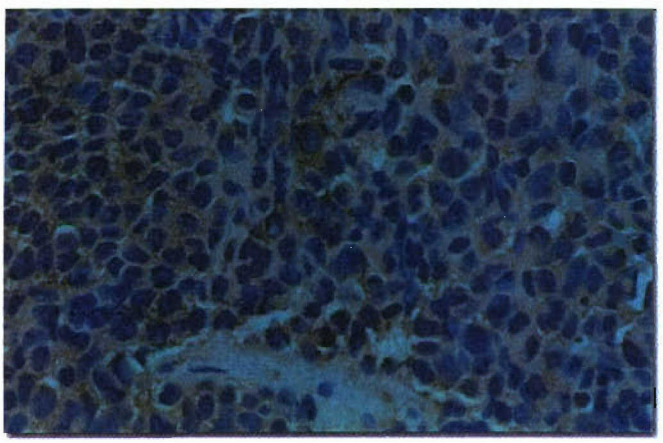

Figure 8. CN Stain-NSE. *Figure depicts strong positive membraneous and cytoplasmic NSE staining in tumor cells. A fibrillary background.*

A portion of this brain tumor was extirpated and processed for in vitro MRS analyses. Aqueous and lipid extracts of brain sample were prepared by dual-phase extraction. High-resolution proton-decoupled ^{31}P and ^{1}H on the brain extract samples were acquired.

The extraction and data acquisition method has been described previously [45]. In vitro MRS data were processed using standard method of apodization, Fourier transformation, and baseline flattening.

MRI/MRS data were obtained using a WKNI MR instrument acquired via cooperative agreement with the USAF. Before the acquisition of any MR spectra, a targeting MR volume was acquired in order to localize the VOI for subsequent CSI. The VOI was selected from the high-intensity signal from gadolinium on T_1W MRI prior to the MRS exam. A large region of interest (ROI), which included tumor as well as remote normal-appearing brain tissue, was defined for selective excitation. These were aligned parallel to the transverse MRI scout slices (in axial plane) and spectra were obtained using a PRESS pulse sequence for volume selection. Water was suppressed by selective excitation. The voxel sizes were chosen to reflect the amount of homogenous abnormal tissue within the voxel. Two sets of CSI data (normal and the lesion site) were acquired using PRESS sequence (TE/TR, 288/1500), FOV 24×24 mm^2; 16×16 phase encoding steps, 10-mm slice thickens; and 2 signal averages per phase encoding step, resulting in a nominal voxel volume of 2.25 cm^3 (1.5×1.5×1 cm^3).

4.5 PL Changes in Hippocampus of Epileptics

4.5.1 Immunohistochemical Studies

4.5.1.1 Monoclonal Antibody against PL

Monoclonal antibody 3sb is an IgM, reacts in enzyme-linked immunosorbent assays (ELISAs) against the negatively charged PL phosphatidic acid, phosphatidylinositol, and phosphatidylglycerol, and does not react with phosphatidylethanolamine (PE) or phosphatidylcholine [46]. This antibody has been tested against two other mouse IgM aPL antibodies. Each monoclonal antibody reacts differently in routine clinical ELISAs with cardiolipin and PS; 3sb reacts only with PS (CL-/PS+), D11A4 reacts only with cardiolipin (CL+/PS-), and BA3B5C4 reacts with both cardiolipin and PS (CL+/PS+). The cofactor dependence of the monoclonals is currently under investigation. Preliminary investigations suggest that 3SB also reacts with PE in a cofactor-dependent manner. IgM concentrations in undiluted tissue culture supernatant were 80 μg/ml.

4.5.1.2 Control Antibodies

Positive control antibodies included purified immunoglobulin fraction of rabbit antisera against NSE (specific for gamma subunits of the enolase of neuronal origin and not for alpha subunits of glial origin), myelin basic protein (MBP; specific for myelin of white matter and to a lesser degree in grey matter), GFAP (primarily specific for astrocytes), and S-100 protein (reactive with both glial and neuronal cells) (Zymed Laboratories Inc.; South San Francisco CA). HB8512, a monoclonal mouse IgM against bacterial peptidoglycan (ATCC; Rockville, MD), served as a class-matched negative control for the aPL antibodies.

4.5.1.3 Control Tissue

Control tissue was normal human hippocampus provided by the Harvard Brain Bank both formalin-fixed and frozen sections.

4.5.1.4 Preparation of Human Hippocampus

Pathologic hippocampal tissue was obtained from surgical excisions of hippocampectomies of epileptic patients. The tissue is provided directly by the neurosurgeon who segregated that needed for the pathological study from that available for research. Tissue was bisected: ½ for immunohistological studies, the other ½ for nuclear magnetic resonance (NMR) spectroscopic analysis. The NMR tissue was placed in a dewar of liquid nitrogen as rapidly as possible, preferably in the OR. Immunohistochemical study tissue was placed in 4% paraformaldehyde in phosphate buffer.

4.5.1.5 Paraffin-Embedded Tissue

The tissues were dehydrated and paraffin-embedded using a Fisher Histo-processor. Sections (5-7 μm) were cut and dried onto positively charged slides for 18 h at 42° C. Sections were de-paraffinized by immersion in xylene, and rehydrated through a series of graded alcohols. Endogenous peroxidase activity was quenched by immersion in 9 parts

methanol/1 part 30% hydrogen peroxide for 10 min. Sections were thoroughly washed in phosphate-buffered saline (PBS) (pH 7.3) prior to immunostaining.

4.5.1.6 Immunoperoxidase Labeling

Non-specific antibody binding was blocked by incubation for 10 min in 10% non-immune goat serum. Monoclonal aPLs were diluted to 15 μg/ml in PBS and added to sections following removal of the blocking solution. Sections were incubated for 1 h at room temperature in a moist chamber. Slides were rinsed for 2 min in flowing PBS and by immersion in PBS for 2 min (×2). Peroxidase-conjugated anti-mouse IgM (Histostain-SP Kit, Zymed Inc.) were placed on each section and incubated for 30 min at room temperature. Parallel sections were treated with positive control rabbit antibodies and biotinylated goat anti-rabbit immunoglobulin was added and processed as described above. After washing and a 10-min incubation with avidin-peroxidase conjugate, control slides were rinsed in PBS. All slides were incubated for 5 to 15 min with aminoethyl carbazole substrate-chromogen reagent, rinsed well with DDH_2O, and mounted with glycerol-polyvinyl alcohol aqueous mounting solution and a cover slip. Sections were evaluated by light microscopy.

4.6 MRS Studies

4.6.1 In Vivo MRI and MRS at Department of Radiology, KMC

All subjects included in the study were undergoing a comprehensive MRI and MRS examination prior to their surgery. MR data was obtained with a standard quadrature head coil on a GE Signa Horizon *NVi* (Milwaukee, Wisconsin) operating at 1.5 Tesla. To reduce motion artifacts, patients were instructed to avoid head motion during the scanning intervals. The MRI acquisition protocol included our standard *Head* protocol and hippocampi volumetric sequence. Our standard head protocol consists of T_1W, T_2W and proton-density weighted (PDW). Sagittal T_1W images were obtained (TE = 30 ms, TR = 400) following simultaneous acquisition of axial and coronal T_2W and PDW images (TR = 2800, TE = 17 and 85, respectively), for the same section using an asymmetrical multiple-echo sequence. The slice thickness for all scans was 5 mm with

1.5-mm gap successive sections for all slices. All images were obtained using 512 ×224 matrix and 22-cm FOV.

The MR acquisition protocol for volumetric measurements consisted of a scout sequence to ensure proper position of the subject's head (9 sec). A fast 3-D SPGR sequence was then used for the volumetric assessment of the hippocampus. Contiguous coronal images in a plane perpendicular to the long axis of the hippocampus were obtained using a fast 3-D-SPGR sequence. The sequence parameters were as follows: TR 6.5 msec, TE 1.6 msec, TI 500, flip angle 60, 256×224 image matrix, FOV 24 cm, 2 acquisition, 1.5-mm slice thickness. An inversion recovery pulse sequence was selected to maximize the gray-white contrast and allow accurate definition of anatomical structures. MRS sequences included a single-voxel spectroscopy using STEAM sequence (TE/TR, 35/1500) in the temporal lobe region followed by 2-D CSI of the same region. The entire imaging time including the scout sequence was less than 30 min. The MRI study, however, was repeated if the image quality was poor due to patient motion during imaging.

4.6.2 In Vitro MRS

4.6.2.1 Tissue Preparation

A portion of pathological and normal brain tissue was processed for in vitro MRS analyses. Aqueous and lipid extracts of brain samples were prepared using a dual-phase extraction procedure described by *Tyagi et al.* with some modification to accommodate brain tissue samples as opposed to cell cultures. Briefly, brain tissues were crudely homogenized under liquid N_2 and then further homogenized by stepwise addition of cold solvents using a glass tissue grinder with a Teflon pestle. The final solvent composition was MeOH:$CHCl_3$:H_2O (1:1:1: v/v/v/; 10.5 mL/g brain). The homogenate was then centrifuged to allow separation into two liquids phases and pellet. The supernatant was transferred to a separatory funnel to allow complete separation of the two phases. The lower phase contains lipids, and the upper phase contains all water-soluble brain metabolites. The lipid extracts were then dried under a stream of N_2, and reconstituted for high-resolution MRS analyses in a solution of $CDCL_3$, D_2O and MeOH with Cs_2 (EDTA) as described previously [44]. The remaining supernatant sample (i.e., aqueous

portion) was lyophilized to dryness. The dried samples were reconstituted in 2 ml of 10 mM EDTA in H_2O:D_2O (5:1 v/v) for MR analyses.

4.6.2.2 High-Resolution MRS

We performed high-resolution proton-decoupled ^{31}P, ^{13}C, and ^{1}H on all brain extract samples. ^{31}P, ^{13}C, and ^{1}H MR spectra were acquired at 145.8, 90.6 and 360 MHz, respectively, using a Bruker AM 360 NMR spectrometer (8.5 T) equipped with a 10-mm broadband probe. The sample temperature was regulated at 293 K for lipid extracts and 298 K for aqueous samples. The lower temperature used for lipid samples helped minimize evaporation of the volatile solvents and improve ^{31}P spectral resolution as demonstrated previously [45]. MRS in vitro acquisition parameters were similar to a previously reported study published by the investigators of this study [44].

As previously stated, in vitro MRS data was processed using standard method of apodization, Fourier transformation, and baseline flattening. Spectral assignments were determined from literature reports and by spiking extract samples with known compounds.

4.6.3 Comparative Analysis of CT and FLAIR for the Detection of Hemorrhage

This study was retrospectively designed, using readily available patient data. At the present time, we have found four patients with active intracranial hemorrhage and 13 patients without intracranial hemorrhage (both defined by CT) to used as study controls. All of the above patients have had a CT scan and MR FLAIR within 30 h of one another. CT and MR FLAIR images of all patients were obtained and presented to three board-certified neuroradiologists for examination. Examiners were blinded to the identity and case history of each patient, and were asked to record their interpretation of each film on a pre-designed worksheet.

4.6.4 Hippocampal Volumetric Measurements

4.6.4.1 Phase 1

4.6.4.1.1 Subjects

Six healthy volunteers, three males and three females, between the ages of 20-45 years were recruited from KMC hospital staff or the local university. After signing an informed consent form approved by KMC Institutional Review Board and completing a safety screening questionnaire, each volunteer was scanned using our newly acquired MRI-*NVi* twice within a two-week time period. The scans were done on the same scanner utilizing the same exact imaging parameters. These sets of two scans were compared to identify scan-to-scan variation.

4.6.4.1.2 Exclusion Criteria

Subjects were not able to participate in the study based on exclusion criteria that were determined based upon the possible impact on the size of the hippocampus and also successful completion of MR exam. The criteria includes the following: 1) depression; 2) dementia; 3) history of drug and alcohol abuse; 4) neurological disorder including history of ischemic stroke, transient ischemic attack (TIA), epilepsy, Parkinson disease or major physical illness (e.g., carcinoma, insulin-dependent diabetes mellitus); and 5) conditions that would preclude the completion of a MRI exam such as claustrophobia, pacemaker or metal objects in body.

4.6.4.1.3 MR Protocol

MR images were obtained with a standard quadrature head coil on a GE Signa A fast 3-D SPGR sequence was then used for the volumetric assessment of the hippocampus. Contiguous coronal images in a plane perpendicular to the long axis of the hippocampus were obtained using a fast 3-D-SPGR sequence. The sequence parameters was the followings: TR 6.5 msec, TE 1.6 msec, TI 500, flip angle 60, 256×224 image matrix, FOV 24 cm, 2 acquisition, 1.5-mm slice thickness. An inversion recovery pulse sequence was selected to maximize the gray-white contrast and allow accurate definition of anatomical structures. The entire imaging time including the scout sequence was less than 5 min. The MRI study was, however, repeated if the image quality was poor due to patient motion during imaging.

4.6.4.1.4 Phantom

Absolute accuracy of our volumetric measurements was obtained using a spherical phantom as described elsewhere [29]. Briefly, a 17-cm diameter sphere was filled with water and treated with sufficient gadolinium (gd)-based contrast agent for adjusting the relaxation time of the protons (0.01ml of gd/50ml of saline solution). The volume of sphere, as determined by a graduate cylinder, served as the absolute reference volume. The imaging protocol was the same as the one used for human brain imaging. Selecting a global threshold to generate a sharp border between the phantom and background allowed an accurate and reproducible measurement of phantom volume. Thresholding was adjusted according to an American College of Radiology (ACR)-defined method , currently being used routinely in our MR department. The exact volume of the phantom via MR data was determined according to the method described below. Phantom was scanned five times to measure the reproducibility of our measurements. Additionally, we assessed the volume of the sphere by measuring the length of four distances present in each of the three plane images of the phantom. The phantom was filled entirely with solution of gd and saline.

4.6.4.1.5 Hippocampal Volumetric Measurements

The image visualization and analysis procedure was conducted at the image-processing laboratory of the Department of Radiology at KMC. First, data processing was conducted on a Silicon Graphics O_2 workstation operating at 300 MHz and utilizing Vitrea™ software version 1.2 package (Vital Images). Data was transferred to a separate workstation (Ultra-SPARC-2, Sun Microsystems) for comparative analysis using a commercially available 3-D display and measurement software, AWW version 3.0 (GE Medical Systems; Milwaukee, Wisconsin). The volumetric approach for both sofwares involved manual outlining and tracing of the ROI on coronal images. The hippocampal structure was outlined manually in AWW software using the mouse-driven painting function. Hippocampal volumes were measured independently by two observers and were reported as cm^3 (mean ± SD). Each observer made the measurements on two separate occasions for each subject's right and left hippocampi. The intra-observer performance was assessed as well. *Watson et al.* described hippocampal boundries [29].

For hippocampal volumetric measurements, the hippocamus proper, denate gyrus, fimbria, subiculum, intralimbic gyrus, and uncinate gyrus were included. The outlining of the hippocampus always proceeded from anterior to posterior. After delineating the hippocampus in the coronal projection, the volume was calculated automatically by the computer programs. To increase the specificity of our measurements, a cut-off value of 0.9, which is 3 SD of variation in pixels signal intensities of structure, was selected for volumetric measurements using AWW. Leveling the window appropriately to delineate the hippocampal structure from the surrounding gray/white and CSF is sufficient in determining the pixels relative signal intensities using Vitrea™.

4.6.4.1.6 Statistical Analysis

Intra- and inter-observer assessment was reported by calculating the mean and standard deviation. The results were reported as percentage of deviations. Error may arise from incorrectly outlining the ROI. Variations among the observers were assessed by an unpaired *t*-test. Those results were considered statistically significant at $p > 0.5$.

4.6.4.2 Phase 2

Five healthy volunteers (mean age = 28 yrs, three female and two male) were scanned twice within a two-week time period. The MR images were acquired on a 1.5 T GE *NVi* scanner. The MR acquisition protocol included thin sagital T_1W slices for measuring the angle of long axis of hippocampi, followed by contiguous oblique images (1.5-mm thickness) in a plane perpendicular to the long axis of the hippocampi using a fast 3-D SPGR-IR prepped sequence. The acquisition parameters are depicted in **Table 1.**

Table 1. MR parameters of appropriate pulse sequences

MR Parameters	**Scout Sequence**	**Fast SPGR-IR Prepped**
Plane	Sagital	Coronal-oblique
TR	100	6.4
TE	1.8	1.5
Inversion Time	NA	500
Flip Angle	20	20
Number of Excitation	1	1
FOV	24×24	24×24
Slice Thickness	5 mm	1.5 mm
Image Matrix	256×160	256×224
Total Acquisition Time	17 sec	2:38 min

We examined several inversion recovery times (T_I = 0-1000 msec), and determined that T_I of 500 ms produced a good contrast between white/gray matter and CSF for hippocampal delineation without compromising significant image acquisition time.

Data processing was initially conducted utilizing Vitrea™ versus 1.2 (Vital Images). Data were then transferred to a separate workstation for comparative analysis using the widely accepted 3-D display and measurement software, AWW version 3. We have only measured the volume of the right hippocampus. The outlining of the hippocampus always proceeded from anterior to posterior in coronal plane and the boundaries of hippocampus were delineated as described by *Watson et al.* [25]. After delineating the hippocampus in coronal section, the volume was calculated automatically by both computer programs.

Additionally, we assessed the absolute accuracy of our volumetric measurements by comparing our MR volumetric measurements of a phantom to its known exact volume (10 mL). The phantom was filled by using a graduate cylinder and served as the absolute

reference volume. MR data for the phantom were also processed using both image-processing softwares. The imaging protocol was the same as the one used for human brain imaging. The phantom was scanned five times to measure the reproducibility of our measurements.

4.6.4.3 Phase 3

This study was designed retrospectively using available patient data and is presently ongoing. All data utilized came from the medical records of the Radiology, EEG and Pathology Departments at KMC. We are attempting to find approximately 10 patients with clinically diagnosed hippocampal sclerosis (i.e., based on the volumetric analysis and EEG recordings) and 10 corresponding normal controls. If available, the pathological data of patients' post-hippocampal resection is also obtained. All MR images interpreted by the radiologists and for the purpose of volumetric analyses were acquired with the Radiology Department's temporal lobe protocol.

The MR images of all patients and normal controls were obtained and presented to several board-certified neuroradiologists for examination. The examiners are blinded to the identity and case history of each patient, and are asked to record their interpretation of each study. Data is entered into a computer database designed by the WKNI, along with pertinent medical history and case information. To preserve patient confidentiality, this database remains in a password-protected computer, and is only accessible by individuals directly involved in this research project.

MR images used for this study must have been obtained with a temporal lobe coil on a GE Signa Horizon *NVi* operating at 1.5 Tesla. The MR acquisition protocol for temporal lobe imaging consists of a scout sequence to ensure proper position of the subject's head (9 sec). A FSE-IR sequence is then used for the high-resolution imaging of the hippocampus. Contiguous coronal images in a plane perpendicular to the long axis of the hippocampus are obtained using a FSE-IR sequence. The sequence parameters are the followings: TR 6.5 msec, TE 1.6 msec, TI 500, flip angle 60, 256×224 image matrix, FOV 24 cm, 2 acquisition, 1.5mm slice thickness. An inversion recovery pulse sequence

was selected to maximize the gray-white contrast and allow accurate definition of anatomical structures.

The image visualization and analysis procedure is conducted at the image-processing laboratory of the department of radiology at KMC. First, data processing is conducted on a Windows NT workstation operating at 300 MHz and utilizing Vitrea™ software version 2.0 package (Vital Images). The volumetric approach involves manual outlining and tracing of the ROI on coronal images. Hippocampal volumes are reported as cm^3 (mean ± SD). After delineating the hippocampus in the coronal projection, the volume will be calculated automatically by the computer programs.

4.6.4.3.1 Statistical Analysis

Inter-observer assessment of radiological interpretations was reported by calculating the mean and standard deviation. The results were reported as a percentage of deviations. The variations among the observers were assessed by an unpaired *t*-test. Those results were considered statistically significant at $p > 0.5$.

4.6.5 Alleviating Claustrophobia with 3-D Audio Display

A within-subject design was used to access the anxiety of 10 undergraduate university subjects (previously identified as having a tendency toward claustrophobia) while in a mock-up MRI scanner, with and without the presentation of a VE. The mock-up MRI machine was constructed to appear similar to a real MRI, except that the sliding gurney and 59-cm diameter tube were at floor-level rather than waist-level. Speakers housed outside the tube presented realistic magnet noise during the experimental procedures. In the non-VE condition, the subject merely laid in the MRI enclosure for 20 min. In the VE condition, the subject laid in the enclosure for 20 min, but viewed and listened to a VE which consisted of five collaborators playing a game of Pictionary* (Hasbro) in a spacious room. The drawing surface was projected on the ceiling and digitally recorded from the perspective of someone lying on the floor (i.e., the position of the subject in the mock-up MRI). Similarly, spatialized virtual audio was recorded by microphones within the ear canals of a Knowles Electronic Manikin for Acoustic Research (KEMAR), which

was positioned next to the digital camera, so as to align the visual and auditory scenes. The game was planned to incorporate activity within the room in order to enhance both the audio and visual simulations. The VE was presented to subjects within the MRI enclosure over a head-mounted display (HMD) and headphones. A number of dependent measures were collected before, during, and after each 20-min exposure to the mock-up MRI. These included physiological (pulse rate, blood oxygen saturation level, and skin conductance) and subjective (Endler Multidimensional Anxiety Scales (EMAS), subjective ratings of comfort and coping ability) measures of anxiety and discomfort. Initial baseline EMAS state and physiological measures were taken before the subject was placed in the MRI enclosure. Physiological responses were continuously monitored during the exposure period. In addition, every 2-min during the exposure, subjects provided ratings on two 10-point Likert scales, indicating their level of emotional comfort and their ability to cope with the situation. Additional EMAS state measurements were taken after each exposure. Each subject participated in two 20-min exposures, one from each condition (VE and non-VE), separated by a 5-min break. The order of conditions was counterbalanced across subjects (***Figures 9-11***).

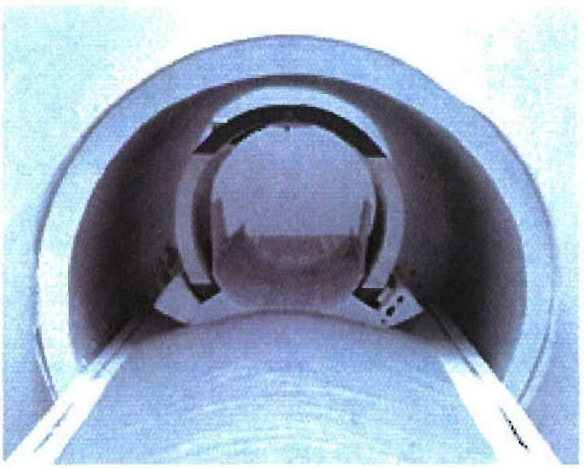

Figure 9. Mockup MRI enclosure demonstrating the size of the tube. *Subjects will lie on the platform (seen in the foreground) that slides in and out of the enclosure on raised rails.*

Figure 10. MRI mockup fully assembled and prepared for running subjects. *Subjects will lie on the platform (seen in the foreground) that slides in and out of the enclosure.*

Figure 11. Person modeling the HMD that will be used to present the VE to subjects.

4.6.6 Active Noise Reduction in the MRI Environment

A device was designed, built and patented for active noise reduction in the MRI environment. The device was built similar in overall structure to the existent *Shimode* algorithm-based device already in use, but incorporated a new method of measuring the

error signal inside the magnet bore without the use of conductive material, and incorporated information from the RF signal in addition to the x, y, and z gradient pulses. Like the *Pla* and *Shimode* system, the present system uses the Filtered-X LMS algorithm.

4.6.6.1 The Filtered-X LMS Algorithm

The noise cancellation system is based on the filtered least mean squares (Filtered-x LMS) ANC algorithm, as described by *Widrow et al.* [47]. This algorithm is adapted from the classic LMS adaptive signal processing algorithm, which adaptively changes the weights of a finite-impulse response filter with k weights $\mathbf{W_k}$ such that the difference between the convolution of $\mathbf{W_k}$ with the last k samples of a reference signal **x[n]** and the last k samples of an arbitrary desired signal **d[n]** is minimized in the least squared sense. According to the LMS algorithm, if an adaptive FIR Filter with k weights is defined as

$$\mathbf{W_k[n]= [w_1[n]\ W_2[n]\ ....\ w_{k-1}[n]\ w_k[n]]^T} \qquad (1)$$

where **n** defines the time index of the filter weight and **k** indicating the tap number of the weight. The last k samples of a reference signal $\mathbf{X_k[n]}$ and a desired signal $\mathbf{D_k[n]}$ are defined in vector form as:

$$\mathbf{X_k[n]= [\ x[n-k+1]\ x[n-k+2]\ ....\ x[n-1]\ x[n]\ ]^T} \qquad (2)$$

$$\mathbf{D_k[n]= [\ d[n-k+1]\ d[n-k+2]\ ....\ d[n-1]\ d(n]\ ]^T} \qquad (3)$$

and an error signal is defined as the difference between the last k samples of the desired signal **d[n]** and the convolution of the adaptive filter $\mathbf{W_k}$ and the reference signal **x(n]**

$$\mathbf{e_k[n]= d[n] - X_k[n]^T\ W_k[n]} \qquad (4)$$

then the adaptive filter $\mathbf{W_k}$ will converge to the filter that minimizes the squared error signal $\mathbf{e_k[n]\ e_k[n]}$ if the filter weights are updated each sample according to the following formula:

$$W_k[n+1] = W_k[n] - \mu\, e_k[n]\, X_k[n], \qquad (5) \quad \textbf{(LMS Algorithm)}$$

where μ is a convergence constant that is used to trade off between the stability of the convergence algorithm and the speed of convergence. The LMS algorithm has been studied extensively and is known to converge under a wide range of conditions.

Figure 12 shows a typical feed-forward noise control application of the LMS algorithm. A Noise Source (1) generates a signal **x[n]** that is filtered by transfer function **P** of the propagation path from the source to the control point, where an Error Microphone (4) senses the sound generated by the noise source , known as the disturbance **d[n].** A sensor at the noise source generates an electrical signal known as the reference signal **(x[n])** that is either exactly the same as the noise source (as shown in this example) or highly correlated with the noise source (for example, a vibration sensor on the noise source or a microphone near the noise source). The reference **x[n]** is convolved with the weights $\mathbf{W_k[n]}$ of the Adaptive Filter (2) and the resulting signal **y[n]** is transduced into an auditory signal by a Control Loudspeaker (3). The electrical signal of the loudspeaker is filtered by the speaker's frequency response and the propagation path **C** from the speaker to the control point, and the Error Microphone (4) picks up the error signal **e[n]** which is the sum of the disturbance signal from the noise source **d[n]** and the filtered output of the control loudspeaker **y[n] *C [n].** Each sample, the control weights $\mathbf{W_k[n]}$are updated with the values of $\mathbf{e_k[n]}$ and $\mathbf{X_k[n]}$ according to the LMS algorithm, shown above in Equation 5. The resulting system adjusts the weights of the adaptive filter to minimize the power of the signal **e[n]** at the Error Microphone. In this case, the weights are adjusted so that in the frequency (z) domain $\mathbf{W_k(z) = P(z)C^{-1}(z)}$, the filter that would make the error signal uniformly zero.

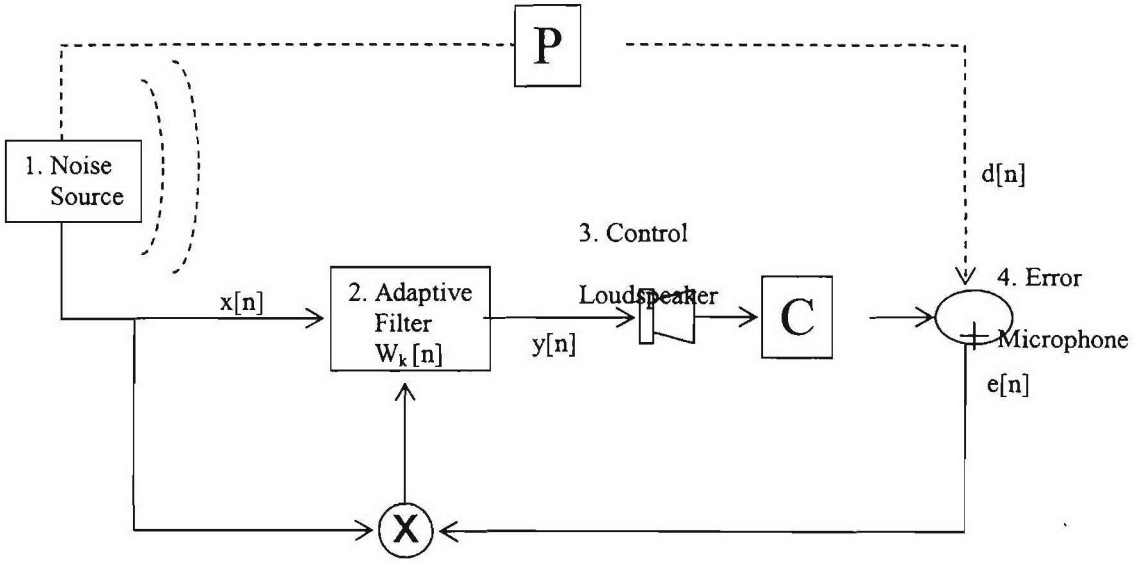

Figure 12: LMS Algorithm in Noise Control Application

A noise source (1) generates a signal **x[n]** that is filtered by transfer function **P** of the propagation path from the source to the control point, where an error microphone (4) senses the sound generated by the noise source, known as the disturbance **d[n].** A sensor at the noise source generates an electrical signal known as the reference signal **(x[n])** that is either exactly the same as the noise source (as shown in this example) or highly correlated with the noise source (for example, a vibration sensor on the noise source or a microphone near the noise source). The reference **x[n]** is convolved with the weights $\mathbf{W_k[n]}$ of the adaptive filter (2) and the resulting signal **y[n]** is transduced into an auditory signal by a control loudspeaker (3). The electrical signal of the loudspeaker is filtered by the speaker's frequency response and the propagation path **C** from the speaker to the control point, and the error microphone (4) picks up the error signal **e[n]** which is the sum of the disturbance signal from the noise source **d[n]** and the filtered output of the control loudspeaker **y[n] *C [n].** Each sample, the control weights $\mathbf{W_k[n]}$ are updated with the values of $\mathbf{e_k[n]}$ and $\mathbf{X_k[n]}$ according to the LMS algorithm, shown above in equation 5. The resulting system adjusts the weights of the adaptive filter to minimize the power of the signal **e[n]** at the error microphone. In this case, the weights are adjusted so that in the frequency (z) domain $\mathbf{W_k(z) = P(z)C^{-1}(z)}$, the filter that would make the error signal uniformly zero.

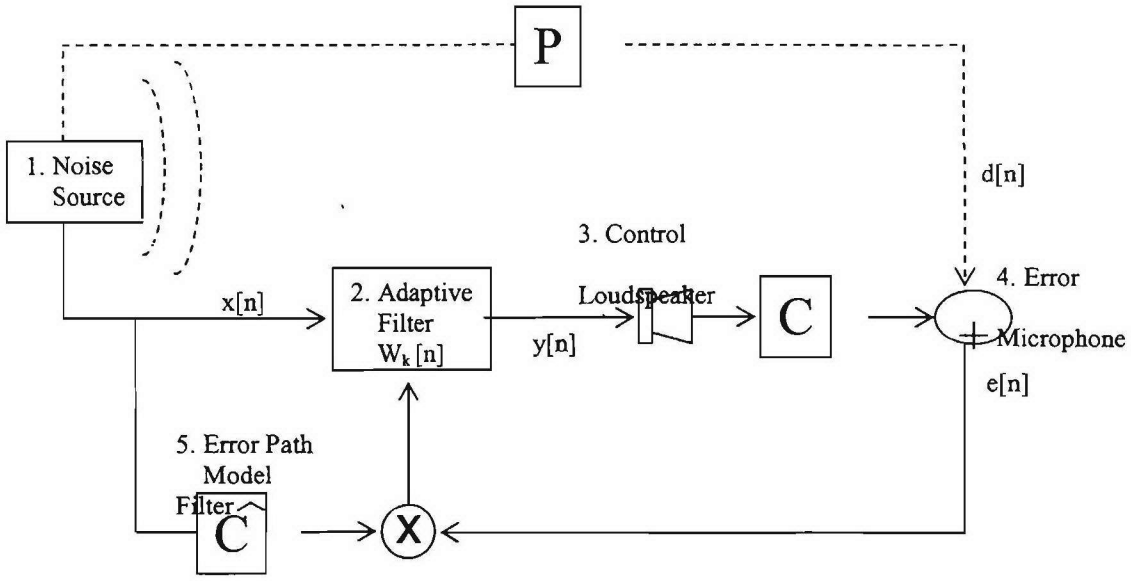

Figure 13. Filtered-X LMS algorithm in noise control application.

A clear problem arises when the propagation path from the control loudspeaker to the error microphone **C** contains a substantial delay component. When this occurs, there is a time lag between the updating of the weights in the adaptive filter $\mathbf{W_k}$ **[n]** and the effects of those updates on the error signal **e[n]**. This time lag introduces instability into the system. Furthermore, if the propagation delay of the control path **C** is longer than the propagation delay from the Noise Source to the error microphone **P** (which, as discussed later, is the case for an MRI noise cancellation system) then the filter $\mathbf{-P(z)\ C^{-1}(z)}$, which the LMS algorithm is attempting to converge to, will be non-causal. The Filtered-X LMS algorithm has been developed to deal with this problem [48]. In the filtered LMS algorithm, shown in Figure 13, the reference signal **x[n]** is convolved with an Error Path Model Filter *t (5)* that approximates the propagation path **C** from the Control Loudspeaker (3) to the Error Microphone (4) to create an error-path compensated reference signal **r[n]** that is used to update the control weights of the adaptive filter $\mathbf{W_k[n]}$:

$$\mathbf{W_k[n+1] = W_k\ [n] - \mu\ e_k[n]\ R_k[n],} \qquad \textbf{(6)}$$

(Filtered-X LMS Algorithm) where

$$\mathbf{R_k[n] = [r[n-k+1]\ r[n-k+2]\ ....\ r[n-1]\ r[n]]^T} \qquad \textbf{(7)}$$

and

$$\mathbf{r[n] = x[n] * t[n]} \bullet \qquad \textbf{(8)}$$

This Filtered-X LMS algorithm has been found to be relatively stable under a wide range of conditions even is the Error Path Model t only roughly approximates the true error path **C**. *Widrow et al.* note that the most important feature of t for stability in the Filtered-X LMS algorithm is that its impulse response has "at least as great a transport delay" as C. However, the introduction of the error model path into the LMS algorithm does have a price in terms of the maximum stable convergence coefficient μ, which determines how quickly the system can adapt to changes in the noise signal. *Elliot et al.* found that

$$\mathbf{max}\ \mu_{LMS} = \frac{1}{\mathbf{rms(x[n])K}} \qquad \textbf{(9)}$$

and

$$\mathbf{max}\ \mu_{Filtered\text{-}LMS} = \frac{1}{\mathbf{rms(r[n])\ (K + \Delta)}}, \qquad \textbf{(10)}$$

where Δ is the overall delay (in samples) in the secondary path **C** and **K** is the number of weights in the adaptive filter $\mathbf{W_k}$. Thus, the maximum convergence speed of the system is reduced when there is a substantial delay in the control path **C**, but stability can still be achieved using the Filtered-X LMS algorithm.

4.6.6.2 Measuring the Error Signal inside the MRI

All active noise cancellation systems require an error microphone at the location of the desired noise cancellation to provide a feedback error signal to the system. In the prior art, we have found three proposed solutions to this problem. The solution, first described by *Goldman et al.*, is to use pneumatic tubes to carry the acoustic signal from the location of the patient's ears inside the MRI to electret microphones located outside the magnet bore. This method is advantageous because it requires no metal parts inside the magnet bore and therefore is not likely to interfere with the medical-imaging process. However, it has serious disadvantages. The use of the tube to carry sound introduces a substantial propagation delay into the impulse response of the microphone, generates attenuation at high frequencies. Friction in the tube causes an attenuation of high-frequency sound in the tube, and the walls of the tubes may pass some acoustic noise that will interfere with the noise signal at the opening of the tube. Furthermore, the signal measured by the microphones is still electronic, and thus susceptible to electromagnetic interference. *Goldman et al.* report they had use an electro-optical transducer to convert the electrical microphone signal to a fiber optic signal to reduce EMI in the signal.

The second solution is to place non-magnetic microphones, either piezoelectric, electret, or capacitance type, inside the magnet bore and measure the sound pressure directly. In this method, the frequency response of the microphone has no propagation delay and much higher bandwidth. However, because the microphone signal wires must run inside the magnet bore, there is a greater possibility of EMI in the microphone signal. Furthermore, all require the insertion of conductive materials inside the magnet bore, where eddy currents could be induced in the materials and interfere with the magnetic field in the MRI and cause artifacts in the medical image. Thus, both of these solutions

in the prior art are problematic. This device provides an alternate technology for measuring noise inside the MRI that has not been proposed before.

4.6.7 Distributed Neuroscience Database Project

The application is designed by working with WKNI users. It is based on an existing proof-of-concept database made available to SPI by WKNI. SPI gathered information by observing and interviewing personnel from each area that will use the application.

Initial development focused on epilepsy research. Implementation of the stroke, tumor, aneurysm, and Gamma Knife research sections will be done as personnel within these areas become available. As development progresses, SPI will work with WKNI to import existing data and will work with the WKNI IS department to access current databases.

4.6.8 Internet Browser-Based Imaging Access

WKNI and WPAFB Hospital, in conjunction with KMCN, implemented a cost-effective solution to resolve the issue of broad image distribution. This solution is the Stentor's iSite web server, which is fed directly from KMCN's PACS system. The server provides access to images and reports via both the Intranet and Internet.

4.6.9 Functional Imaging in Tumefactant MS

A 36-year-old female presented with the complaints of subacute (10 days) onset of dysarthria and right hemi-paresis. Gadolinium-enhanced magnetic resonance imaging (gd-MRI) of the brain was performed at the time of admission. PET scanning using ^{18}F-FDG and ^{11}Cmet was done. Further characterization of the lesion was undertaken using ^{11}C-cho PET and ^{1}H-MRS. A CSF analysis was then carried out to substantiate MS. A repeat MRI scan done three weeks later.

4.6.10 Spectroscopic Imaging Biopsy Guidance

MRI/MRS data were obtained using the WKNI MR instrument acquired via cooperative agreement with the USAF. Before the acquisition of any MR spectra, a targeting MR volume was acquired in order to localize the VOI for subsequent CSI. The VOI was

selected from the high-intensity signal from gd on T_1-W MRI prior to the MRS exam. A large ROI, which included tumor, as well as remote normal-appearing brain tissue, was defined for selective excitation. These were aligned parallel to the transverse MRI scout slices (in axial plane) and spectra were obtained using PRESS pulse sequence for volume selection. Water was suppressed by selective excitation. The voxel sizes were chosen to reflect the amount of homogenous abnormal tissue within the voxel. Two sets of CSI data (normal and the lesion site) were acquired using PRESS sequence (TE/TR, 288/1500), FOV 24×24 mm^2; 16×16 phase encoding steps, 10-mm slice thickens; and two signal averages per phase encoding step, resulting in a nominal voxel volume of 2.25 cm^3 (1.5×1.5×1 cm^3).

A board-certified neuroradiologist examined the MR spectra data and selected the voxel in which maximum changes in choline/Cr ratio and reduction in NAA were noted. MRS data were then fused with 3-D anatomical data and transferred to the neuronavigational system.

4.6.11 High-Speed Neuroimaging in Management of Stroke

We began recruiting patients in December 2000. We screened 36 patients and one was enrolled in the study.

4.6.11.1 Procedure

Patients who were admitted to our ER for the possible neurological deficits that resemble those of hemorrhage, TIA or stroke were offered the possibility of participating in the study. The neurological deficits must have occurre less than 24 h prior to their admission; furthermore, prior to admission to the study, all patients must meet the inclusion criteria as stated in our Internal Review Board protocol. Trained examiners conduct NIHSS evaluations at the time of presentation. Once the consent form was signed, the patients were scanned by our standard CT protocol followed by the complete MRI stroke sequences. Subjects enrolled in the study had a second MRI, CT and NIHSS evaluations at discharge (i.e., 4 days post-admission). CT and MR data were provided to blinded neuroradiologists without providing any substantial medical history. MR images

were obtained using WKNI research MR. The entire MR protocol including patient handling takes approximately 30 min. Image analysis includes creation of online isotropic DWI trace images, ADC maps and MTT images.

Timeline (h)	Procedure
0.0	Admission of subjects with possible cerebrovascular accident of < 24 h
0:30	Patients meeting all the inclusion criteria will be admitted into the study
0:35	CT examination
0:45	Comprehensive MR stroke protocol in the following order: 1. 3D localizer 2. Sag. T_1 FSE 3. Ax. T_2 FSE 4. Ax. EP-DWI-FLAIR 5. Ax. EP-PWI 6. Creation of online isotropic DWI trace images, ADC maps and MTT images
1:15	Neuroradiologist first evaluation of MR and CT scans for the possible presence of hemorrhage or hyperacute stroke
1:15	NIHSS test score

1:30	rTPA treatment for the selected patients

Day 6-10: *Follow-up Examination*

1. Comprehensive MR stroke protocol

2. NIHSS test score

>Day 10: *Data Analysis*

1. Lesion VOI measurements of all time-points by two neuroradiologists blinded from CT and MR exams

2. NIHSS score tests data analysis

3. Statistical analysis by the investigators

4.6.11.2 Human Factors Analysis of System

KMCN and WKNI organized a stroke team to provide for rapid care of stroke patients, with the goal to provide TPA therapy to ischemic stroke patients within 60 min after arrival at the ER. A human factors assessment was done by *Jennie J. Gallimore*, Ph.D. (Humanwise, Inc., Bellbrook, OH) to identify systems concerns and provide some initial recommendations for system improvement. The study was limited to interviews with the stroke team members including a stroke nurse coordinator, stroke team researcher, CT technicians, radiology file clerk, lab supervisor, ER nurse manager, and a neurologist. Each member described their understanding of the process and their roles, and the roles of their staff members. They also discussed any concerns or issues related to the process.

Based on the interviews, the stroke care process as described in the interviews was outlined, followed by system concerns.

4.6.12 Brain Functional Imaging Data Deliverance to Stereotactic Neuronavigational Instruments

3-D brain functional imaging data were delivered to stereotactic neuronavigational instruments utilized in the neurosurgery operating theatre: the main objectives of this projects were accomplished in a close collaborative effort among neuroimaging team and neurosurgeons in the following three phases: 1) optimizing MR data acquisition methods, MR data were acquired using WKNI GE with Real-Time Image Processing software; 2) image transformation and post-processing. (Data were post-processed using commercially available software Medx. Brain activation maps were calculated by correlation of measured signal time course with a time-shifted boxcar function); and 3) 3-D neuronavigational compatibility of functional data.

We have devised a computer hardware/software device for the simultaneous task activation and MR data acquisition. Developing such a product has enabled accurate timing in our data acquisition.

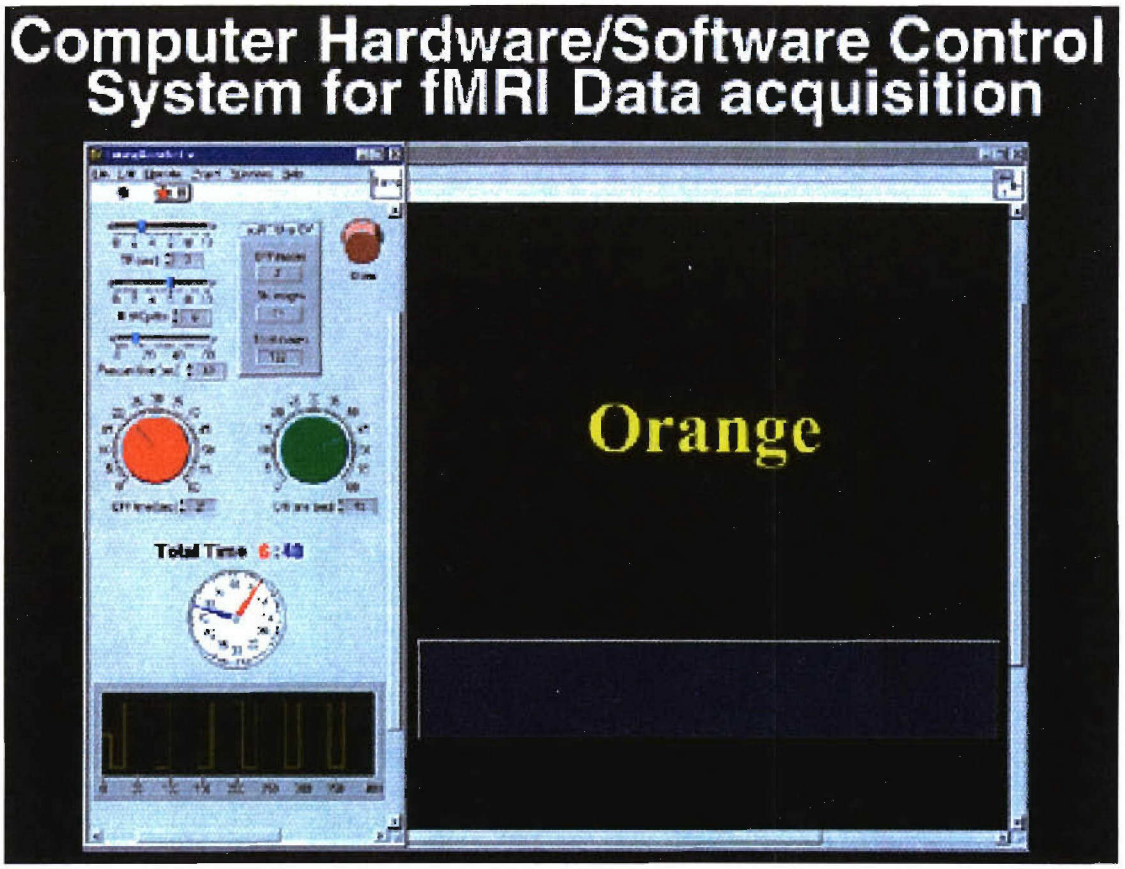
Computer Hardware/Software Control
System for fMRI Data acquisition
Orange
Total Time

Figure 14

5.0 Results

5.1 In Vivo Characterization of Human Brain Tumors by MRS

At WKNI, image data obtained using MRI are now routinely supplemented with MRS data to evaluate brain tumors. More importantly, several studies have suggested that MRS can also improve the in vivo classification of intracranial tumors and monitoring response to treatment. Indeed, we have joined the several other research laboratories in the process of developing mathematical models to perform PR analysis of MRS spectra for the characterization of brain tumor types. We are correlating the in vivo spectroscopic data with surgical pathologic finding and supplemental MR spectroscopic studies performed on surgical tissue specimen in determining the clinical value of the MRS in characterization of tumor types in vivo. In addition, KMC neurosurgeons have begun using MRS data as a valuable tool in the OR in determining tissue state and mapping of surgeries.

Another benefit from this project was software development for MRS analysis. To calculate the ratios of the different metabolites, as well as integrate the area under the metabolic peaks, we developed software at KMC called *Integrex*. *Integrex* produces a spectrum of MRS data from a text file (***Figure 15***). Using this spectrum, one can very easily determine the area under each metabolic peak, with no calculation involved. This software also readily reports the ratios of the various metabolites. It is very user-friendly; limited MRS knowledge is needed. *Integrex* can produce a metabolic spectrum from a text file using any multi-modality post-processed MRS data. It is very easy to import and analyze data with this program; to import data to *Integrex*, one simply follows the prompt on the first screen and selects a text file. Users can set the baseline value when integrating the metabolic peaks; all that is really needed is a mouse. Four vertical, different colored lines are used to delineate the beginning and ending of the area to be integrated; two peaks can be integrated at once. Using this data, *Integrex* then calculates the ratio between the two peaks being measured. Many hours of research time are saved, and persons of lesser skills can be incorporated into data analysis.

5.1.1 USAF Relevance

Our clinical experience with PR models has yielded significant and direct future military applications. Models and analytical software package resulted from the current investigation could be utilized in screening/diagnostic instruments for prediction for large-scale application in the military field. These include large image data base processing, automatic detection of pathologic cases by enhancement of details and recognition of patterns, accurate measurements of the changes and distortions in the processed images, prediction of results to allow planning of treatment, simulation, and training on computerized cases. Further application will be in the field of toxicogenomics, which currently focuses on the application of large-scale differential gene expression (DGE) data to toxicology. Our PR models could be a valuable tool in predictive toxicology which is of a significant interest to United States Air Force.

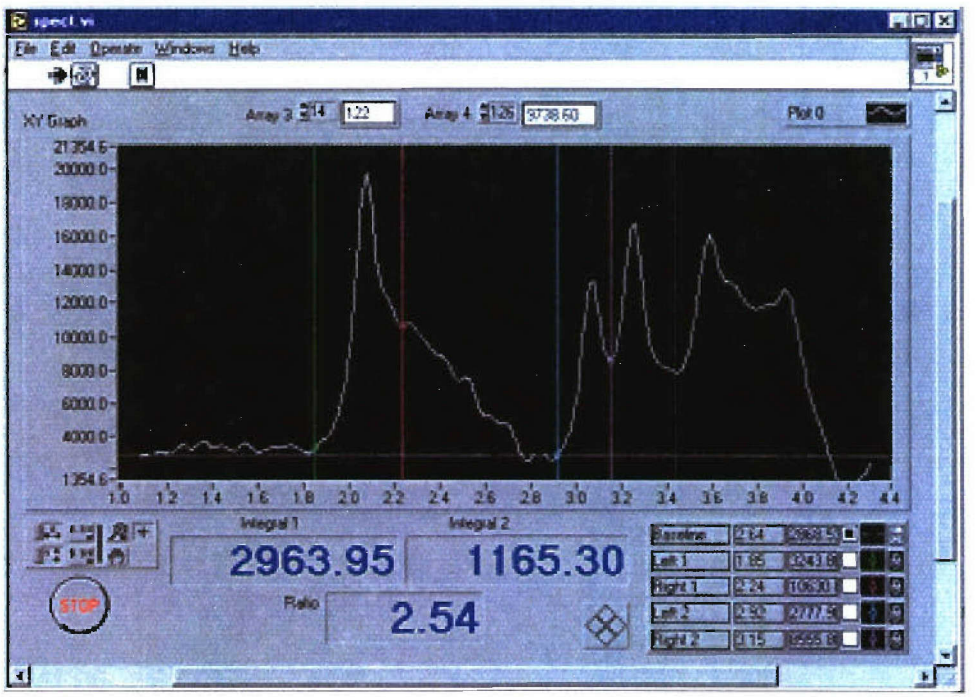

Figure 15

5.1.2 Future Directions

The work completed in this project has paved the way for future projects involving application of MRS in solving biomedical questions including MRS and Gamma Knife Radiosurgery in the management of brain metastases. Metastases are defined as

secondary cancerous growths formed by transmission of cancerous cells from a primary growth located elsewhere in the body. Metastases can happen anywhere in the body, and can occur from any type of primary cancer. Brain metastases are the most common type of brain tumor; up to 50% of cancer patients will develop brain metastases, and half of these patients will demonstrate neurological symptoms due to these tumors. The current standard of therapeutic treatment assessment is evaluating change in lesion volume as determined by MRI. However, MRI techniques can only evaluate gross morphologic changes in tumors, and give no information about possible links to changes in cell biology. The goals of radiosurgery treatments, such as Gamma-Knife, are local tumor control, improved quality of life, and prolonged survival. Because patients with brain metastases have such short survival times, an earlier indicator is needed to adequately assess the ability of Gamma Knife to meet these goals. We hypothesize MRS could be the technique of choice for early detection of morphological changes. We will apply the MRS software package developed under sponsorship of our cooperative agreement with USAF in analyzing data from this project.

5.2 Choline Metabolism in Human Brain Tumors with ^{11}C-PET and ^{1}H-CSI

The choline study of the brain with PET demonstrated generally decreased choline metabolism in the brain except for a focal area of increased choline uptake in the right temporal region corresponding to the abnormality noted in the MRI. ***Figure 16*** depicts the sleeted axial slices from MRI, PET and co-registered MRI and PET data. MRI data post-contrast indicated an enhancing mass in the right temporal lobe. The patient also had completed a methionine-PET (22 mCi) uptake study as well as glucose uptake PET (8 mCI of ^{18}F-deoxyglucose) study. The results of these studies also indicated a right temporal lobe tumor (data not shown).

Corresponding MR, PET and Fused PET/ MR Images

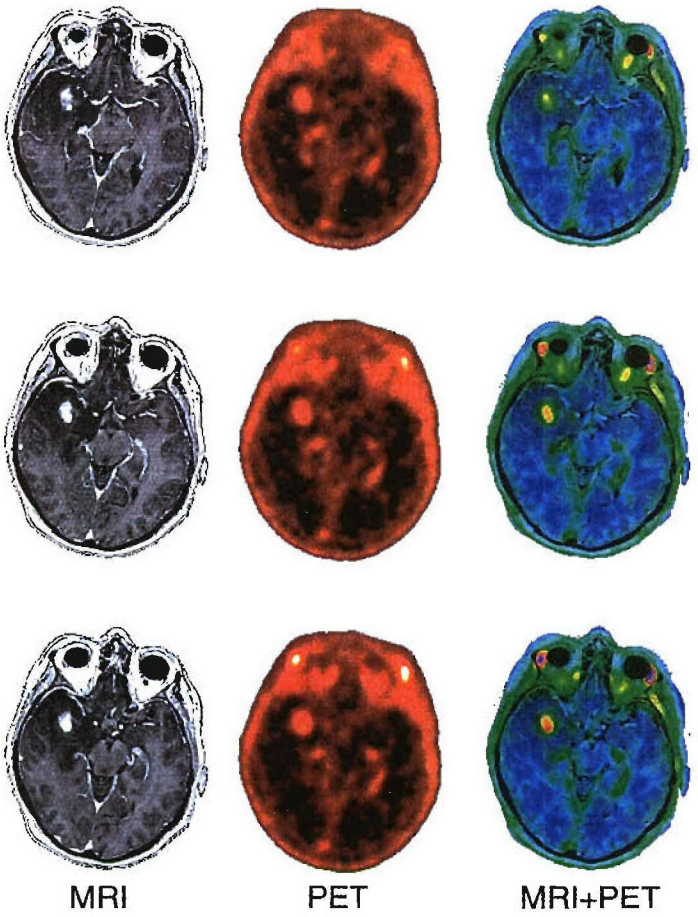

Figure 16. The selected T_1 MR images obtained post contrast, corresponding PET images and fused PET/MR data.

The ratio of choline/Cr and NAA/Cr in the area of lesion enhancement was 2.3 and 1.5, respectively. In the normal cortex of the same patient, these ratios were 1.2 and 2.7, respectively. ***Figure 17A-D*** demonstrates the 2-D-multivoxel CSI fused with the corresponding anatomical MR image and ^{11}C-choline PET Data (17A). Also shown in this figure is the average CSI spectra from the enhanced region (Figure 17B; ROI approximately 2.25 cm^3). For comparison, we also show non-pathological ***in vivo*** spectrum for the same volume of the same patient (Figure 17C).

Multiparametric studies such as this, integrating MRI anatomical, MRS and PET biochemical information into a single image and incorporating in vitro analysis provide a

more comprehensive representation of changes occurring in the brain than previously available. The methods of integrating this data we describe enabled rapid availability of the information, providing physicians and researchers with valuable insight into the status and progression of neurological changes for determination of therapeutic choice and potential cause-and-effect relationships in metabolic pathways in the brain. The applications of these integrative methods are far-reaching and may extend to neurological effects of chemical compounds as well as naturally occurring disease progression.

5.2.1 USAF Application and Future Directions

Future directions and applications include:

1) Animal models for the effects of compounds can be developed that provide comprehensive detailed biochemical evaluations of tissue status. These can also be correlated with behavioral studies and kinetic analysis to provide a "living" picture at the level of organism, organ and cell of changes due to compound exposure or disease progression.
2) Multi-parametric studies such as this can be extended to a multiplicity of naturally occurring and induced disorders in humans to provide clues as to their origins, progression over a time course and effects of various therapies. Following biochemical and metabolic changes may provide for early detection and be of predictive value in decision-making for both medical and research applications.

5.3 Choline PET and MRS Imaging of a Human Astrocytoma

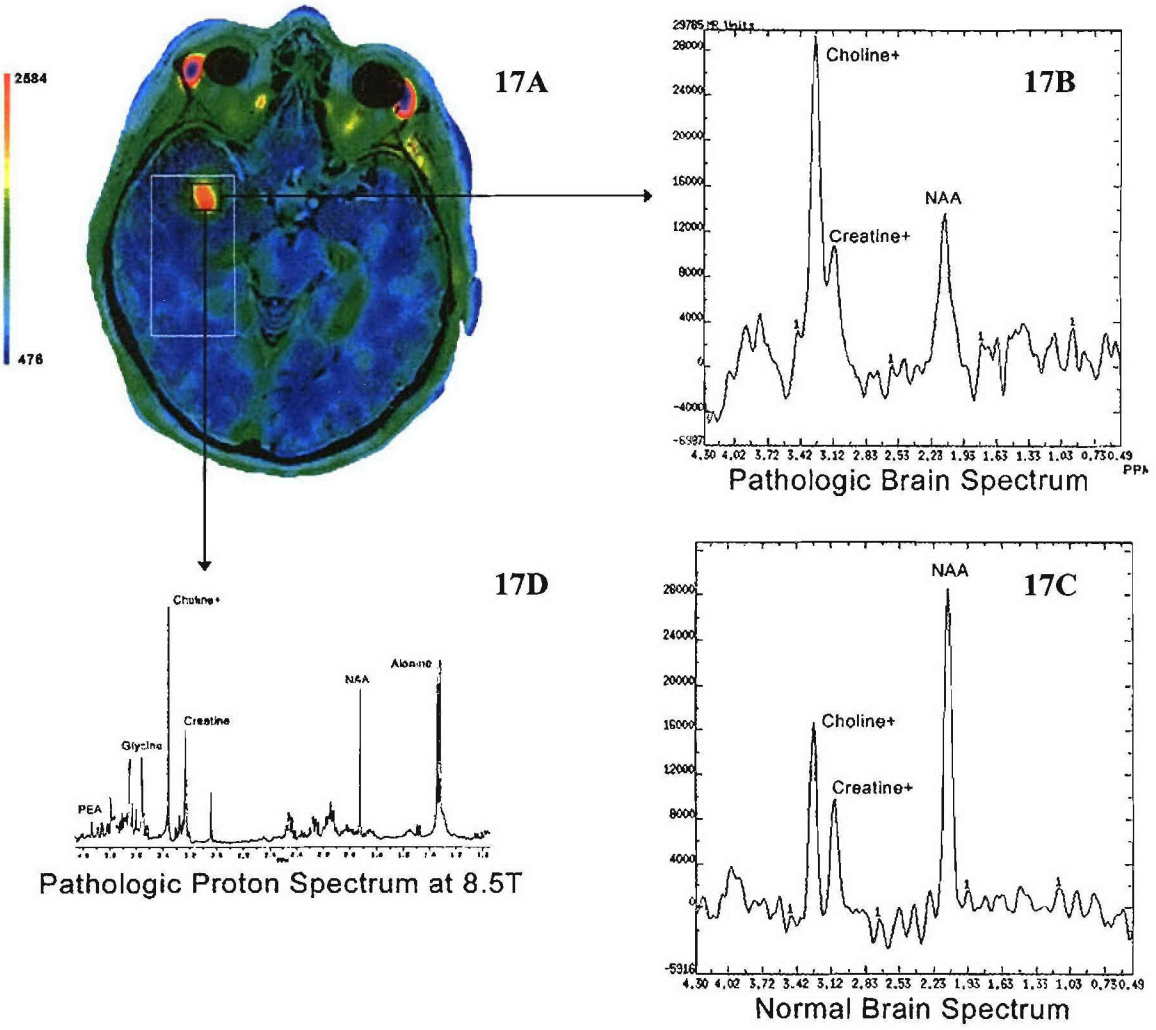

Figure 17A depicts the 2-D multivoxel CSI fused with the corresponding anatomical MR image and ^{11}C-choline PET data. *The white rectangle represents the excitation volume for CSI. The area of red represents the high choline uptake as determined from PET.*

Figure 17B and 17C represent the in vivo MR Spectra obtained using PRESS sequence. *MR data acquisition parameters are given in the text. Figure 17B is the average spectrum from the region depicted as the black square in the Figure 17A; the area of signal enhancement on MR T_1 post-gd and high choline uptake. The approximate volume is 5 cc. Figure 17C represents the non-pathological spectrum from the normal region (i.e. reomote from the tumor site). Both MR spectra represent approximately 5 cc of biological tissue. The same axial T_1-MR image was utilized for both CSI data*

acquisition.

Figure 17D depicts the high-resolution proton spectrum of aqueous extract of the astrocytoma specimen acquired at 8.5T. *See text for the acquisition parameters. Note the significant elevation in the choline-containing compound signal (3.26 ppm). Our subsequent analysis confirmed that the enhancement in this signal is due to the elevation in GPC concentration.*

Concentrations of metabolites of interests as measured by MRS in the region of lesion enhancement were as follows: choline and Pcho (3.26 ppm) 13.46 μmol/g; cr (3.1 ppm) 8.94 μmol/g and NAA 8.26 (1.94 ppm) μmol/g. The high resolution in vitro MRS is shown in Figure 17. The subsequent analysis of ^{31}P aqueous sample demonstrated that the enhancement in the choline signal in proton spectrum in vivo and in vitro is mainly due to a marked elevation in GPC content rather than Pcho (data not shown).

Our data suggest elevated concentration of tumor GPC content. GPC is a major by-product of PtdC degradation and may be indicative of PL turnover. Others have observed increases in GPC following upregulation of PtdC synthesis by addition of excess phospholipid in HeLa cells [49] and overexpression of CTP:Pcho cytidylyltransferase in COS cells [50]. They attributed this to an increase in turnover as a mechanism to maintain PL content.

5.3.1 USAF Relevance

The need for prompt and accurate recognition of a low- to high-grade progression and/or of a post-therapeutic recurrence in cerebral neoplasms has given impetus to the search for novel neuroimaging methods. PET provides insight into tumor cell metabolism and has emerged as a powerful method to assess the biological behavior of cerebral neoplasms. MRS has also shown to be an important diagnostic and research tool because of its ability to detect brain metabolites and their changing concentrations, which correlate with physiologic and pathologic processes. This is the first documented study of in vivo choline metabolism with MRS in conjunction with PET. MRS provides data with respect to choline concentration, which complements PET's rate of choline uptake in tumors.

Data from the current study clearly show the feasibility of performing correlative investigations with PET and MRS. Such data may prove useful for characterizing tumor proliferation status in vivo.

Furthermore, our current investigation has demonstrated the importance in utilization of multi-parameter biochemical imaging in studying the in vivo metabolism. Such studies provide an important framework for future investigation relevant to US military, most significantly to the military Tri-Service (Army, Navy & Marines, Air Force) Deployment Toxicology Assessment Program (DTAP). MRS and newly synthesized PET radio-ligands could potentially be utilized in human risk assessment to various chemicals/neurotoxins during military deployment. A good example of how our echniques could provide benefit to military toxicology program will be applying our techniques to study Gulf War Syndrome.

5.3.2 Future Directions

Future studies will be undertaken to understand how such alterations might be impacted by tumor type. Our objective will be to utilize the combination of these imaging techniques in identifying and grading brain tumors. We will collect data from patients who have received a comprehensive PET examination including FDG, methionine and choline in conjunction with MRS and MR. We will then use the PR models developed under sponsorship of our cooperative agreement in assessing the predictive value of these techniques in grading brain tumors.

5.4 Choline PL Metabolism in Human Brain Tumor Cell Lines

The pools of Pcho, Peth, PtdC, and PtdE remained constant from 0 - 60 min during the infusion of substrates (analysis of variance; ANOVA). ***Figure 18*** shows portions of the ^{13}C NMR spectra from rat liver lipid extracts before and 60 min after infusion with ^{13}C-labeled substrates.

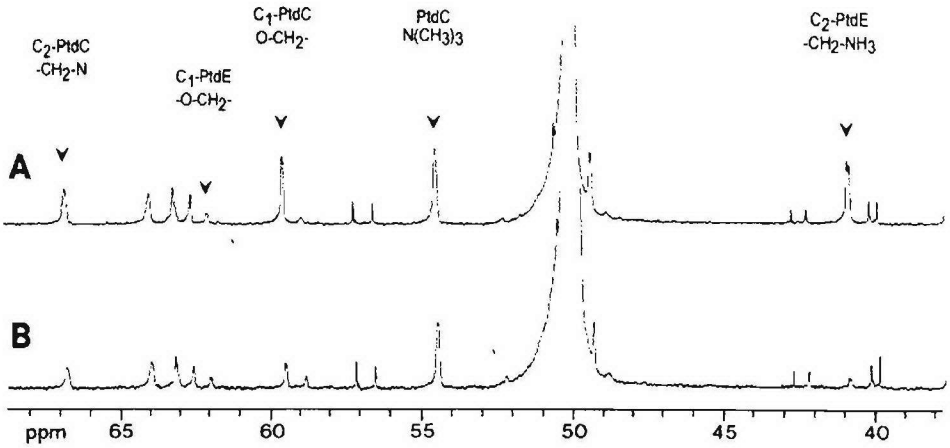

Figure 18. Proton-decoupled ^{13}C NMR spectra (40-70 ppm region) of rat liver lipid extracts before (B) and 60 min after (A) infusion with [1-13C]choline + [2-13C]ethanolamine. *Note the incorporation of ^{13}C labels into C1-PtdC, C2-PtdC, and C2-PtdE. The N(CH3)3 and C1-PtdE signals show natural abundance intensities for PtdC and PtdE, respectively. The strong signal at 50 ppm is from the MeOH solvent. Spectra were acquired using a 8.0 ms pulse (60¡ flip angle), 20 kHz bandwidth, 1.64 s acquisition time, 3.65 s interpulse delay, 64 K data points, and ~12 h of signal averaging. Chemical shifts are relative to TMS at 0.0 ppm.*

Figure 19. Biosynthesis via choline pathway

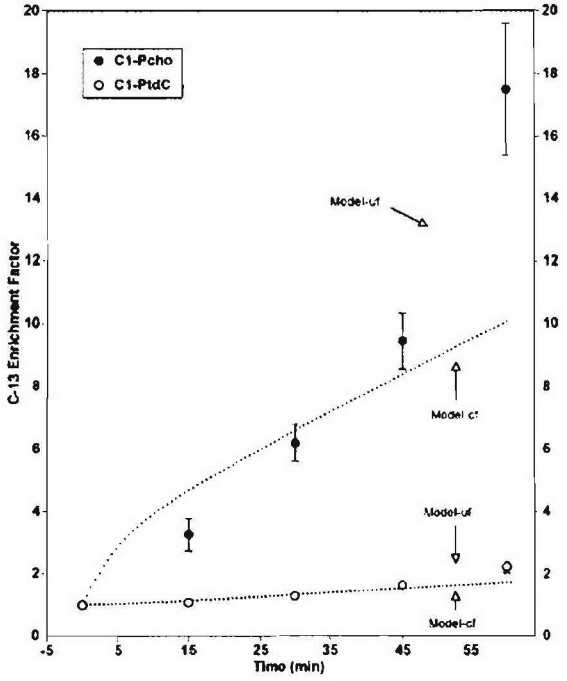

Figure 19. The ^{13}C enrichment factors (EFs) for Pcho and PtdC, and during infusion of labeled choline. *Data points are from the NMR experimental measurements (mean ± SE), while the lines represent the kinetic model predictions. Model predictions are based on constant reaction rates (Model-cf), or upregulated flux (Model-uf). Alternative kinetic models were examined to obtain a reasonable fit of the experimental data; for further explanation see Discussion section.*

These MR methods are superior to earlier radioisotope studies since they provide simultaneously in one experiment information about the specific metabolic pathways of PL biosynthesis. The results of the current study indicated that metabolites derived from exogenous choline and ethanolamine are preferentially utilized in the pathways for PL synthesis. Biosynthesis of PtdC and PtdE through the CDP pathways is a channeled process. We also show for the first time that channeling is involved in the PEMT pathway for interconversion of PtdE into PtdC.

These preliminary studies in rat liver provide the basis for performing these assays in cultured human brain tumor cells in vitro. Future studies will increase our understanding

of the biosynthesis and metabolism of these PL that affect processes of signal transduction, cell proliferation, differentiation and apoptosis, including carcinogenesis in brain tumors.

5.5 CSI of Human CN

The integrated peaks for enhanced lesion area depicted in the voxels 1, 2, 4 and 5 with the remote normal-appearing brain tissue in voxels were compared. 2-D multivoxel CSI was overlaid on the corresponding anatomical image (***Figure 20, 21A, 21B***). The corresponding averaged individual spectra (1-16) are also shown (Figure 21B).

Figure 20. T_1-W Images Post-Contrast

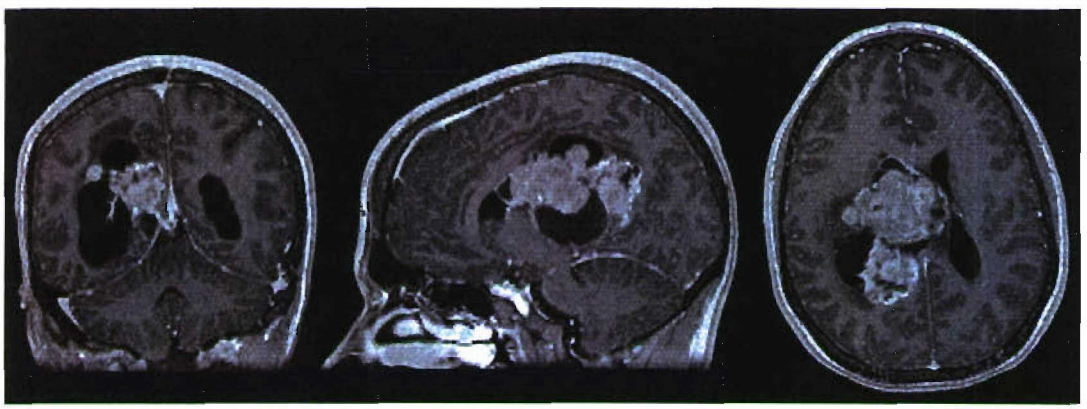

Figure 20. Selected sagital, axial and coronal images from a patient with CN. Images were acquired using a T_1 post-gd for pre-surgical planning.

Figure 21: CSI of CN

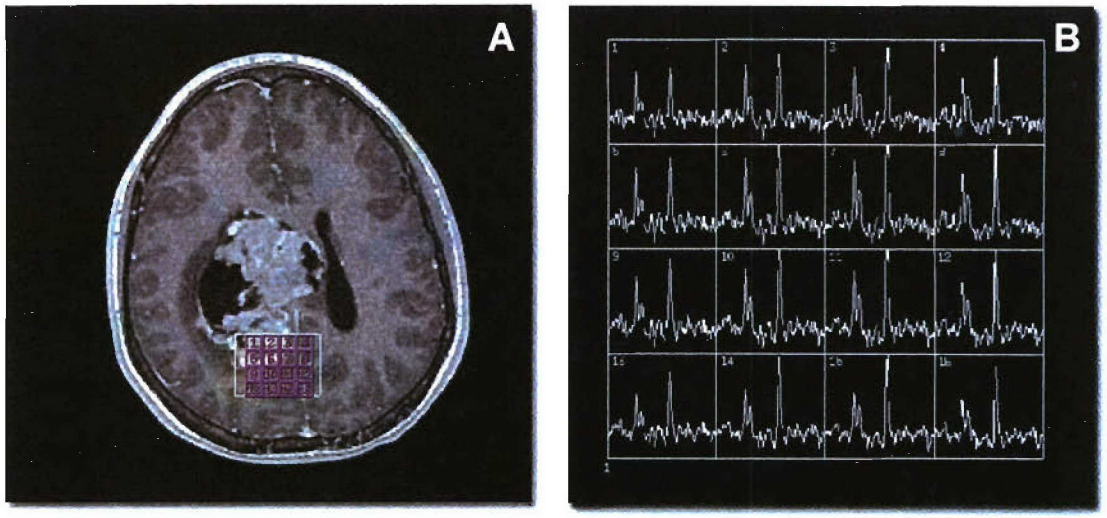

Figure 21A. Proton CSI of a patient with CN. *Data acquisition parameters are given in the text. The voxel numbers on the MR image corresponds to the individual spectrum in Figure 21B.*

CN brain tumors indicated enhancement of choline/Cr ratio (2.7) compared to normal subjects (1.8), and a decrease in the NAA/Cr ratio (2.5) compared to normal subjects (3.12) on anatomical images. The high-resolution proton spectrum of normal (***Figure 22***), an astrocytoma (***Figure 23***) and a CN tumor (***Figure 24***) extracts are compared. The total amount of Cr was lowered by more than 54% in human CN tumors compared to previously reported data for normal human brain. Choline-containing groups are increased by 23% and total NAA content is reduced nearly threefold.

Figure 22. Normal Brain Spectrum

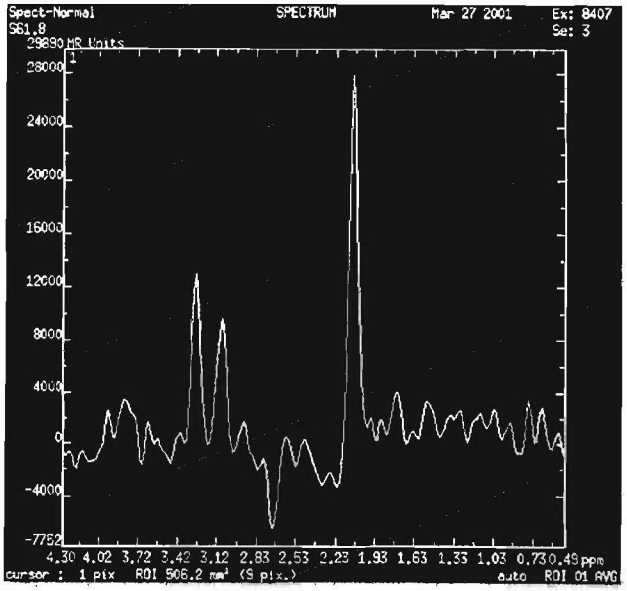

Figure 22 depicts the normal brain spectrum obtained from a volunteer. *Data acquisition parameters are given in Method section. The ratios for choline/Cr and NAA/Cr is 1.2 and 2.75, respectively.*

Figure 23. Spectrum of Astrocytoma

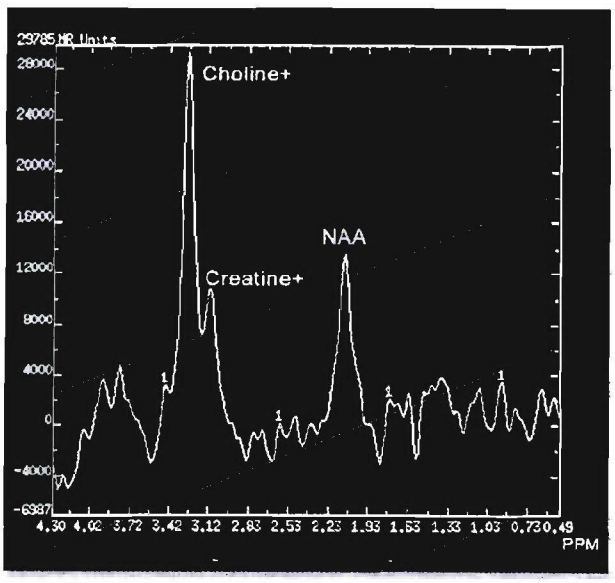

Figure 23 depicts the proton spectrum obtained from a patient with brain tumor astrocytoma. *Note the marked elevation in choline/Cr ratio.*

Figure 24. High-Resolution Proton Spectrum

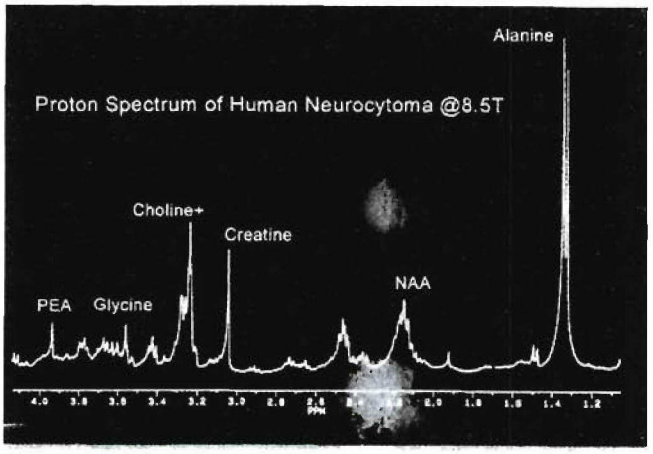

Figure 24. High-Resolution proton spectrum of neurocytoma specimen extract.

The in vitro MRS of CN brain tumor was characterized in order to provide a better interpretation of the spectra obtained by in vivo MRS. An especially interesting finding of this study was the indication that the ratio of choline/Cr ratio in vivo for CN is misrepresented due to the drastic reduction in total Cr content. It is generally accepted that in vivo levels of Cr remain constant in neoplasms, which can then be used as a reference for other metabolite changes. Alterations in choline-containing metabolites are likely related to changes to alterations in cell membrane integrity. Changes in NAA are indicative of neuronal or axonal loss or dysfunction. The high in vivo Cr signal indicated that Cr is not a stable and reliable reference metabolite in ^{1}H-MRS studies, thus emphasizing the importance of quantitation in ^{1}H-MRS studies for detecting altered brain metabolism.

5.5.1 USAF Relevance

In the future, US military forces will be faced with opposing forces that have chemical and biological weapon capabilities. As demonstrated in the following study, MRS could provide the very first choice for in vivo metabolic imaging for risk assessment. MRS could provide surrogate markers indicative of biochemical or physiologic measurements that can demonstrate the direct effect of a potential toxin.

5.5.2 Future Direction: MNS in Diagnosis and Classification of Various Memory Disorders

MRS can detect structural alteration and biochemical abnormalities in the brain of demented subjects and may help in the differential diagnosis and early detection of affected individuals, monitoring disease progression, and evaluation of therapeutic effect. Most recently, researchers have reported that increased levels of cytosolic choline, a precursor pool for acetylcholine synthesis, were associated with greater progression in memory impairment during treatment. Others have reported that MRS findings are useful indicator of neuronal/axonal loss in the white matter of the frontal lobes which precedes cognitive impairment. Most recently, it has been reported that MRS differentiates mild cognitive impairment from normal brain aging. Moreover, a recent review concludes that NAA alone may be more useful as a prognostic marker for monitoring neurodegeneration, stabilization, or improvement, and for evaluating therapeutic response to novel drugs. Thus, MRS has promise for predicting cognitive status and monitoring pharmacologic efficacy, and can assess cortical and subcortical neurochemical change. Our goal at WKNI will be to take the utility of MRS to the next natural progressive step which is the MNS. Application of MNS for the classification of memory disorders has been very limited due to small number of sites capable of performing such studies. We are fortunate that as the result of our cooperative agreement with AFRL, we were able to upgrade our spectroscopy capabilities to the MNS. Indeed, MNS in conjunction with our PR models can aid in processing large amount of information collected from this project. Our center will be able to contribute significantly to this up-and-coming filed.

5.6 PL Changes in Hippocampus of Epileptics

Preliminary data from immunohistochemical observations of hippocampal excisions of two epileptic patients reveal similar labeling by the monoclonal 3sb against PS-dependent antigen. Pathologic labeling differs considerably from normal tissue (***Fig. 25***). Normal tissue granular layer neurons reacted (Fig.25a), as did pyramidal cells (Fig. 25b). Antibody binding in normal hippocampus was throughout the cytoplasmic region of cells, but was less intense or absent in nuclei. In contrast, labeling of granular cells of both

pathologic patients was weak in intensity, and was not cytoplasmic. There appeared to be some labeling on the periphery of granular cells of one patient, while the other was not reactive (Fig. 25c,e). Pyramidal cells did not label in pathologic tissue. However, there was labeling of what appears to be the periphery of a number of small cell bodies or processes in both pathologic patients (Fig. 25d, f).

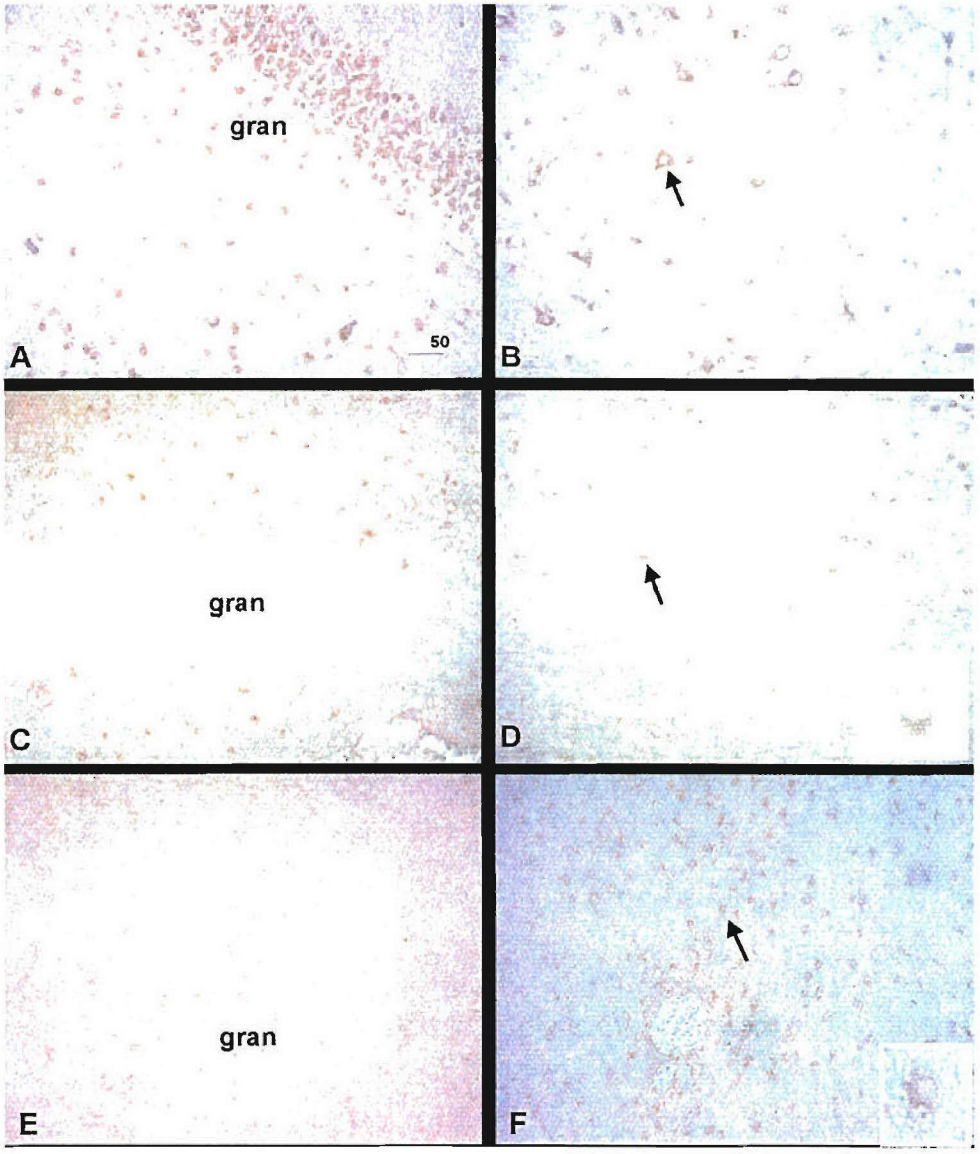

Figure 25. Reactivity of monoclonal aPL antibody 3sb in normal and sclerotic-fixed paraffin-embedded hippocampus. *3sb reacted with normal tissue granular layer (gran) and pyramidal neurons with cytoplasmic labeling (25a,b). In pathologic hippocampus 1 (25c,d) granular cell reactivity as confined to the periphery of cells (25c). The antibody did not react with granular layer cells of pathologic patient 2(25e). There was also*

scattered reactivity with small cells or processes in both pathologic tissues (arrows25e,f). At higher magnification (insets), labeling did not appear cytoplasmic but restricted to the periphery.

5.6.1 Case Report 1

A 46-year-old gentleman presented with medically intractably epilepsy of complex partial seizures since age 11. The frequency has been described as occurring three times a month. Patient presented with a normal physical presentation but was noted to be cognitively slow. Past medical history was noted for a ruptured appendix at age 11 and a bowel obstruction at age 28 with an abdominal abscess.

A work up was done with MRI and PET, which showed medial temporal sclerosis. Specifically, an asymmetry of the right anterior-to-mid hippocampal gyrus that is consistent with atrophy was noted. An incidental partially empty sella was also noted on the MRI images. Finally, no mass effect was noted within the brain, and flow void in the major vessels was normal. Subsequent volumetric analysis indicated an assymetrical atrophy in the hippocampi (***Figure 26***). The volume of left hippocampus was reduced to 2.3cc in comparison to the right one (5cc). CSI data further indicated NAA loss in the left hippocamapal area (***Figure 27***). The choline/Cr ratio was elevated in the left side compared to the corresponding right hippocampus.

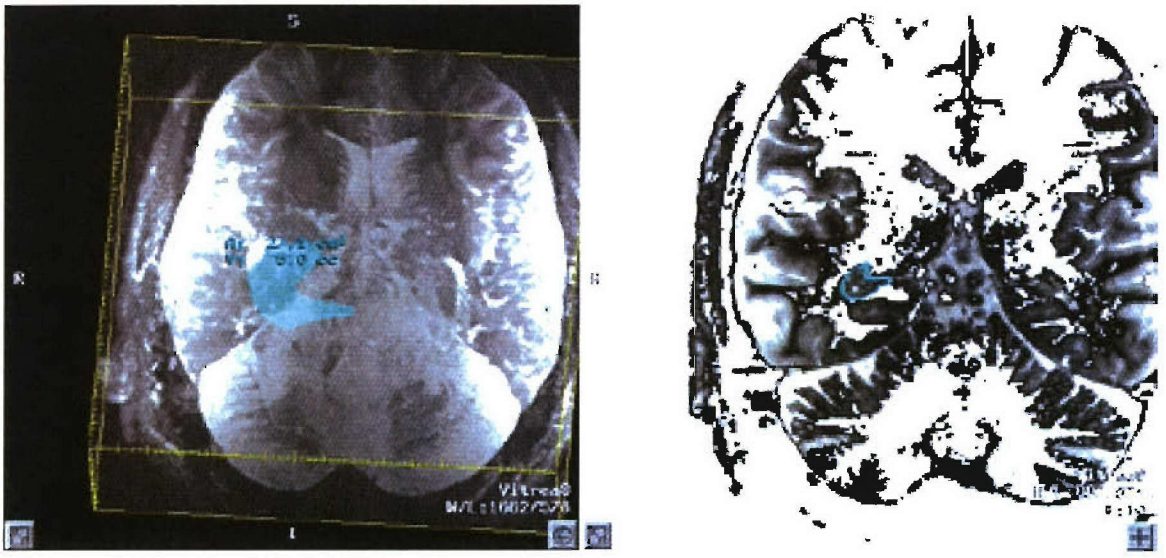

Figure 26a and b

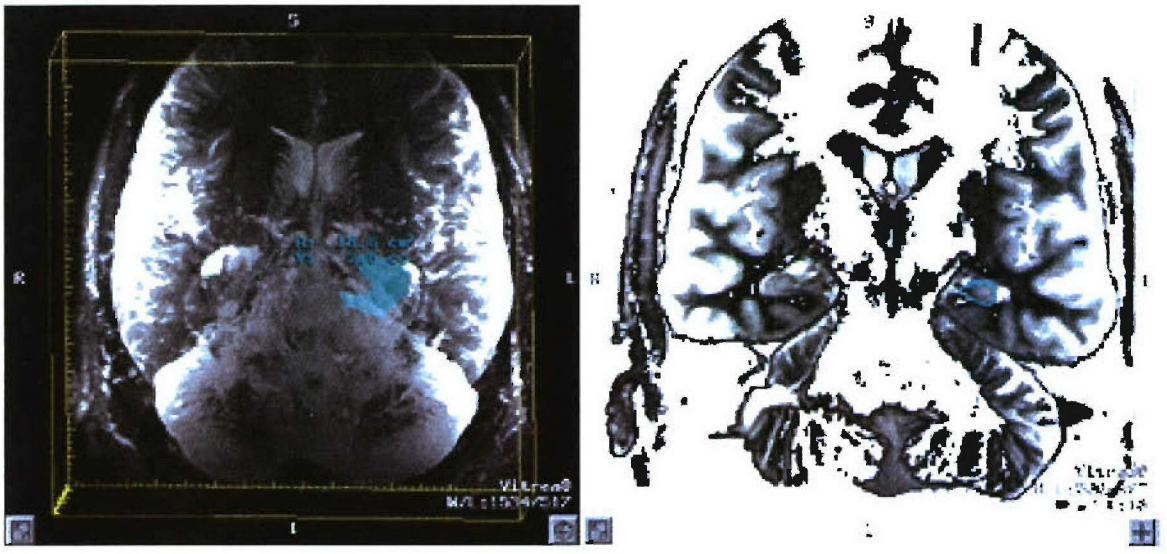

Figure 26c and d

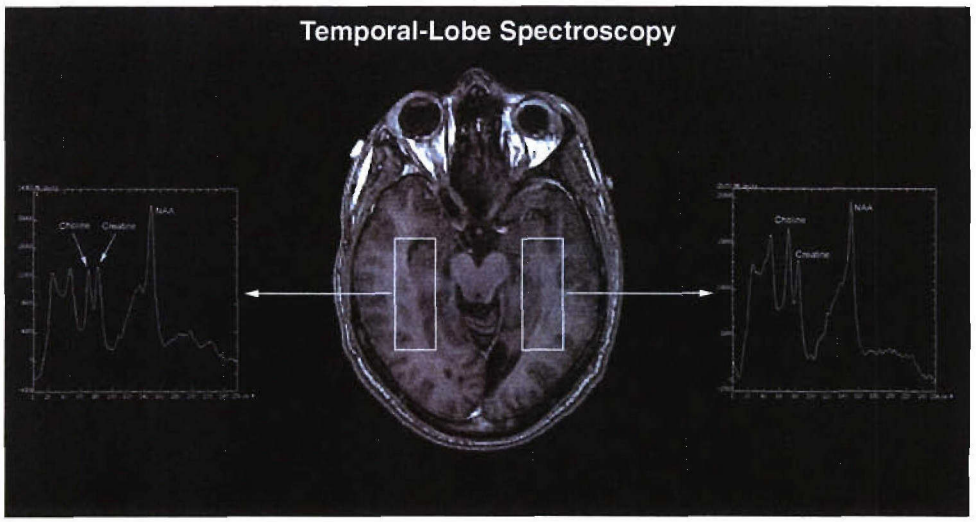
Temporal-Lobe Spectroscopy
Choline
Creatine
NAA
Choline
Creatine
NAA

Figure 27

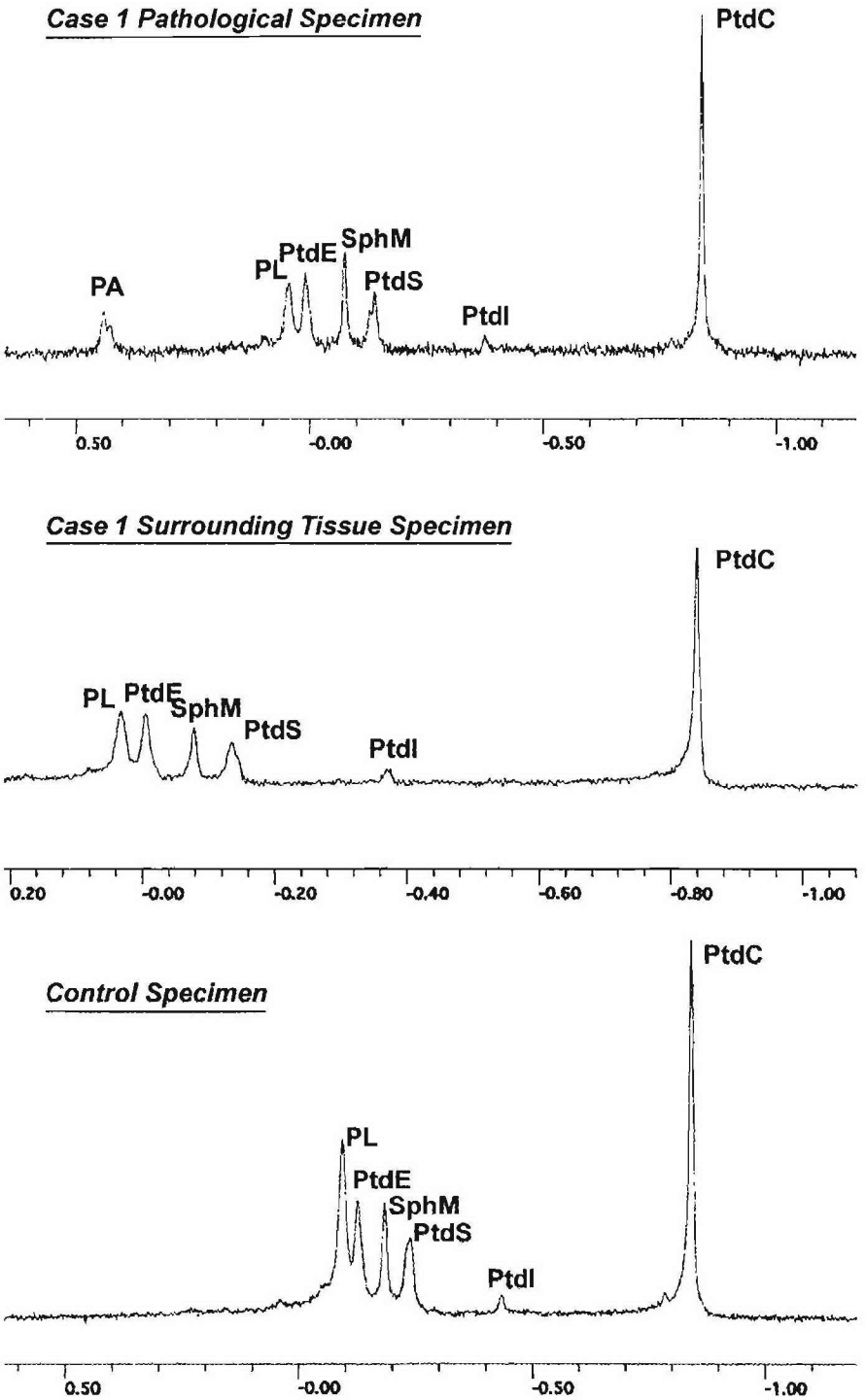
Case 1 Pathological Specimen
PtdC
PA
PL
PtdE
SphM
PtdS
PtdI
0.50
-0.00
-0.50
-1.00
Case 1 Surrounding Tissue Specimen
PtdC
PL
PtdE
SphM
PtdS
PtdI
0.20
-0.00
-0.20
-0.40
-0.60
-0.80
-1.00
Control Specimen
PtdC
PL
PtdE
SphM
PtdS
PtdI
0.50
-0.00
-0.50
-1.00

Figure 28

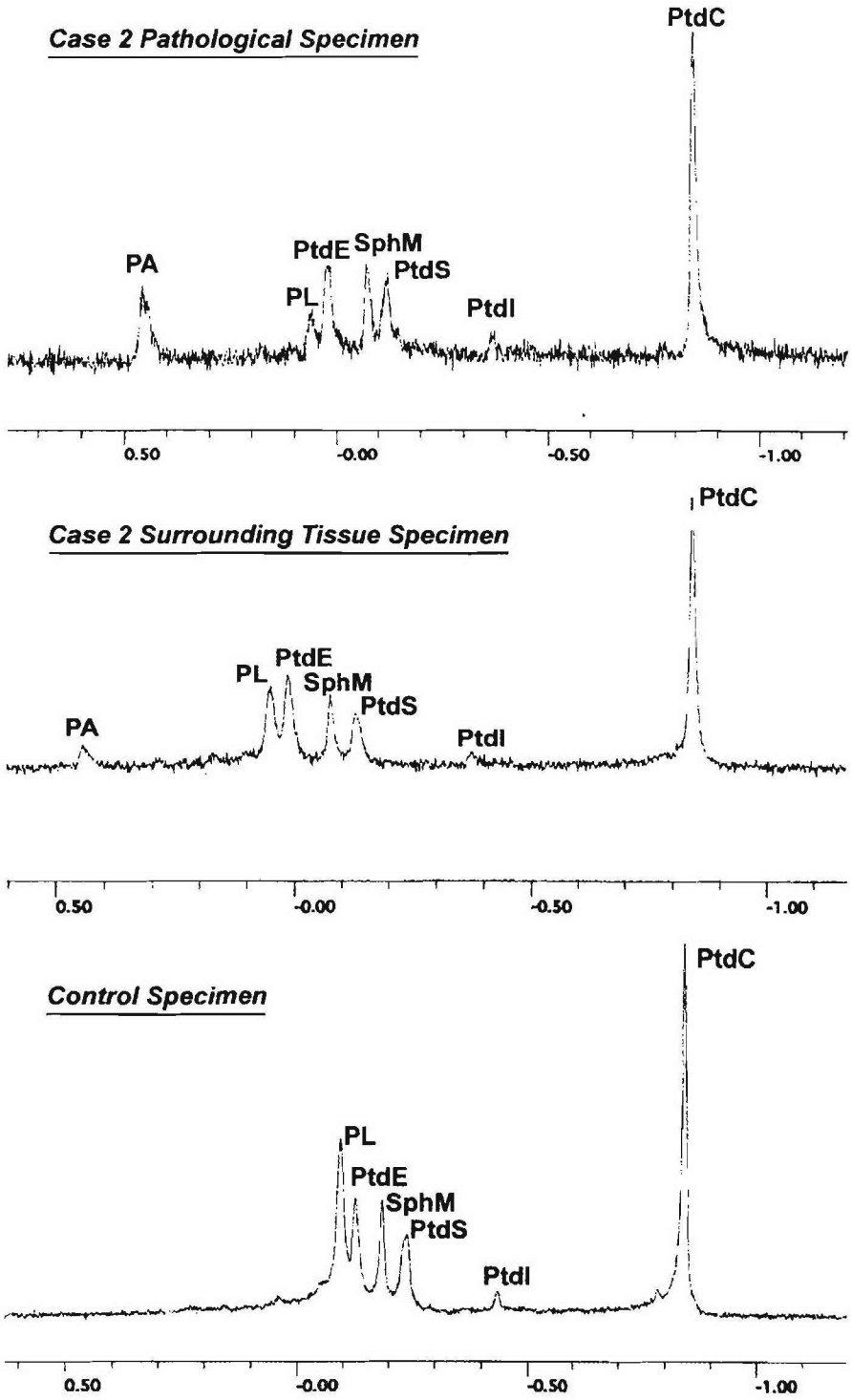
Case 2 Pathological Specimen
PtdC
PA
PtdE
SphM
PtdS
PL
PtdI
0.50
-0.00
-0.50
-1.00
Case 2 Surrounding Tissue Specimen
PtdC
PL
PtdE
SphM
PtdS
PA
PtdI
0.50
-0.00
-0.50
-1.00
Control Specimen
PtdC
PL
PtdE
SphM
PtdS
PtdI
0.50
-0.00
-0.50
-1.00

Figure 29

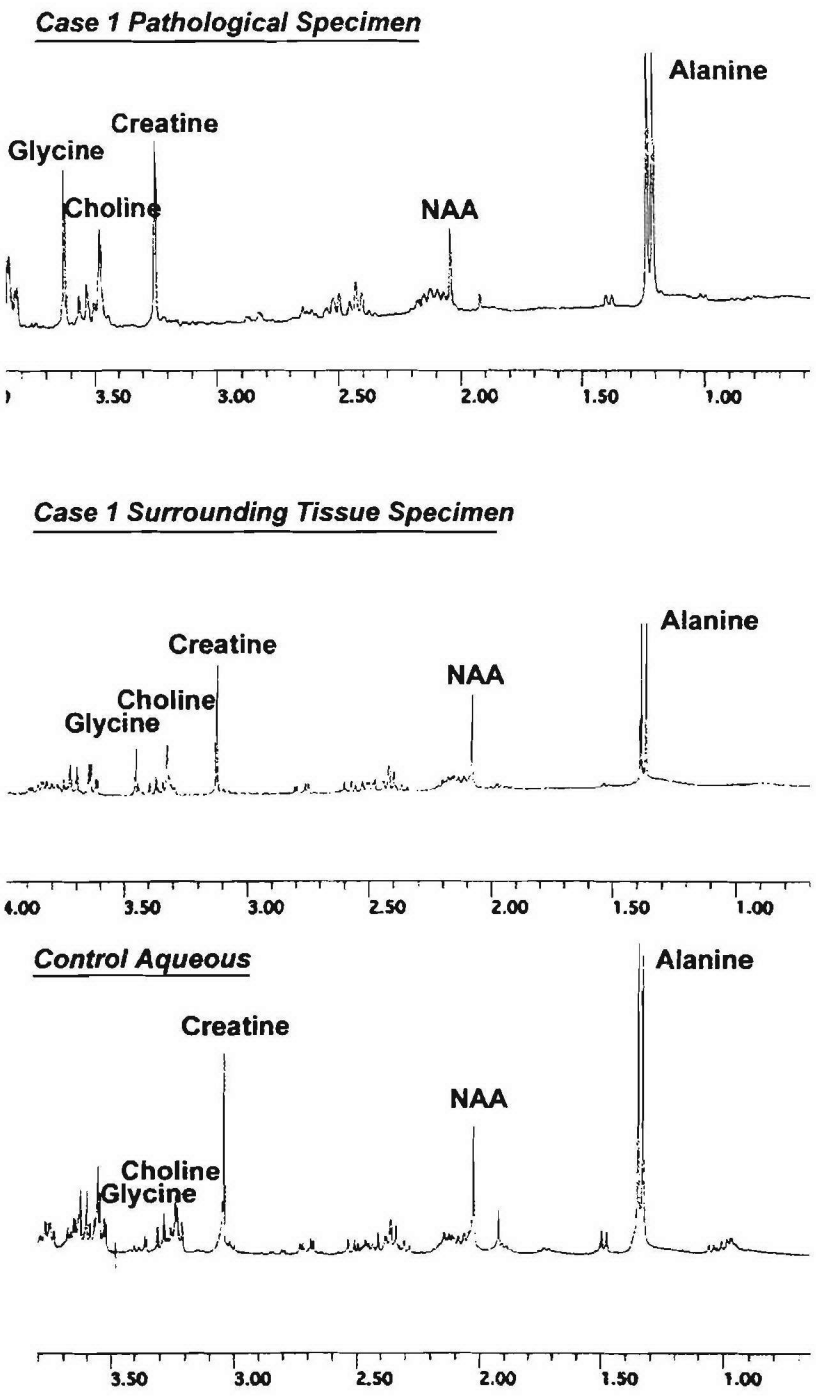
Case 1 Pathological Specimen
Alanine
Creatine
Glycine
Choline
NAA
3.50
3.00
2.50
2.00
1.50
1.00
Case 1 Surrounding Tissue Specimen
Alanine
Creatine
NAA
Choline
Glycine
4.00
3.50
3.00
2.50
2.00
1.50
1.00
Control Aqueous
Alanine
Creatine
NAA
Choline
Glycine
3.50
3.00
2.50
2.00
1.50
1.00

Figure 30

Case 2 Pathological Specimen

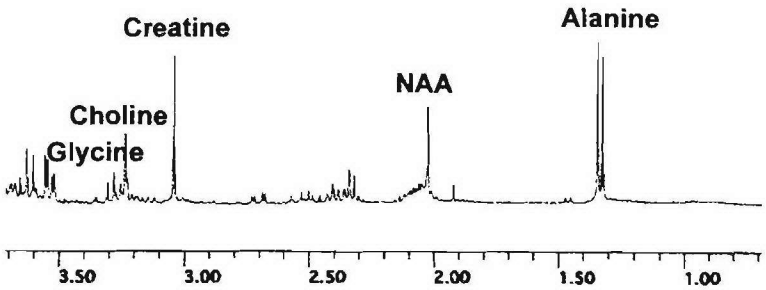

Case 2 Surrounding Tissue Specimen

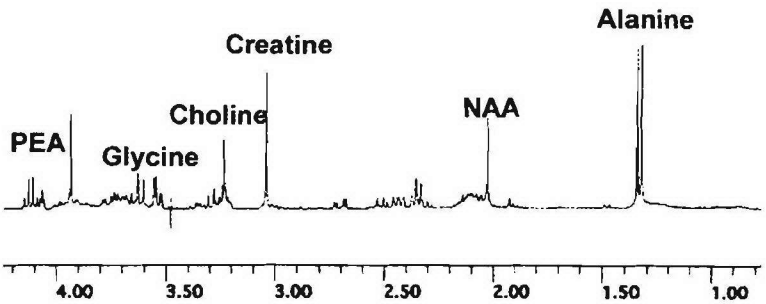

Control Aqueous

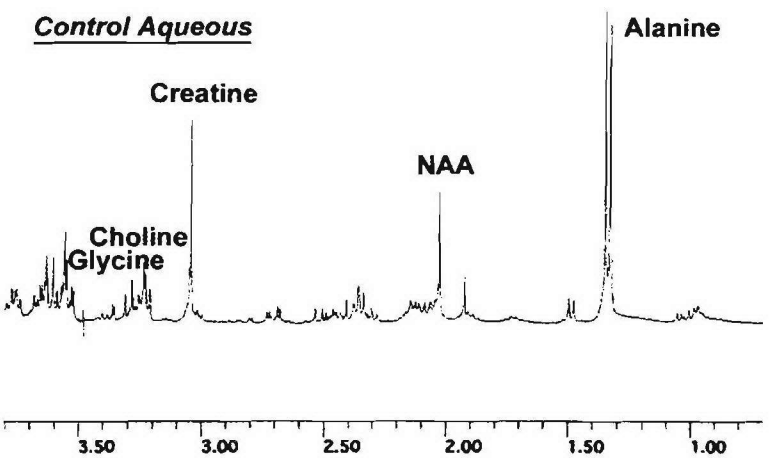

Figure 31

A video EEG was done with implantation of bilateral sphenoidal electrodes, which showed seizures in the left temporal region. After reviewing all testing as well as previous history, it was determined that the patient was a candidate for a left frontal temporal craniotomy. Patient had surgery done with pathology report reviewed. The temporal cortex revealed a hyper cellular molecular layer demonstrating multi foci of small aggregates of round to oval glial cells and a few astrocytes wit stray neurons in the center of some of them. It was best described as a glioneuronal homartia.

Post-surgery the patient has done well. Short-term memory has improved per family but long-term memory still remains a problem. Neuropsychological testing revealed that the patient had returned to pre-surgery baseline. Neurologically, the patient has ataxia and nystagmus post-surgery, but an elevated Dilantin level had been noted. Patient is seizure-free since OR and Dilantin continues to be weaned.

5.6.2 Case Report 2

A 36-year-old gentleman presented with medically intractable epilepsy of complete partial seizures since age 10. The frequency has been described as occurring one to six times a day with the posturing of the right extremities, involving staring and some clicking sounds. The patient reports that he seems to have a warning but his aura is very ill-defined.

The physical exam was normal. The neurological exam noted right homonymous hemianopia due to a focal area of atrophy in the left mesial occipital region. This was most likely a congenital abnormality or perinatal infarct. A decrease in the left deep tendon reflex was also noted. Past medical history is significant for a fever of 105° as a baby as well as hitting his head at age 4-5 after falling from a truck. Patient smokes 1-11/2 packs of cigarettes a day with a history of inability to sleep well.

A work up was done consisting of MRI, PET, and EEG. The MRI exam revealed an abnormal scan consistent with axial temporal sclerosis with sclerosis of the left hippocampal gyrus. No masses were demonstrated, but increased signal was noted

surrounding the temporal horn of the left lateral ventricle and to a lesser degree, the right lateral ventricle. A PET scan demonstrated hypo metabolism of the left temporal region. The EEG noted sharp focus in the left temporal region.

After reviewing all testing as well as past history, it was determined that the patient was a candidate for a left temporal lobectomy. The patient proceeded with the surgery and has been seizure-free for three months. The patient's only complaint at this time is an off-and-on headache. Patient remains on two anticonvulsants at this time.

5.6.2.1 Discussion

This preliminary data suggests differences between epileptic and normal hippocampi in the patterns and intensity of labeling by a monoclonal aPL against a PS-dependent epitope.

This research is ongoing and these preliminary results should be interpreted with caution. The methods used did not allow ultrastructural localization of the antigen to inner or outer membrane leaflet. However, the apparent peripheral labeling of numbers of small cells or processes with the absence of cytoplasmic reactivity in both pathologic hippocampi, contrasted with cytoplasmic labeling in the normal hippocampus, was of particular interest. Specific histological targets are currently being investigated. Preliminary observations of controls suggest reactivity in pathologic tissue is glial. These differences may reflect alterations in PL distribution in hippocampal sclerosis. However, the differences may also reflect changes in antigenic properties from sample treatment. While normal control tissue is from deceased subjects, removed and fixed 6 to 12 h post-mortem, patient tissue was fixed within minutes of excision. These concerns are currently being addressed through an animal model. These preliminary data suggest alterations in PS distribution may occur in hippocampal sclerosis.

In vitro MRS data are depicted in ***Figures 28-30***. Our preliminary in vitro MRS analysis for both subjects yielded some interesting findings:

1. The ratio of PtdS+SphM /PtdE+PL is elevated consistently from the pathological area to the surrounding tissue to control specimen
2. PtdA is markedly elevated in pathological specimen compared to surrounding tissue and control specimen
3. PtdC/PtdE is increased in the pathological specimen.
4. Glycine content is elevated in the pathological specimen compared to the surrounding tissue and normal control

Work is in progress to understand the significance of these preliminary biochemical findings in only two patients. While we are unsure of the significances, the difference between pathologic hippocampi and both surrounding normal tissue and control normal hippocampus were unmistakable. The increase in PtdA may be related to phospholipase D activity and membrane breakdown. The elevated glycine levels may relate to localized neurotoxicity. These differences may represent changes indicative of an active causal process in the sclerotic hippocampus, or merely be epiphenomenal markers of tissue deterioration. Future studies will address this question. We are in the process of expanding the number of patients in a multi-center investigation

Figure 32. PL AND Lipid Kinases

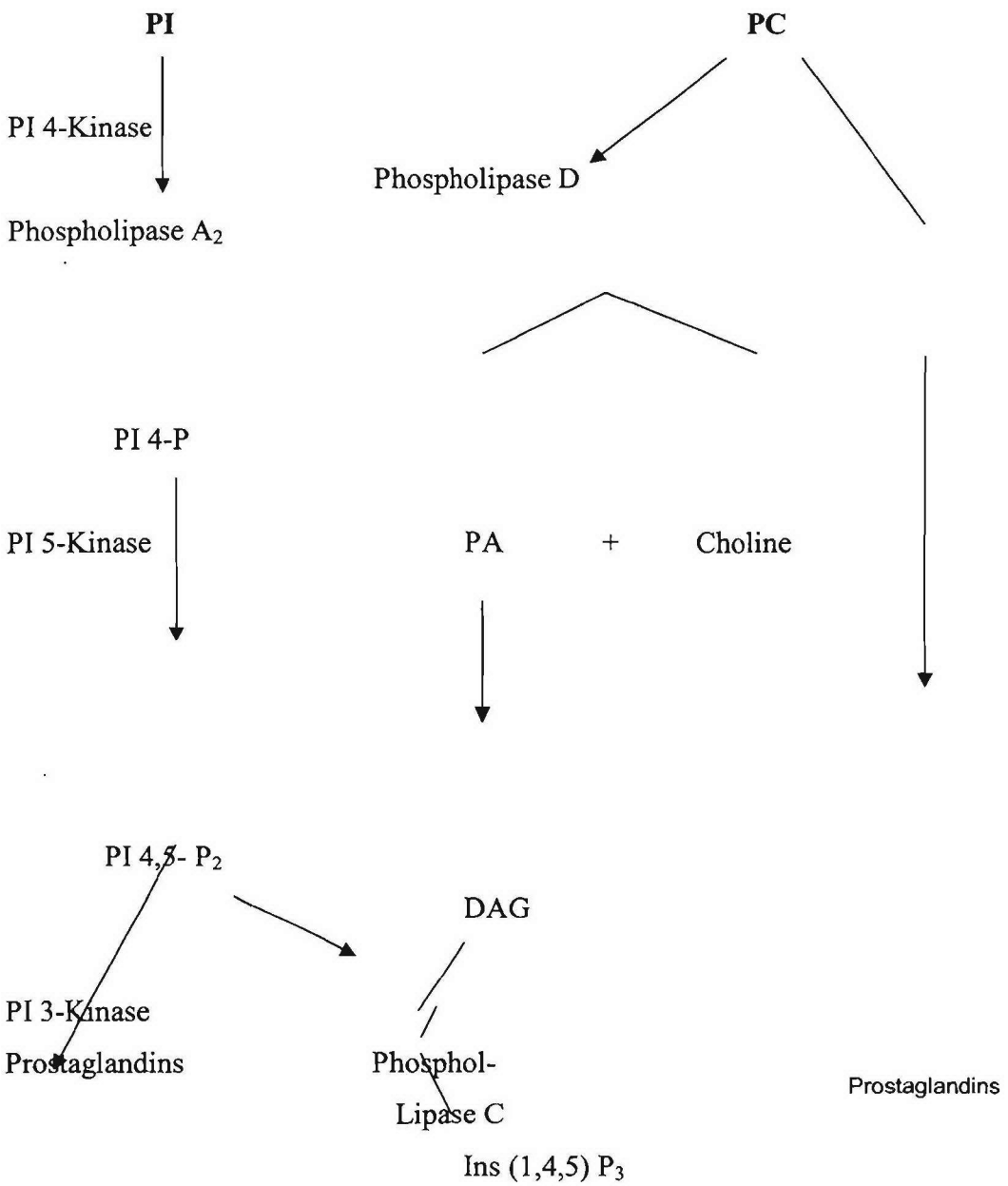

These studies suggest biochemical differences between normal hipp[illegible]mpal tissue and tissue from epilepsy patients diagnosed with hippocampal sclerosis. Work continues to understand the significance of these preliminary data. Conventional MRI and MRS defined the localization of changes and assisted neurosurgeons in determining the location and extent of surgical excision. In vitro MRS of excised hippocampus compared to adjacent temporal lobe and normal tissue showed unmistakable biochemical differences that suggest membrane breakdown and neurotoxicity. The complementary addition of immunohistochemistry may contribute to elucidation of the biochemical changes seen in MRS. The differences in neuronal labeling by a PS-dependent monoclonal antibody between normal control and pathologic hippocampi suggest changes that may be consistent with that seen in in vitro MRS. Whether this reflects upon an apoptotic PS externalization process remains unclear, as these studies were conducted on fixed tissue in which both membrane-bound and cytoplasmic PS targets were exposed. However, combining the MRS and immunohistochemical data suggests that the biochemical differences seen in MRS may not be accounted for by the loss of neurons alone. (Note: These results reflect investigations of only a few patients, and the study is ongoing to confirm and expand observations as tissue becomes available.)

5.6.3 Future Directions and Applications

1) Further studies of additional epilepsy patients by MRS and using anti-PS and additional antibodies against biomarkers are planned to elucidate the results seen in these preliminary studies.
2) Complimentary immunohistochemical and MRI/MRS investigations of animal models of epilepsy may prove useful in elucidating mechanisms of injury and response to therapies.
3) Integration and complementation of multi-parametric observations such as MRI, MRS and immunohistochemistry are providing information previously unavailable. New antibodies capable of identifying markers of biochemical processes and cellular metabolites indicative of abnormal processes are emerging rapidly. Development of batteries of immunohistochemical tests in conjunction

with MRI and MRS may prove useful in characterizing cellular mechanisms of disease processes or compound exposure.

4) Neurobehavioral testing of disease process and neurotoxicological compounds may be complimented by MRS and immunohistochemical studies. Complementation of comprehensive batteries of tests of each category is expected to provide exceptional insight into the function, biochemistry, and effect of injury in the brain.

5.7 Comparative Analysis of CT and FLAIR for the Detection of Hemorrhage

A total of 45 CT scans and 51 MR FLAIR images were read by the three neuroradiologists. The median age of the patients was 64 years (mean = 61, mode=82). The average time between patients' CT scan and MR FLAIR was 17 h and 28 min. All of the neuroradiologists' interpretations were compared to the CT scan findings. The total error rate for the CT scan readings was 2.27%, while the total error rate for the MR images was 9.80%. **Table 2** and **Table 3** show a break down of the total amount of correct and incorrect readings on both the bleeds and the controls.

	TOTAL CORRECT	TOTAL INCORRECT
CT CONTROL	36	1
CT BLEEDS	8	0
TOTAL	44	1
% ERROR RATE	2.27	

Table 2. CT scan readings: total correct and incorrect

	TOTAL CORRECT	TOTAL INCORRECT
FLAIR CONTROL	35	4
FLAIR BLEEDS	11	1
TOTAL	46	5
% ERROR RATE	9.80	

Table 3. MR FLAIR readings: total correct and incorrect

Two patients presented with highly identifiable acute intracranial hemorrhages on both CT and MR FLAIR images. A 55-year-old female presented to the ER with complaints of nausea and headache which she described as being behind her eyes and located in the middle of her head. She had been unsteady on her feet for a couple of days with previous falls noted. A physical exam was performed with the patient unable to open her eyes except for a slight slit. Her pupils were dilated and fixed and irregular. Lateral deviation of both eyes was noted as well the inability to look up or medially. A physical exam of the head revealed tenderness of the left occipital area. Past history is significant for hypertension, trigeminal neuralgia, psychosis and intermittent chest pain.

A CT was performed 1 h after admission to the hospital which showed an intracerebral hemorrhage localized to the cerebral peduncles, at midline (***Figure 33A***). An MRI was performed at 22 h past admission which also showed hemorrhage in the cerebral peduncles at midline (***Figure 33B***). Areas of ischemic demyelination in the right side of the cerebellum, in the basal ganglia and centrum semiovale bilaterally were also noted. Patient was discharged to a regional rehab center 10 days past admission with stable hypertension and inappropriate affect and behavior. On physical exam she could not open her eye lids related to the third nerve palsy. She then was admitted to a nursing home with significant apoptosis of the right eye and was considered legally blind. She continued to have frequent falls.

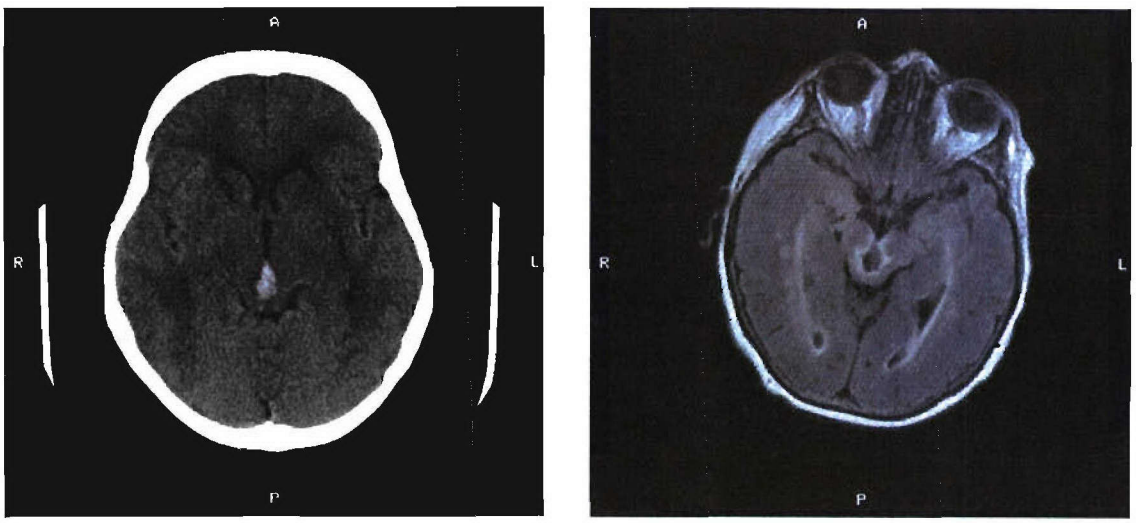

Figure 33A and B

A 64-year-old female was found unresponsive at home by her husband. Her husband stated that he heard her fall and found her lying on the bedroom floor. She has a history of diabetes and a blood sugar was initially done which was noted to be 141. She awoke by the time she arrived in the ER with no initial complaints. In ER she became symptomatic with complaints of nausea, vomiting, and headache. Physical exam noted right pupil round, left pupil irregular related to cataract removal, and paresis on lateral gaze of the left eye. Her facial folds were assymetrical with a facial droop on the left side below the eyes and at the nasolabial fold. A positive heart murmur was noted. Decreased deep tendon reflexes were noted on the left, as well as decreased muscle strength on the right. She was not able to do heel-to-shin on the left and a positive babinski reflex was noted on the left. Past history included diabetes type I since age 8. Patient has a history of probable transient ischemic attack (TIA), cataract removal from left eye, depression, diabetic retinopathy and a 50-year, 2 pack-a-day smoker.

Patient initially had completed the CT examination four and a half hours after arrival to ER which showed an intracranial hemorrhage around the intraventricular falx cerebri area (***Figures 34A and 34B***). Subsequent FLAIR MRI study demonstrated a right interhemispheric subdural hematoma with right frontal parietal interhemispheric cortical hypersignal involving the motor sensory region and cortex (***Figures 35A and 35B***). MR

data were obtained 20 h and 18 min following CT study. Basal ganglia and brain stem hypersignal consistent with small vessel disease was also noted. Patient did have surgery to remove the hematoma.

Figure 34A & B

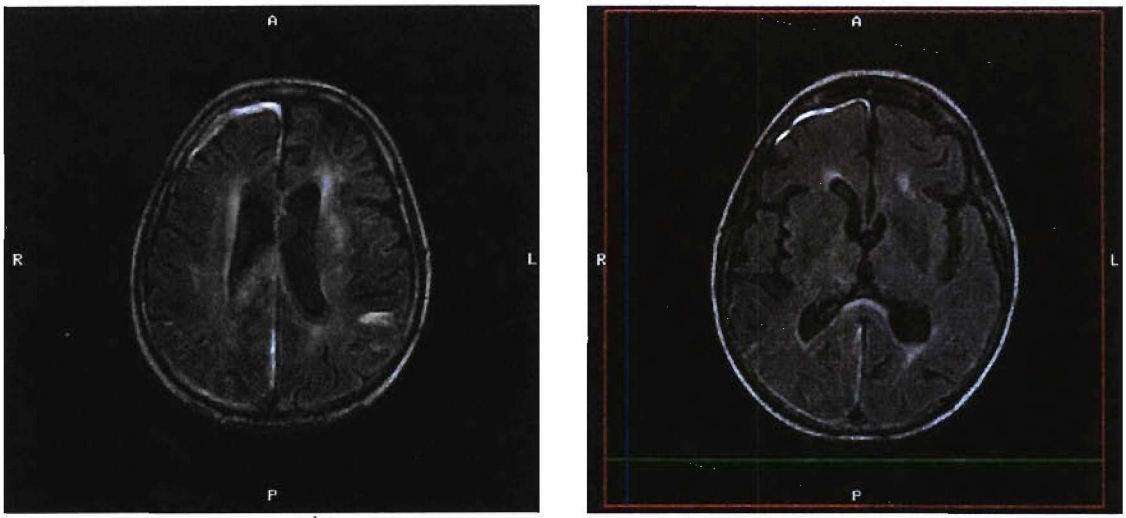

Figure 34A and B

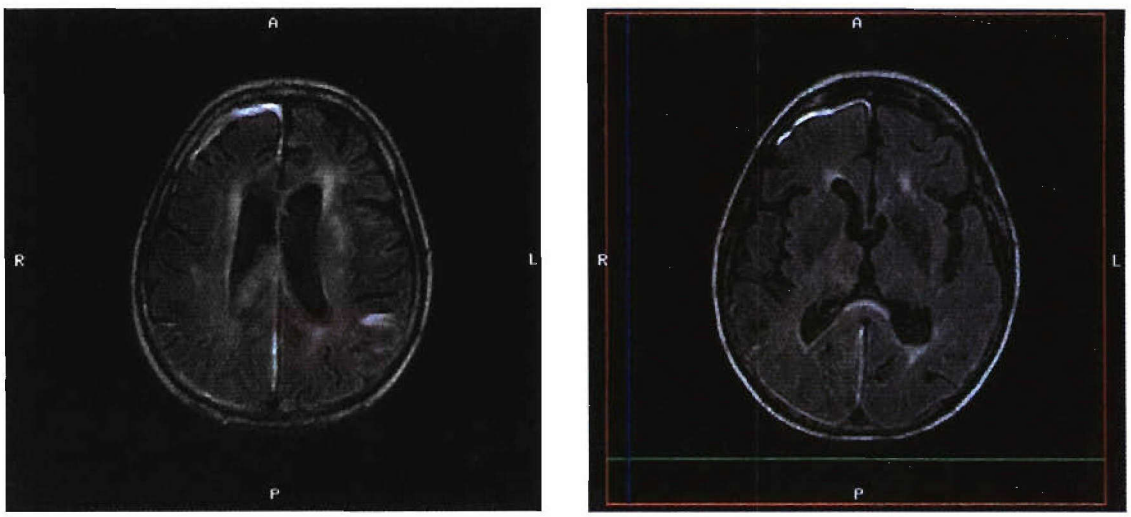

Figure 35A and B

Our results reflect the fact that more work is needed to determine MR FLAIR's role in the detection of hemotoma. The higher percent error rates for the radiologists' interpretation of the MR FLAIR images suggest that this method may not be as diagnostically accurate for the detection of acute and hyperacute intracranial hemorrhage (HICH). However, Case Studies 1 and 2 depict an accurate representation of hemorrhage in both CT scans and MR FLAIR images. We feel that the results of this study are confounded by a small sample size; more patients will be recruited to determine the efficacy of MR FLAIR in the detection of acute and HICH.

5.7.1 USAF Relevance

In our experiences as a community-oriented medical center, we believe that developing a stroke imaging center could be a great help to military health facilities in search of providing similar services to active personnel and veterans. We believe that the true value of MRI is that it offers information that shows the area and location of the infarct, the dynamic process going on, the pathophysiology, and the reduction in blood flow and increase in cerebral blood volume. The future of imaging in acute stroke management will be that MRI can be used "stand alone" to diagnose acute stroke and direct therapy.

5.7.2 Future Direction

We are proposing to use MRI in clinical trials to evaluate its potential role in management of stroke. The following will be our main focus:

1. Patient selection: The goal of image-based patient selection is to collect and analyze imaging data from stroke patients in acute and post stroke in order to narrow the range of patient characteristics with respect to their clinical manifestations and outcome. Studies will focus on acute DWI images in predicting final infarct size and the role of DWI/PWI mismatch in predicting salvageable area.
2. Proof of pharmacologic principle: We will examine the potential role of MRI as a marker of response to therapy, replicating the pre-clinical experiments in patients. The fundamental promise of drug discovery in acute stroke is that treatment will reduce the lesion size. MRI will be a cost-effective and rational imaging modality to make such evaluations in phase II or III of drug trials.

3. As an outcome measure; further studies in DWI/PWI characteristics will provide data regarding the efficacy of these techniques in predicting outcome.
4. Possible role of MRA in predicting stroke risk

5.8 Hippocampal Volumetric Measurements

5.8.1 Phase 1

The volume (Mean ± SD) of the right hippocampus was 2.86 ± 0.2 $cm^3$and 2.92 ± 0.2 cm^3 for measurements using AWW and Vitrea™, respectively. We did not observe any statistical significance between the two softwares as determined from a standard student *t*-test ($p = 0.8$). Our volumetric measurements compared favorably with reported literature values [2]. Study-study variations and intra-operator variations did not indicate significant variability as determined from the coefficient of variance in our volumetric measurements using either image-processing softwares. The error in our repeated MR measurements of the phantom volume (Mean, $n = 5$) compared to its known volume, was less than 3% using either Vitrea™ or AWW.

Our study confirms that the images processing software, Vitrea™, can produce reliable and accurate volumetric measurements. In the following, we summarize our findings:

Disadvantages of Using Vitrea:

1. Cost
2. Requires its own dedicated workstation.
3. Direct 3-D segmentation is not an option. One can segment the structure in 2-D and the software will reconstruct the results in 3-D.
4. The software does not allow users to use histogram data in making a decision about the voxels' relative signal intensity. Instead, voxels' relative signal intensity is obtained simply be leveling the window and visual instant feedback. This feature, however, can potentially making volumetric measurements more practical in a routine clinical setting.

Advantages of Using Vitrea™:

1 User-friendly software.
2 Vitrea™ allows both surface and volume rendering which can theoretically improve the accuracy of visual delineation as well as the volumetric measurement of the hippocampus.
3 Less time-consuming with respect to this particular application relative to the more widely used AWW 3.0.
4 Real-time volume rendering feedback in 3-D

5.8.2 Phase 2

Figure 36 depicts the process of hippocampal volumetric measurements on images acquired using temporal lobe coil and FSE-IR sequence post minimal pixal intensity (MIP) processing. The volume (Mean ± SD) of the right hippocampus was 3.01 ± 0.2 cm^3 and 2.95 ± 0.2 cm^3 using FSE-IR and SPGR-IR, respectively. The average time in minutes (Mean ± SD) for delineation using images obtained by FSE-IR sequence with a temporal lobe coil and SPGR-IR with a regular head-coil were 11.3 ± 1.5 and 18.0 ± 4.0, respectively. There was no statistically significant difference between the two sequences as determined by standard student *t*-test ($p = 0.8$). Study-study variations and intra-operator variations indicated no significant variability as determined from the coefficient of variance in volumetric measurements using either sequences.

We have shown that FSE-IR MR sequence using a temporal lobe coil could enhance clinical utilization of hippocampal volumetric measurements. One of the concerns was the acquisition time in which it normally takes approximately 11-14 min for acquiring images with FSE-IR in comparison to 4 min with SPGR. Consequently, we limit using this sequence to patients who can sustain prolonged scan times.

5.8.3 Phase 3

The KMC IRB has approved this project, and data is currently being prepared for the radiologists to analyze.

Hippocampal Volume Measurement in Vivo; Structure Tracing in Coronal Plane

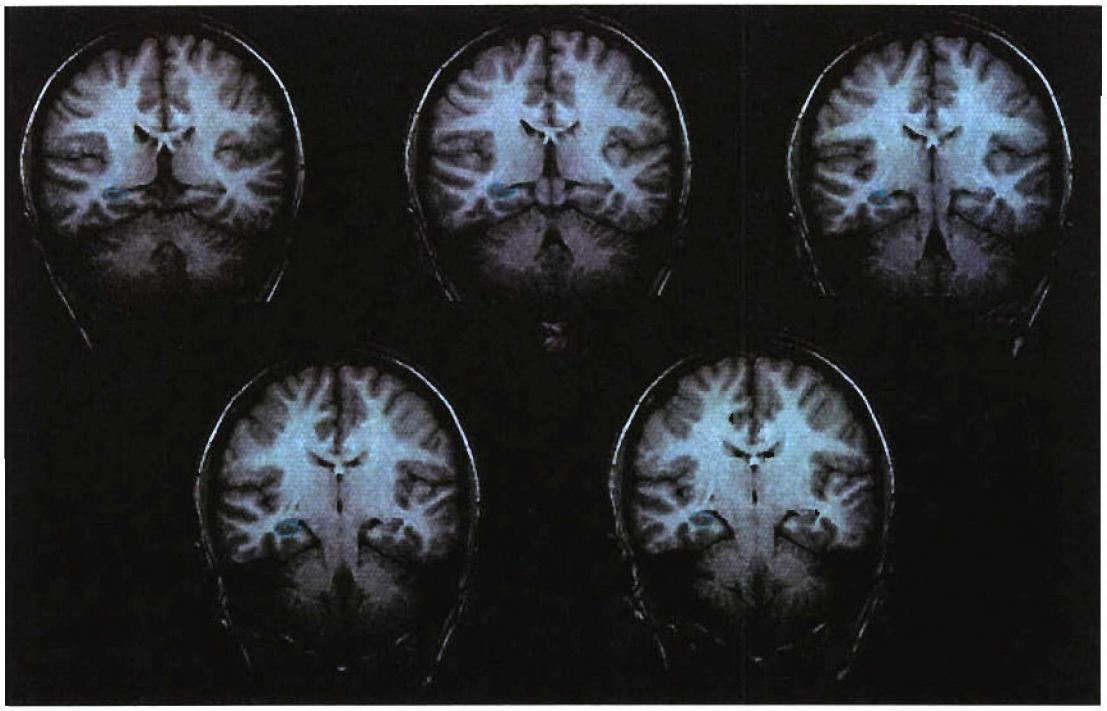

Figure 36. Samples of coronal images acquired with 3-D volumetric fSPGR pulse sequence (TI = 500 msec). *Images were acquired from a normal 25-year-old volunteer. Hippocampus outlining was performed using Vitrea™.*

In Vivo Segmentation of the Hippocampus

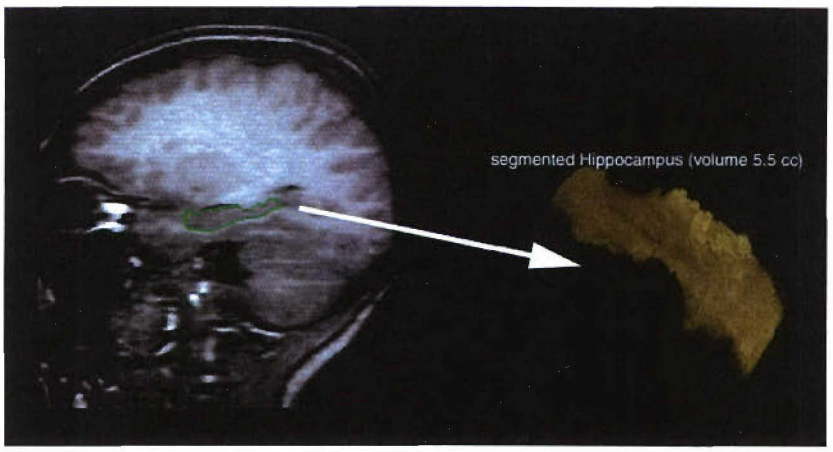

Figure 37. The process of sagital viewing of the hippocampus post-surface rendering in the coronal plane. *Such an operation enables the operator to assess the accuracy of hippocampal contouring in the coronal images. A segmented right hippocampus of a 25-year-old volunteer is also displayed. For hippocampal volumetric measurements, the hippocamus proper, denate gyrus, fimbria, subiculum, intralimbic gyrus, and uncinate gyrus will be included. The outlining of the hippocampus always proceeded from anterior to posterior.*

5.9 Alleviating Claustrophobia with 3-D Audio Display

Preliminary analysis of the results from these initial 10 subjects shows a number of significant differences between the VE and non-VE conditions. Subjects' subjective ratings of comfort were higher in the VE condition than in the non-VE condition, but this difference failed to reach significance, $t(7)=1.56$, $p=0.08$. Similarly, subjective ratings of their ability to cope with the situation were significantly higher in the VE than the non-VE condition, $t(7)=2.30$, $p=0.03$. Although the physiological data have not yet been analyzed, the Autonomic-Emotional scale of the EMAS state measure was significantly lower after the VE condition than after the non-VE condition, $t(9)=-2.03$, $p=0.04$. In addition, although all 10 subjects were able to complete the full 20-min exposure under the VE condition, two of these same 10 subjects could not complete the 20-min exposure under the non-VE condition.

This research is ongoing and these preliminary results should be interpreted with caution. Nevertheless, these findings are very encouraging and indicate that VE technology has the potential to significantly reduce the claustrophobic response in MRI patients.

5.9.1 USAF Applications

The military could potentially benefit from virtual reality environment for the creation of simulation training programs. Such VE can provide a risk-free realistic learning environment for the spectrum of field training. This will, in turn, enhance limited hands-on training opportunities and revolutionize the way we train in peace. High-fidelity modeling developed in our research program will permit manufacturers and military affiliated contractors to prototype new VE-based devices

5.9.2 Future Direction

In collaboration with our colleagues at WSU and WPAFB, we plan to experiment with other forms of VE and their impact on human psycho-physiological responses. We hypothesize that VE also could potentially aid in overcoming problems such as claustrophobia that may be encountered by personnel in enclosed settings such as cockpits.

5.10 Active Noise Reduction in MRI Environment

Using a fiber optic microphone and transducers developed under contract for the AFRL, a predictive algorithm was developed and will be incorporated into a custom circuit board (***Figure 28***). The device was designed and patented for active noise reduction in the MRI

environment (Attachment # 1 hereto.)

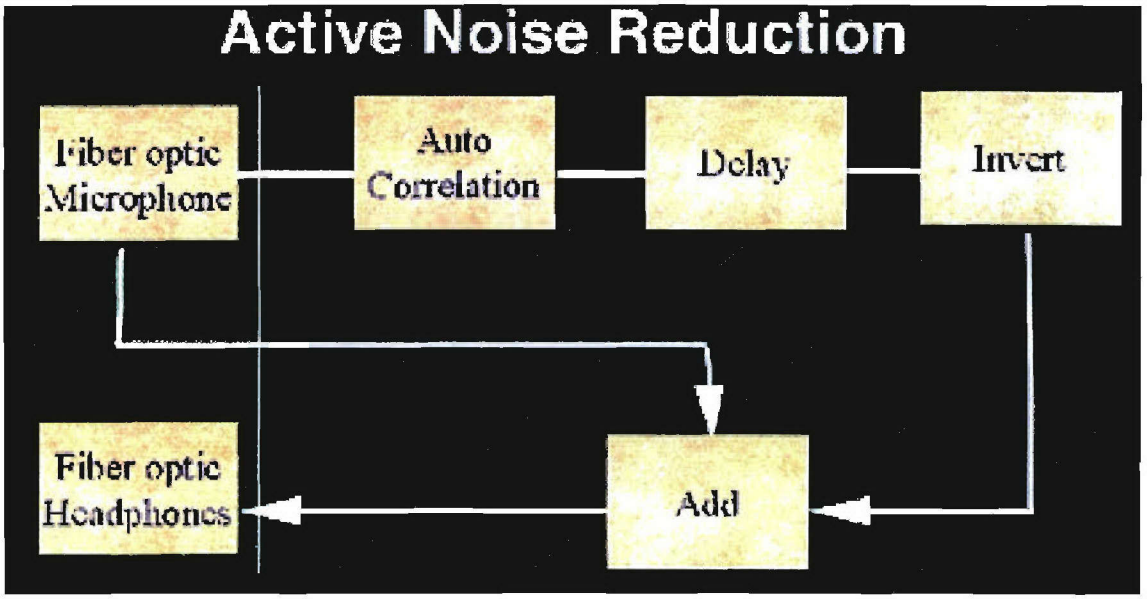

Figure 38

The device will now enter the testing phase and is expected to provide significant noise reduction, allowing for greater comfort and hearing safety in the MRI environment. This is not only significant for current MRI use, but may be important for increasing the power and subsequent noise in future MRI development.

5.11 Distributed Neuroscience Data Project

The first phase of the project began June 15, 2000. The segments of the first phase are: 1) Patient Records; 2) Epilepsy and 3) Tumor. These segments have been designed and are being tested. Plans are underway to include Stroke, Gamma Knife, Aneurysm, and Sleep Lab in the database.

An important developmental objective was ease of use. If an application is too complicated, it will not be used. In addition, a poorly designed interface may cause users to incorrectly enter information. By creating an engaging, easy-to-use interface, common data can easily be shared between all users. ***Figure 39*** illustrates the common toolbar that users will see when they launch the program.

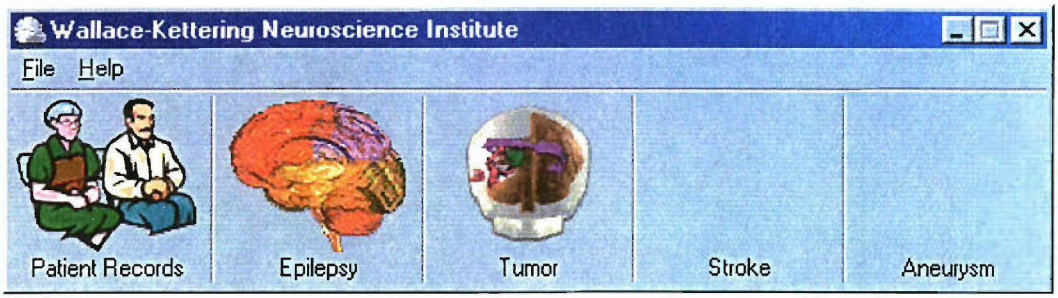

Figure 39. The design is simple and the interface is easy to use. *The application is divided into Patient Records, Epilepsy, and Tumor. More areas such as stroke, aneurysm, and gamma knife are being developed. Each screen allows a user to easily capture medical information. The starting screens within each area are shown below.*

Patient Records screen

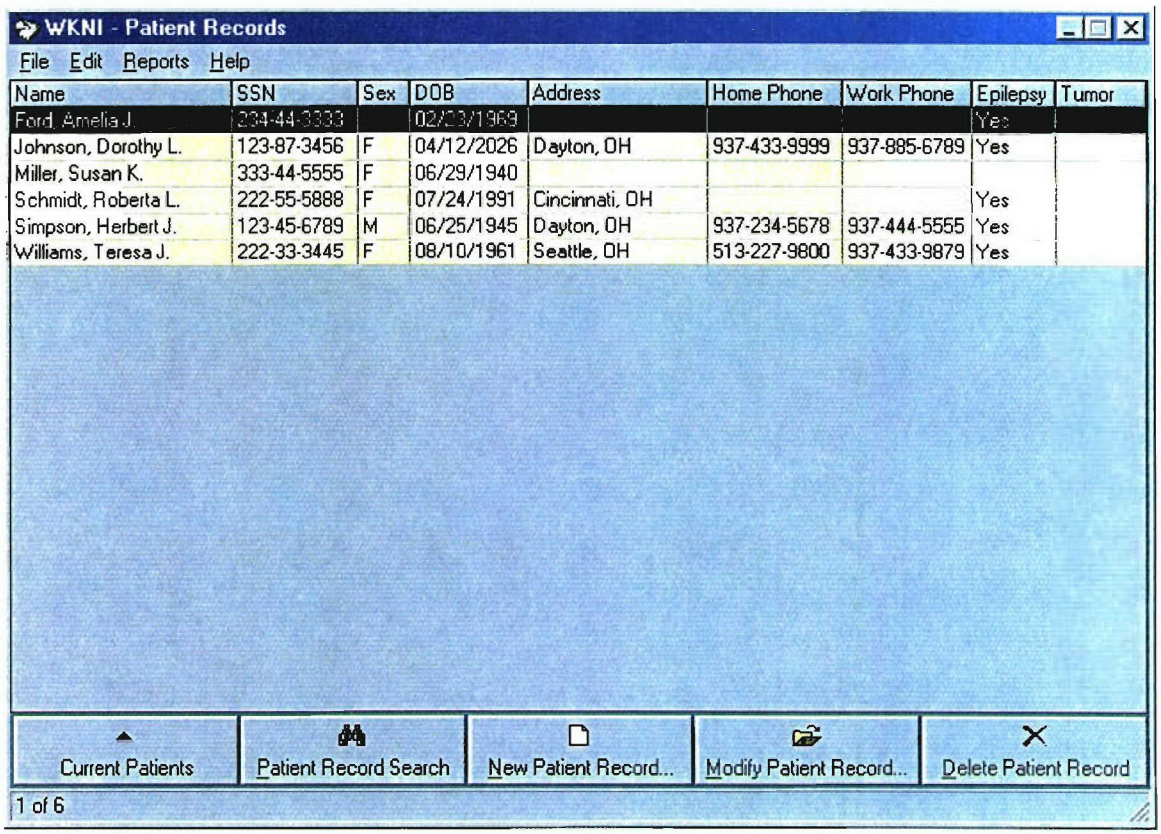

Figure 40. All patient demographic information such as Name, Social Security Number, Sex, and Date of Birth is entered on the Patient Records screen (all above

data is fictitious). *This is common data that is accessible to all doctors and researchers at WKNI. This functionality speaks to another important objective, which is creating an environment that allows researchers in different areas to share common data. From this screen, any user can easily add, modify, or delete patient demographic information.*

Epilepsy screen

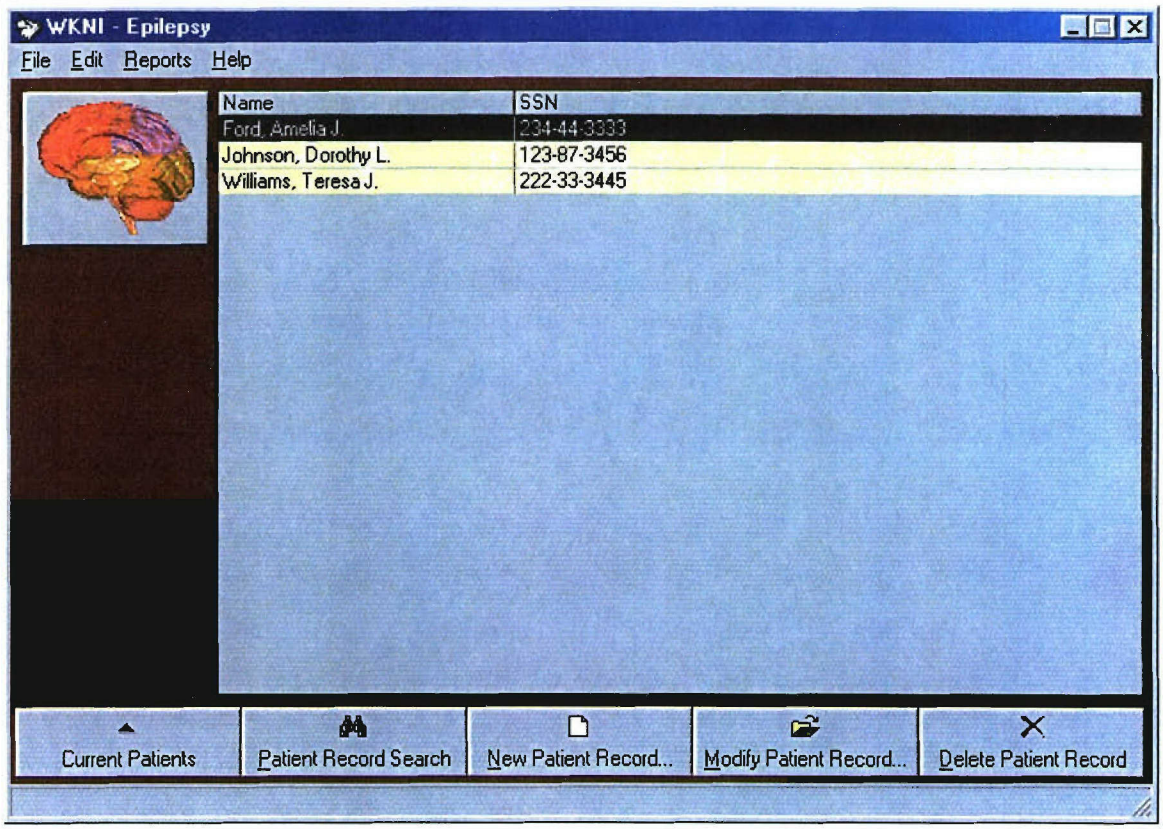

Figure 41. Details about an epilepsy patient's condition and treatment are entered in the epilepsy screens (all data above is fictitious). *Here, a user can view current patients, deceased patients, or inactive patients. The user can easily add, modify, or delete an epilepsy patient from this screen.*

Tumor screen

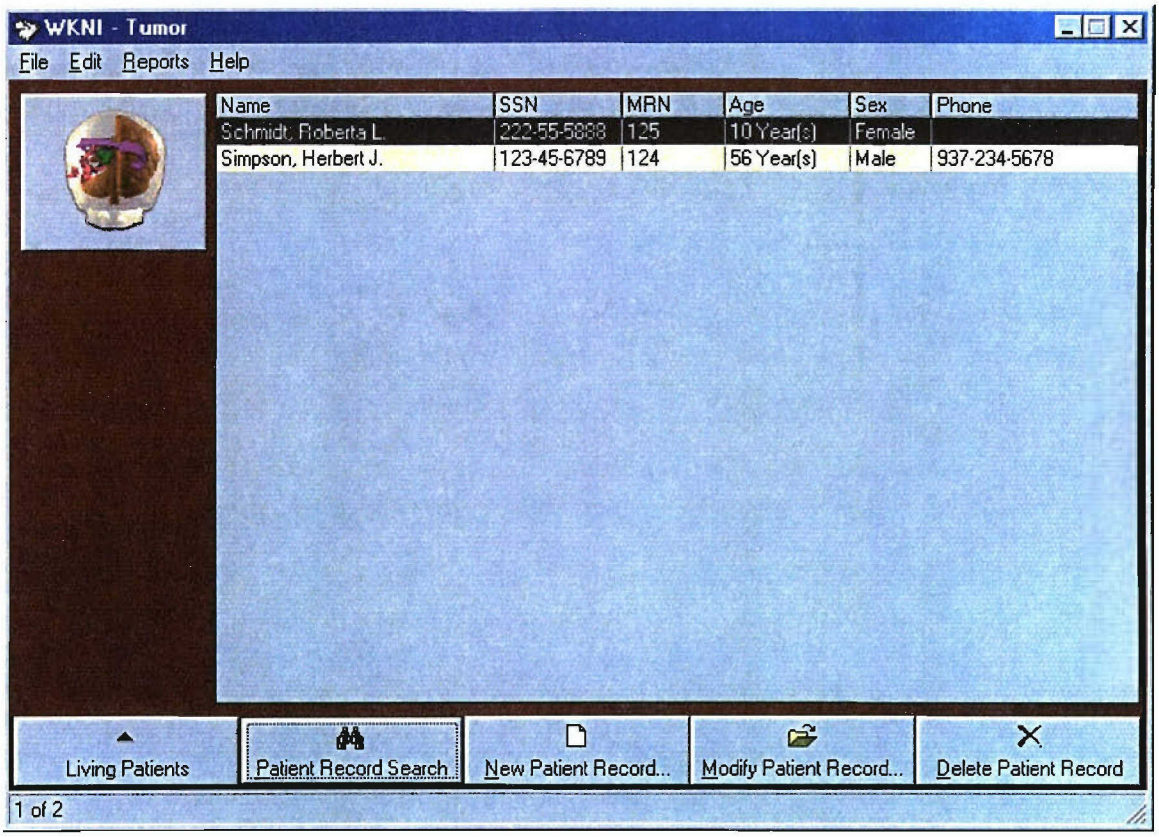

Figure 42. Details about a tumor patient's condition and treatment are entered in the tumor screens (all data above is fictitious). *Here, a user can view living or deceased patients, or may view both on the same screen. Users may also view inactive patients on this screen. Here too, the user can easily add, modify, or delete a patient. A user can perform a search or generate a report from any of the screens above.*

5.11.1 Future Directions and Applications

1) The database will be implemented throughout the WKNI community of physicians and scientists, and include epilepsy, stroke, tumor, schizophrenia and MS. Other categories will be added as needed.
2) Because the database is secure, it can be implemented or accessed from multiple sites, including WPAFB, WSU, or any KMCN facility.
3) The database can also be implemented in other locations and be tailored securely for access to the organization's targets.

5.12 Internet Browser-Based Imaging Access

The WKNI and WPAFB Hospital, in conjunction with KMCN, implemented a cost-effective solution to resolve the issue of broad image distribution. This solution was the Stentor's iSite web server, which is fed directly from KMCN's PACS system. The server provides access to images and reports via both the Intranet and Internet. This system eliminated the need for costly diagnostic workstations and, yet, provides the same image quality and tools needed to evaluate a study. This system also provides the ability for multiple users at multiple locations to view the same image simultaneously. This allows for more expedient patient diagnosis, physician-to-physician consultation from remote locations, and the correction or improvement of poor images, in addition to the obvious reductions in film costs and expense for courier service. Another valuable aspect for patient care is the ability of physicians to be out of town and still view the study that they need by simply opening a web browser and connecting to the Stentor server.

The Stentor iSite Web Server provides advantages over alternatives through the use of the Stentor iSyntax technology, which matches the delivery of image data to the speed of human perception. Based on the mathematical representations of images called wavelets, iSyntax delivers only the coefficients that are required for the displayed view, thus making the Stentor image delivery method more efficient and effective than alternative competitive techniques running with the same fidelity. iSyntax technology provides full resolution images in real-time without compromising speed, image quality, or the hospital network. This eliminates the traditional separation between radiology and the other parts of the hospital, allowing collaboration from any computer terminal with an Internet connection, without compromising patient confidentiality.

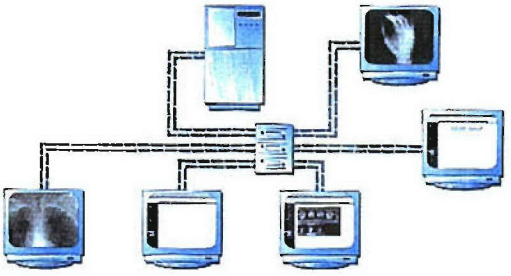

Figure 43. Syntax™ technology network transfer.

5.12.1 Future Directions and Applications

The Stentor image access system can be implemented from any location and provide secure, real-time, high resolution image presentation to physicians and researchers at multiple selected locations. This system provides for 3-D image presentation previously unavailable for transmission. Therefore, applications are wide for both medical, research and military applications. A limitation of Stentor is the ability to manage only one file format. A future focus may be to adapt this system for a multitude of images and image types and formats tailored for specific demand.

5.13 Functional Imaging in Tumefactant MS

A 36-year-old female presented with complaints of subacute (10 days) onset of dysarthria and right hemi-paresis. She had no neurological complaints prior to the present illness. She gave a history of mild hypertension for 2 years not requiring medication and was a chronic smoker. She had a family history for hypertension and diabetes.

Gadolinium-enhanced magnetic resonance imaging (gd-MRI) of the brain at the time of admission revealed a single enhancing 1.2×1.4 cm area of hypersignal in the left corona radiata on T_2-W images. (***Fig. 44***). Differential diagnoses entertained were a low-grade tumor versus a tumefactant plaque of MS and more remotely an infarct.

Given these differential diagnoses, it was decided to study the lesion further by metabolic imaging. PET scanning using ^{18}F-FDG and ^{11}Cmet was done. The glucose images demonstrated glucose uptake in the lesion that was more than white matter but much less than in cortical regions. The methionine study demonstrated a focal area of increased ^{11}Cmet uptake in the deep white matter of the left frontal parietal region corresponding to the enhancing abnormality noted on the MRI scan (Fig.44). The impression therefore on the glucose and methionine PET images was a low-grade glioma. Nevertheless we could not definitively rule out an inflammatory lesion, even though an infarction was ruled out.

Since the differentiation of tumor versus an inflammatory lesion could not be resolved fully by the above imaging, further characterization of the lesion was undertaken using ^{11}C-cho PET and ^{1}H-MRS. It was presumed that a positive choline uptake would make the diagnosis in favor of a tumor and vice-versa. However, ^{11}C-cho PET imaging, contrary to expectations, revealed a mild focus of choline uptake, which certainly was unlike any tumor, but was not entirely negative (Fig.44).

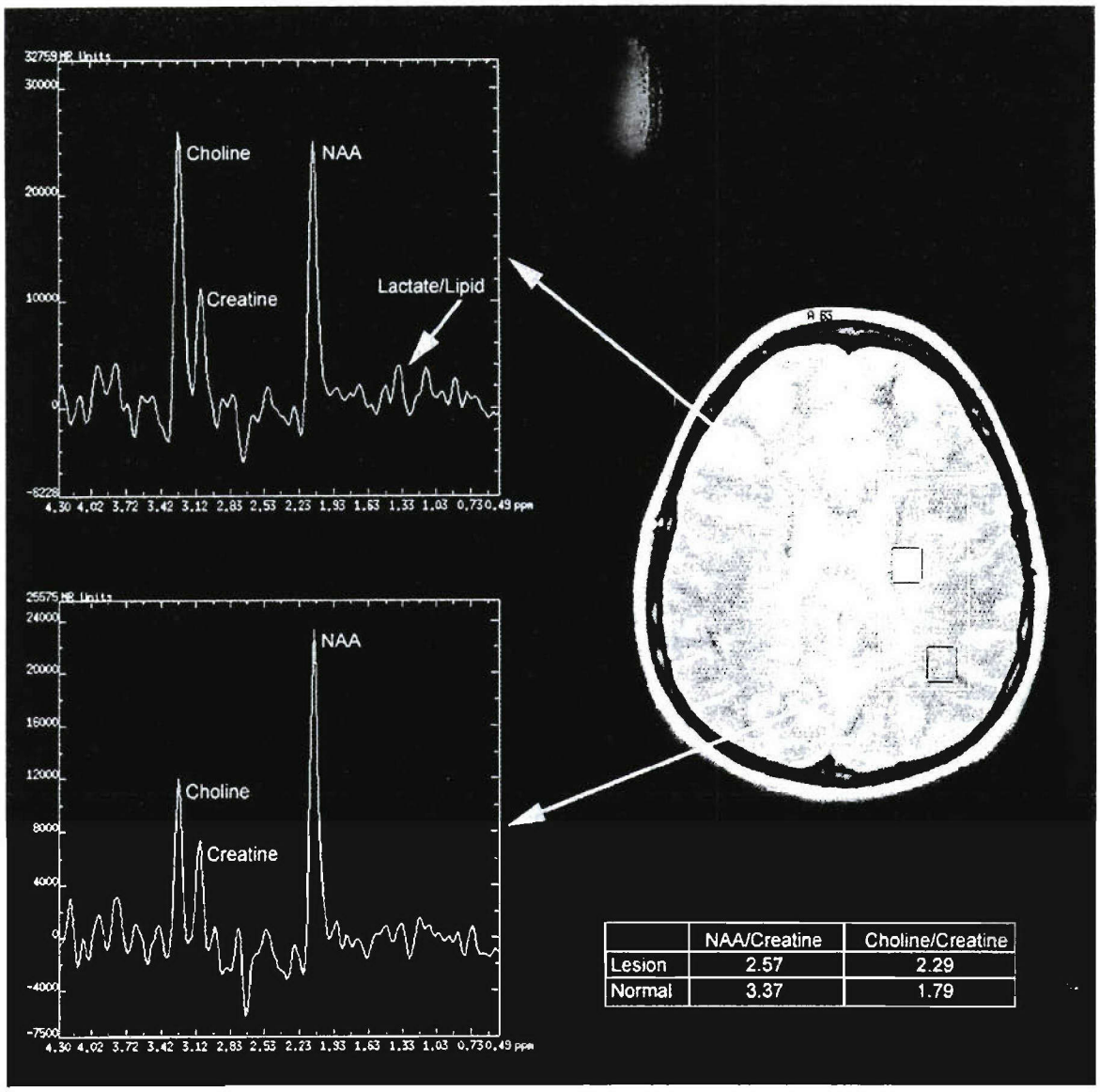

Figure 44. Gd-MRI and the co-registered images of PET showing a single enhancing 1.2×1.4 cm area of hyper signal in the left corona radiata on T_2W images on the MRI of the brain; prominent ^{11}Cmet, mild glucose and choline uptake in the lesion. *^{1}H-MRS image showing an increased peak of choline with a mean choline/Cr ratio of 2.29 as against a control of 1.79 and a reduced NAA peak with a mean NAA/Cr ratio of 2.57 as against 3.37 in the* control.

^{1}H-MRS showed an increased peak of choline with a mean choline/Cr ratio of 2.29 against a control of 1.79. The mean NAA peak was reduced with a mean NAA/Cr ratio of 2.57 against 3.37 in the control. An elevated lactate peak was also noted (***Fig. 45***). The

lesion volume was 2.6 cc. The findings on MRS strongly suggested a demyelinating pathology (Fig. 45).

A CSF analysis was then carried out to substantiate MS. CSF analysis showed no cells and an elevated protein of 65 mg%. There were no oligoclonal bands but MBP was positive.

Following the CSF report, the patient was started on a short course of high-dose steroids (1000 mg of solumedrol/i.v/day/3 days) followed by oral steroids tapered over the next 10 days. She improved rapidly and recovered fully with no residual neurological deficit over the next 10 days.

A repeat MRI scan done three weeks later showed a mild decrease in the initial hyperintense lesion in the left corona radiata. However, two other lesions were now seen on the FLAIR sequence in the white matter. This lends further credence to primary demyelinating plaques as the etiology. Repeat MRS study done at the same time showed a decrease in the ratios closer to normal (NAA/Cr: 2.53 versus 2.9 and choline/Cr: 2.26 versus 2.1) (**Table 4**).

	Initial Study		**Repeat Study**	
	NAA/Cr	Choline/Cr	NAA/Cr	Choline/Cr
Patient	2.57	2.29	2.53	2.26
Control	3.37	1.79	2.9	2.1

Table 4

Imaging studies in MS usually reveal multiple small plaques ranging from a few millimeters to 16 mm in size [51]. However, MS sometimes presents as a large solitary mass lesion that is indistinguishable from a brain tumor. Recognition of a limited mass effect and surrounding edema in considering the size of the lesion favored a demyelinating lesion in our case. MS simulating a single mass lesion has been described in literature.

Acute plaques are characterized by edema and some demyelination, while chronic plaques are characterized by gliosis, and to some extent, neuronal loss. There have been several studies of MRS in MS [22-24, 43, 52]. Acute plaques can show an increase of choline, lactate (Lac), and mobile lipid peaks (products of myelin breakdown). The increase of choline signal is due to the release of Pcho and GPC during active demyelination. In MS plaques, ^{1}H MRS has shown a reversible decrease of NAA, which suggest axonal damage and/or impairment. We found a relatively decreased NAA/Cr ratio and an elevated choline/Cr ratio in the lesion. This agrees with reports in the literature. An elevated lactate peak represented inflammation. In contrast, low-grade gliomas in contrast, are characterized by low NAA, strongly elevated choline and inositol and variable lactate levels.

PET showed a very minimally increased glucose uptake in our case, which was consistent with an inflammatory lesion. It is possible that, in this instance, the stage of the lesion was sub-acute to chronic.

Unlike the high uptake seen in tumors, we found a very faint uptake of choline in our patient. Once again, this may represent a stable plaque with relatively decreased rate of ongoing demyelination.

The above report therefore sums up the metabolic characterization of a demyelinating lesion, which may mimic a neoplasm on structural imaging such as an MRI. The demyelinating plaque in our case exhibited a low-glucose uptake, prominent methionine uptake and a minimal choline uptake on the PET studies. MRS data showed an increased choline/Cr ratio and a decreased NAA/Cr ratio which demonstrated a return to near normal ratios on follow-up study.

5.13.1 USAF Relevance

Our current investigation has further demonstrated the importance in utilization of multi-parameter biochemical imaging in studying the in vivo metabolism. Such studies provide

an important framework for future investigations relevant to US military, most significantly to the military Tri-Service (Army, Navy & Marines, Air Force) Deployment Toxicology Assessment Program (DTAP). MRS and newly synthesized PET radio-ligands could potentially be utilized in human risk assessment to various chemicals/neurotoxins during military deployment. A good example of how our techniques could provide benefit to military toxicology program will be applying our techniques to study Gulf War Syndrome.

5.13.2 Future Directions

Future studies will be undertaken to understand how such metabolic alterations might be impacted by various neuropathologies. Our objective will be to utilize the combination of these imaging techniques in identifying various lesions that are indistinguishable. We will collect data from patients who have received a comprehensive PET examination including FDG, methionine and choline in conjunction with MRS and MR. We will then use the PR models developed under sponsorship of our cooperative agreement in assessing the predictive value of these techniques in various neurological disorders.

5.14 Spectroscopic Imaging Biopsy Guidance

5.14.1 Case Report

A 39-year-old gentleman presented to his family care physician with headaches occuring over the past 6 weeks. The headaches frequently occurred in the morning. He had a history of sinusitis and it was felt that this was a sinus infection. Patient was treated with antibiotics without relief of the headaches and then developed right arm numbness. A CT was performed which showed a left thalamic lesion measuring 3x3.6 cm with mass effect and a left-to-right shift with hydrocephalus. Patient's past history is significant for sinusitis, hypertension and a broken nose. A physical exam was performed which was noted for a drift on the right side, and decreased rapid alternating movements on the right side. A stereotactic brain biopsy was performed which showed a grade 4 astrocytoma. Patient is now undergoing chemotherapy and requires a walker for balance.

We have utilized a simple model to predict the site within tumor that might possibly provide the highest yield for biopsy. Data were post-processed and delivered to the surgical suite. Surgical biopsies were obtained from locations referenced on MR images by guidance with a surgical navigation system. Studies are in progress to determine the efficacy of this procedure.

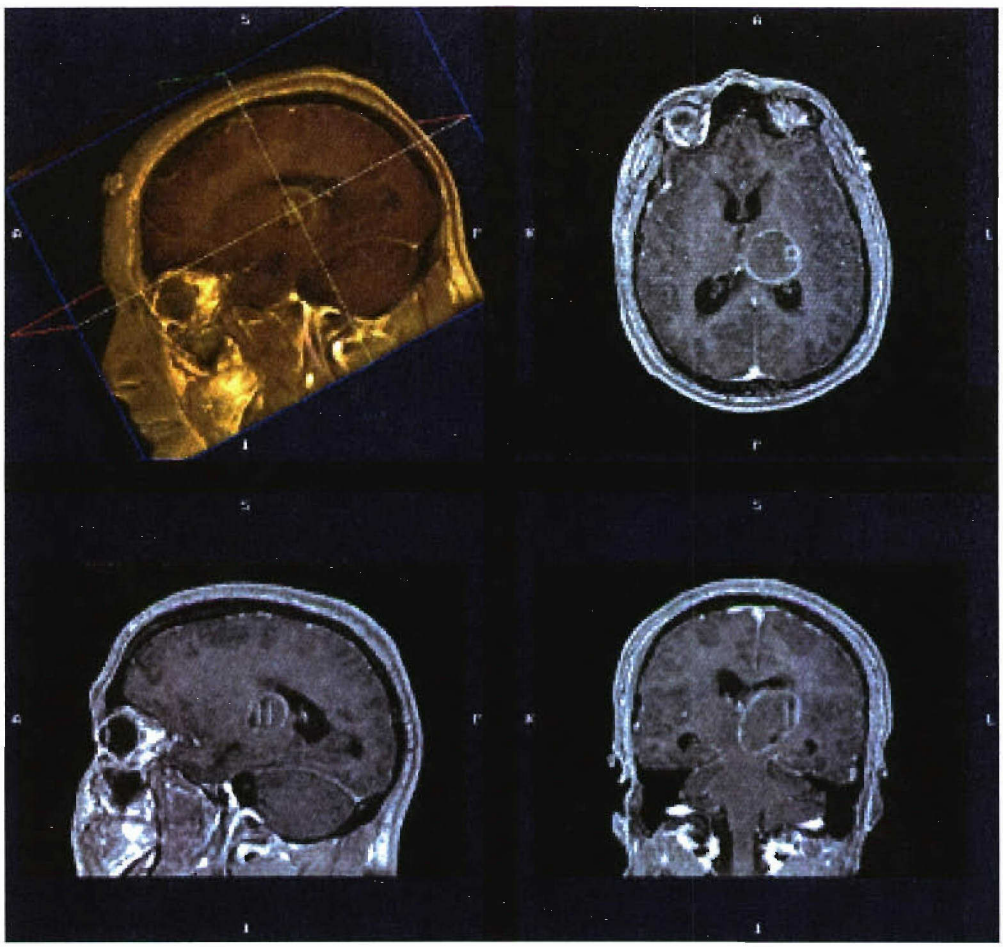

Figure 45

5.15 High-Speed Neuroimaging in Management of Stroke

5.15.1 Procedure

Patient was a 73-year-old white male with a previous history of one episode of vasovagal syncope approximately 5 years ago and no other significant past medical history, who developed the sudden onset of confusion and a receptive aphasia, at approximately 2:00-2:30 pm. According to his family, however, the symptoms might have occurred earlier in

the morning. At 2:30 pm, he began to stagger and walked about in a confused manner after exiting a store. There was no cardiac history or history of hypertension. MR and CT data were acquired approximately 3 h post-arrival in the ER. The patient was transported to the inpatient unit for further evaluation. There the patient remained under observation, during which time clinical observations were made for evidence for worsening and recurrence. Patient was discharged to a rehabilitation center in stable condition.

A second set of MR and CT scans were acquired prior to discharge. Data from CT scan indicated no acute abnormality (data not shown).

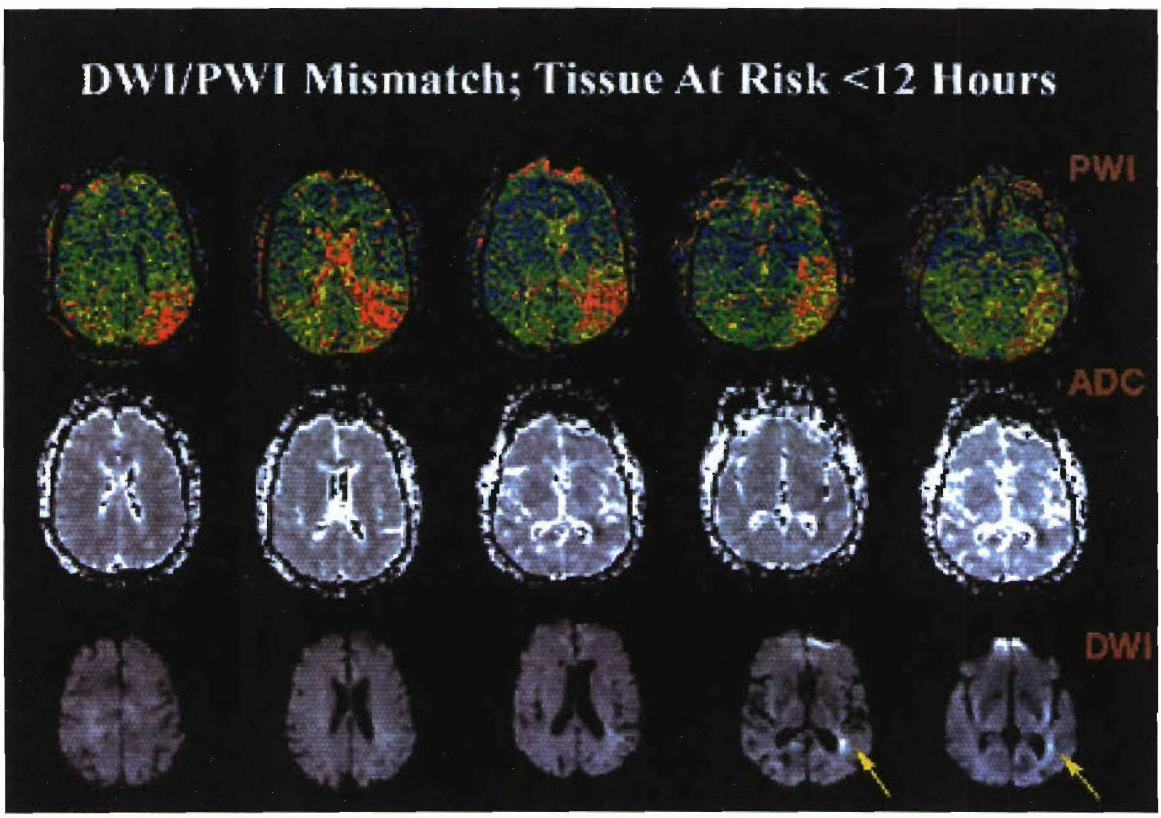

Figure 46

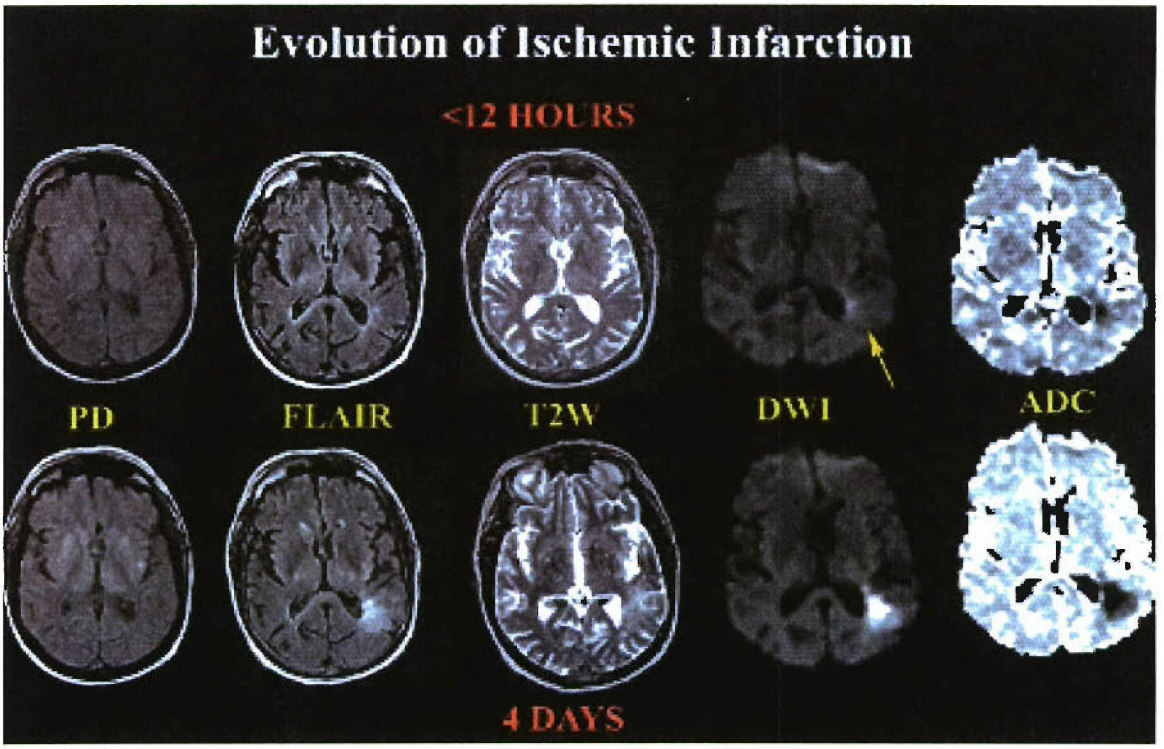

Figure 47

5.15.2 Human Factors Analysis

The results of the human factors analysis of the stroke team system indicated that team members are attempting to move toward a common goal, but there are issues relating to teamwork, communication and situation awareness. The team members did not share a common mental model of the entire process which can cause some systems to slow while team members are trying to communicate and coordinate with each other. A two-way paging system was tested to solve this problem, but only allowed some team members to communicate and reach one another easily. Team members were sometimes unaware of which stage they were in the process, could not always associate times within each stage, or determine what their role was during that stage.

In addition, the system lacked a central place to which all information converges. As a result, team members were often contacting various members to determine what they had accomplished, at which stage they were, and the results and locations of other team members.

A summary of initial recommendations includes:

1) Conduct an in-depth human factors analysis to gather objective data, including measurements of timing of information and variability in the process;

2) Develop a system in which information and current stages in the process converge to provide a quick update to team members;

3) Develop a technique to notify everyone in the ER when there is a stroke patient so that all tasks can begin in parallel;

4) Develop specific communication protocols for using the paging system;

5) Make results from lab and radiology more readily available to all team members;

6) Provide training to ER nurses on the stroke procedures and NIHSS to become certified in its use;

7) Use the EMS time in transit to prepare for the stroke patient;

8) Evaluate the pharmaceutical delivery process to determine the variability of drug availability in the Pyxis system;

9) Evaluate staff workload;

10) Determine ways to provide for a more rapid incorporation of stroke care training, techniques and protocols; and

11) Evaluate the layout of the ER as it directly affects workload and communication.

5.16 3-D Brain Functional Imaging Data Deliverance to Stereotactic Neuronavigational Instruments

A 49-year-old male presented with a sudden onset of localized right facial and right upper extremity seizures. Patient reported a 7-10-day prior history of trouble picking up objects with his right hand that required fine motor control. Patient's past history is only significant for knee surgery. The patient physical exam revealed mild right facial weakness, decreased grasp of 4/5 of the right arm, and decreased right arm swing. An unsteady, wide-based gait was also noted.

A CT was performed which showed a left-sided lesion. An MRI was then performed which showed a 3-cm mass in the posterior left frontal lobe. A biopsy was performed which showed a high-grade glioma. A surgical resection was not possible because of the proximity of the lesion to the motor strip. Chemotherapy/radiotherapy was recommended with Gamma Knife stereotactic radiosurgery performed. Patient is now undergoing chemotherapy.

Our objectives were met in this study and they include: 1) optimizing MR data acquisition methods; 2) post-processing of data using Medx; and 3) 3-D brain functional imaging data were delivered to stereotactic neuronavigational instruments utilized in neurosurgery operating theater.

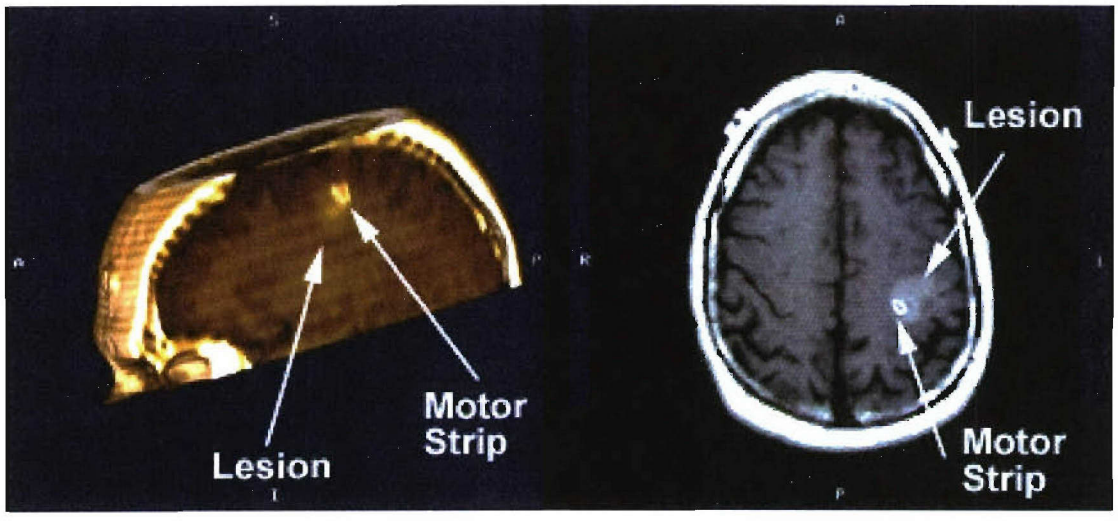

Figure 48

6.0 Future Use of Acquired Equipment

6.1 MRI Hardware and Software Equipment

1. Development of novel MR imaging techniques for automated MR volumetry.
2. Designing fMRI paradigms for diagnosis and monitoring therapy in memory disorder patients.
3. MRS and Gamma Knife radiosurgery in the management of brain metastases.
4. Software tool development for MRS analysis.
5. Development and implementation of 3-D brain functional imaging data including BOLD, CSI and tensor for stereotactic neuronavigational instruments utilized in the neurosurgery operating theater.
6. MNS in diagnosis and classification of various memory disorders.
7. Surface coil development for high-resolution imaging.
8. Functional imaging in MS patients.
9. MNS spectroscopy in schizophrenia.

6.2 Computer Hardware and Software

1. Visual cortex mapping of schizophrenics.
2. 3-D brain functional imaging data deliverance to stereotactic neuronavigational instruments.
3. Development of novel and secure methods for internet browser-based imaging access.
4. Development of computer-assisted communication technologies in acute patient care.
5. Develop technologies assisting in inter-disciplinary data communication including remote access to brain monitoring units to stroke team in management of stroke.

6.3 WKNI Laboratory Equipment at COX Research Institute

1. Nicotinic receptors on circulating lymphocytes of smokers and recovering tobacco users.
2. PL metabolism in human brain tumor cell lines.
3. Understanding the pathophysiologic mechanisms of brain damage and translating this insight into improved patient care in stroke.
4. Physiological role of aPLs in pathogenisis of neurological disorders.

References

1 Castillo M, Kwock L. Proton MR spectroscopy of common brain tumors. Neuroimaging Clin N Am 1998;8(4):733-752.

2 Nelson SJ et al. Volume MRI and MRSI techniques for the quantitation of treatment response in brain tumors: presentation of a detailed case study. J Magn Reson Imaging 1997;7(6):1146-1152.

3 Nelson SJ, Vigneron DB, Dillon WP. Serial evaluation of patients with brain tumors using volume MRI and 3D 1H MRSI. NMR Biomed 1999;12(3):123-138.

4 Tate AR et al. Towards a method for automated classification of 1H MRS spectra from brain tumours. NMR Biomed 1998;11(4-5):177-191.

5 Freeman JJ. Regulatory mechanisms of choline production. Life Sci 1996;58(22):1921-1927.

6 Bruton JD. The effect of lithium and nitrate on potassium contractures in a glycerol-treated slow-twitch muscle of the rat. Jpn J Physiol 1988;38(5):735-739.

7 Cendes F et al. MRI volumetric measurement of amygdala and hippocampus in temporal lobe epilepsy. Neurology 1993;43(4):719-725.

8 Harrison G et al. Residence of incident cohort of psychotic patients after 13 years of follow up. Bmj 1994;308(6932):813-816.

9 Kim JJ, Yoon KS. Stress: metaplastic effects in the hippocampus. Trends Neurosci 1998;21(12): 505-509.

10 Scheltens P. Early diagnosis of dementia: neuroimaging. J Neurol 1999;246(1):16-20.

11 Vance DE. Phosphatidylethanolamine N-methyltransferase: unexpected findings from curiosity-driven research. Eur J Med Res 1996;1(4):182-188.

12 Dreifuss FE. Classification of the epilepsies: influence on management. Rev Neurol (Paris) 1987;143(5):375-380.

13 Garcia PA, Laxer KD. Magnetic resonance spectroscopy. Neuroimaging Clin N Am 1995;5(4):675-682.

14 Allen PS, Thompson RB, Wilman AH. Metabolite-specific NMR spectroscopy in vivo. NMR Biomed 1997;10(8):435-444.

15 Blankenberg F, Ohtsuki K, Strauss HW. Dying a thousand deaths. Radionuclide imaging of apoptosis. Q J Nucl Med 1999;43(2):170-176.

16 Bevers EM et al. Lipid translocation across the plasma membrane of mammalian cells. Biochim Biophys Acta 1999;1439(3):317-330.

17 Bevers S, Xiang G, McLaughlin LW. Importance of specific adenosine N3-nitrogens for efficient cleavage by a hammerhead ribozyme. Biochemistry 1996;35(20): 6483-6490.

18 Brey RL, Escalante A. Neurological manifestations of antiphospholipid antibody syndrome. Lupus 1998;7(Suppl 2): S67-S74.

19 Kent M et al. Monoclonal antiphosphatidylserine antibodies react directly with feline and murine central nervous system. J Rheumatol 1997;24(9):1725-1733.

20 Yehuda S et al. Essential fatty acid preparation improves biochemical and cognitive functions in experimental allergic encephalomyelitis rats. Eur J Pharmacol 1997;328(1):23-29.

21 Barber PA et al. Identification of major ischemic change. Diffusion-weighted imaging versus computed tomography. Stroke 1999;30(10):2059-2065.

22 Motto C et al. Hemorrhage after an acute ischemic stroke.MAST-I Collaborative Group. Stroke 1999;30(4):761-764.

23 Broderick JP et al. Guidelines for the management of spontaneous intracerebral hemorrhage: A statement for healthcare professionals from a special writing group of the Stroke Council, American Heart Association. Stroke 1999;30(4):905-915.

24 Del Bigio MR et al. Experimental intracerebral hemorrhage in rats. Magnetic resonance imaging and histopathological correlates. Stroke 1996;27(12):2312-239; discussion 2319-2320.

25 Noguchi K et al. Acute subarachnoid hemorrhage: MR imaging with fluid-attenuated inversion recovery pulse sequences. Radiology 1995;196(3):773-777.

26 Noguchi K et al. Subacute and chronic subarachnoid hemorrhage: diagnosis with fluid-attenuated inversion-recovery MR imaging. Radiology 1997;203(1):257-262.

27 Bakshi R et al. Fluid-attenuated inversion-recovery MR imaging in acute and subacute cerebral intraventricular hemorrhage. AJNR Am J Neuroradiol 1999;20(4):629-636.

28 Linfante I et al. MRI features of intracerebral hemorrhage within 2 hours from symptom onset. Stroke 1999;30(11):2263-2267.

29 Deweer B et al. Memory disorders in probable Alzheimer's disease: the role of hippocampal atrophy as shown with MRI. J Neurol Neurosurg Psychiatry 1995;58(5):590-597.

30 Laakso MP et al. MRI of the hippocampus in Alzheimer's disease: sensitivity, specificity, and analysis of the incorrectly classified subjects. Neurobiol Aging 1998;19(1):23-31.

31 Friday PJ, Kubal WS. Magnetic resonance imaging: improved patient tolerance utilizing medical hypnosis. Am J Clin Hypn 1990;33(2):80-84.

32 Schneider JW. Lens-assisted in vivo desensitization to heights. J Behav Ther Exp Psychiatry 1982;13(4):333-336.

33 Vince GS et al. Interleukin-6, tumour necrosis factor and soluble tumour necrosis factor receptors in women with pre-eclampsia. Br J Obstet Gynaecol 1995;102(1):20-55.

34 North MM, North SM, Coble JR. Virtual reality therapy: an effective treatment for phobias. Stud Health Technol Inform 1998;58:112-119.

35 Ravicz ME, Melcher JR, Kiang NY. Acoustic noise during functional magnetic resonance imaging. J Acoust Soc Am 2000;108(4):1683-1696.

36 Ziarati M. Three-Dimensional high resolution MRI video and audio system and method. 1999: US.

37 Goldman AM, Gossman WE, Friedlander PC. Reduction of sound levels with antinoise in MR imaging. Radiology 1989;173(2):549-550.

38 Hedeen RA, Edelstein WA. Characterization and prediction of gradient acoustic noise in MR imagers. Magn Reson Med 1997;37(1):7-10.

39 Shimode SI, Inouye, Hiroshi et al. *Active Noise cancellation in MRI apparatus*. 1995: US.

40 Kates RD. Atkinson, and Brant-Zawadzki M. Fluid-attenuated inversion recovery (FLAIR): clinical prospectus of current and future applications. Top Magn Reson Imaging 196l;8(6):389-3896.

41 Brant-Zawadzki M et al. Fluid-attenuated inversion recovery (FLAIR) for assessment of cerebral infarction. Initial clinical experience in 50 patients. Stroke 1996; 27(7):1187-1191.

42 Singer MB, Atlas SW, Drayer BP. Subarachnoid space disease: diagnosis with fluid-attenuated inversion-recovery MR imaging and comparison with gadolinium-enhanced spin-echo MR imaging--blinded reader study. Radiology 1998;208(2):417-422.

43 Karonen JO et al. Combined diffusion and perfusion MRI with correlation to single-photon emission CT in acute ischemic stroke. Ischemic penumbra predicts infarct growth. Stroke 1999;30(8):1583-1590.

44 Reo NV, Adinehzadeh M. NMR spectroscopic analyses of liver phosphatidylcholine and phosphatidylethanolamine biosynthesis in rats exposed to peroxisome proliferators-A class of nongenotoxic hepatocarcinogens. Toxicol Appl Pharmacol 2000;164(2):113-126.

45 Reo NV et al. Perfluorodecanoic acid, a peroxisome proliferator, activates phospholipase C, inhibits CTP:phosphocholine cytidylyltransferase, and elevates diacylglycerol in rat liver. Toxicol Lett 1996;86(1):1-11.

46 Rote NS et al. Immunologic detection of phosphatidylserine externalization during thrombin-induced platelet activation. Clin Immunol Immunopathol 1993;6(3):193-200.

47 Widrow B, Stearns S. Adaptive Signal Processing. 1985.

48 Elliot SJ. Active Noise Control. IEEE Signal Processing Magazine 1993(October 1993):12-35.

49 Baburina I, Jackowski S. Cellular responses to excess phospholipid. J Biol Chem 1999;274(14): 9400-9408.

50 Walkey CJ, Kalmar GB, Cornell RB. Overexpression of rat liver CTP:phosphocholine cytidylyltransferase accelerates phosphatidylcholine synthesis and degradation. J Biol Chem 1994;269(8):5742-5749.

51 Schellinger PD et al. A standardized MRI stroke protocol: comparison with CT in hyperacute intracerebral hemorrhage. Stroke 1999;30(4):765-768.

52 Ebisu T et al. Hemorrhagic and nonhemorrhagic stroke: diagnosis with diffusion-weighted and T2-weighted echo-planar MR imaging. Radiology 1997;203(3): 823-828.

Next Generation [Image-Guided] Neuronavigation

Project

Principle Investigator:

Martin Satter, Ph.D.

Chief PET Physicist
Kettering Medical Center

1.0 Executive Summary

1.1 Purpose

The overall purpose of the Next Generation [Image-Guided] Neuronavigation (NGN) project was to enhance the neurosurgical capabilities at Kettering Medical Center (KMC) by integrating hardware and software with elements potentially useful in both military and civilian applications. The Air Force pilot requires a wide variety of information from different sources to navigate through a predefined air space around barriers to a predefined target. This is analogous to a neurosurgeon accessing multiple sources of information, such as magnetic resonance (MR) and positron emission tomography (PET) images, input to image-based computer guidance systems to enable precise navigation through brain anatomy during surgery. Using multiple data inputs, this project sought to obtain and couple (co-register) data from these disparate sources while augmenting the ability to accomplish a successful surgery or mission to the operator (pilot or surgeon).

The neurosurgeon's abilities to visualize and discriminate a target (i.e., tumor or aneurysm) from normal brain tissue are critical factors in performing successful neurosurgery. Unfortunately, direct target visualization during surgery is often impossible without additional technology to augment the limited view of the surgeon because he/she can only directly observe structures on the exposed brain surface. As neurosurgical techniques continue to progress toward more minimally invasive procedures (smaller craniotomies), direct visualization of the target in this way is becoming virtually impossible.

Computer-based technologies such as Image-Guided Neuronavigation Systems (IGNS) are evolving to compensate for this shrinking visual field as well as provide pre-surgical planning capabilities. These intraoperative image guidance systems for neuronavigation have been developed along two seemingly parallel tracks, one utilizing image data acquired prior to surgery and the other calling for real-time imaging during the surgical procedure. Intraoperative imaging provides visual updates of patient anatomy, organ or tissue displacement, and target-to-instrument hand-to-eye orientation. Multiview x-ray projection fluoroscopy, 3-D ultrasound and intraoperable (portable) magnetic resonance

(MR) and computerized tomography (CT) scanners provide the imaging capabilities necessary to perform many straightforward biopsy and intravascular procedures.

To improve the accuracy of these surgical procedures, especially for those targets buried in deep brain structures, these various imaging modalities can be combined to create a virtual brain of the patient. The virtual brain can be a composite of anatomical images (CT, MR), vascular images (MR angiography), and physiological images (fMRI and PET), as well as images reflecting biochemical activity (PET and SPECT).

1.2 Methods and Procedures

The NGN project was executed along two parallel tracks involving hardware assessment and acquisition along with software development and deployment.

1.2.1 Hardware

Time is a mission-critical factor for both pilots and neurosurgeons. A drawn-out mission leads to increased exposure, potential detection and unnecessary conflict for the pilot, whereas an extended surgery increases the rate of infection and complications due to anesthesia. Fatigue translates to a greater probability for human error in both disciplines. Therefore, a primary goal in this project was to investigate technologies to input information from a number of sources and integrate them into a single sensory display system, culminating in reduced fatigue and increased attention levels throughout the operating field. The Principle Investigator studied improvements in man-machine interfaces by electronically combining input from disparate components and presenting information in approximate real-time to the surgeon and the surgical team.

Hardware was acquired to provide the neurosurgeons with the most advanced navigation technology for brain and spinal surgery including a Mayfield Intraoperative CT scanner (Ohio Medical Instrument Company; Cincinnati, OH), two Medtronic Stealthstation™ systems (both of which were coupled to a Ziess NC4 Surgical Microscopes), a Medtronic FluoroNav™ spinal navigation system, a JVC high-definition camera and recorder

system, a Medtronic FrameLink™ Stereotactic Planning/Linking system, and a Medtronic StealthServer™.

To improve the surgeon's visibility of the target, a Virtual Retinal Display™ was delivered by MicroVision (Bothell, WA) for alpha testing and returned to the manufacturer with upgrade recommendations to enable suitable beta testing in the neurosurgical suite.

Finally, the need to observe the output from endoscopes, microelectrode recording systems and traditional anesthesiology and patient physiology monitoring systems led to the acquisition of a NEC PlasmaSync™ 5000W Plasma Screen and video mutliplexer to provide a consistent focal point for the neurosurgeon and attending staff.

1.2.2 Software

Analogous to the Air Force pilot's task of navigating through a predefined air space to a predetermined target using radar and other tracking technologies, the neurosurgeon utilizing IGNS technology can navigate through the brain or spine of a patient with an accuracy approaching 2-3 millimeters. IGNS technology works by creating a virtual brain or spine via complex computer graphics of patient data that can be a composite of many imaging modalities including but not limited to: CT, MRI, MRA, PET, 3-D ultrasound, fMRI, spectroscopy, single photon emission CT, EEG-derived cortical maps, standard X-rays and optical images including infrared.

Once the virtual brain or spine is created, it is brought into alignment with the actual patient's brain or spine via a process called co-registration. The co-registration step involves touching the patient's anatomy at several distinct points, registering the 3-D location of those points via tracking technology similar to GPS, and correlating the position of these patient landmarks with their homologous locations on the virtual anatomy displayed on the computer. With the completion of co-registration, the patient has effectively been mapped to the coordinate system of the virtual brain or spine, and the location of any surgical instrument relative to the patient anatomy can be visualized on

the computer by positional data updates from the tracking system. As the pilot's target is approached, he/she requires near real-time image updates to complete the mission, just as the surgeon requires visual updates as his/her plan changes based on new data such as brain shift during surgery.

Using AFRL input and participation where possible, specialized technology was combined with software developed for the rapid co-registration and display of 3-D medical image data. One challenge centered on developing a way to display the information in an understandable way that is scaled and stored in a common format. Another challenge was to take 3-D information and make it available on 2-D displays while maintaining 3-D cues. A final objective was to increase the types of information to be displayed and interpreted in context while insuring that the different data sources do not interfere with one another or the operator's ability to function efficiently.

In addition, it was necessary to update computer images based on the position of the aircraft or surgeon's tools, thereby presenting the operator with the most relevant data at a specific time and place. By obtaining a picture of the microscope objective and using it as a pointing device for surgical navigation, the system establishes the anatomical or biochemical relevance of the data based on the <X,Y,Z> location of the surgeon's instrument (i.e., scalpel or microscope). The ability to specifically receive the most relevant data to both the neurosurgeon during an operation, and the pilot navigating through unknown terrain, allows both to operate more efficiently and effectively in the completion of the mission.

Much of the work to date reported on the co-registration of the 3-D medical images has been based on the utilization of intensity information encompassing the complete set of volumes from which to derive the co-registration parameters. The approach adopted for the NGN project extracts only those sub-volumes (templates) with high mutual information to determine the transformation. Co-registration, region-of-interest (ROI) analysis, advanced visualization, segmentation, and image-processing software was developed under this project to solve these potential problems.

1.3 Results and Recommendations

1.3.1 Hardware

Keeping in mind the parallel between the mission of both the surgeon and the Air Force pilot, the Principle Investigator sought improvements in man-machine interface by electronically combining input from disparate components and presenting information in approximate real-time where possible to the operator (surgeon and the surgical team and/or pilot) for case planning and surgical procedures.

With mobile CT in the operating room (OR), it is possible to obtain CT scans during the surgical procedure to update the image data in the navigation system as required, i.e., when there is a high degree of brain shift. This system can also be used for brain biopsy, an assessment of the degree of brain tumor resection, to check for brain bleeds in the OR, and for pedicle screw insertion for fixation of the spine. Another advantage of this particular mobile scanner is that it can be used outside of the neurosurgical suite in areas such as the emergency room (ER) and the surgical intensive care unit (SICU). The intraoperative CT scanner is also useful for other surgical procedures outside of neurosurgery including radiofrequency ablation of liver tumors, CT-guided colorectal surgery, liver surgery and more.

1.3.2 Software

Software development for the NGN was a joint effort between the Wright State University (Dayton, OH) and Wallace-Kettering Neuroscience Institute (WKNI), and has resulted in methodologies and software that are currently in use at WKNI. Both image co-registration and segmentation are new capabilities that have been accepted for publication in reputable image analysis journals. These state-of-the-art capabilities should uniquely enable the WKNI surgeons to provide the best patient care possible in the community, and may have application to the pilot as he/she performs military missions.

2.0 Summary of Objectives

2.1 Hardware

2.1.1 Virtual Retinal Display™

Integration of a Virtual Retinal Display (VRD™) in an IGNS Medtronic StealthStation™ was the first objective of this project. This head-mounted system allows the neurosurgeon to select from a variety of data inputs without jeopardizing his/her focus on the craniotomy site and the StealthStation™ display screen. WKNI partnered with MicroVision (Seattle, WA), a high-technology firm, and other medical equipment manufacturers to develop the VRD™. After alpha-testing the VRD™ unit, it was returned to MicroVision with upgrade recommendations for further testing in the clinical setting. Potential exists for this technology to improve Air Force pilot target recognition in a more user-friendly and accurate manner.

2.1.2 Multiplexed Projection System

The second hardware objective was to plan and build a Multiplexed Projection System to allow the entire surgical team to view the small area of the craniotomy site (microscope output) or exposed brain that normally only the neurosurgeon can see during the operation.

2.1.3 Ziess NC4 Surgical Microscope

The next objective was the integration of 2 Zeiss NC-4 surgical microscopes into the IGNS to give the surgeon a magnified view of the patient's brain, particularly the vital areas controlling speech or motor function, as well as the brain stem, optic nerve and chiasm. In this case, the focal point of the microscope acts as the pointing device, enabling visualization of tissue beyond the exposed surface.

2.1.4 Positron Probe

The last objective called for the development/acquisition of the positron probe that can identify tissue in situ, which could potentially allow the surgeon to adjust for brain shift and delineate tumor from nontumor at the tip of the probe. The positron probe will be

used in conjunction with established radiopharmaceuticals with a proven track record in the detection/delineation of cancer with PET scanning.

2.2 Software Development

PET biochemical data fused with the morphologic data from MR or CT through image co-registration reveals additional diagnostic and therapeutic information. The image processing and analysis of co-registered, fused data sets can change the course of patient management and improve surgical/clinical decisions by detection and precise localization of disease where anatomical imaging alone was negative or indeterminate. A goal was to develop automated software for the rapid intra/inter-modality co-registration of brain images. In particular, the objective of the software was to enable co-registration to be performed within the neurosurgical OR where there exists much higher requirements for minimal user interaction and processing time than in the diagnostic arena.

Development of software was required to update the 3-D positional data via the virtual pointer location of the microscope, fusing the output image of the microscope with the 3-D image data from the IGNS, and making the 3-D image data accessible for display on the VRD™ and crew displays from a variety of input selections.

3.0 Background

3.1 Statement of Need

The overall purpose of the Next Generation Neuronavigation (NGN) project was to enhance the neurosurgical capabilities at Kettering Medical Center by integrating hardware and software with elements potentially useful in both military as well as civilian applications. The Air Force pilot requires a wide variety of information from different sources to navigate through a predefined air space around barriers to a predefined target. This is analogous to a neurosurgeon accessing multiple sources of information, such as magnetic resonance (MR) and positron emission tomography (PET) images, input to image-based computer guidance systems to enable precise navigation through brain anatomy during surgery. Using multiple data inputs, this project sought to obtain and couple (co-register) data from these disparate sources while increasing the ability to accomplish a successful surgery or mission to the operator (pilot or surgeon).

The overall success of neurosurgery depends upon the surgeon's ability to define the safest route to the target, i.e., tumor or aneurism, without disturbing vital brain structures, especially those buried deep within the brain. Affordable previous technology allowed the surgeon to view only the exposed surface of the patient's brain, a problem made more difficult as neurosurgical techniques continue to progress toward more minimally invasive procedures. Pre-surgical planning includes designating the location and size of the scalp incision, craniotomy, corticotomy, and the surgical resection. Theoretically, the complete spectrum of surgical planning capabilities must include computer software design and visualization technology providing tactile (haptic) simulation capabilities, as well as the ability to predict and correct for tissue deformation and organ shifts.

A further challenge facing neurosurgeons is knowing at all times precisely where their surgical instruments are inside the patient's brain. Prior to the advent of neuronavigation technology, the skill of the neurosurgeon relied heavily on his/her ability to calculate 3-D spatial coordinates from a 2-D film displayed on a light box. Uncertainties in this

complex calculation resulted in craniotomies that were unnecessarily large in order to guarantee access to a lesion or aneurism. This uncertainty also translated to unnecessary damage to normal tissue.

Computer-based tomographic and medical imaging such as MR and CT scanning revolutionized diagnostic and therapeutic medicine including neurosurgery and radiotherapy. Current high-field MR scanners provide some technologies necessary for real-time high-precision target definition for the surgeon; however, they are expensive, difficult to incorporate into a typical neurosurgical suite, and possess many logistical and technical constraints. Portable battery-powered CT scanners developed for the military have the potential to be incorporated into neuronavigation systems.

3.1.1 Hardware

In response to the prerequisite for the most accurate delineation of targets, especially targets in deep brain structures, neuronavigation systems are evolving and redefining the standard of care in modern neurosurgical practice.

The modern IGNS combines patient data gathered from different imaging modalities to create a virtual brain. This virtual brain can be a composite of anatomical (CT, MR), vascular (magnetic resonance angiography; MRA), and physiological (MRI, PET) images, as well as images reflecting biochemical activity such as glucose or oxygen utilization (MRS, PET). Patient-specific brain data from these various imaging modalities are then combined through a complex mathematical process termed "co-registration," which may then be displayed as spatially aligned data sets via fusion techniques such as alpha-bending.

WKNI has established a reputation as a pioneer in the utilization of neuronavigation technology, especially with regard to incorporation of functional data to guide complex neurosurgical procedures. Computer navigation utilizing a simulated virtual brain built

from accurate image data from a variety of modalities at the WKNI enables successful neurosurgical procedures to be performed even near high-risk regions of the brain where speech and motor function are controlled ***(Figure 1).***

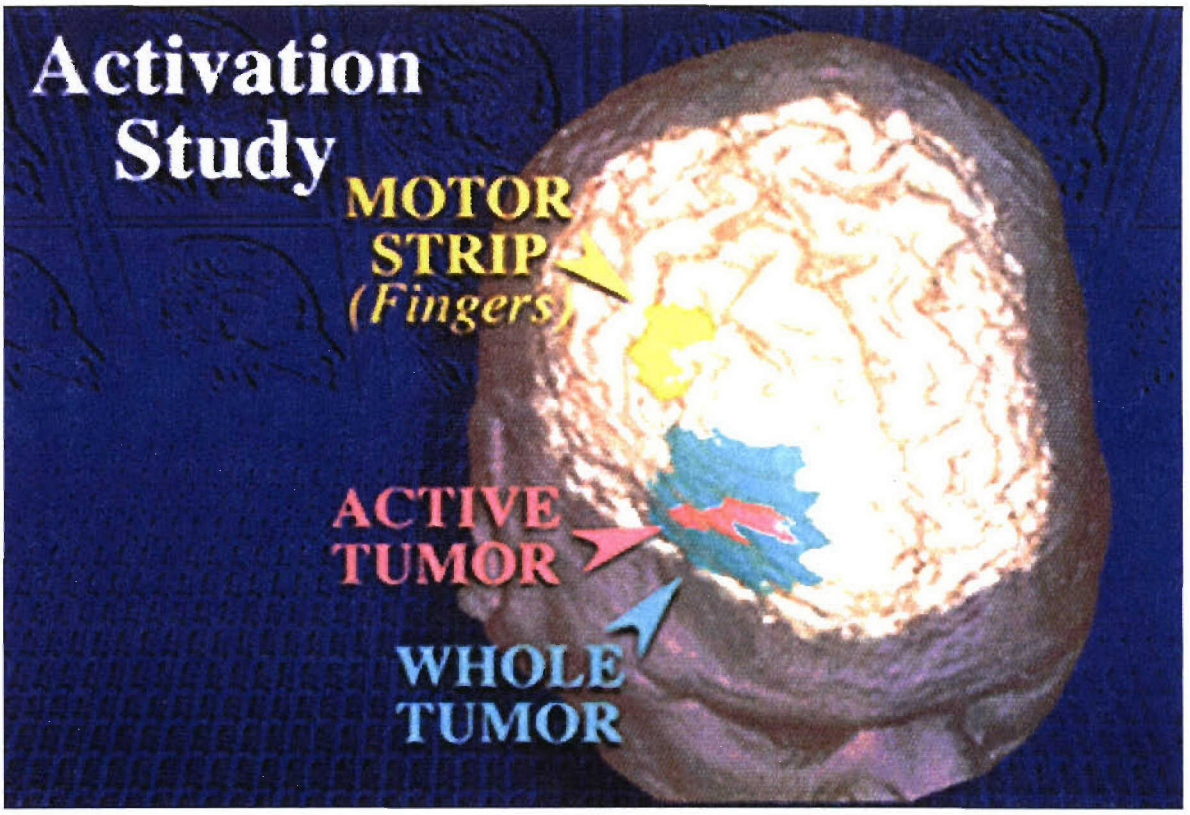

Figure 1. PET Activation Study in the Case of a 76-Year-Old Female with Glioblastoma Multiforme (IV). *An FDG PETscan revealed the active volume of the tumor - based on glucose metabolism.. Prior to entrance to an experimental protocol (boron neutron capture therapy), an aggressive resection was required. A PET activation study was performed to localize the motor strip. Post surgery, there were no significant motor deficits.*

Neuronavigation-based surgery requires that 3-D tomographic data sets of a patient's brain be obtained prior to surgery. The key step in the neuronavigation process is the co-registration (spatial alignment) of the patient's 3-D "MR/CT virtual brain," which exists on the neuronavigation computer, with the patient's actual brain. After registration, the position of any surgical equipment can be tracked in the anatomical coordinate system established by the 3-D image data. With neuronavigation technology, the "mind's eye"

of the neurosurgeon has been replaced with complex computer graphics displaying real-time 3-D anatomical information on high-resolution monitors.

Intraoperative image guidance systems for neuronavigation have been developed along two seemingly parallel tracks, one utilizing image data acquired prior to surgery and the other calling for real-time imaging during the procedure. Intraoperative imaging provides visual updates of patient anatomy, organs or tissue displacement, and the target-to-instrument hand-to-eye orientation. Multi-view x-ray projection fluoroscopy, 3-D ultrasound and intraoperative (portable) MR and CT scanners provide the necessary imaging capabilities to perform many straightforward biopsy and intravascular procedures. High-field MR scanners such as the General Electric Signa SP provide the requisite tissue contrast, resolution and multiplanar acquisition capabilities for performing complex, real-time frameless stereotactic image-guided procedures. However, the GE Signa SP system is expensive to purchase and incorporate into a typical neurosurgical suite, has limited availability, and suffers from some logistical and technological constraints and therefore, is not a practical solution in a typical neurosurgical environment.

Clearly, neuronavigation-based surgery can only be as effective as: 1) the determination of the exact spatial location of the target and its relationship to normal brain structures in the acquired 3-D image data; 2) the integration of practical display technologies to the operation room (OR) to provide real-time visualization of navigation information; and 3) the minimization of, or correction for, brain shift during the procedure. Prior to neuronavigation technology, the estimation of the target location and the craniotomy size and site came via an extrapolation by the neurosurgeon of 2-D image data (film) to the 3-D skull surface. Neuronavigation technology has in effect leveled the playing field by replacing educated inference with previously unattainable positioning accuracy, resulting in the ability to map the brain with an accuracy of less than 4 millimeters.

3.1.2 Computer-Aided-Design (CAD) Environment for Image Segmentation - Software Development

Similar to the Air Force pilot's task of navigating through a predefined air space to a predetermined target, the neurosurgeon navigates through a virtual brain or spine that can be a composite of many modalities including CT, MRI, MRA, PET, 3-D ultrasound, fMRI, spectroscopy, single photon emission CT, EEG-derived cortical maps, standard x-rays and optical images including infrared.

As the pilot's target is approached, he/she requires image updates approximating real-time to complete the mission, just as the surgeon requires visual updates as his/her plan changes based on new data such as brain shift during surgery.

Using AFRL input and participation where possible, we developed a set of instruments combined with software development that allows for rapid co-registration of 3-D image data. One challenge centered on developing a way to display the information in an understandable way that is scaled and stored in a common format. Another challenge was to take 3-D information and make it available on 2-D displays while maintaining 3-D cues. A final objective is to increase the types of information to be displayed and interpreted in context while insuring that the different data sources don't interfere with one another or the operator's ability to function efficiently.

Image segmentation is the process of partitioning an image into meaningful regions. For regions to be meaningful, they should represent objects or their components. For example, in medical practice, segmentation is required to define tumor volumes for diagnosis, surgical resection and radiotherapy targeting. If rapid, accurate segmentation can be realized, the clinical impact of quantitative radiology can be investigated. For example, segmentation tools could be used to determine subtle volumetric changes in a brain tumor or hippocampus as a function of time. In addition, segmenting out a tumor and tracking its volume and position in time enables modeling the changes as a net vectoral displacement. This displacement vector could be used to predict behavioral or motor abnormalities that could benefit therapeutic strategies.

Difficulties arise when properties within objects vary or boundaries of objects are not well defined. The problem is exacerbated when scanner inaccuracies exist and create noisy images. These variations, which are often unpredictable, make it all but impossible to develop an automated method that can correctly segment medical image data consistently.

Image segmentation is perhaps the most studied topic in image analysis and every year a great number of publications and conference proceedings are devoted to this subject. These segmentation methods often take into consideration various properties of images or objects. When properties of images or objects deviate from those anticipated, errors occur and inaccurate segmentation results. Even for a limited class of images, for instance high-resolution MR brain images, various methods have been developed. However, none of these methods to date is guaranteed to provide segmentation that does not require further user modification. Since an error-proof segmentation cannot be guaranteed, user assistance is needed to revise the result of an automated segmentation. At present, we believe the best possible approach is: 1) automatically or manually segment an image; and 2) enable the user to rapidly correct the segmentation via 3-D editing of the region surface.

3.2 The Team

The team was comprised of neurosurgeons and scientists at the WKNI and Wright State University, Dayton, Ohio. The principal investigator on the project was *Martin Satter*, Ph.D., Chief PET physicist at the Kettering Medical Center PET Department. The physicians were lead by *Dr Theodore Bernstein*, Medical Director of the WKNI. Also participating were *Dr Gary Krauss* and *Dr Raymond Poelstra*, neurosurgeons from the WKNI. Software development was the result of collaboration between the WKNI and the Wright State University Computer Science department; with *Ardy Goshtasby*, Ph.D. the key individual at WSU.

The NGN project integrated technology from several different vendor partners including Medtronic (Minneapolis, MN), MicroVision (Bothell, WA) and Ohio Medical Instrument Company (Cincinnati, OH).

3.3 Potential Benefits

3.3.1 WKNI

The IGNS technology potentially benefits all patients whose diagnoses are based primarily on medical imaging. Neuronavigation-guided surgery can be performed with less perturbation to healthy tissue and will result in fewer complications and faster recovery times, and a dramatic reduction in costs; in fact, it has been estimated that neuronavigation-based surgery can potentially reduce costs in the overall U.S. healthcare industry by as much as $1.5 billion annually.

The complex medical image-processing developed in this project to more accurately identify and target brain tumors for therapeutic resection, namely co-registration of biochemical and anatomical images and rapid segmentation with 3-D region-of-interest (ROI) editing, can also be used by radiologists to improve sensitivity and specificity of their diagnoses and therapists for more accurate radiotherapy targeting and surgical resection. This is evidenced by recent scanner configurations that combine, in a single gantry, anatomical (CT) and biochemic PET) imaging capabilities to provide hardware-based co-registration.

3.3.2 USAF/AFRL

Technologies to be developed under this project can potentially provide support to both WKNI and the USAF AFRL/HE missions. WKNI seeks to improve the neurological health of the community by providing excellent patient care and education, and conducting research to integrate neuroscience advances which will significantly improve patient outcomes. Through investigation of better ways to develop, display, and utilize medical information, this project supports the Air Force effort to lead the discovery, development, and timely transition of affordable, integrated technologies to keep the Air Force the best in the world. Research and development of imaged-guided surgery can

also benefit the Human Effectiveness Directorate mission of developing, integrating and transitioning science and technology products for the selection and training of personnel, the protection and sustenance of crew members, and the improvement of human interfaces with weapon systems to assure the preeminence of US air and space forces.

This research sought to find improved techniques for the end-user to visualize information to enable better decision-making in complex neurosurgical cases. The delivery of complex information and process visualization are rapidly developing technology areas, and development and application of these technologies have potential utility in image and data integration, as well as team coordination observations such as the position of equipment in work areas and team knowledge of what is going on, for both WKNI and the USAF AFRL/HE.

4.0 Methods and Procedures

4.1 Overview

The NGN project was executed along two parallel tracks involving hardware assessment and acquisition along with software development and deployment. Hardware was acquired to provide the neurosurgeons with state-of-the-art navigation technology for brain and spinal surgery. Evaluations were made of cutting-edge display technologies, which led to alpha-testing of a head-mounted display as well as the acquisition of two large plasma screens. Finally, software was developed to enable co-registration of PET, functional MRI (fMRI) or MRS images with anatomical images to identify biochemical or functional targets and input the location of these unique targets into the neuronavigation systems to guide resection.

4.2 Hardware

4.2.1 Medtronic Stealthstation™

At the beginning of this project, the WKNI Neurosurgery Department had only the Viewing Wand™ from Elekta Instruments (San Diego, CA) as a navigation system (***Figure 2***). In 1995, WKNI was only the third site in North America to have a Viewing Wand™ installed, and was the first clinical site in the U.S. to utilize biochemical targeting for a tumor resection. However, several inadequacies had been identified in this system including: 1) the positioning was accomplished via a six-jointed electromagnetic arm that was relatively cumbersome and expensive to maintain; 2) the system software was in need of an upgrade to simplify input of biochemical and/or functional data; and 3) a restrictive image transfer methodology via DAT tape was required and Elekta was noncommittal about eventual DICOM 3.0 support for image transfer.

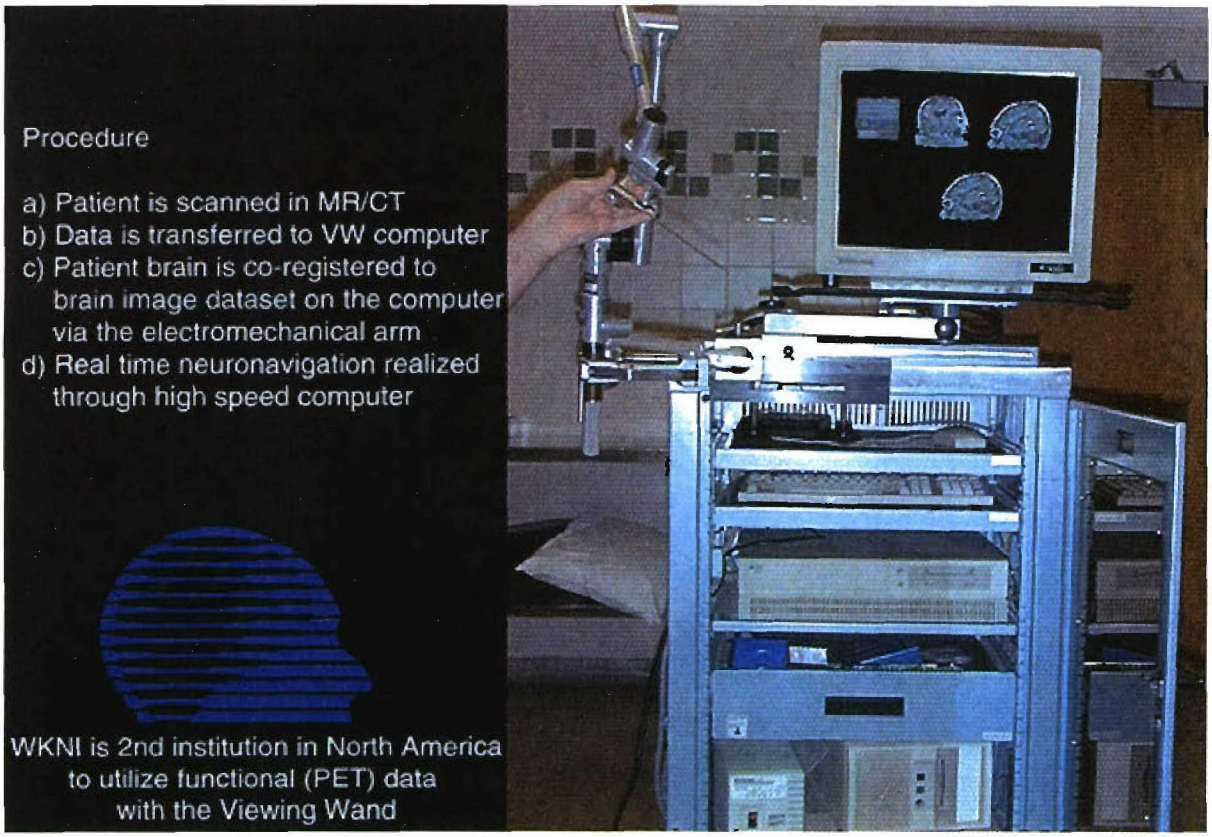

Figure 2. The Elekta Instruments Viewing Wand™. *The Viewing Wand was the first neuronavigation system utilized by the WKNI. Note the use of the six-jointed electromechanical arm as the pointing device.*

By 1998, over a dozen vendors were selling neuronavigation equipment and after assessing the top five vendors, two Medtronic Stealthstation™ systems were installed in late 1998 and early 1999. These Stealthstation™ systems have several software packages designed for various surgical procedures (i.e., brain and spinal) and utilize infrared tracking of any surgical instruments on which passive reflectors can be affixed. They also provide full DICOM 3 "receive" support, which enables network transfer of information, precluding the need for the awkward "sneaker net" system used for the viewing wand.

4.2.2 Ziess NC4 Surgical Microscope

A Ziess NC4 Surgical Microscope was incorporated into the IGNS as an alternative pointing device during the installation of the second Stealthstation™ in the second quarter of 1999. With this configuration, the focal point of the microscope became the

virtual pointer for real-time positioning updates. Because the majority of neurosurgical cases are performed under the magnification of a microscope, the dual role of microscope and pointing device improved the logistics in the cramped condition around the patient bed resulting from all the equipment employed in modern neurosurgery ***(Figure 3)***.

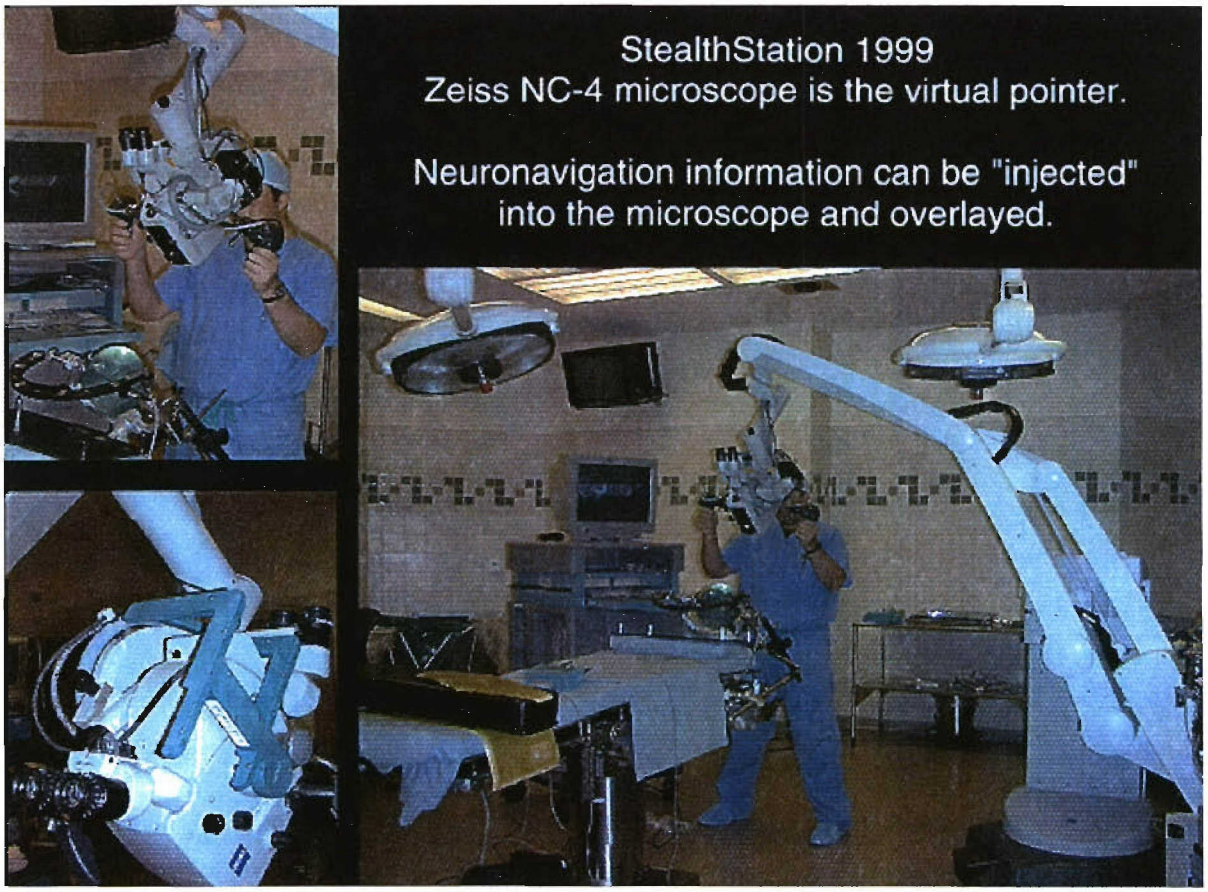

Figure 3. Stealthstation™ with the Zeiss NC-4 microscope as the virtual pointer.

The second Zeiss NC-4 microscope was integrated into the remaining StealthStation in the Fall of 2001. It provided additional technology to overlay real-time 24 bit video images into the ocular.

4.2.3 Medtronic Framelink™ Stereotactic Planning/Linking Station

WKNI purchased a Framelink™ Stereotactic Planning/Linking system in the first quarter of 1999, which provides for the integration of a patient-specific atlas and analysis within

micro-stereotactic space. It can be used as a stand-alone surgical-planning station and features a simplified target and trajectory planning mode, quick and accurate coordinate calculations for all popular stereotactic frames, and advanced visualization tools for planning biopsies and stereotactic craniotomies.

4.2.4 Medtronic FluoroNav™ Spinal Navigation System

A Medtronic FluoroNav™ Spinal Navigation System was purchased and installed in the second quarter of 1999. This system is designed for spinal surgery, providing precise navigation without the need for acquisition of CT data of the patient's spine prior to surgery. The system works in conjunction with the portable x-ray machines (C-arm) currently utilized in most complex spine cases.

The FluoroNav™ system overlays real-time instrument positions in multiple views from fluoroscopic images acquired from a C-arm. FluoroNav™ reduces the radiation exposure per procedure by reducing the number of fluoroscopic views acquired (eliminates the need for C-arm repositioning) and has nearly unlimited applications for complex spinal procedures. The WKNI FluoroNav™ installation was the first non-university-based installation in the U.S., and the first navigation-related intraoperative imaging performed at WKNI ***(Figure 4)***.

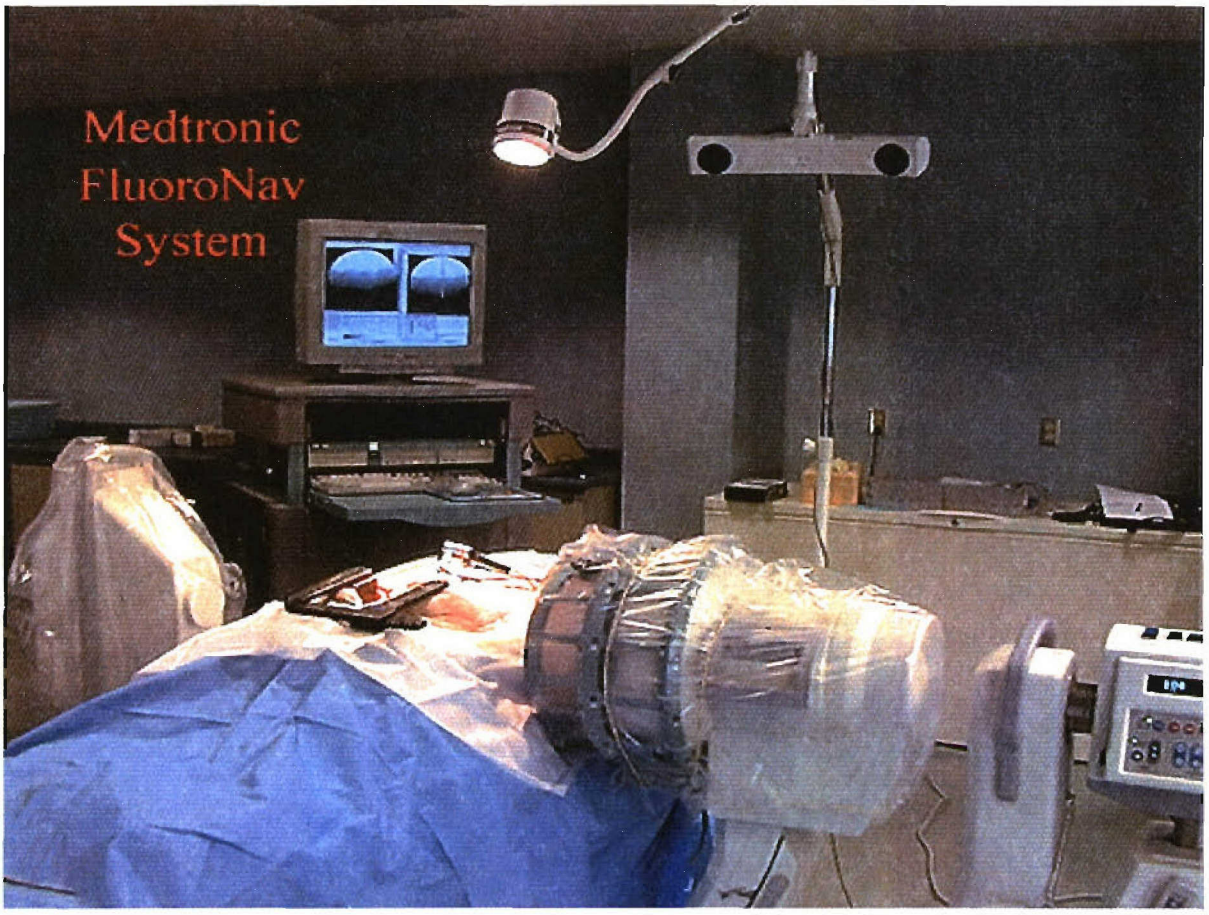

Figure 4. Medtronic FluoroNav™ system. *The FluorNav is used to provide real-time spinal navigation via infrared tracking of instrument positions registered to fluoroscopic images from the C-Arm.*

4.2.5 Medtronic StealthServer™

A Medtronic StealthServer™ was purchased and installed in the third quarter of 1999. The StealthServer™ computer connects to the hospital network and enables full-time DICOM receive functionality as well as storage for the image data utilized for neuronavigation cases at WKNI. Full-time DICOM receive functionality became a requirement as the number of cranial and spinal neuronavigation cases increased, and image data transfer directly to the StealthStation™ was not possible because they were in use and were disconnected from the network during surgery.

In addition, the StealthServer™ supports radiologic image review on any computer platform including Unix, Windows, Macintosh and Linux via ZMED software. This

software was installed on the StealthServer™ in the first quarter of 2001 and provides physicians with full-time, anywhere-access to patient image studies from a digital radiography PACS network. The browser-based ZMED software can be run under any operating system via a pure Java environment and provides the full suite of DICOM tools including Query/Retrieve, Send, Receive and Print.

4.2.6 The Virtual Retinal Display (VRD™0 System

Surgeons at WKNI have been performing computer-guided surgery since it first became available in the U.S. in 1994. Using complex computer software and hardware that enables the fusing of anatomical data (CT/MR) with biochemical data (PET/MRS), computer guidance allowed the neurosurgeons to target lesions in the brain and spinal cord with safer and more accurate procedures. This neuronavigation technology was developed as a technology transfer project with USAF/AFRL and has improved surgical outcomes dramatically. Today, approximately 60% of all neurosurgery is done with some computer-assisted guidance to better visualize and map the surgical field.

The influx of visual display technology into the OR brought a new set of problems. For instance, the video display on the conventional CRT computer screen is too small for neurosurgeons to view from across the OR during surgery. Because of the crowded conditions around the operating table, the computer monitors cannot be moved closer to the surgeon, and the surgeon cannot move closer to the monitor. WKNI tested new display technologies during this project to address this problem, including projecting images onto a screen with a high-powered, high-resolution projector and employing a VRD™ system from MicroVision, Inc. that uses low-power lasers to project the display directly onto the surgeon's retina.

Neuronavigation-based surgery has required that the surgeon divide his focus between the craniotomy site and the various computer screens displaying navigational, radiological, and patient information. The ideal visualization technology would enable the neurosurgeon to raster through any number of display inputs without necessarily losing sight of the craniotomy site. Not only would this greatly reduce surgeon fatigue, it

would insure a continuous visual link to the surgical instruments at the craniotomy site, or when implanting pedicle screws in complex spinal surgery.

Our research identified that MicroVision, Inc. had a VRD™ that could potentially meet the ideal visual display requirements (i.e., light weight, head-mountable, high SXGA (1280×1024) resolution, full color, and a flexible control over the projected "virtual reality," from a fully immersive environment to a see-through environment). This VRD™ is fundamentally different from previous display technologies because it uses a modulated, low-power beam of red (635 nanometers), green (532 nanometers) and blue (457 nanometers) laser lights to deliver an image directly on the retina. Because there is no intervening screen, the system can be adjusted to produce a fully immersive display environment, or adjusted to be partially or fully transparent.

The VRD™, whose visual output could ultimately be controlled via voice and/or menu options on the StealthStation™, could enable the neurosurgeon to select from a variety of data inputs; in particular, images from the computer neuronavigation screen, the output from a Ziess NC4 surgical microscope, or various imaging modalities incorporating both anatomical, physiological and biochemical patient data. Thus, the visual data necessary at any point in the procedure can be accessed by the neurosurgeon without a concomitant head rotation and loss of visual focus anchored to the craniotomy site. The theoretical resolution and color capabilities of the VRD™ (due to substituting the retina for a CRT or LCD screen) are clearly superior to any current helmet-based system, making the VRD™ the ideal choice for integration.

The Whidbey Retinal Scanning display VRD™ (***Figure 5)*** was built by MicroVision and delivered in the third quarter of 1999 to WKNI for alpha-testing with the following specifications:

· System Unit: 2.5′× 2.5′×1′ package that houses the laser light sources, the drive electronics, the interface to SVGA, the power supply, etc.;
· Resolution/Color: SGVA (800×600)/Full RGB, (8 bits per color mode);

· Luminance: 100′ lambert maximum;

· Exit pupil: 15 millimeter;

· Field of view: 30° horizontal, 22° vertical, see-through binocular and;

· Form factor: head-mounted, weighing less than 32 oz.

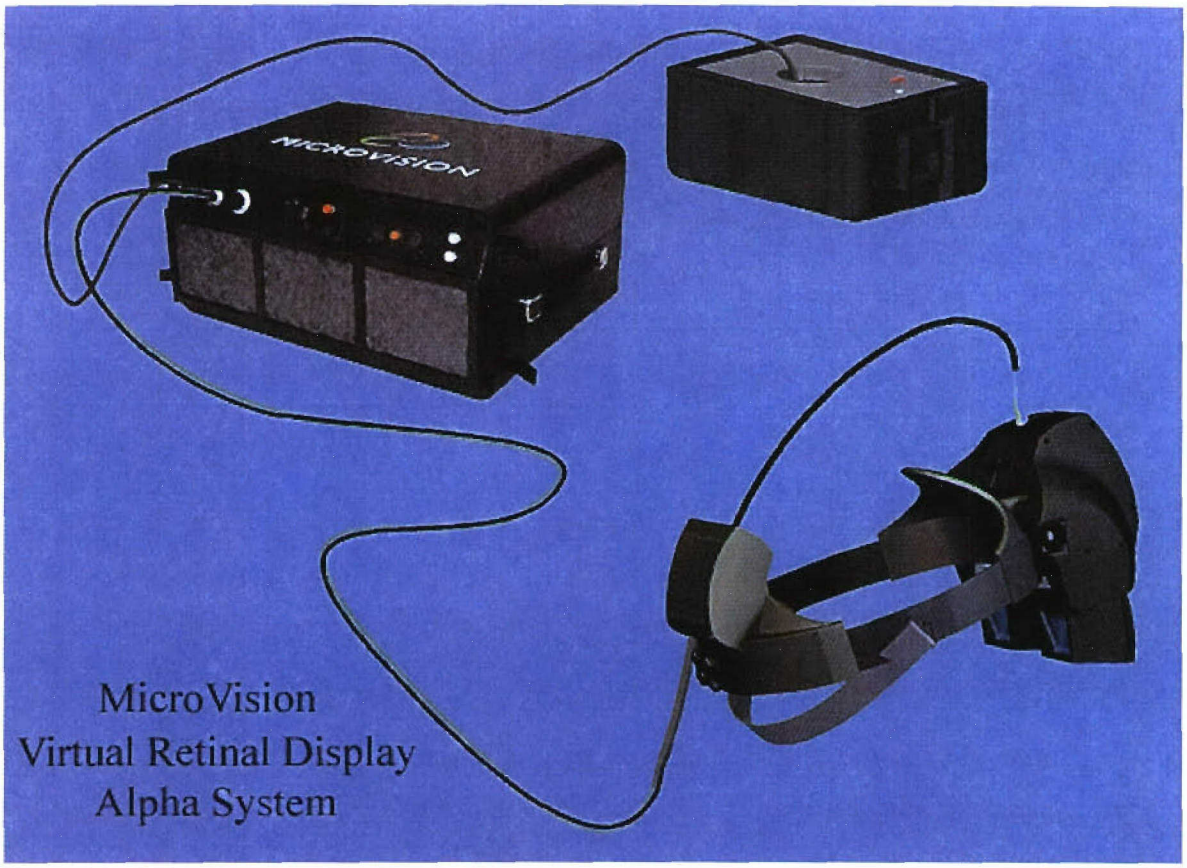

Figure 5. The MicroVision Virtual Retinal Display™ system: component view.

Extensive testing of the system ensued for approximately 1 year and there were two main obstacles to overcome in testing the system during actual surgical procedures. The VRD™ would frequently blow 20 amp fuses in the OR and an unidentified safety interlock would inappropriately shut down the VRD™.

4.2.7 NEC PlasmaSync™ 5000W Plasma Screen

Concurrent with the increase in the number of computer-assisted devices in the OR has been the number of video and/or computer outputs that must be displayed. A current list

of WKNI Neurosurgery Department image-guided systems includes an Eletkta Viewing Wand, two Medtronic Stealthstations™ (one coupled to a Ziess NC4 Microscope) and a Medtronic FluoroNav™ system for spinal surgery. A JVC high-definition television (HDTV) camera was also acquired to capture the video output from the Ziess NC4 microscope. Additional output from endoscopes, microelectrode recording systems and traditional anesthesiology and patient-monitoring systems led to the acquisition of a high-resolution plasma screen and video multiplexer to provide a consistent focal point for the neurosurgeon and the support staff for real-time updates of all mission-critical information.

The NEC PlasmaSync™ 500W plasma screen was chosen because it provided the largest viewable area (43.5" wide × 34" high), a small footprint (4" thick), the highest native pixel resolution (1375×768), a 400:1 contrast ratio and full 24-bit color. Acceptable computer-generated RGB inputs to the plasma screen ranged from VGA to SXGA while standard video signal compatibility included NTSC, PAL, SECAM, S-Video, composite and high definition television (HDTV). The plasma screen was installed within in a hand-made protective case equipped with a hydraulic lift to maintain cleanliness and ease of use. The large screen (50" diagonal) and high-resolution display enabled multiplexing several visual inputs to the plasma screen.

An RGB Spectrum SuperView™ 1000 video multiplexer was employed to combine the video inputs to the plasma screen. The multiplexer accepts up to two RGB (computer) and two composite or S-Video inputs. Thus a wide range of video and computer displays employed in modern surgery such as x-ray (fluoroscopy), MR/CT/PET, an HDTV video camera output, real-time physiological data, and the images from navigational guidance systems can be simultaneously displayed on the plasma screen. The multiplexer is programmable, accepting the various outputs of the equipment in the surgical suite and outputting them alone or in combination.

4.2.8 Acquisition and Development of an Intraoperative CT

The next logical development in neuronavigation-based surgery was to enable real-time updating of MR or CT maps used to guide the surgeon when the patient's brain anatomy has been altered. Both CT and MR have hardware and imaging characteristics amenable to imaging in the neurosurgical OR.

With mobile CT in the OR, it is possible to obtain CT scans during the surgical procedure to update the image data in the navigation system as required; for example, when there is a high degree of brain shift. It can be used for brain biopsy, brain tumor resection, to check for brain bleeds in the OR, and pedicle screw insertion for fixation of the spine.

In spinal surgery, accurate navigation through a complex anatomy is a prerequisite. Fluoroscopic systems show the position of anatomical structures but fail to provide proper 3-D information, especially after modification of the spine as in complex cervical spinal cases. A particular problem is that of screw fixation in spinal surgery, where even the most experienced surgeons perforate the cortex in up to 40% of cases.

The advantage of this particular mobile scanner for WKNI and KMC is that it can be used outside of the neurosurgical suite in areas such as the ER and SICU. In fact, it has been estimated that up to $500 in transfer costs per patient can be saved when the patient can be scanned on site in the ICU. The inter-operative CT is also useful for other surgical procedures such as radiofrequency ablation of liver tumors, intra-operative-guided colorectal surgery, liver surgery, etc.

Our vendor partner was Ohio Medical Instruments Company because they expressed a desire to collaborate with WKNI to advance the capabilities of intraoperative CT imaging with their MobileScan™ CT product ***(Figure 6)***.

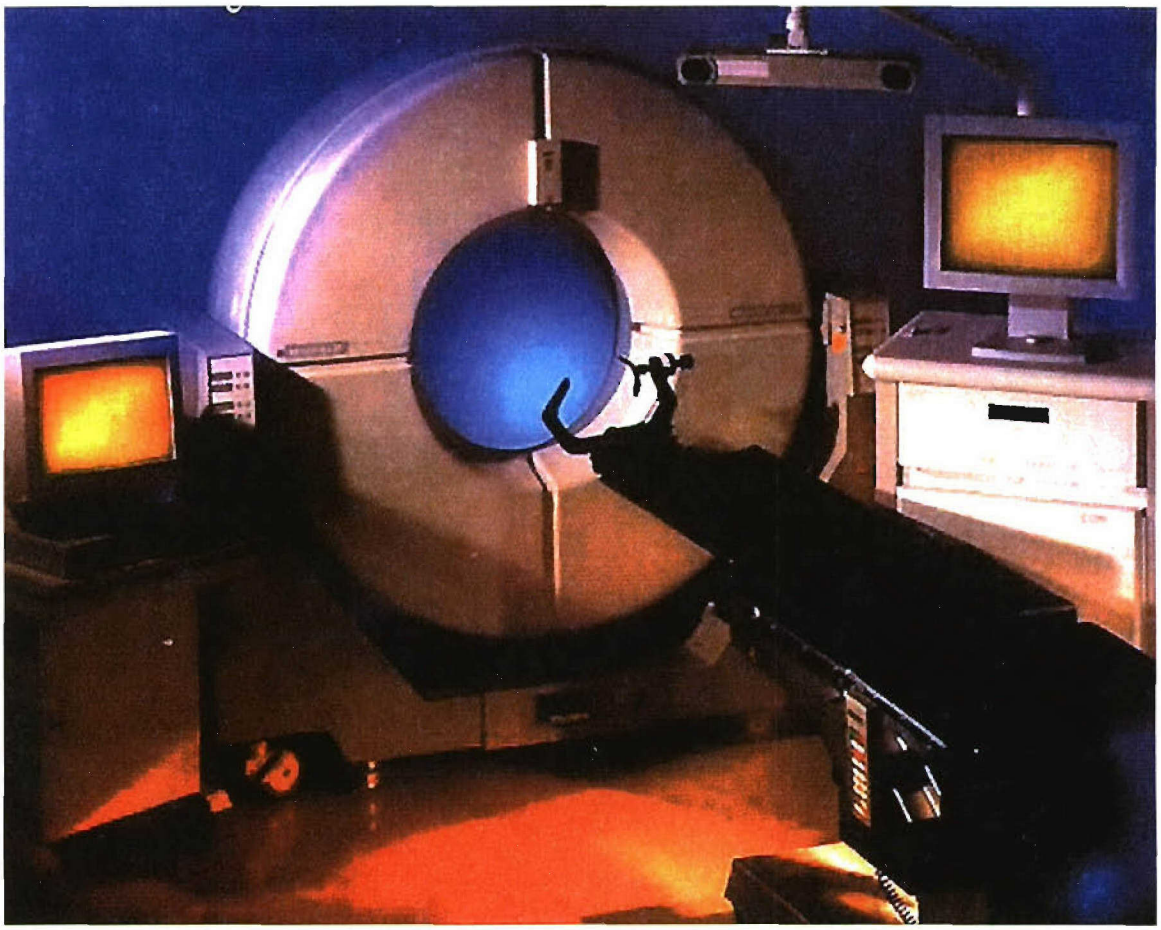

Figure 6. Ohio Medical Instruments MobileScan™ CT. *The complete system replete with the dedicated OR table including radiolucent Mayfield clamps. Also pictured is the ACCISS electromagnetic tracking system, soon to be undergoing beta-testing at the WKNI.*

4.3 Software Development

4.3.1 Co-Registration: Utilization and Development

Image co-registration, or sensor fusion, is the mathematical process of determining the correspondence between all points in different images of the same scene. Along with the co-registration of the atmospheric, astronomic, or satellite data, this technique is growing in importance in the field of medical imaging. This includes both inter-modality (PET to MR) and intra-modality (MR to MR) co-registration.

The primary goal in the software development portion of the NGN project was to create CRASIS, a software program for the rapid, automated co-registration of biochemical PET images to morphological MR or CT data with the added criteria that it could be routinely used in the clinical setting. The WKNI has long recognized that co-registration and fused data sets provide additional needed diagnostic as well as therapeutic information for the physician ***(Figure 7)***.

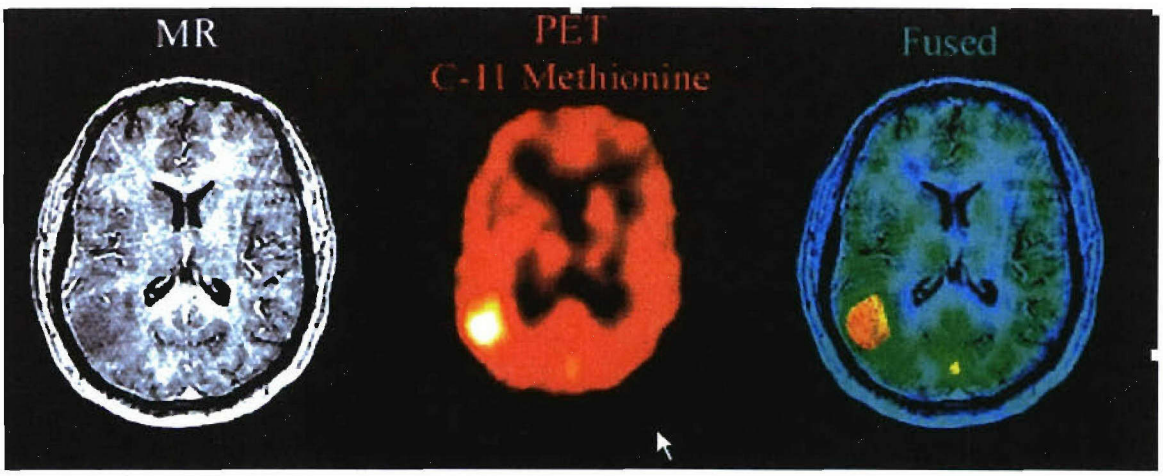

Figure 7. Case of a 32- year- old female with a lesion that did not enhance on T_1-weighted MR scans (left). *Fluorodeoxyglucose (FDG) PET scans were unremarkable. However, carbon-11- labeled methionine had a well-defined focal uptake as observed on the PET scan (middle). The methionine ROI volume was painted on the MR data set (post co-registration) for a neuronavigation based resection of the astrocytoma (II/IV).*

Prior to the development of CRASIS, co-registration of multimodality images at the WKNI was performed with the computer program Register, which was graciously provided by the PET department of the Montreal Neurological Institute [1]. With image processing software written by the KMC PET department, MRI or CT and PET image volumes were read, displayed and then converted into a MINC file format as input into the Register program. MINC files are medical imaging specific NetCDF files. The Register program requires that an operator via mouse control select homologous points from each image volume. Then a transformation is computed utilizing linear least squares that best aligns all the homologous (paired) points by minimizing their root-mean square distance. Registration errors have been determined for this technique to be ~2 millimeters at the brain center and ~4 millimeters at the brain surface [2].

The Register program was used to co-register over 300 image volume sets (PET to MRI, PET to CT, magnetic resonance angiography-MRA to MRI and PET to PET) prior to the onset of the NGN project. The biggest problem with the Register program was the 15-20 minutes required by the operator to perform homologous point selection. This degree of user interaction did not permit the co-registration of multimodality images to become a routine clinical procedure. The CRASIS program was designed to automatically find homologous points through the process of template selection.

4.3.1.1 Template Selection

Much of the work reported on the co-registration of 3-D medical images to date has been based on the utilization of intensity information encompassing the complete set of volumes from which to derive the co-registration parameters. The approach adopted for the NGN project extracts only those sub-volumes (templates) with high mutual information to determine the transformation. This global approach, which utilizes entire volumes, may not produce the optimum results when the images have partial intensity and/or geometric differences. A detailed account of the software package CRASIS (Co-registration, region-of-interest analysis, advanced visualization, segmentation and image-processing software) can be found in Attachment #1 hereto.

Image volumes to be co-registered (MR, CT, PET, MRS) are read into the program without the need for any preprocessing. The CRASIS program automatically selects highly detailed and unique templates (6-12 sub-volumes) from the target and locates the best-matching templates in the reference (***Figure 8***). The centroids of the best correspondences are then used to determine the transformation that re-samples the target to the reference.

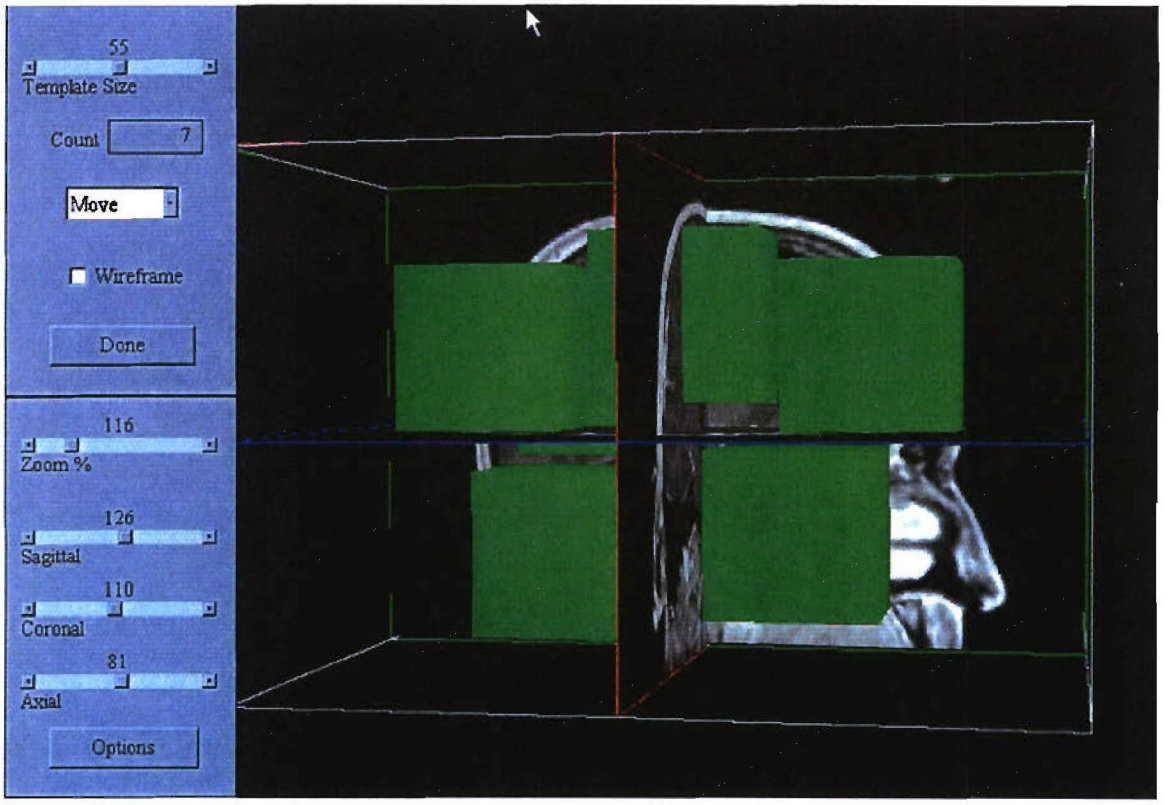

Figure 8. Template selection is the first step performed in the CRASIS co-registration software. *The green cubes represent templates extracted by the CRASIS program within the MR brain volume. The templates were chosen based on their degree of information content. Template selection can be performed automatically (via the algorithm) or manually selected by the operator.*

To achieve an accurate co-registration, the templates selected from the target (the volume to be reoriented and re-sampled) must represent highly detailed, unique regions. The detail or information content in a template is determined by accessing the number of high-gradient edges from a computation of the sum of gradient magnitudes.

The templates are then put in order as a function of their gradient magnitude values (information content) and the top 5% are extracted. As many of the templates overlap one another, those that overlap by greater than 50% are removed. Among the remaining target template, up to a dozen of the most unique are kept for matching to templates in the reference (the volume to which the target is aligned).

Template uniqueness is characterized by calculating the eigenvalues of the inertia matrix of each template [3]. A template containing all large eigenvalues represents a locally unique sub-volume in the 3-D volumes. A template with only two large eigenvalues may not be unique because of its similarity to many templates in its neighborhood along a line. A template with only one large eigenvalue may be similar to many templates in its neighborhood along a plane.

4.3.1.2 Calculation of Transformation Matrix

Once the templates in the target have been identified, matching is performed. Template matching is the process of finding the location of the templates inside the target that possesses the highest similarity to templates in the reference. Once a number of matching templates are found, their centers are defined as corresponding to homologous points at identical spatial locations in each volume. An affine transformation is then calculated that minimizes the distance between the homologous points via rotation and translation of the target. The search for template matches is facilitated by the generation of a similarity matrix whose entries correspond to the similarity value between all combinations of the templates.

Different metrics (similarity measures) have been reported in the literature; no single similarity is known to produce the best result for all situations. Depending on the image modalities involved, one metric may produce better template matching than another. Some of the similarity metrics tested were: 1) sum of absolute differences [4]; 2) cross-correlation coefficient [5]; 3) geometric distance (Chamfer matching) [6]; 4) mutual information [7]; and 5) invariant moments [8]. However, the similarities measures (1-4) listed above cannot be used to extract the actual similarity between image sub-volume if the target and reference volumes have a large rotational difference.

Invariant movements are employed to correct for rotational differences. Moments are features that characterize the geometry of a spatial pattern, and can be normalized to be invariant of the position and orientation of the pattern. Assuming highly detailed and unique templates are found in the target, template matching is achieved by: 1) aligning templates via their principal axes (as derived from their invariant moments); 2)

generating similarity matrices for template pairs; and 3) selecting the optimum template matches (spatial locations) from a search through the similarity matrices. Among the similarity matrices mentioned, the cross-correlation coefficient, geometric distance, and invariant moments provide the most unique measures. However, with the top priority at WKNI being the registration of inter-modality images, mutual information is used as the similarity metric in the CRASIS program. The flexibility of utilizing mutual information is that as long as a function exists that can map intensities between the target and reference templates, a high similarity value will be found.

To find the match position of templates, a course-to-find approach as implemented. First image volumes are reduced in scale and approximate match positions are determined. Then the scaling of the volumes is increased in two to three steps back to their original resolution. At each step, potential match positions are found with associated confidence levels and the search for the next step includes only those high-confidence matches. When the image volumes are approximately co-registered, the search area is small and an exhaustive search through all match combinations quickly determines the optimum alignment transformation.

An approximate or course registration can be performed by utilizing mouse-controlled rotation and translation in CRASIS. The best-match positions reduce to a set of homologous points for the corresponding templates. Given a set of homologous points (at least four), the rotation and translation differences between the image volumes can be calculated. Knowing the rotation and translation variances that exist between the volumes, the affine transformation that co-registers (aligns) the target to the reference can be determined.

4.3.2 Image Segmentation Software Development

Image segmentation is the process of partitioning an image into meaningful regions. For the regions to be meaningful, they should represent objects and/or their components. For example, in the medical arena, segmentation is required to define tumor volumes for diagnosis, surgical resection and radiotherapy targeting. Difficulties arise when properties within objects vary or boundaries of objects are not well defined. The problem is exacerbated when scanner inaccuracies exist and create noisy images. These variations,

which are often unpredictable, make it all but impossible to develop an automated method that can correctly segment medical image data consistently.

Image segmentation is perhaps the most studied topic in image analysis. Every year a great number of publications and conference proceedings are devoted to image segmentation. These segmentation methods often take into consideration various properties of images or objects. When properties of images or objects deviate from those anticipated, errors occur and inaccurate segmentation results. Even for a limited class of images, for instance high-resolution MR brain images, various methods have been developed, none of which to date is guaranteed to provide segmentation that does not require further user modification.

Since an error-proof segmentation cannot be guaranteed, user assistance is needed to revise the result of an automated segmentation. To address these issues, specific software was developed to automatically segment an image and enable the user to rapidly correct the errors via 3-D editing of the region surface. The software, written in IDL, can aid the user in revising the result of an automatically derived segmentation. With the assumption that a region obtained by an automated method contains voxels, whose bounding surface represents the object of interest, the method developed fits a parametric surface to the object and then overlays the surface within the volumetric image. By viewing both the image data and the extracted surface, the user can edit the surface until the desired shape is obtained.

5.0 Results

5.1 Overview

Utilization and alpha-testing of the VRD™ system in the initial phase of the NGN project cast WKNI and the USAF/AFRL into the national spotlight in the form of over 250 newspaper articles nationwide, and five local and two national television reports (Fox National News and NBC Dateline). This national recognition brought WKNI and the NGN project to the forefront in the list of potential collaborators. One such collaborator, Ohio Medical Instruments Company has subsequently partnered with the WKNI to determine the efficacy of intraoperative CT imaging in the neurosurgical OR. The WKNI continues to lead by testing, developing and incorporating intraoperative imaging into the neuronavigation technology arsenal.

Through the collaborative efforts of WKNI and WSU, two software programs were developed that enable the fully automated co-registration, fusion and visual display of all combinations of volumetric brain image data, such as MR-MR, CT-CT, PET-PET, MR-CT, MR-PET, CT-PET, etc. Once co-registration has been performed, target volumes can be segmented through a computer-assisted design environment that enables 3-D manipulation of segmented surfaces. A Masters level thesis and two Ph.D. theses were completed by students at the WSU Computer Science Department during the course of this work.

The software was written in IDL from Research Systems, a Kodak company, and can be run across all platforms including Windows (98, NT, 2000), Macintosh and all common unix variants such as Linux, Sun, and SGL. This software has proven to be extremely valuable for targeting lesions due to better demarcation of lesion boundaries culminating from the fusion of biochemical and anatomical information. It is also anticipated to be of great value in the evaluation phase of patient treatment.

In addition, many new neuronavigation technologies were acquired, evaluated and eventually incorporated into the neurosurgical OR. In all, over 200 FluoroNav™ (spine)

and 300 cases utilizing a StealthStation™ were performed during the course of this project

5.1.1 Medtronic Stealthstation™

The Medtronic Stealthstation™ was evaluated as a replacement for the outdated Viewing Wand system. It proved to be an adequate vehicle for the co-registration of patient data for the surgeon. The first Stealthstation™ was linked to the focal point of the lens of the Ziess NC4 microscope. However, the neurosurgeons found no advantage to this element of the StealthServer™-Zeiss NC4 integration because it was necessary to break visual contact with the patient and look away to where the image was being projected. Another obstacle to its effectiveness in the OR was due to limitations of the software. Although it was anticipated that the second Stealthstation™ would be connected to the VRD™ for spinal surgery, the VRD™ as delivered from MicroVision was too primitive for integration and upgrades could not be accomplished within the period of performance of the 12-month WKNI-MicroVision contract.

5.1.2 Ziess NC4 Surgical Microscope

The WKNI was one of the first facilities to perform beta-testing of the Ziess NC4 microscope as a guidance tool in neurosurgery. Although the microscope provided much clearer and brighter optics, and integrated well into the IGNS, using the focal point of the microscope as the pointing device was determined not to be an advantage for the following reasons: 1) the system was too cumbersome as it relies on the line of sight with the infrared camera and because the microscope moves in complex positions, the line of sight is sporadically lost; 2) no definitive reference point in its guidance could be established; the surgeon has to assume the microscope focal point is the point of reference and then verify this with some external point; and 3) image injection from the Stealthstation™ into the microscope was too crude; the microscope did not have the necessary optical connections.

5.1.3 Medtronic FluoroNav™ Spinal Navigation System

The Medtronic FluoroNav™ system was evaluated for its surgical navigation capabilities with positioning information from intraoperative fluoroscopy. The FluoroNav™ system was evaluated to be accurate and effective. WKNI was the third beta test site for this system worldwide and approximately 300 procedures were performed with FluroroNav™ over the course of the project, with early results sent to Medtronic to as part of the beta-test agreement.

The precision and magnification provided by this system address documented health risks associated with pedicle screw placement, where incorrect placement can result in spinal damage, breach of bone, or nerve irritation. The optical magnification provided by FluoroNav™ affords the surgeon precision on two planes so that a 5.5-millimeter screw can be safely and quickly inserted into a 7-millimeter pedicle.

The accuracy of the FluoroNav™ also allows for a marked reduction in the time required for spinal and intracranial surgeries, which in turn results in markedly minimized radiation exposure and OR time for both the surgeon, the neurosurgery team and the patient. A procedure that once took 30-60 min can now be completed in 10-15 minutes.

The WKNI is currently continuing research by developing different reference points for this system so that patient movement during surgery can be tracked.

5.1.4 Medtronic Framelink™ Stereotactic Planning Station

The Medtronic Framelink™ Planning Station was evaluated and proved to be an effective tool for visualizing the relevant co-registered data during pre-surgical planning. However, because of a delay in the Food and Drug Administration 510k approval, it was only used in one case.

Due to the proven value of the system as determined in this case, it was eventually added to the IGNS and updated to incorporate current stereotactic frames data for use in more

advanced functional neurosurgeries (i.e., tremors, mood disorders). Potential future applications include treatment for obesity and pain control.

5.1.5 Medtronic StealthServer™

The Medtronic StealthServer™ proved to be a 100% uptime DICOM-Receive server. The StealthServer™ provided: 1) a depot for patient image data coming from many different departments on the KMC picture archives and communications system (PACS) network; and 2) tranfer capability to the StealthStations™. It also served as a primitive mini-PACS system, providing a temporary storage (~ 1 year) of patient data sent to the OR. However, this system is limited in the context of providing all mini-PACS functionality necessitated by the appearance of the Mayfield Intraoperative CT. This system shortened surgical time by allowing multitasking and access to all co-registered data (i.e., MRA, MRI, etc.) for pre-surgical planning.

5.1.6 VRD™

Extensive testing of the system ensued for approximately 1 year and there were two main obstacles to overcome in testing the system during actual surgical procedures. The VRD™ would frequently blow 20 amp fuses in the OR and an unidentified safety interlock would inappropriately shut down the VRD™. The argon ion gas-powered blue laser was identified as the cause of the blown fuses, primarily due to inefficient cooling. The VRD™ employed solid-state components to generate both the red (laser diode) and green (diode-pumped) lasers. After considerable debugging, the interconnect coupling the optical fiber from the helmet to the system source was the cause of the shutdowns. Following modifications by MicroVision in the first quarter of 1999, the system was ready to be tested in the OR ***(Figure 9)***.

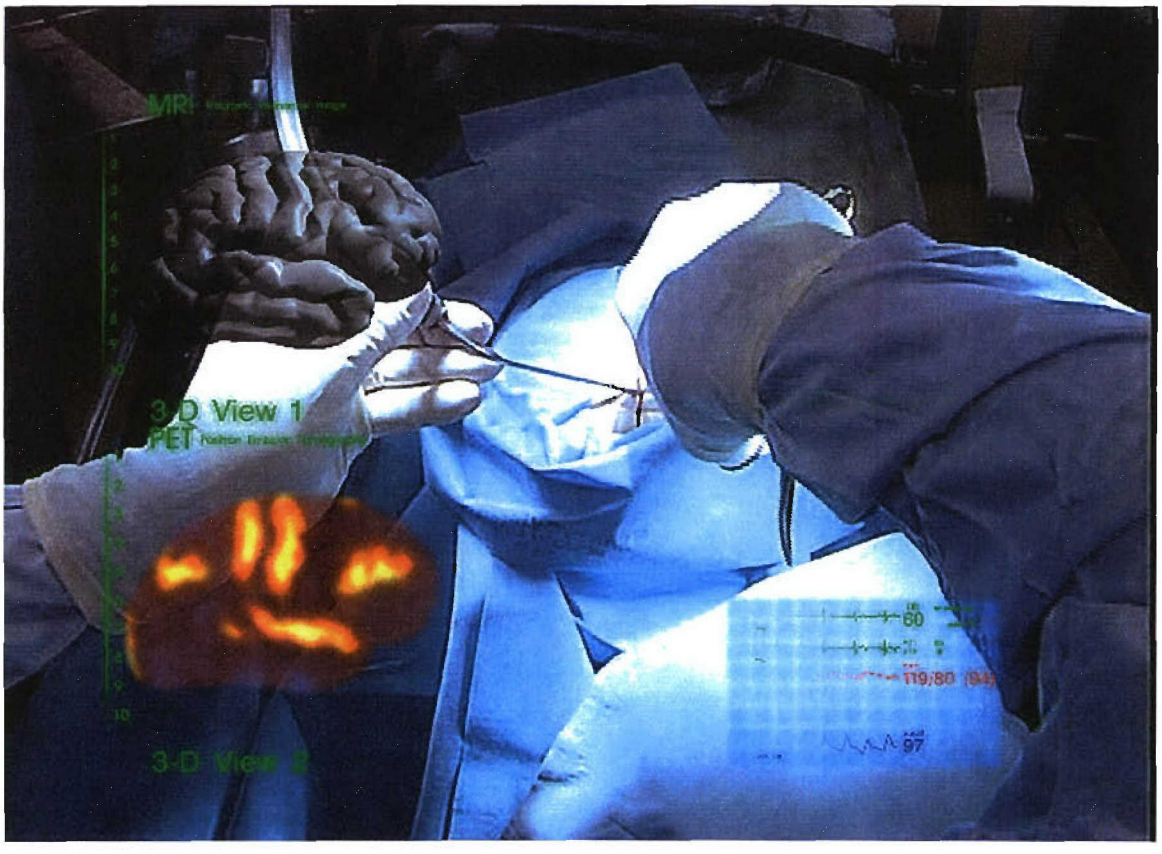

Figure 9. Simulated view through the VRD™. Simulation illustrates how PET, MR and patient physiology data can be overlayed.

The VRD™ was first tested in an actual surgical procedure on May 11, 1999, by *Dr. Theodore W. Bernstein*, Chief of Neurosurgery at KMC. *Dr. Bernstein* utilized the head-worn VRD™ to monitor the output of the FluoroNav™ image-guided surgery system to tap into place, confirm, and verify placements of pedicle screws for a multilevel spinal fusion procedure. The system was also tested by the Chief OR nurse, *Mr. Tim Gillum*, who investigated the value of having the attending staff monitor the video output of the Ziess NC4 microscope with the VRD™ while assisting neurosurgeons in resecting brain tumors ***(Figure 10)***.

Figure 10. The VRD™ from MicroVision during alpha-testing at the WKNI.

The VRD™ was returned to the manufacturer in the third quarter of 2000 with the following upgrade recommendations from WKNI for suitable beta-testing in the neurosurgical suite:

· The argon ion gas blue laser should be replaced with a solid state blue laser component;
· The head-worn display was incorrectly balanced (nose-heavy) and should be reduced in weight by at least 50%;
· The VRD™ resolution should be increased to XGA (1024×768) as an intermediate step, with the final resolution of at least SXGA (1280×1024) to properly display high-resolution medical images;
· The color depth should be improved to a true 8 bits (the VRD™ tested was estimated to be 5-6 bits);
· Allowance should be made for flexible monocular or bi-ocular use; and

· User-friendly GUI-based software should be developed for setup and calibration of the system.

The WKNI was the first and only site to test the full color VRD™ from MicroVision. Overall, the VRD™ was evaluated during the performance of six neurosurgeries and was found to provide improved image resolution, especially for pedicle screw placement. Also, the surgeon found the ability to fade the retinal displays in and out very valuable, as he/she could perform two tasks simultaneously without having to look away from the surgical site.

5.1.7 NEC PlasmaSync™ 5000W Plasma Screen

Concurrent with the increase in the number of computer-assisted devices in the OR has been the number of video and/or computer outputs that must be displayed. A current list of WKNI Neurosurgery Department image-guided systems includes an Eletkta Viewing Wand™, two Medtronic Stealthstations™ (one coupled to a Ziess NC4 Microscope) and a Medtronic FluoroNav™ system for spinal surgery. Additional output from endoscopes, microelectrode recording systems and traditional anesthesiology and patient-monitoring systems led to the acquisition of a high-resolution plasma screen and video multiplexer to provide a consistent focal point for the neurosurgeon and the support staff for real-time updates of all mission-critical information(***Figure 11***).

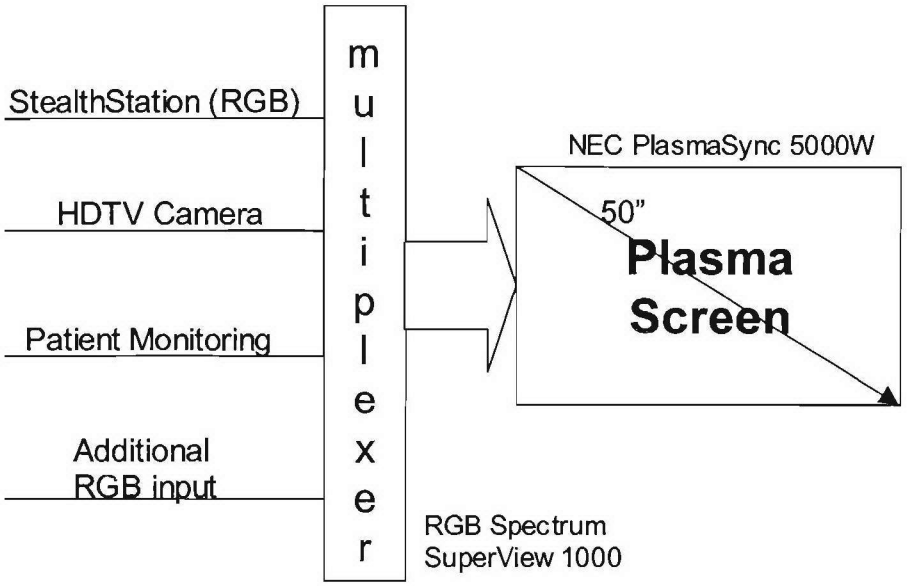

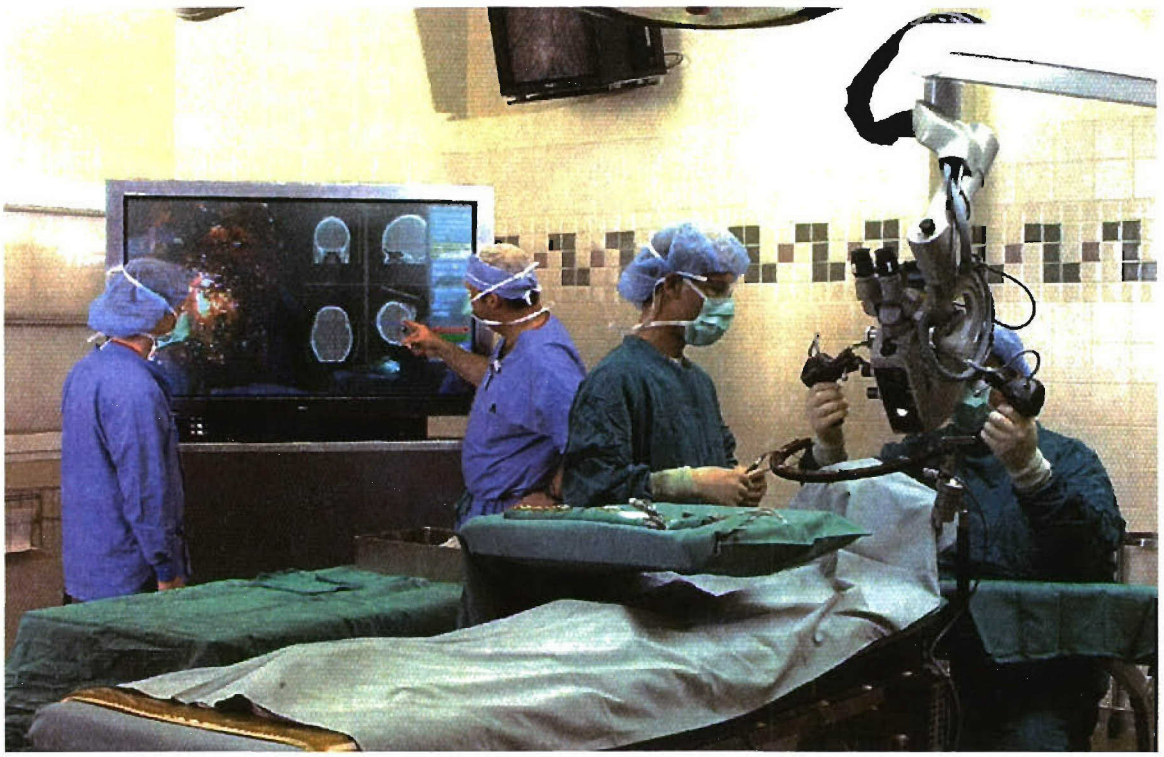

Figure 11. Schematic of the multiplexer-plasma screen setup (above). Mock surgical setup showing plasma screen utilization in the OR (below).

This plasma screen was initially evaluated during six neurosurgery cases and was determined to be an extremely valuable tool, solving a number of problems. First, it

aided in reducing surgical time because it provided an augmented view of all necessary images, providing an excellent magnified images especially useful for guidance during the placement of pedicle screws in spinal surgery. It also solves the problem of crowding of equipment during surgery around the patient, and improves the effectiveness and efficiency of the entire surgical team by providing a complete view of what is going on at any specific point in time during the operation.

The surgeon can then select specific information to be monitored and petition the plasma screen according to his need. The large screen can be easily observed across the OR, making the data available to all staff. At WKNI, all the vital visual information can now be processed by the neurosurgeon with a simple turn of the head from the surgical microscope. The plasma screen is now routinely implemented in nearly all neuronavigation-based surgery cases. The merging of technologies, plasma screen and multiplexer, has potential application in both consumer and military products.

5.1.8 Mayfield Intraoperative CT

Intraoperative CT allows the surgeon to start with pre-surgical images, updating these images throughout the operation, and provides a baseline for post-surgical evaluation and treatment.

The first clinical case involving the intraoperative CT was a craniotomy in the OR on Wednesday, December 12th 2001 by *Dr. Theodore Bernstein*. The MobileSCAN CT was used to provide a pre-operative CT scan, followed by a post-operative CT scan to check the extent of resection and for any bleeds or complications prior to the patient leaving the OR. *Dr. Bernstein* was pleased with the image quality and the ease in which they were made.

The second and third clinical uses occurred on Thursday, December 13, 2001 with a craniotomy in the morning, and a spine case in the afternoon. In both instances the scans were taken in minutes and image quality was found to be acceptable by *Dr. Bernstein, Dr Poelstra* and *Dr Kraus*. Introperative CT scans were used in a total of

eight neurosurgical cases, including a spine case, before the end of the Cooperative Agreement period of performance on January 31, 2002.

The Intraoperative CT will be incorporated by WKNI for active online registration of data to enhance future neurosurgical guidance. Incorporation of intraoperative CT imaging is more affordable than MRI, is smaller and portable, and provides more bone detail. It is anticipated that intraoperative CT has future application for surgical guidance throughout the human body.

5.1.9 Co-registration Software

The goal was to develop a co-registration software program for clinical use with the following specifications: 1) automated co-registration of multimodality brain images; 2) manual point matching; 3) a mouse-controlled (rotation/translation) rapid manual registration; 4) overall 2-4 min processing time on typical PCs; 5) the manual selection of templates for those unusual cases where automatic template selection is impossible because there is instrumentation in the field of view, such as stereotactic frames, head holders, etc.; and 6) an accurate registration and user-friendly program.

With the CRASIS program, in the first iteration the initial affine transform is applied to the *target* volume and the process of template selection and matching is repeated to find the second transform parameters. This second transformation is applied only if the average distance between homologous points is reduced from the first iteration. The process continues up to an operator-selected number of iterations or until the average distance between all of the points fall below a preset limit.

The accuracy of CRASIS was determined from co-registering the Vanderbilt brain image data sets [9, 10]. The results for intra-modality MR co-registration are shown in **Table 1**. The results for inter-modality images MR to CT and PET to MR are shown in **Table 2**. For the Vanderbilt data, each image pair was approximately aligned using the mouse (to control rotation and translation), and then automatic registration was initiated (iterations set at 2). Entries in Table 1 indicate the mean, median and maximum errors for each data set. The CRASIS program performs nearly as well as the best method reported to date using the Vanderbilt intra-modality (MR to MR) data. The average mean, median and maximum errors are 0.2, 0.15 and 0.24 mm higher than those of the best method reported.

Table 1

CRASIS mean, median, and maximum errors (in millimeters) using 8 intra-modality MR volumes from the Vanderbilt dataset [9, 10]. Errors from the best method reported are in parentheses.

DATA SET	MEAN	MEDIAN	MAXIMUM
1	3.23 (2.78)	3.20 (3.80)	3.46 (2.90)
2	1.75 (1.81)	1.77 (1.83)	1.92 (1.88)
3	2.01 (1.65)	2.07 (1.61)	2.61 (2.12)
4	4.03 (2.58)	3.99 (3.62)	4.47 (2.12)
5	2.79 (3.06)	3.63 (2.99)	3.71 (3.36)
6	3.52 (3.46)	3.48 (3.36)	4.12 (4.19)
7	2.64 (2.54)	3.67 (2.41)	3.74 (3.45)
8	2.10 (2.62)	2.10 (2.66)	2.84 (3.31)

Table 2 shows results for inter-modality image co-registration, with entries 1-7 MR to CT and entries 8-13 PET to MR. Again, the results compare favorably with the best method reported with the Vanderbilt data, especially comparing the PET to MR co-registration where CRASIS had an average mean, median and maximum error of 3.47, 5.87 and 7.9 mm compared with the best method reported of 5.87, 2.85 and 40.1 mm. With CRASIS the median error is worse than that of the best method; however, the mean and maximum errors are substantially less. CRASIS appears to be more "stable" because it utilizes similar information from the image volumes to determine the transformation and avoids

Table 2

CRASIS mean, median, and maximum errors (in millimeters) using 13 intermodality volumes from the Vanderbilt dataset [8, 9]. Errors from the best method reported are shown in parentheses. Note: Data sets 8-13 are for PET to MR registration.

DATA SET	MEAN	MEDIAN	MAXIMUM
1	3.00 (2.16)	2.81 (2.09)	6.28 (3.75)
2	2.52 (1.49)	2.29 (1.47)	6.28 (2.68)
3	2.93 (2.02)	2.41 (2.01)	5.24 (4.47)
4	1.83 (0.86)	1.70 (0.88)	4.11 (1.84)
5	1.59 (0.84)	1.27 (0.66)	4.45 (1.97)
6	2.22 (1.08)	2.11 (0.78)	5.56 (3.89)
7	2.17 (1.02)	2.12 (0.98)	4.65 (2.04)
8	3.05 (7.35)	3.12 (3.27)	6.74 (62.2)
9	3.76 (4.09)	3.74 (2.63)	9.44 (23.4)
10	3.36 (8.41)	3.13 (2.50)	8.99 (64.2)
11	4.37 (9.71)	4.16 (2.96)	10.9 (72.0)
12	2.77 (2.18)	3.82 (2.13)	4.81 (5.01)
13	3.52 (3.55)	3.72 (2.23)	7.63 (14.0)

using dissimilar regions. However, when images do not contain partial intensity and/or geometric differences, the use of the entire volumetric data tends to produce more accurate results.

The CRASIS program meets or exceeds specifications as follows: 1) the program was written in IDL from Research Systems, Inc., and can be run on any OS; 2) co-registration via manual point selection is supported; 3) rapid registration via mouse-controlled rotation/translation is supported; 4) the program co-registers brain volumes (256"×256"×124") in approximately 2-4 minutes on a generic PC (800Mhz CPU and 256 Meg of RAM); 5) manual selection of templates is supported and; 6) the program is accurate and user-friendly. Visual inspection shows excellent alignment between the reference and re-sampled target volumes. Analysis of CRASIS with the Vanderbilt test data sets produced a median error of approximately 2.8mm.

The CRASIS software is utilized the WKNI for the co-registration of PET glucose, methionine, choline, fallypride and flumazenil images to MR or CT. Beyond the diagnostic advantages that derive from image co-registration, the biochemical data is often transferred to the MR or CT scans and used to target lesions for resection or radiotherapy and to mark speech or motor areas to be avoided (***Figure 12).***

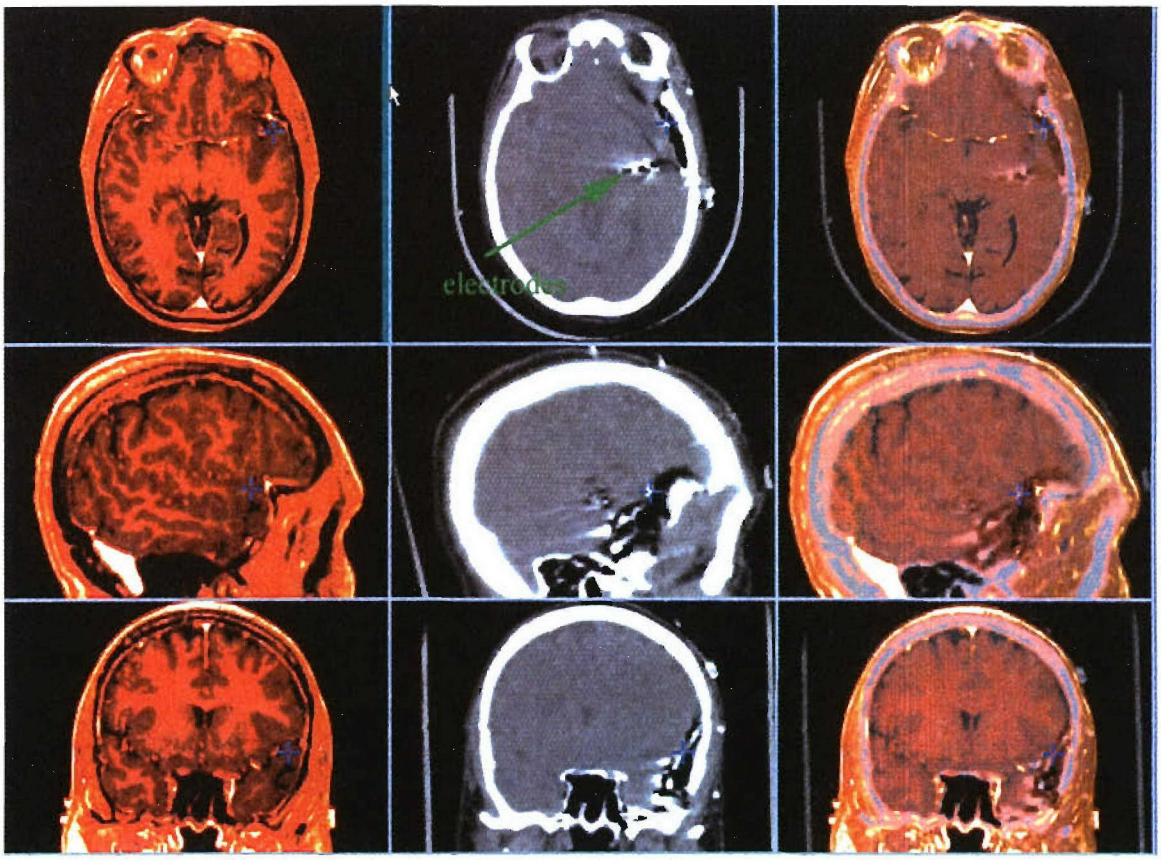

Figure 12. Co-registration with CRASIS of CT to MR scans of a patient with intractable epilepsy. *After placement of electrodes to identify the seizure focus, considerable brain shift (edema) occurred. The use of template matching based on mutual information from each image modality resulted in an accurate registration.*

5.1.10 CAD Environment for Image Segmentation – Software Development

The result of a typical 3-D segmentation is an interconnected set of voxels that form the bounding surface of an object, referred to as a volumetric region or digital shape. Since voxels belonging to an arbitrary shape often do not form a regular grid, surface parameterization methodologies that require a regular grid of control points such as B-splines and Non-Uniform B splines (NURBS) are precluded. However, a rational Gaussian (RaG) formulation [11, 12] does not require a regular grid of control points to represent a free-form shape. The key steps of the process are: 1) parameterizing the voxels in the digital shape and 2) finding the control points of the RaG surface approximating the shape by the least-squares method. Once the RaG surface is created, it is overlaid on the image data and the user can revise the surface by moving its control points via the mouse ***(Figures 13 - 15)***.

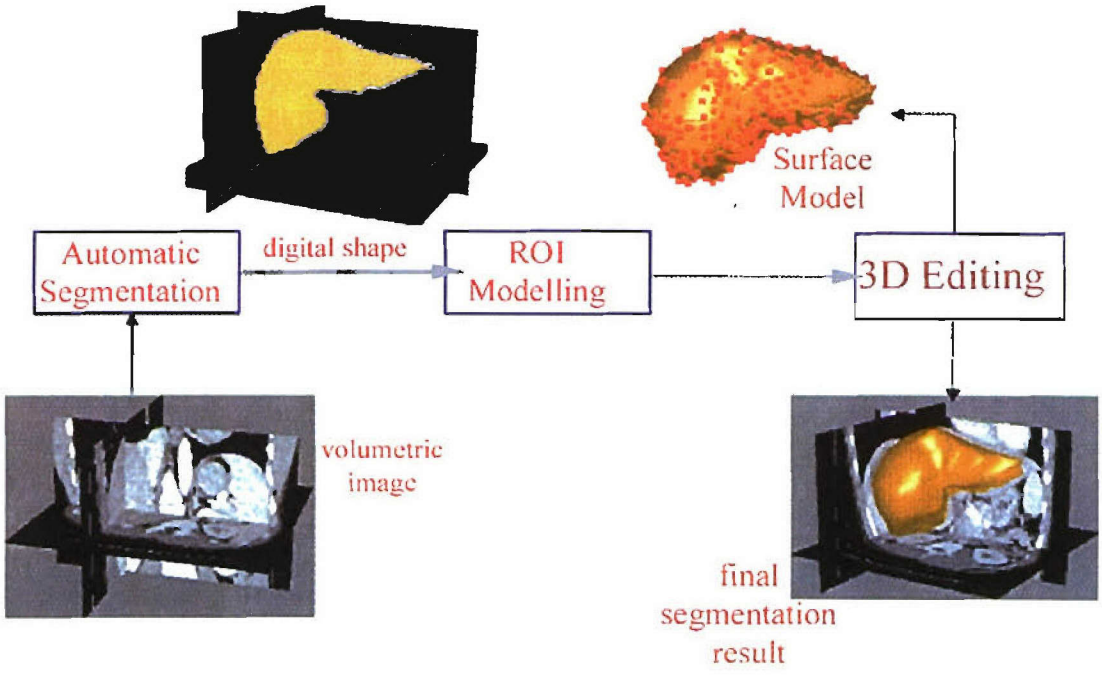

Figure 13. The workflow for a 3-D ROI editing. *A digital shape is extracted from the volumetric image via an automated or manual segmentation. The digital shape is then modeled as a surface (sum of Gaussians) with a reduced number of control points. The surface model (free-form parametric surface) is overlayed on the volumetric image. The operator can then revise the surface in 3-D while viewing the 2-D contours produced by the intersection of the surface with the orthogonal planes (axial, coronal and sagittal).*

The CAD 3-D editing environment developed for the NGN project requires only a fraction of the time needed to produce a 3-D segmentation slice by slice (2-D mode). Although modification is done in 3-D, the user can go through image slices in any desired view (axial, coronal and sagittal). Since the final result is in surface form, a smooth rendering of the segmented region can be performed. This representation also enables rendering of a segmented region in high resolution. Because a region of interest is represented by a parametric surface, the data can be sent to a computer-aided manufacturing system for actual construction of the object shape. A full description of this work can be found as Attachment 2 hereto.

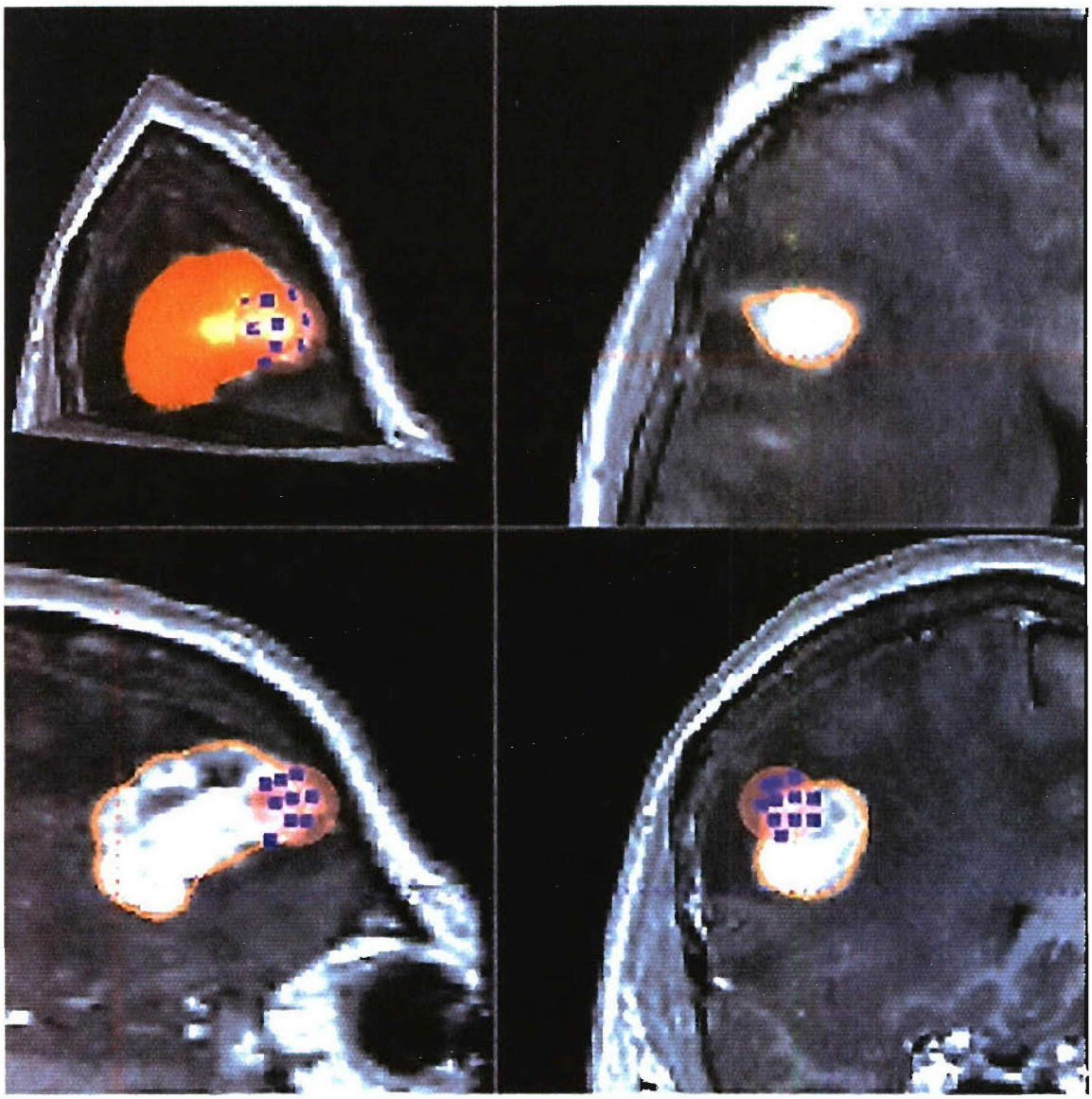

Figure 14. CAD surface editing. *A small sphere attached to the cursor selects a number of control points for near-real time editing. As the user performs editing in one view, the surface is revised in all four windows.*

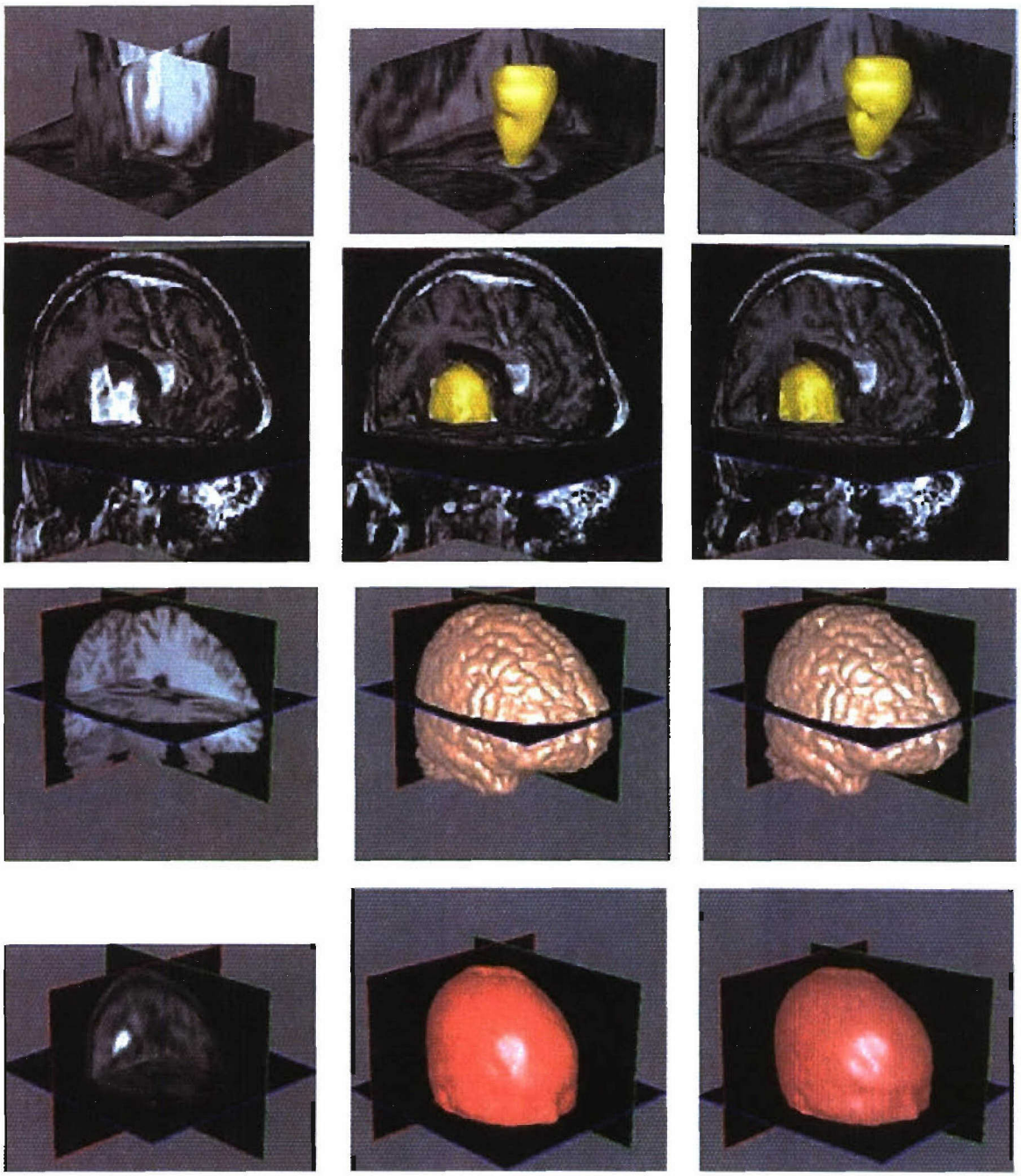

Figure 15. First row: Short-axis cardiac MR image and segmentation of left ventricular cavity; Second row: MR brain image and segmentation of the tumor; Third row: MR brain image and segmentation of the brain; Fourth row: PET image and extraction of the surface of the head. *The first column shows the original images, the middle column shows the initial segmentation results, and the right column shows the results after surface fitting and surface modification.*

5.2 Additional Opportunities

WKNI was presented with additional opportunities in the NGN project to utilize neuronavigation technology for placement of deep brain stimulators (DBS), which tested the system's resolution to the highest degree at the maximum limits of the surgical field. The DBS surgical implantation represents a recent advance in controlling the aberrant motor activity that afflicts patients with advanced Parkinson's disease or essential tumor. The procedure is complex in that the stimulators (microelectrodes) must be placed with sub-millimeter accuracy in deep brain structures to work effectively.

To assist in the placement, a special manual microelectrode driver was fabricated (insert-***Figure 16).*** By attaching the driver to the Leksell stereotactic frame, the position of the electrodes can be monitored at all times. To better identify the exact position of the microelectrodes, an Axon microelectrode recording system was purchased from Axon Instruments, Inc., in the first quarter of 1999. This system is used to measure and display characteristic electrical signals that can uniquely identify the brain structure in which the electrode tip is implanted (***Figure 16***).

The first DBS case was performed at WKNI in November 1999 on a patient suffering from essential tremors of the head and hands. The microelectrode recording mapped the brain's electrical activity and provided a pattern that matched the pattern of the patient's neuronal activity to guide the insertion of the stimulator accurately. This system is more precise than using CT or MRI for guidance, thereby requiring fewer passes through the brain and making the procedure safer for the patient. The results of the DBS implantation restored control of movement to the patient following stimulation of the electrodes. The use of the microelectrode recording system was therefore considered to be a very effective technique for the treatment of essential tremors. Potential use of this technology also includes treatment of Parkinson's disease.

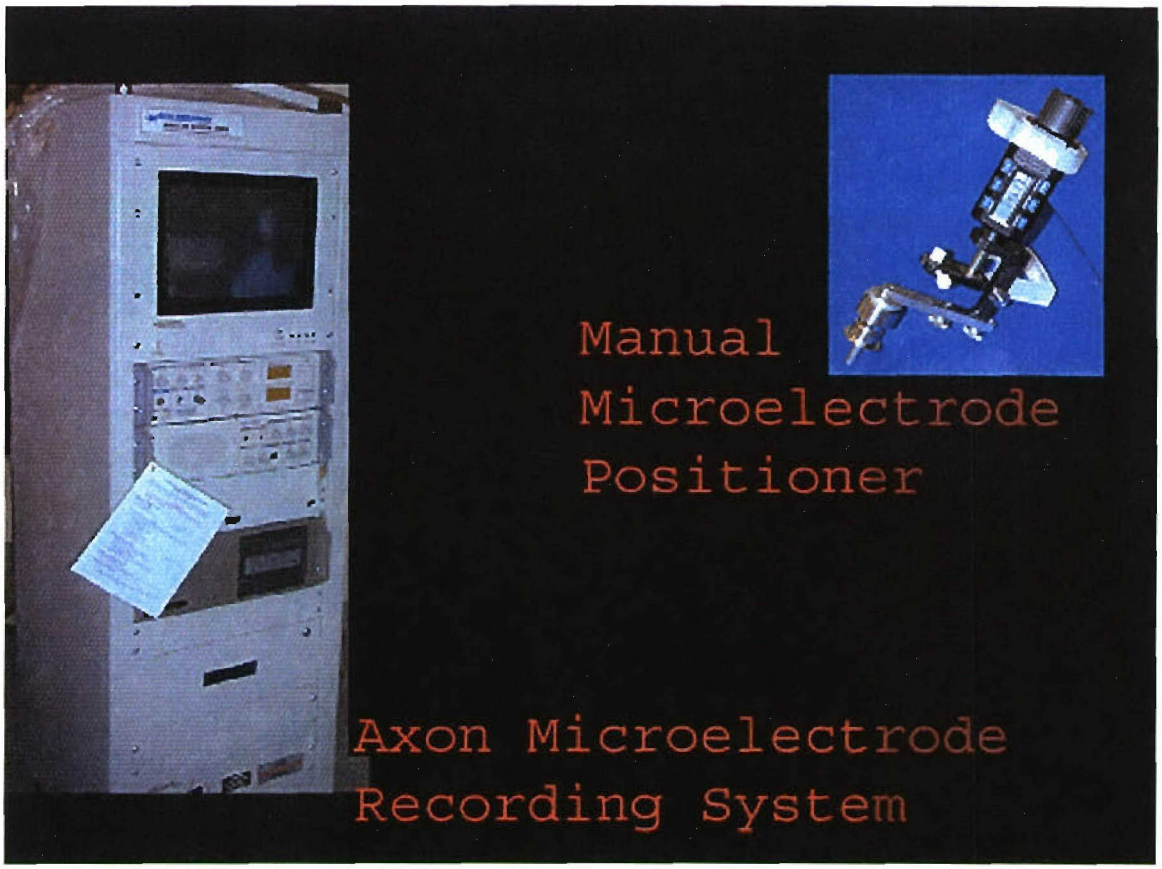

Figure 16. The Axon Microelectrode Recording System (left), and the microelectrode positioner. *These components enabled the precision implantation of microelectrodes for DBS surgery.*

5.3 Objectives Not Achieved

Brain tissue physiologic markers could be monitored with miniaturized "smart" probes capable of detecting lactate, pH, tissue fluorescence, water content, optical reflectance, pO2, pCO2, ion concentration, EEG-evoked potentials, temperature, blood flow, or radiolabeled biochemical markers. For the original implementations of the NGN project, it was proposed to cultivate a vendor partner relationship that would lead to the fabrication and testing of such a smart probe that could be integrated into a StealthStation™ as the pointing device. We felt this configuration could prove to be extremely valuable, especially in adjusting for brain shift and the ability to delineate tumor from nontumor at the probe tip.

Neurosurgeons and scientists at WKNI have pioneered the use of PET scanning for the diagnosis and treatment planning of brain tumors, including neuronavigation-based resection and X-knife and Gamma Knife radiotherapy. ^{11}C-MET and ^{18}F glucose are radioactive markers that have been utilized extensively at WKNI to reveal the altered biochemistry of tumors from normal brain tissue. These radiopharmaceuticals could be utilized during neurosurgery in conjunction with a highly sensitive positron probe capable of discriminating between the disparate uptake of radioactivity between tumor and brain tissue.

At the initiation of the NGNP, the United States Surgical Corporation (USSC) had been working for several years developing a handheld gamma detector probe system for detecting metastases (axillary node involvement) for breast cancer patients. USSC had committed $50,000 to the WKNI Neurosurgery department to collaborate in the development of the positron probe for neurosurgery. However, the collaboration dissolved when the Tyco Corporation acquired the USSC in 1999 and the project was shelved until a new vendor partner can be identified.

6.0 Future Directions

6.1 Software Development

The research proposal outlined below represents a continuing joint effort between the Intelligent Systems Laboratory at WSU and WKNI to develop methodologies and software to fuse multimodal brain images, segment brain images into different compartments, delineate tumors in images, visualize brain structures, and quantify various brain structure and tumor features.

During the past two years, this joint effort has resulted in methodologies and software that are currently in use at WKNI. Both image co-registration and segmentation are new capabilities that have been accepted for publication in peer reviewed computer science journals. These state-of-the-art capabilities should uniquely enable WKNI surgeons to provide the best patient care possible to the Miami Valley community.

6.2 Nonlinear Brain Image Registration

Preliminary work in this area has already begun. An edge-based method has been designed that elastically deforms a target brain to take the shape of a reference brain. The process involves determination of: 1) edge surfaces in the reference and target volumes; 2) correspondence between edge elements in the two images; 3) a nonlinear transformation function that will elastically deform structures in the target image to align with structures in the reference image; and 4) the use of obtained transformation function to resample the target image to overlay the reference image.

Additional work has been initiated to extract 3-D structures in volumetric brain images. The approach is based on a 3-D edge-detection algorithm, which finds edge surfaces in volumetric images. Weak and noisy edges are filtered out and only structures that are typically found in brain images are kept. Future work is planned to develop a method that establishes correspondence between two image structures as well as a method that determines a nonlinear transformation function from the correspondence to register the images. The nonlinear brain image registration being developed is in volumetric form

and will require minimal user interaction, similar to the CRASIS linear co-registration software.

The primary interest in nonlinear brain image registration is to develop software to map a patient's brain to a standard atlas, or to estimate brain shift and brain deformation caused by removal of a tumor.

6.3 Brain Shift Determination

In conjunction with nonlinear brain image registration software, a plan is underway to develop a flow visualization program that can detect the deformation existing between a target image and a reference image. The nonlinear image registration program in effect determines correspondence between all points in two brain images. From the correspondences, the magnitude and direction of the deformation are computed. Since the flow vectors are in 3-D, flow in cross-sectional images can be generated quickly for visualization of local brain shifts. Interactive tools to provide quantitative output of the amount of shift or displacement will be provided. A 2-D version of this capability is near completion. The work to be performed in this project will extend the 2-D method to 3-D and make it an integral part of the nonlinear image registration program.

6.4 Quantification of Brain Deformation in Serial Images

This capability, which will be built on top of the brain shift estimation program, will enable quantification and tracking of brain deformation patients with neurodegenerative diseases such as epilepsy and AD, as well as tracking brain shape of a patient after removal of a tumor. This new program will receive a sequence of images for processing. By nonlinearly registering consecutive images, a flow-path diagram will be generated. Each flow path will consist of a sequence of vectors, each showing the motion of a point from one time frame to the next. To provide an effective visualization of flow paths, a capability to change the density of vectors in an image will be provided. A capability to merge flow paths with brain structures displayed with desired degrees of transparency

will also be provided. This will enhance visualization of brain deformation as a function of time.

6.5 3-D Reconstruction and Visualization

Techniques to visualize and navigate through brain structures will be developed. Effective means to visualize edge structures or surface structures in brain images are currently underway. Also, use of transparency to view occluded structures and the capability to move the position of the light source to enhance viewing of local details will be provided.

When the cortical surface extracted, the user will have the capability to interactively move a predefined grid over the brain surface and fix it at a desired location. This should be useful in executing grid placement for the determination of seizure focus in epilepsy cases.

Speed will be a major factor in visualization. A method to subdivide digital brain structures into polygon meshes of a desired resolution will be developed. This should enable rendering of brain structures at a desired resolution or navigation of brain structures at a desired speed. The visualization software will be integrated with the image segmentation software to enable viewing of regions of interest obtained as a result of the segmentation. It also will be integrated with the image registration software to enable evaluation of a completed registration.

6.6 Active Snake and Balloon Models for Image Segmentation

Currently an active contour model known as the "snake" is being developed to segment brain image slices. With this software, a boundary of an object of interest is roughly drawn and the program then revises the boundary by optimizing an energy function. This is currently being made a part of the segmentation program. In the present segmentation program, the user has the option of accurately drawing region boundaries in image slices. With the snake capability, the user will need only

to roughly draw the boundary of a region of interest on a few slices and the process will reposition the contour by minimizing an energy function. By observing the final result of the snake, the user will be able to refine the segmentation result, if needed.

A 3-D energy-minimizing model, known as "active balloon," will be developed to determine the surface of an object of interest in a volumetric image. The user will initiate a spherical balloon interactively inside an object of interest. The balloon will then deform to the shape of the object by reducing its energy. The minimum energy state of the balloon is taken as the final segmentation result. The balloon will be overlaid with the given image. At this time, the user will have the ability to revise the balloon by going through image slices and pulling or pushing it locally to obtain a desired shape.

The research team will consist of two investigators and four graduate students. One of the investigators, *Ardeshir Goshtasby*, is a computer scientist in the Department of Computer Science and Engineering, WSU, and the second investigator, *Dr. Martin Satter*, is the Chief PET physicist at WKNI, KMC. The graduate research assistants will consist of four Ph.D. students. The investigators will design the methodologies that provide the required capabilities and guide the students responsible for implementing and testing the software. The research performed by the students will become a part of their theses.

Goshtasby has considerable experiences in the design of medical image analysis systems and is internationally well known. He has edited two special issues of international journals on image registration and image analysis. He also has numerous publications in the area of medical image analysis. *Dr. Satter*, a PET physicist, well understands the capabilities that are required by the neurosurgeons, neurologists and radiologists. He is aware of commercial software packages and can guide the research team towards creating useful medical image processing software ahead of commercial production. He has been programming in IDL for over a decade. The graduate students have extensive experience in software design and, in particular, image analysis and have a great desire to develop their own research that will lead to advanced degrees. The proposed team is believed to be ideal to carry out the proposed work as evidenced by software created through their previous collaborations.

References

1 Evans AC, Marrett S, Collins L et al. Anatomical-functional correlative analysis of the human brain using three dimensional imaging systems. Proc. SPIE-MI III 1989;1092:264-274.

2 Neelin P, Crossman J, Hawkes DJ et al. Validation of an MRI/PET landmark registration method using 3D simulated PET images and point simulations. Comp Med Imag Graphics 1993;17(4/5):351-356.

3 Ding L, Goshtasby A, Satter M. Volume image registration by template matching. Journal of Imaging & Vision Computing 2001;

4 Galvez JM, Canton M. Normalization and shape recognition of 3D subjects by 3D movements. Pattern Recognition 1993;26(5):667-682.

5 Devijever PA, Kittler J. Pattern recognition: a Statistical Approach. 1983; Prentice Hall:Englewood Cliffs, NJ, p. 232.

6 Anura PE. Spatial registration of multispectal and multitemporal digital imagery using fast fourier transform techniques. IEE Transactions on Geoscience Electronics 1970:8(4):353-368.

7 Borgerfors G. On digital distance transforms in 3D. Computer Vision and Imaging Understanding 1996;64:420-433.

8 Maes F, Collignon A, Vandermeulen D et al. Mutlimodality image registration by maximization of mutual information. IEE Transactions on Medical Imaging 1997;16(2):187-198.

9 http://cswww.vuse.vanderbilt.edu/~image/registration/results.html

10 http://cswww,vuse.vanderbilt.edu/~image/registration/reg_eval_html/ding.html

11 Lo CH, Don HS. 3D moment forms: their construction and application to object identification and positioning. IEE Transactions on Pattern Analysis and Machine Intelligence 1989;11(10):1053-1055.

12 West J, Fitzpatrick JM et al. Comparison and evaluation of retrospective inter-modality brain image registration techniques. Journal of Computer Assisted Tomography 1997;21(4):554-566.

Positron Emission Tomography (PET) Biochemical Imaging

Principle Investigator:

Joseph Mantil, M.D., Ph.D.
Director, Department of Nuclear Medicine/PET
Kettering Medical Center

1.0 Executive Summary

1.1 Purpose

The Positron Emission Tomography (PET) Biochemical Imaging project focuses on using biochemical imaging of tumors for improved diagnosis, target delineation and treatment evaluation.

1.1.1 Use of Biochemical Imaging for Tumor Diagnosis

By measuring chemical changes within the body, PET biochemical imaging offers many advantages over other technologies available for the detection and treatment of brain tumors and other neurological diseases. Noninvasive biochemical brain mapping performed by PET scan can immediately elucidate the marked differences between normal brain tissue and tumor tissue for the physician, long before the anatomical changes recorded by computerized tomography or magnetic resonance imaging can be detected.

1.1.2 Development of Radiotracers and Radiopharmaceuticals for PET Imaging

In order to understand the biochemical processes in tumor, PET allows the use of selective radiotracers (or biomarkers) that enables the analysis of tumor pathology, location and volume. Biochemical imaging thus assists in the efficacy of neurosurgery, radiotherapy, and chemotherapy. The development of new radiotracers for use in PET scanning aids studies of patients with brain tumors, schizophrenia, stroke, Alzheimer's disease (AD) and Parkinson's disease.

Radiopharmaceuticals will also be developed, and the production of currently used radiopharmaceuticals will be streamlined. Methods for the routine production of several radiopharmaceuticals for human use have now been established. These include ^{11}C-choline for studying lipid synthesis in tumors, ^{11}C-flumazenil for studying benzodiazepine receptor sites in epilepsy, and ^{18}F-fallypride for dopamine receptors in neuropsychiatric illnesses.

1.1.3 Software Development for Quantitative PET Image Analysis

The development of software for quantitative PET image analysis is necessary for state-of-the-art modeling of neuroreceptor location and function that will support studies in many areas of interest to both the Wallace Kettering Neuroscience Institute and the USAF Air Force Research Laboratory including AD, nerve gas poisoning, stress reactions, schizophrenia, movement disorders, and the development of posttraumatic stress disorder. This work involved: 1) defining a metric which accurately described the ligand-receptor binding process; 2) developing an experimental protocol for measuring this metric; and 3) devising a method which simplified both the data acquisition and analysis for the measurement of this metric.

1.1.4 Optimization of Therapy for Brain Tumors

Further objectives were to utilize the information from PET imaging to develop strategies for improving therapeutic response, and investigate the application of 2-deoxy-D-glucose as a differential radiomodifier to optimize therapy of malignant brain tumors.

1.2 Methods and Procedures

1.2.1 Use of Biochemical Imaging for Tumor Diagnosis

A protocol was developed to utilize three target radiotracers to study brain tumors in human subjects: ^{18}F-fluorodeoxyglucose (^{18}F-FDG) for glucose metabolism; ^{11}C-methionine (^{11}C-MET) for amino acid transport and protein synthesis and; ^{11}C-choline for lipid synthesis. The uptake and incorporation of these radiotracers were evaluated using PET in astrocytoma patients who were suspected of having World Health Organization (WHO) grade II or grade III tumors.

Seventeen patients with suspected astrocytomas (nine grade II and eight grade III) were studied by PET with ^{18}F-FDG and ^{11}C-MET, and one patient (grade III) was studied with ^{18}F-FDG, ^{11}C-MET and ^{11}C-choline. The uptake of PET radiotracers was quantitated based on tumor to corresponding-contralateral-region uptake ratio, tumor to mean-cortical-uptake ratio, and tumor to white matter uptake ratio. Radiotracer uptake was also correlated with the WHO histologic grading system and clinical follow-up. To better understand the potential underlying mechanisms of radiotracer uptake in the tumors, we

also carried out in vitro studies with the tracers in a grade III HTB-14 human astrocytoma cell line.

1.2.2 Development of Radiotracers

The installation of the General Electric-Nuclear Interface (GE-NI) system was completed and used to produce high-specificity activity methyliodide for production of various receptor-specific radiopharmaceuticals. The system consisted of two phases: the first phase that produced the high-specificity methyliodide, and the second that used the methyliodide to label the various radiopharmaceuticals. Installation of the entire system required the assembly of shielding, laying out of various utilities, and appropriate ventilation of the shell for the two phases.

The GE-NI was also used to streamline the production of several carbon-11 radiotracers, including ^{11}C-choline, ^{11}C-MET and ^{11}C-flumazenil, all of which are produced routinely for human-use purposes.

1.2.3 Development of Software for PET Analysis

Software was developed to permit quantitation of the binding characteristics of novel neuroligands. This involved: 1) defining a method that accurately described the ligand-receptor binding process; 2) developing an experimental protocol for measuring this metric and; 3) devising a method that simplified both the data acquisition and analysis for measurement of this metric.

An analytical method was developed and validated for ^{18}F-fallypride for measuring a metric that is representative of dopamine, D-2, receptor density. A rigorous compartmental analysis was first performed to define the "gold standard" of the in vivo tracer kinetics. Simplified models were then applied to test the tradeoffs between parameter bias and computational rigor.

1.3 Results

The successful completion of the PET Biochemical Imaging Project involved state-of-the-art positron labeling and detection technologies, as well as the development of visualization software, interactive 3-D rendering, biochemical-based image segmentation, co-registration, and software for neuroreceptor imaging and modeling.

1.3.1 Use of Biochemical Imaging for Tumor Diagnosis

Our results suggest that a combination of ^{18}F-FDG and ^{11}C-MET is useful in predicting the histologic grade of astrocytomas. Moreover, ^{11}C-MET is better than ^{18}F-FDG in delineating tumor boundary for low-grade gliomas.

Our in vitro studies demonstrate that ^{3}H-MET is incorporated into proteins, suggesting that protein incorporation is one of the major driving forces in the uptake of ^{11}C-MET that has been observed in PET imaging.

Experiments with these radiotracers in vivo in animal models will be useful in further characterizing the biochemistry of tumors. These findings may then be correlated with the findings in human subjects.

Receptor studies with ^{18}F-fallypride have potential USAF application because this type of metabolic measurement could be used to study the effects of nerve gas poisoning on the central nervous system, and possibly improve upon methods to counteract its effect.

1.3.2 Radiotracer Development for PET Imaging

We evaluated our automated tandem system, the GE-NI, for the clinical production of the radiopharmaceuticals ^{11}C-choline, ^{11}C-MET and ^{11}C-flumazenil. ^{11}C-flumazenil was used to study the gamma aminobutyric acid receptor complex, because ^{11}C-flumazenil binds to sites that have been shown to be overly expressed in epilepsy patients. PET imaging with this radiopharmaceutical can potentially supply the adequate diagnostic and localizing information needed for epilepsy patients to receive relief from their disease.

The radiochemistry developed and streamlined under this project provides a potential benefit to the military where it can be used to analyze the biochemical effects of toxic compounds, or measure their pharmacokinetics once they are labeled. PET imaging can create quantitative 3-D images that can be used to evaluate the effects of such compounds.

1.3.3 Software Development for Quantitative PET Image Analysis

We found that a simplified method of analysis, yielding a parameter of distribution volume ratio, could accurately describe the binding process without the need to sample arterial blood from the patient. This model can now be applied to human studies without the full course of validating studies.

It is also possible to apply this model of in vivo binding characteristics to answer relevant scientific questions. ^{18}F-fallypride was used to measure antipsychotic drug occupancy for the D-2 dopamine receptor site, and showed that very small amounts of the typical antipsychotic, haloperidol, result in almost complete blockage of the targeted D-2 receptor, which causes an overmedicating of the patient. These measurements were also made for atypical antipsychotic medications such as risperidone and clozapine.

2.0 Summary of Objectives

2.1 Biochemical Imaging of Tumors for Diagnosis, Target Delineation and Evaluation of Treatment

The first objective was to improve the diagnosis of brain tumors, target delineation and treatment evaluation of these tumors. In order to understand the biochemical processes in tumor, PET allows the use of selective radiotracers (or biomarkers) to improve the analysis of tumor pathology, location and volume. Biochemical imaging can thus assist in the efficacy of neurosurgery, radiotherapy and chemotherapy.

2.2 PET Scanning to Determine Tissue Viability Post-Stroke

The objective of this subproject was to develop a protocol to identify and measure salvageable brain tissue post-stroke using PET scanning. Currently, stroke patients medically evaluated within three hours of the onset of stroke symptoms, and whose computerized tomography (CT) scan indicates that symptoms are not due to cerebral hemorrhage, are candidates for tissue plasminogen activator (TPA). Some patients who have extensive areas of irreversibly injured cerebral infarct will benefit little from this therapy; however, patients who have small areas of cerebral infarct and significant areas of reversibly injured penumbra are likely to benefit substantially from TPA therapy. In the absence of a diagnostic procedure to differentiate these two types of stroke patients, both are exposed to the inherent risks of TPA therapy; therefore, less than 10% of stroke victims currently receive TPA treatment. The development of a rapid diagnostic procedure that can differentiate between these two patient populations will enable the clinician to initiate TPA therapy in patients for whom the benefits outweigh the risks.

2.3 Tracer Development for PET Imaging

The first goal under this objective involved development of new radiotracers for research and protocol development. The initial challenge was to develop the radiochemistry for labeling ^{11}C-choline, an analog of naturally occurring choline, to allow for evaluation of the growth of cell membranes, specifically malignant cell growth. Another area to be

explored was the production of radiochemistry to produce a high-specific activity ^{11}C-flumazenil to trace neurotransmitter receptor activities.

The second goal under this objective was to streamline the production of radiopharmaceuticals currently in clinical use in ongoing PET studies of patients with brain tumors, schizophrenia, stroke, Alzheimer's disease (AD), and Parkinson's disease (PD).

PET glucose metabolism imaging is employed to diagnose brain tumors, epilepsy, AD and stroke and currently, ^{18}F-FDG is the tracer of choice.

Perfusion imaging with PET is utilized to map brain function, determine the volume of hypoperfusion due to stroke, predict individuals who may benefit from endarectomy, and localize the brain areas responsible for movement and speech. While oxygen-15-labeled water is currently the tracer of choice, we plan to evaluate the utility of fluorine-18-labeled fluoromethane as a perfusion agent in assessing tissue viability post-stroke, and for activation studies to identify vital brain regions to be avoided during a surgical resection.

The Wallace-Kettering Neuroscience Institute (WKNI) has done research with carbon-11 methionine (^{11}C-MET), a naturally occurring amino acid, which has shown to be a good tracer for amino acid transport and metabolism. Specifically, it has shown tremendous potential as a marker for brain tumors. A goal of this subproject was to streamline the radiochemical synthesis of ^{11}C-MET for routine clinical production.

2.4 Software Development for Quantitative PET Image Analysis

The final objective of the PET Biochemical Imaging Project was to develop software for quantitating the binding characteristics of novel neuroligands to potentially eliminate the need for arterial blood sampling from patients undergoing PET receptor scanning. This work involved: 1) defining a metric that accurately describes the ligand-receptor binding process; 2) developing an experimental protocol for measuring this metric; and 3)

devising a method that simplifies both the data acquisition and analysis for the measurement of this metric.

3.0 Background

Positron Emission Tomography (PET) is a powerful imaging modality that enables biochemical and physiological imaging of the entire body, including the brain. The novelty of PET scanning stems from the associated PET radiochemistry, which labels highly specific radiopharmaceuticals and physiologic markers with positron-emitting radioisotopes such as carbon-11 (^{11}C; 20-min half-life; $t_{½}$), oxygen-15 (2-min $t_{½}$), nitrogen-13 (10-min $t_{½}$) and fluorine-18 (110-min $t_{½}$). PET scanning enables regional brain function to be monitored in a noninvasive manner, essentially utilizing biochemical probes to perform radioassays. PET imaging is extremely sensitive, producing radioassays in the nanomolar to picomolar range. Thus, PET scanning is a true tracer technique employing concentrations of radiopharmaceuticals that do not perturb the biological system. PET biochemical imaging is an in vivo analog of standard autoradiography and can provide unique information regarding the underlying biochemistry of the disorders of the body.

By measuring chemical changes within the body, PET biochemical imaging offers many advantages over the other techniques available for detection and treatment of brain tumors and other neurological diseases. Noninvasive biochemical brain mapping performed by PET can immediately elucidate the marked differences between normal brain and tumor tissue for the physician, long before the anatomical changes recorded by CT or magnetic resonance imaging (MRI) can be detected. PET scanning is an ideal tool for examining the neural response to sensory, motor, cognitive and drug stimulations, and the development of biochemical markers that can provide an early indication of central nervous system (CNS) disorders.

PET can also determine tissue viability post-stroke, enabling a more accurate determination of whether a patient may receive acute stroke therapy to rescue salvageable brain tissue. The development of new radiotracers for use in PET scanning will aid in studies of patients with brain tumors, schizophrenia, stroke, AD or PD. Finally, the development of software for quantitative PET image analysis is necessary for state-of-the-art modeling of neuroreceptor location and function that will support studies in many

areas including AD, nerve gas poisoning, stress reactions, schizophrenia, movement disorders, and the development and treatment of posttraumatic stress disorder.

3.1 Biochemical Imaging of Tumors for Diagnosis, Target Delineation and Evaluation of Treatment

The biochemistry of normal brain tissue is markedly different from tumor. As tumor grows, its biochemistry fingerprint can be detected before visual alterations are observed in the tumor-to-brain tissue interface from the classical diagnostic imaging modalities such as CT or MRI. With MRI or CT imaging, the tumor:brain tissue interface is typically enhanced by the use of contrast agents which permeate the primitive (leaky) blood brain barrier of a tumor. Thus, until the tumor vasculature develops, a lesion may remain invisible to contrast-enhanced MRI or CT imaging. This chronological sequence, biochemistry differences culminating in anatomical contrast, enables early detection of a brain tumor for diagnosis and treatment planning with PET imaging.

3.2 PET Scanning to Determine Tissue Viability Post-Stroke

Stroke affects approximately 500,000 people in the U.S. each year, where it is the third leading cause of death. In addition to mortality, stroke is the leading cause of morbidity in the U.S., which imposes an enormous economic burden on stroke victims, their families and society. A recent study by the Stroke Prevention-Patient Outcomes Research Team estimated the economic burden of stroke in the U.S. to be in excess of $30 million in 1993; $17 billion in direct medical costs and over $13 billion in indirect costs associated with lost earnings. Over the next decade, it has been estimated that about 15 million people will suffer acute stroke in Europe and the U.S., and approximately 85% of the strokes will be ischemic in origin. Cerebral vascular thrombus is very often the cause of ischemic stroke. Very early in this ischemic episode, the affected cerebral tissue exhibits a core of anoxic (irreversibly injured) tissue surrounded by an ischemic penumbra, which is a zone of ischemically threatened but potentially viable (reversibly injured) tissue.

Restoration of blood flow (and oxygen) to the ischemic zone at the earliest possible time is crucial to salvaging reversibly injured tissue and eventual recovery of normal or near-normal cerebral function. With vascular thrombus-induced cerebral ischemia, early intervention with thrombolytic agents may significantly improve the patient's prognosis. Several randomized clinical trials [1-5] have evaluated the efficacy and safety of intravenous thrombolysis. The European Cooperative Acute Stroke Study suggested benefits with the use of tissue plasminogen activator (TPA) within 6 h of stroke onset with patients whose initial CT scan does not indicate major signs of early infarction [4]. However, the use of both streptokinase and TPA are accompanied by an increased risk of cerebral hemorrhage. The timing of the thrombolysis is critical [6], since the National Institute of Neurological Disease and Stroke (NINDS) trial found a benefit with TPA without an increase in mortality when treatment was begun within 3 h of symptom onset [5]. *Infield et al.* also suggest that earlier treatment is associated with a better outcome [6]. They proposed the concept of a chronological "therapeutic window" to rescue the dynamic penumbra, which has the potential for recovery but without intervention transforms into the core of irreversible infarction. It has been suggested by *Heiss et al.*, based on PET studies of tissue deoxygenation, that this window may be extended up to 48 h in some patients [7].

Currently, stroke patients evaluated medically within 3 h of the onset of symptoms, and whose CT scan indicates that symptoms are not due to cerebral hemorrhage, are candidates for TPA therapy. Some patients who have extensive areas of irreversibly injured cerebral infarct will benefit little from this therapy. Patients who have small areas of cerebral infarct and significant areas of reversibly injured penumbra are likely to benefit substantially from TPA therapy. In the absence of a diagnostic procedure to differentiate these two types of stroke patients, both will be exposed to the risks of TPA and for this reason, less than 10% of stroke victims currently receive TPA treatment. Therefore the potential use of PET scanning to develop a protocol to identify and measure salvageable brain tissue is critical.

3.3 Radiopharmaceutical and Tracer Development for PET Imaging

A key component to the development of a successful protocol to identify and measure salvageable brain tissue post-stroke, and the diagnosis and treatment of tumor and other CNS-related disorders, is the development of radiopharmaceuticals and radiotracers (biomarkers) to enable the analysis of tumor pathology, location and volume. The biochemical imaging afforded by the use such tracers will assist in the efficacy of neurosurgery, radiotherapy and chemotherapy. Meanwhile the development of novel radiotracers, as well as streamlining the production of currently used radiopharmaceuticals, for use in PET scanning will aid in studies of patients with brain tumors, schizophrenia, stroke, AD or PD.

3.4 Software Development for Quantitative PET Image Analysis

3.4.1 Neuroligand Modeling Software Development

PET receptor studies are considered minimally invasive to the patient because only arterial blood sampling is performed to obtain the input function for the pharmacokinetic model. However, obtaining arterial blood samples can be a relatively painful experience and carries some risk of arterial damage, which sometimes precludes the use of this technique for routine clinical or pediatric studies. Therefore, the development of methods for the quantitative measurement of neuroligand/receptor interactions without the need for these arterial blood samples is of value.

The time-activity curve of the arterial plasma is termed as the input function, indicating the concentration of the radiotracer presented to the tissue over the course of the experiment. In general, the shape of this curve determines the kinetics of the radiotracer as measured by the PET scanner. Knowledge of the input function is crucial to accurately quantitate the kinetics of the radiotracer. Once this necessary step has been completed, it is possible to validate model simplifications, such as the use of a reference region or pseudo-equilibrium technique. Reference region techniques refer to using an area in the brain that can provide an estimate of the ligand concentration where specific binding is negligible. A study of how the implementation of software reference region techniques could impact the clinical setting would allow relatively complex ligand/receptor systems

and processes to be investigated, and PET data to be acquired through a straightforward method suitable in the clinical setting.

3.4.2 PET Activation Data Analysis

With the advent of advanced medical imaging instruments such as functional MRI (fMRI) and PET, it is now possible to localize areas of cerebral function noninvasively not only in diseased patients, but healthy subjects as well. This methodology has evolved into a rapidly growing field termed "brain mapping" or "function activation," and is widely used by all disciplines of neuroscience. Functional activation studies refer to locating specific regions in the brain that are used while performing some type of task or exhibiting some behavior.

Original PET investigations in noninvasive functional activation were conducted by *Fox and coworkers* [8]. These studies operated under the premise that as a specific region of the brain is utilized to perform a task, its energy consumption increases. The increase in energy consumption (or glucose utilization) is accompanied by an increase in local blood flow. Therefore, measuring changes in local cerebral blood flow (CBF) will indicate regions of the brain that are active during a task.

Because these changes in CBF can be very small, it became necessary to devise a method of analysis that could accurately determine areas of activation. As in all medical diagnoses, the goal of this statistical analysis was to make sure that all areas of activation are found (sensitivity) while limiting the number of false activations (specificity).

In early PET activation studies, oxygen-15-labeled water was employed to measure CBF. Experiments consisted of making two measurements of blood flow, one at rest and one while performing a task (activation). The areas of activation were then identified by subtracting the resting scan from the task can, which resulted in a "difference" image. Though the statistical details of identifying the areas of activation have advanced dramatically since this original work, the underlying technique of comparing the two conditions remains the same.

As the power and utility of this technique gained in popularity, attempts were made to measure very subtle activations (i.e., 1-2% change in blood flow), such as those observed while performing higher cognitive functions. This required larger sample sizes to increase statistical power. Statistical parameter mapping (SPM) was developed to account for the inter-subject variations and establish a statistically rigorous standard for researchers to analyze these studies. SPM analysis consists of spatially normalizing the images into a standard space to allow inter-subject comparison, and applying the General Linear Model to generate statistical maps of t, Z and F statistics. Because of the large size of the image sets, up to 128*128*50 voxels, the analysis software includes capabilities for multiple comparisons and defining the correlation between pixels inherent to image construction. These issues are addressed using the theory of continuous random fields.

Though widely used and accepted by the scientific community, there are still several shortcomings in using SPM for activation analysis. The primary problem is the low degree of freedom associated with these studies. This becomes a limiting factor in using SPM analysis for clinical applications where only a single subject is scanned, as in the case of identifying motor or speech areas in a patient with a brain tumor. Statistical maps are calculated using an estimate of the variance at each voxel. For a single-subject study with at most five scans per condition, the variance estimate becomes highly unstable. This in turn results in a prohibitively noisy t or F map. Some estimations set a lower limit of 24 degrees of freedom for accurate t maps.

To counter the limited degrees associated with single-subject studies, several groups have proposed nonparametric analysis techniques [9, 10]. Nonparametric analysis eliminates many of the assumptions associated with SPM, such as normally distributed data that is derived from continuous random fields with a stationary covariance structure. Nonparametric techniques simply assume that under the null hypothesis of no activations, the experimental labels of the data can be switched and a null hypothesis can be expected. In implementation, rest and task scans are mixed and randomly grouped to form a

randomization distribution. The hypothesis can then be tested by comparing the labeled data with this distribution.

Another novel technique has been suggested for analyzing activation experiments of single subjects by partitioning the dynamic PET image sequence into smaller temporal segments [11]. This method effectively increases the degrees of freedom without decreasing the signal-to-noise ratio of the data set. Our goal was to develop the optimum activation software to analyze PET activation data, especially for single-subject studies.

4.3 Tumor-Volume Measurement (3-D Display)

Precise tissue-volume measurement is critical in all phases of research and surgical application at WKNI. For example, tissue-volume measurement is necessary in pre-surgical planning, both in terms of localization of eloquent cortex and tumor imaging. Accurate tissue-volume measurement requires some form of objective image segmentation, and therefore a certain degree of automation [12-14]. Manual methods of separating data according to the various tissue types that they are sought to represent are inherently prone to operator subjectivity and can be very time-consuming. Therefore we sought to implement software with a segmentation procedure based on morphological edge detection to determine the volume of tumors and specific brain regions under study. This software would potentially calculate tissue volumes from physiological data obtained from PET studies and co-registration techniques involving fusion of PET, MR and CT images.

3.5 Study of 2-Deoxyglucose as a Differential Modifier

The prognosis of patients suffering from malignant gliomas has remained dismal despite the application of sophisticated multi-modal therapy based on medical radiation technology. Failure of local tumor control is the major contributor to the failure of radiotherapy, implying that the conventional treatment is inadequate to locally control the tumor. The poor response is attributed primarily to the presence of hypotoxic, repair-proficient and intrinsically radio-resistant sub-populations of cells in the tumor. The delivery of larger radiation doses is restricted due to the limited tolerance of normal

tissue. Therefore, strategies directed towards differentially enhancing radiation damage in tumor cells, while reducing the damage to normal tissues could significantly improve the treatment efficacy of radiotherapy, leading to better local control.

Differences in glucose-dependent energy metabolism between malignant tumor and normal cells (i.e., that glucose usage in malignant tumors is significantly higher compared to normal cells) are well known. ^{18}F-FDG-PET imaging has shown that the glucose uptake correlates directly with the degree of malignancy and inversely with the treatment response. We investigated using 2-deoxyglucose (2-D), a glucose analog and inhibitor of the glucose transport and glycolytic pathway, to induce energy-linked differential modulation of post-irradiation repair responses for enhancing radiation damage to tumors, while reducing the same in normal tissues.

4.0 Methods and Procedures

4.1 PET Scanner Acquisition

The success of the PET Biochemical Imaging Project was dependent upon the acquisition of a state-of-the-art PET scanner. A scanner capable of imaging the entire brain volume was required to capture the interplay of the complex network of structural subunits working in concert for a specific brain function. A scanner with a high spatial resolution was necessary to improve the accuracy of surgical resection or X-knife radiotherapy when PET imaging is employed for tumor (target) delineation. Finally, a scanner with a high temporal sampling capability was important to allow for detection of rapid changes in brain function as well as define the pharmacokinetics of CNS-acting drugs. The Seimens Exact HR$^+$ PET scanner, the scanner of choice at the vast majority of neuroscience institutes worldwide, was the scanner acquired for this project. After installation and performance of appropriate testing, this scanner is now being used routinely for clinical and research applications.

4.2 Biochemical Imaging of Tumors for Diagnosis, Target Delineation and Evaluation for Treatment

WKNI developed a protocol to utilize three target radiotracers to study brain tumors in human subjects: ^{18}F-FDG for glucose metabolism, ^{11}C-MET for amino acid transport and protein synthesis, and ^{11}C-choline for lipid synthesis. The uptake and incorporation of these radiotracers were evaluated using PET in astrocytoma patients who were suspected of having grade II or III tumors.

Seventeen patients with suspected astrocytomas (nine grade II and eight grade III) were studied by PET with ^{18}F-FDG and ^{11}C-MET, and one patient (grade III) was studied with ^{18}F-FDG, ^{11}C-MET and ^{11}C-choline. The uptake of PET radiotracers was quantitated based on tumor to corresponding-contralateral-region uptake ratio (T/CCR), tumor to mean-cortical-uptake ratio (T/MCU), and tumor-to-white-matter-uptake ratio (T/WM). Radiotracer uptake was also correlated with the World Health Organization (WHO) histologic grading system and clinical follow-up.

To understand the potential underlying mechanisms of radiotracer uptake in the tumors, in vitro studies were also carried out with these tracers in a grade III HTB-14 human astrocytoma cell line. Uptake of ^{3}H-methionine, ^{3}H-choline, and ^{18}F-FDG and their incorporation into lipid, RNA, DNA, and protein at different times of incubation (0.5, 1, 2, and 4 h) were investigated in the cell line.

4.3 PET Scanning to Determine Tissue Viability Post-Stroke

The original objective to determine post-stroke tissue viability was not realized because of difficulty in establishing a successful protocol for performing rapid assessment using PET scans.

4.4 Tracer Development for PET Imaging

^{11}C-choline, ^{11}C-MET and ^{11}C-flumazenil are routinely produced for human purposes, and production of these radiopharmaceuticals was standardized under this project. Currently, ^{11}C-MET is used along with ^{18}F-FDG in studies of brain tumors, and ^{11}C-choline continues to be tested for efficacy in detecting prostate and brain tumors.

The most commonly used method of carbon-11 labeling is to couple carbon-11-labeled methyliodide ($[^{11}C]CH_3I$) with the labeling precursor of interest. There are two ways to convert the cyclotron-produced carbon-11 carbon dioxide ($[^{11}C]CO_2$) into $[^{11}C]CH_3I$. The classical method is to use $LiAlH_4$ to reduce $[^{11}C]CO_2$ to an intermediate metal complex, then to use aqueous HI to yield $[^{11}C]CH_3I$ through $[^{11}C]CH_3OH$ [15]. The contemporary method is to use hydrogen gas to reduce $[^{11}C]CO_2$ to $[^{11}C]CH_4$ on a nickel catalyst, then use I_2 to convert $[^{11}C]CH_4$ into $[^{11}C]CH_3I$ at a high temperature.

The commercially available GE [C-11]CH_3I synthesizer is an automated apparatus taking advantage of the newly developed methodology. Nuclear Interface (NI) made the PC DOS-programmed [C-11]Methylation Module commercially available. Our goals for this part of the project were to evaluate an automated system by connecting the methyliodide synthesizer (GE box) and methylation module (NI box) in tandem to replace the older, labor-intensive system that uses $LiA1H_4$ and hydriodic acid to convert $[^{11}C]CO_2$ into

[^{11}C]CH_3I. This automated tandem system was then evaluated for the routine clinical production of ^{11}C-MET, ^{11}C-choline and ^{11}C-flumazenil.

^{11}C-flumazenil is a radiopharmaceutical for the study of the gamma-aminobutyric (GABA) receptor complex. Flumazenil binds to the benzodiazepine sites in the GABA complex, sites that have been shown to be overly expressed in epilepsy. ***Figure 1*** shows the binding of ^{11}C-flumazenil in a normal volunteer, where binding of the radiotracer in cortical regions, which are known to contain a high concentration of the benzodiazepine receptor sites, is detected.

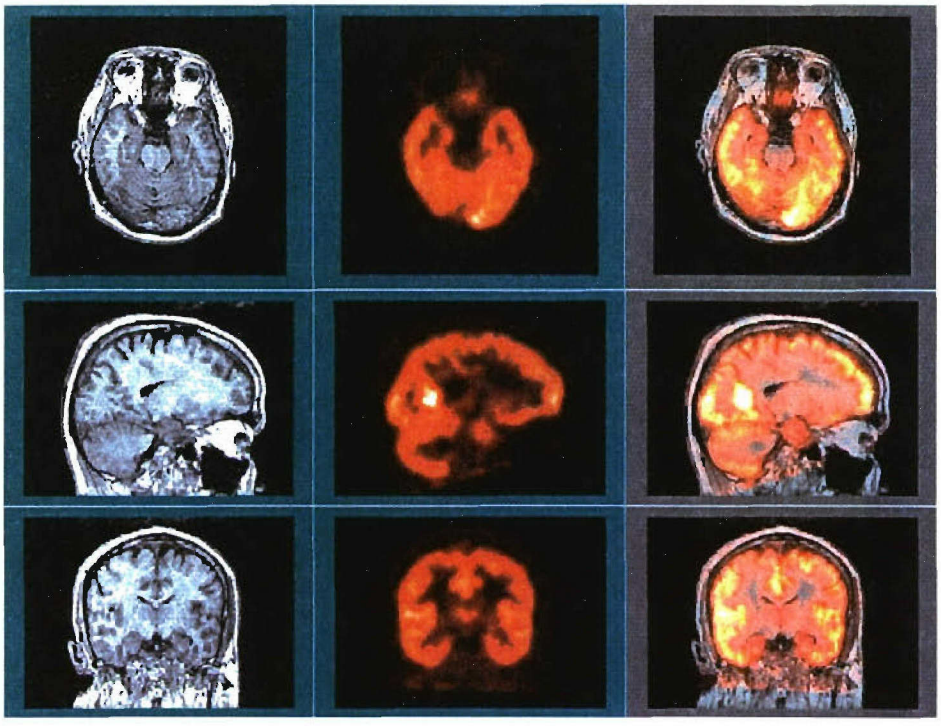

Figure 1

4.5 Software Development for Quantitative PET Image Analysis

For ^{18}F-fallypride, an analytical model was developed and validated for measuring a metric that is representative of dopamine, D-2, receptor density. This work involved performing preliminary work on monkeys to measure the binding potential of ^{18}F-fallypride for the D-2 receptor site. A rigorous compartmental analysis was first performed to define the "gold standard" of the in vivo tracer kinetics. Simplified models

were then applied to test the tradeoffs between parameter bias and computational rigor. It was found that a simplified method of analysis, yielding a parameter of distribution volume ratio (DVR), could accurately describe the binding process without the need to sample arterial blood from the subject [15]. This model can now be applied to human studies without the full course of validating studies.

4.6 Study of 2-DG as a Differential Radiomodifier

Early observations on yeast and mammalian cell cultures showed inhibition of radiation-induced (x-ray, ultraviolet; UV) and 2-DG-induced DNA damage in cells with high rates of glucose utilization and glycolysis. A relative decrease in the rate of DNA repair correlated in a sigmoid manner with the relative reduction in glycolysis in the presence of 2-DG. In the absence of respiratory metabolism, the inhibition in DNA repair was higher and irreversible. In human tumor cell lines, 2-DG-induced enhancements in cell death were related in a sigmoid fashion with the rates of cellular glucose utilization [16].

In murine tumor models, administration of 2-DG (i.v., 1-3 g/kg body weight) just before or after local irradiation of the tumor (10-20 Gy) increased tumor cell loss rate, delayed tumor growth, and increased survival in a dose-dependent manner. Interestingly, administration of 2-DG in similar doses to whole body-irradiated mice reduced cytogenetic damage in the bone marrow and increased survival [17].

5.0 Results

5.1 Biochemical Imaging of Tumors for Diagnosis, Target Delineation and Evaluation of Treatment

In all patients, PET images of ^{11}C-MET and ^{18}F-FDG provided higher T/WM than T/CCR and T/MCU. In grade II patients, ^{18}F-FDG did not exhibit a significant increase in tumor uptake, while ^{11}C-MET was a good predictor for ratios of approximately 1.50±.30. In grade III patients, both ^{18}F-FDG and ^{11}C-MET exhibited higher ratios for grade II patients, with ^{11}C-MET being the greatest, possibly suggesting enhanced protein synthesis. In the single patient who was evaluated with all three radiotracers, ^{11}C-choline appeared to be equal or slightly better than ^{11}C-MET for tumor delineation. ***Figure 2*** compares the PET scans done with ^{11}C-choline, ^{11}C-MET and ^{18}F-FDG versus the MRI scan.

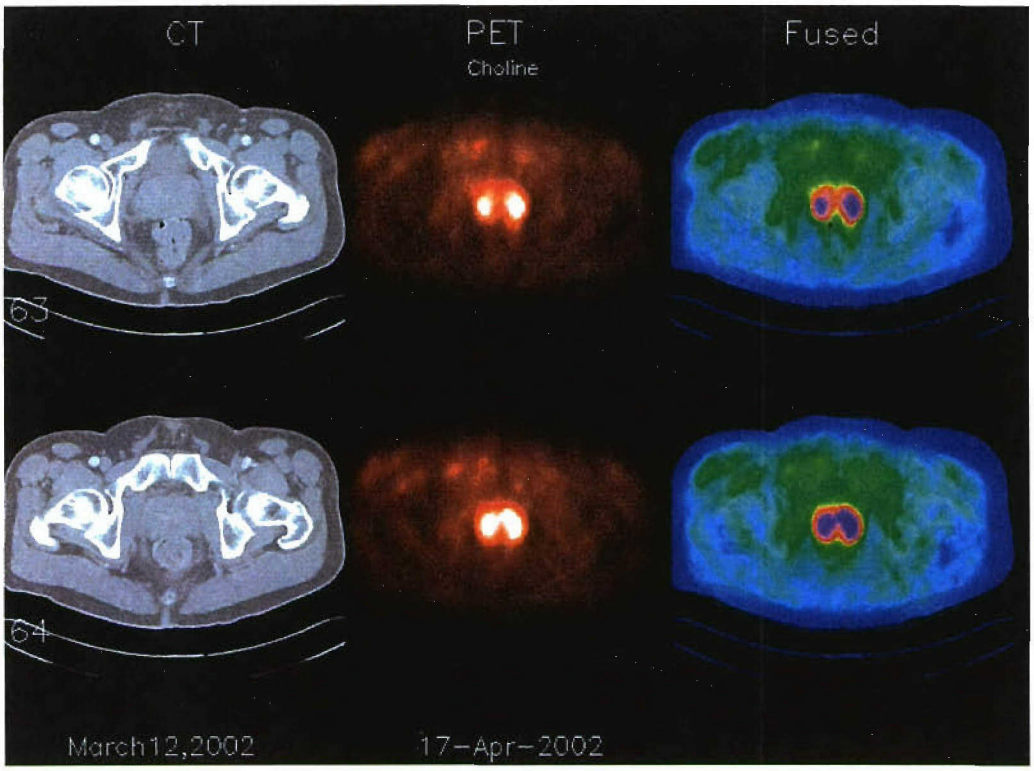

Figure 2

In our in vitro studies with these radiotracers, methionine uptake increased with longer incubation time, and the percentage of incorporation of methionine into DNA, RNA, and protein increased concomitantly with increased uptake. Incorporation into DNA and

RNA showed an increase with longer incubation time at 0.5 h, 1 h, 2 h, and 4 h, whereas increased incorporation into protein was seen between 0.5 h, 1 h, and 2 h. Incorporation of methionine into lipid was constant at all time points.

Similar to methionine uptake, choline uptake increased with longer incubation times in the cell line. No significant increase in choline incorporation into lipid was seen between 2 h and 4 h; however, at 0.5 h and 1 h, the percent incorporation of choline into lipid was 33.15±2.35% and 62.94±0.15%. Choline incorporation into RNA and protein constitutes less than 0.1% at all time points, and there was no incorporation into DNA. Uptake of ^{18}F-FDG showed a time-dependent increase at 0.5 h, 1 h, and 2 h. Total uptake of ^{18}F-FDG was completely accounted for in the free pool supernatant fraction, and there was no incorporation into RNA, DNA, or lipid and protein fractions.

These results suggest that a combination of ^{18}F-FDG and ^{11}C-MET is useful for the prediction of histologic grade of astrocytomas. Moreover, ^{11}C-MET is better than ^{18}F-FDG in delineating tumor boundary for low-grade gliomas. Our in vitro results demonstrate that ^{3}H-methionine is incorporated into proteins, suggesting that protein incorporation is one of the major driving forces in the uptake of ^{11}C-MET that has been observed in PET images. Experiments with these radiotracers in vivo in animal models will be useful in further characterizing the biochemistry of tumors. These findings may then be correlated with the findings in human subjects.

Further work is being done with choline as a radiotracer for imaging prostate cancer and brain tumors. ***Figure 3*** shows an ^{11}C-choline scan of a prostate tumor, demonstrating the power of this radiotracer to detect tumor margins. Several patients have been scanned to determine whether choline can provide the physician with a better marker for improved tumor delineation.

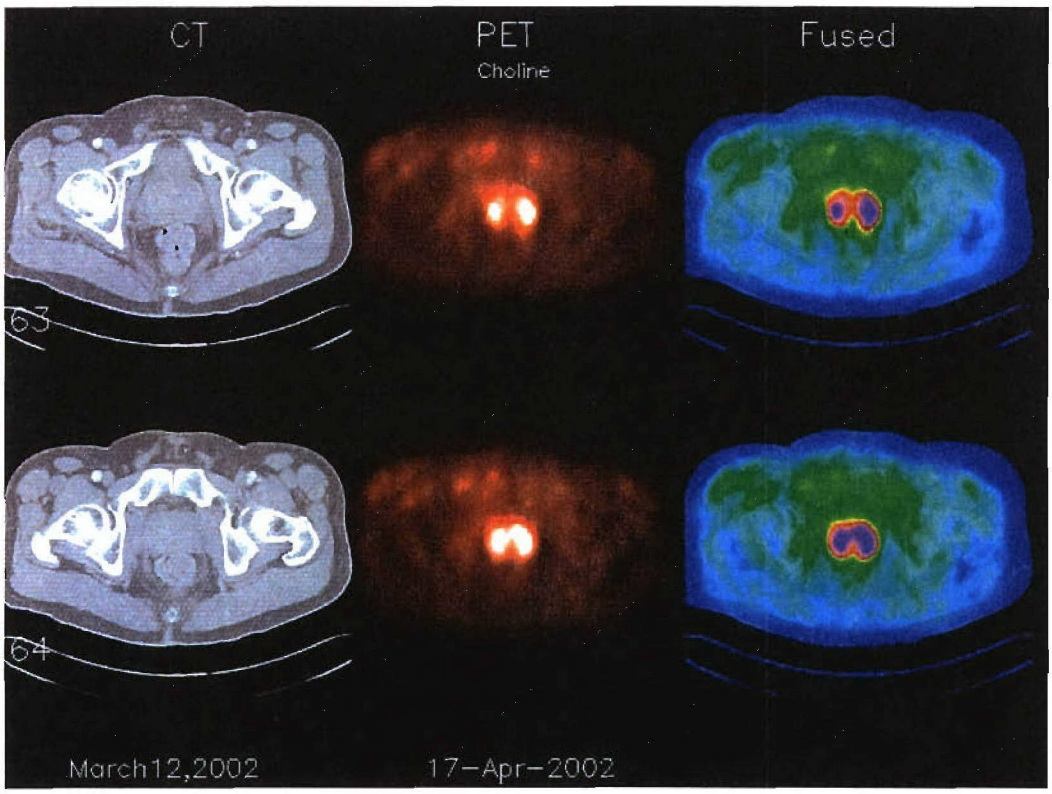

Figure 3

5.2 PET Scanning to Determine Tissue Viability Post-Stroke

As stated in the Methods, our efforts were redirected to more viable portions of this project because of difficulty in establishing a successful protocol in a timely manner for performing rapid assessments by PET scans.

5.3 Tracer Development for PET Imaging

Our continuing studies with flumazenil found that it may play a unique role in helping epileptic patients get relief from their disease. Approximately 70-80% of epilepsy patients may obtain adequate control of their seizures with medication. Of the remaining 30% of medically intractable patients, approximately 50% may be candidates for epilepsy surgery. However, in order to successfully resect the focus, the lesion must be clearly localized using neuroimaging studies, such as MRI, PET, or CT. This may be difficult in some cases, where these imaging techniques are not sensitive enough to discern subtle differences between different types of foci.

For example, noninvasive studies, including electroencephalography (EEG)/video monitoring, high-resolution MRI, ^{18}F-FDG, PET, neurophychological testing and Wada tests supply adequate diagnostic and localizing information in about 75% of temporal lobe epilepsy patients. Many times it is difficult to distinguish mesial temporal from lateral (neocortical) temporal lobe epilepsy. The use of ^{11}C-flumazenil may offer a potential solution to this problem. The reduction in ^{11}C-flumazenil binding reflecting selective loss of GABA receptors appears to be relatively limited to the mesial temporal region, in mesial temporal epilepsy, as opposed to the wider area of hypometabolism demonstrated on ^{18}F-FDG PET.

Experts from the Epilepsy Center of WKNI are currently using ^{11}C-flumazenil on epileptic patients, comparing them with other measurements such as the standard ^{18}F-FDG scans, MRI scans, and EEG findings, in attempts to determine the sensitivity of flumazenil binding in detecting seizure foci. Mapping of the distribution of flumazenil in normal individuals is also being completed for comparison. ***Figure 4*** demonstrates the binding of ^{11}C-flumazenil in the brain of an epileptic patient.

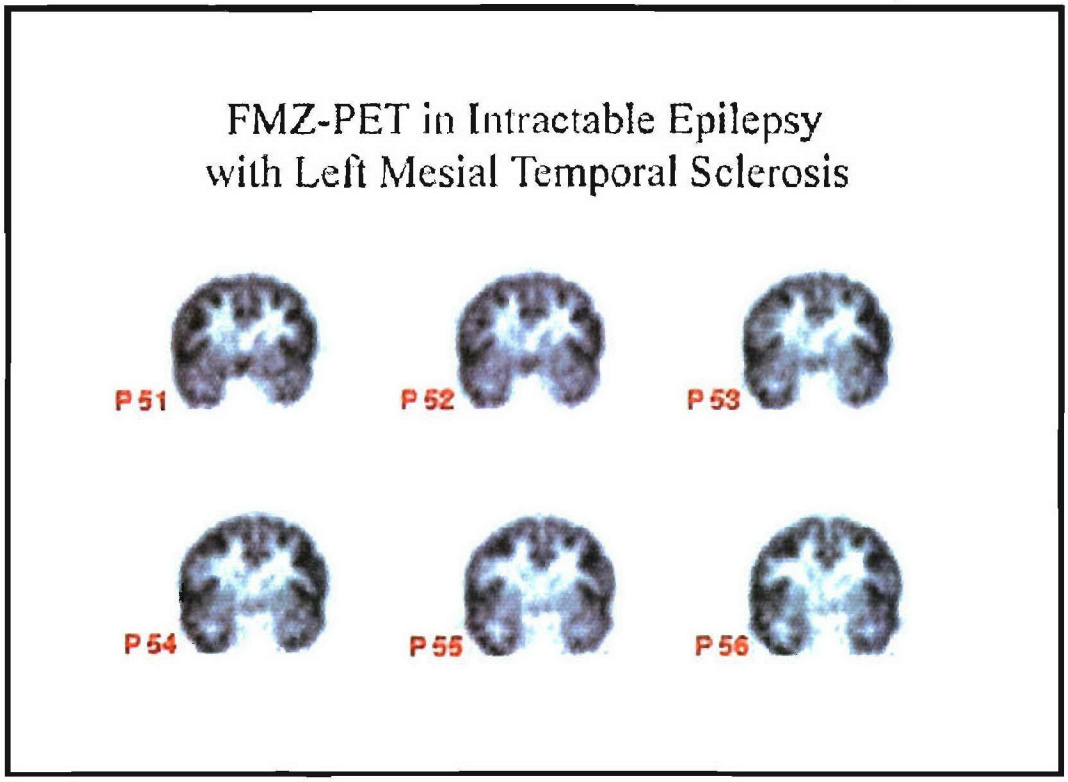

Figure 4

Other unique radiotracers are being developed and used in PET scanning studies at WKNI. The D-2 dopamine receptor antagonist, fallypride, has been labeled for use in studying schizophrenic patients. Fallypride binds to dopamine receptor sites and can be used to measure receptor density and occupancy. We used ^{18}F-fallypride to complete receptor studies in monkeys and normal humans (***Figure 5***), and work is now underway to study fallypride binding in drug-naïve schizophrenic patients.

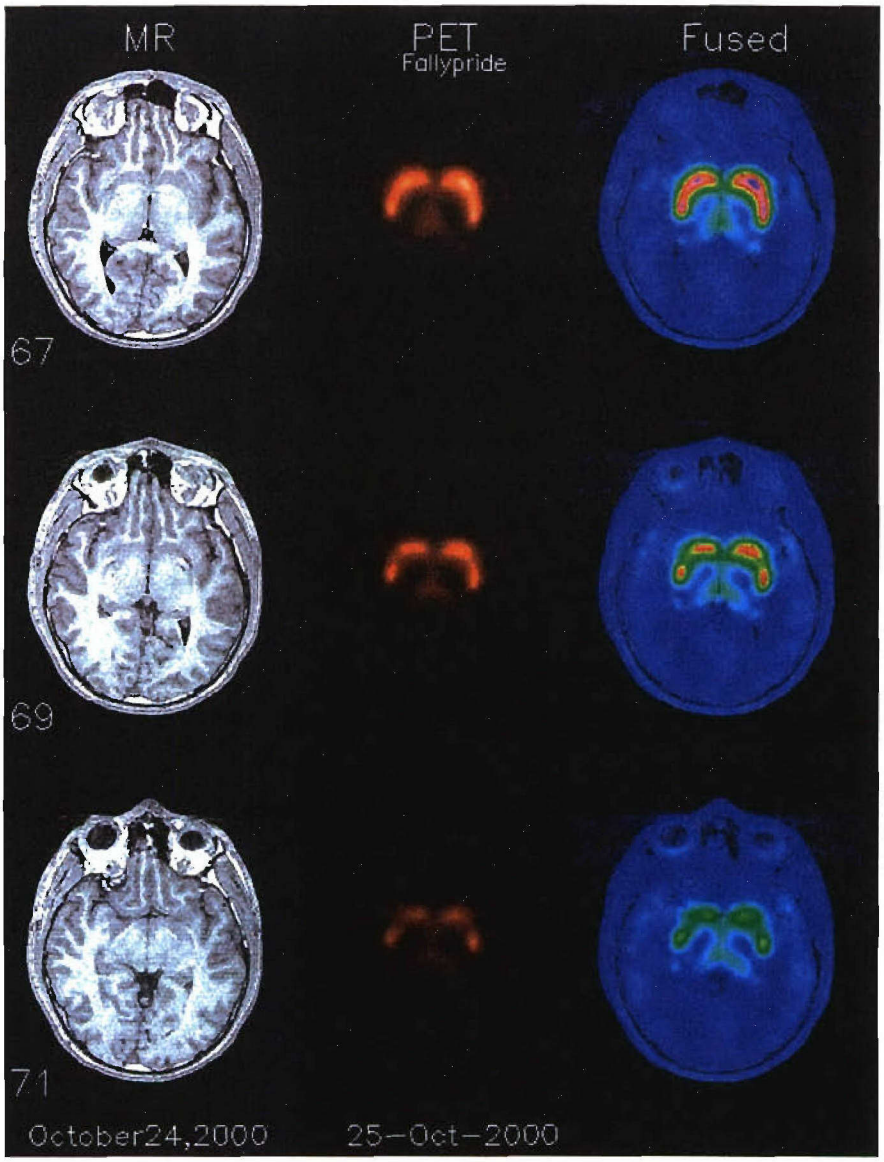

Figure 5

5.4 Software Development for Quantitative PET Imaging Analysis

With the knowledge gained through our development of software for quantitating the in vivo binding characteristics of novel neuroligands, it is also possible to apply this model to answer relevant scientific questions. For this work, antipsychotic drug occupancy for the D-2 dopamine receptor site was measured using ^{18}F-fallypride. We found that very small amounts of the typical antipsychotic, haloperidol, resulted in almost complete blockage of the targeted D-2 receptor, which results in overmedicating the patient [18].

These measurements were also made for atypical antipsychotic medications such as risperidone and clozapine.

5.5 Study of 2-DG as a Differential Radiomodifier

Phase 1 and 2 clinical trails on patients (n=10) with glioblastoma showed that 2-DG given orally (200-300 mg/kg body weight) 20-30 min before large fraction gamma-irradiation (7×5Gy/frction/week) was well tolerated and safe; transient side effects similar to hypoglycemia were observed. Two-year survival with good quality-of-life was 40%, which is significantly higher than conventional treatment.

6.0 Future Directions

Further research in these areas would allow for the continuation of several key studies which were successfully initiated under this Cooperative Agreement. These studies provided a significant base from which to gain understanding into several serious neurological disease states, including cancer, epilepsy, and schizophrenia. Additional funding will be sought to expand these studies and build on this knowledge base. This information can significantly impact and improve human health and provide technological advances for both the general public and the USAF, as well as contribute toward the development of related commercial products.

6.1 Choline and Methionine

The study utilizing choline for delineating brain tumors should be expanded to increase the size of the brain tumor patient database. Subsequent studies could be done to determine whether choline could be used in conjunction with MRS for further improving brain tumor demarcation, and ^{11}C-choline radiotracer could be used for whole body tumor detection, particularly for prostate cancer.

Future work should be completed to learn more about the potential mechanisms of methionine and choline uptake in brain tumors. Uptake kinetics have been studied in high-grade tumors, and these experiments could now be reapplied to the low-grade tumor environment to determine if methionine and choline can be used for delineating other tumor types.

Because it is not fully understood why methionine is selectively taken up in brain tumors, more work is needed to better understand the potential mechanisms of methionine tracer uptake. It is possible that, in addition to increased protein synthesis in the tumors, there may be an additional role that methionine is playing that results in its increased uptake on PET scans.

More work is also needed to determine whether the correlation of co-registered MR/PET images with tumor volumes can be used in the clinical setting for improved diagnosis and

treatment. Does an increased uptake value on PET scans correspond to increased tumor growth? Compared to MR, PET appears to provide a much earlier indication of tumor growth. Do changes in the PET tumor volume provide better diagnostic information than corresponding MR or CT tumor data? Additional studies are needed to determine whether this difference is significant and if it can be used to enhance treatment planning. We also need to better understand how uptake ratios for methionine can be used to enhance diagnosis, and surgery and radiation treatment planning for clinical practice.

6.2 Flumazenil

The flumazenil project, in which flumazenil is being tested to determine its utility compared to other standard, noninvasive tests for localizing epileptic foci, is being continued to include 25 epilepsy patients and five normal controls.

6.3 ^{18}F-Fallypride

The studies using fallypride are being completed; to date, several normal controls have been studied with this radiotracer. The next phase includes drug-naïve schizophrenics to determine the baseline receptor status in these patients, and to discern how that receptor status is impacted once drug treatment is administered. We hope that this will provide more insight into the underlying causes of schizophrenia and potentially offer clues to improve treatment options.

Receptor studies using ^{18}F-fallypride have potential military application because they can be used to study the effects of nerve gas poisoning on the CNS and improve upon methods to counteract the transmission of neurotoxins. The creation of quantitative images aids in the evaluation of the effects of the poisoning by providing a measure of toxicity, or other negative environmental factors, which in turn helps to determine how to counter these effects. In addition, the PET scanner and high performance liquid chromography columns are tools that can be used in studies to establish an infrastructure to study neurotoxins and biological agents (i.e., Anthrax).

6.4 Study of 2-DG as a Differential Radiomodifier

Clinical trials to study the feasibility and efficacy of 2-DG+SRS in patients with malignant brain tumors showing high glucose uptake (measured by ^{18}F-FDG-PET) are planned. Approvals from the Federal Food and Drug Administration and Internal Review Boards (KMC and WSU) for these studies have been obtained and we are preparing to recruit patients

6.4.1 Development of Predictive Assays

Research work using DNA microarrays to study 2-DG-induced changes in gene expression profiling needs to be extended to irradiated cells, other glioma cell lines and surgical specimens to develop predictive assays. This is required to select suitable patients and individualization of treatment. Analysis of large amounts of data collected in the global measurements of gene expression after different treatments is a challenging task. Appropriate methods and software for identifying the most relevant genes affecting the treatment responses need to be developed. Neuronal network and pattern recognition techniques may be employed for this purpose.

6.4.2 Enhancing Radioprotection of Normal Tissue

The minor-groove DNA ligand Hoechst-33342 has been shown to effectively protect DNA against strand breakage induced by irradiation in aqueous solutions, cells in vitro and in vivo [19-21]. The radioprotective effects of H-33342 in whole-body irradiated mice are further enhanced by 2-DG [22]. Interestingly, radioprotection in tumors transplanted in mice was not observed [23]. It would therefore be worthwhile to undertake in-depth studies on the radioprotective effects of H-33342 and its analogs alone and in combination with 2-DG. This could be useful not only for cancer patients, but also for persons receiving high radiation doses in planned (space travel, reactor maintenance) or unplanned exposures (nuclear reactor accidents, terrorist attacks using nuclear weapons).

6.4.3 Radiosensitization of Tumor Tissues

Several recent studies have shown that many tumor types including glioma, breast and prostate express very high density of peripheral benzodiazepine receptors (PBR) which

are mainly located in the outer membranes of mitochondria and associated with the permeability transition pore (PTP) multi-protein complex [24]. Our studies with the U-87 glioma cell line have confirmed over-expression of PBR. The PTP complex has been shown to play a crucial role in cell death through the apoptotic pathway. PBR ligands such as porphyrins have been shown to reduce respiration and enhance glucose uptake in tumor cells [25]. A combination of porphyrin derivative (HpD) with 2-DG enhanced the radiosensitization in cell lines derived from human tumors [26]. HpD acts as a photosensitizer and therefore may induce phototoxicity in patients. Recent work has shown that another PBR ligand, PK11195, can increase the susceptibility of tumor cells to apoptotic death induced by radio/chemotherapeutic drugs [27]. PK11195 can be easily labeled with radioactive isotopes (C-11, F-18, and I-131) and has been used for imaging [28]. Possibly, PK11195 labeled with an appropriate radioisotope could also be developed as an agent for targeted radiation therapy. It is therefore proposed to study the combination of 2-DG with PK11195 in model systems to verify its usefulness in improving radiotherapy of glioblastoma and breast tumors.

6.4.4 Dose Sculpting

FDG-PET and hypoxia images can be used to optimize treatment planning in radiotherapy and radiosurgery. In view of the fact that cells with high glucose uptake and low oxygen (hypoxic) environment are more radioresistant, it would be reasonable to treat them with higher radiation doses. The high glucose usage and hypoxic regions can be identified by PET scanning and incorporated, with appropriate software, in treatment planning procedures. This could further facilitate the use of 2-DG in optimizing tumor radiotherapy.

References

1 Donnan GA et al. Trials of streptokinase in severe acute ischemic stroke. Lancet 1995;354:578-579.

2 Homel M et al. Termination of trial streptokinase in severe acute ischemic stroke: MAST study group. Lancet (letter) 1995;3457-357.

3 Multicenter Acute Stroke Trial–Italy (MAST0I) Group. Randomized controlled trial of streptokinase aspirin, and combination of both on treatment of acute ischemic stroke. Lancet 1995;346;1509-1514.

4 Hacke W et al. Intravenous thrombolysis with recombinant tissue plasminogen activator for acute hemispheric stroke: the European Cooperative Acute Stroke Study (ECASS). JAMA 1995;274;1017-1025.

5 The National Institute of Neurological Disorders and Stroke rTPA Stroke Study Group. Tissue plasminogen activator for acute ischemic stroke. N Eng J Med 1995;333:1581-1587.

6 Infield B et al. Streptokinase increases luxury perfusion after stroke. Stroke 1996;27(9):1524-1529.

7 Heiss WD, Herholz K. Assessment of pathophysiology of stroke by PET. Eur J Nucl Med 1994;21:455-465.

8 Fox and Raichle, 1984.

9 Arndt 1996.

10 Holmes 1996.

11 Andersson 1998.

12 Vaidyanathan et al. 1997

13 Gibbs et al., 1996

14 Valthuizen et al., 1995

15 Marazano 1997.

16 Dwarakanath BS, Zolzer S, Chanda T et al. Heterogeneity in 2-deoxy-D-glucose induced modifications in energetic and radiation responses of human tumor cell lines. Int J Rad Oncol Biol Phys 2001;51:1151-1161.

17 Singh SP, Singh S, Jain V. Effects of 5-bromo-2-deoxyuridine and 2-deoxy-D-glucose on radiation induced micronuclei in mouse bone marrow. Int J Rad Biol 1990;58:791-797.

18 Larsen, 1995.

19 Adhikary A, Jain V. Studies on the modulation of DNA damage 1. A simple kinetic model for radioprotection of DNA in aqueous solution. Indian J Biochem Biophys 1997;34(5):409-418.

20 Adhikary A, Bothe E, von Sonntag C et al. DNA radioprotection by Bisbenzimidazole derivatine Hoechst 33258: model studies on the nucleotide level. Radiat Res 1997;148(5):493-494.

21 Dwarakanath BS, Kapoor N, Chandna JS et al. Radiomodifying effects of the DNA ligand Hoechst in transformed and mammalian cells. In: Sharan RN, ed. Trends in Radiation and Cancer Biology, Bilateral Seminars of the International Bureau, Julich. 1998;29:81-89.

22 Singh SP, Jayanth VR, Chandna S et al. Radioprotective effects of DNA ligands Hoechst-33342 and 33358 in whole body irradiated mice. Indian J Exp Biol 1998;36:375-384.

23 Dwarakanath BS, Singh S, Jain V. Optimization of tumor radiotherapy: Part V-Radiosensitization by 2-deoxy-D-glucose and DNA ligand Hoechst-33342 in a murine tumor. Indian J Exp Biol 1999;37:865-870.

24 Beurdeley-Thomas A, Miccoli L, Oudard S et al. The peripheral benzodiazepine receptor: a review. J Neuro Oncol 200;46:45-46.

25 Khanum F, Jain V. Effects of hematoporphyrin derivatives on the cellular energy metabolism in the absence and presence of light. Photochem Photobiol 1989;50:647-650.

26 Dwarakanath BS, Adhikari JS, Jain V. Hematoporphyrin derivatives potentiate the radiosensitizing effects of 2-DG in cancer cells. Int J Radiat Oncol Biol Phys 1998;43:1125-1133.

27 Hirch T, Decaudin D, Susin SA et al. PK11195, a ligand of the mitochondrial benzodiazepine receptor, facilitates the induction of apoptosis and reverses Bcl-2-mediated cytoprotection. Exp Cell Res 1998;241:426-434.

28 Pike VW, Haldin C, Crouzel C et al. Radioligands for PET studies of central benzodiazepine receptors and PK (peripheral benzodiazepine) binding sites – current status. Nuc Med Biol 1993;20:503-525.

Symbols, Abbreviations and Acronyms

ACR	American College of Radiology
AD	Alzheimer's disease
ADC	apparent diffusion coefficient
AFRL	Air Force Research Laboratory
ANC	adaptive noise cancellation
ANOVA	analysis of variance
aPL	antiphospholipid
^{31}C	carbon
CBF	cerebral blood flow
CDP	cytidine diphosphate
CN	central neurocytoma
CNS	central nervous system
CR	creatine
CSF	cerebral spinal fluid
CSI	chemical shift imaging
CT	computerized tomography
DA	discriminatory analysis
DAG	diacylglycerol
DBS	deep brain stimulators
d[n]	desired signal
DWI	diffusion-weighted imaging
ED	Emergency Department
EEG	electroencephalography
EF	environmental factor; enrichment factor
ELISA	enzyme-linked immunosorbent assay
EMAS	Endler Multidimensional Anxiety Scales
EMI	electromagnetic interfaces
EPI	echo-planar imaging
ER	emergency room
FDG	fluorodeoxyglucose
FID	free induction decay
FLAIR	fluid attenuated inversion recovery
fMRI	functional magnetic resonance imaging
FSE	fast spin echo sequence
GFAP	glial fibrillary acidic protein
gd	gadolinium
gd-MRI	gadolinium-enhanced magnetic resonance imaging
GPC	glycerophosphocholine
^{1}H	proton
HICH	hyperacute intracranial hemorrhage
HMD	head-mounted display
IRB	internal review board

KEMAR	Knowles Electronic Manikin for Acoustic Research
KMC	Kettering Medical Center
KMCN	Kettering Medical Center Neurology
LDA	linear discriminatory analysis
MBP	myelin basic protein
MiniP	minimal intensity projection
MIP	minimum pixal intensity
MNS	multinuclear spectroscopy
MR	magnetic resonance
MRI	magnetic resonance imaging
MRS	magnetic resonance spectroscopy
MS	multiple sclerosis
MTLE	mesial temporal lobe epilepsy
MTT	mean transient time
NAA	*N*-acetyl aspartate
NIHSS	National Institute of Health Stroke Study
NMR	nuclear magnetic resonance
NSE	neuron-specific enolase
ODV	optimum discriminatory vector
OR	operating room
^{31}P	phosphorous
PACS	picture archives and communications system
PBS	phosphate-buffered saline
PCA	principal component analysis
Pcho	phosphocholine
PCr	phosphocreatine
PDW	protein density-weighted
PE	phosphatidylethanolamine
PEMT	PtdE-*N*-methyltransferase
PET	positron emission tomograhy
Pi	inorganic phosphate
PKC	protein kinase C
PL	phospholipids
PR	pattern recognition
PtdC	phosphatidylcholine
PS	phosphatidylserine
PWI	perfusion-weighted imaging
RF	radio frequency
ROI	region of interest
rTPA	recombinant tissue plasminogen activator
SPGR	3-D Spoiled Gradient Recalled Acquisition Steady State
SPI	tissue plasminogen activator
SV	single voxel
SV-MRS	single voxel magnetic resonance imaging
T_1W	T 1 weighted
TIA	transient ischemic attack

TLE	temporal lobe epilepsy
TMS	tetramethylene silacycline
USAF	United States Air Force
VE	virtual environment
VOI	volume of interest
WHO	World Health Organization
W_k	K weights
WKNI	Wallace-Kettering Neuroscience Institute
WPAFB	Wright-Patterson Air Force Base
WSU	Wright State University
x[n]	referenced signal